# Late Holocene environmental change: evidence from Lake Xiaolongwan, north east China and Lake Arachlei, south eastern Siberia

Virginia Natalie Panizzo

For submission for a Doctorate of Philosophy, Department of Geography, UCL

I, Virginia Natalie Panizzo confirm that the work presented in this thesis is my own. Where information has been derived from other sources, I confirm that this has been indicated in the thesis.

## Acknowledgments

There are many people to whom I feel indebted to for their support through the completion of my thesis. First and foremost, I would like to express my gratitude to my supervisor Dr. Anson Mackay, who has been a fantastic friend, mentor and whose insight and knowledge I greatly value. He has given me the inspiration to continue with my research in this field over many years.

I would also like to extend my thanks to my co-supervisors, Prof. Jonathan Holmes, Prof. Melanie Leng and Dr. Patrick Rioual. Their expert knowledge in their subject fields has been very valuable. I would like to thank Patrick further for giving me the opportunity to visit China and the Long Gang Volcanic Field. In particular, for planning our fieldwork in 2007. Without him and Dr. Wang Luo it would not have been possible or at all as enjoyable!

I would also like to thank Prof. Neil Rose for conducting SCP analyses on this project and Dr. Handong Yang for advice on my chronology formulation. Furthermore, Dr. Gavin Simpson, who has helped me greatly in the conducting of advance numerical techniques, designed specifically for this project and Dr. Nadia Solovieva for translating key Russian literature.

I would also like to thank the many members of the ECRC, in particular Prof. Rick Battarbee, Prof. Tim Atkinson, Dr. Carl Sayer, Dr. Tom Davidson Dr. Viv Jones, Dr. Helen Bennion and Dr. Ben Goldsmith, who throughout my Ph.D have provided valuable ideas and comments. They have been very important in shaping this thesis. Fellow Ph.D students, past and present (there are so many to name, sorry) have been essential in helping me to complete my thesis, providing entertainment, much advice and on other occasions, distractions. Thank you to you all!

I would also like to take the opportunity to thank Janet Hope, Tula Maxted and Ian Patmore, whose help in the lab and in organising fieldwork were an important part of my research. Thank you also to Jim Davy, Earth Sciences, who went out of his way whenever possible to book me in for the SEM and showed me the ropes. I would like to express my gratitude also to Hilary Sloane and Carol Arrowsmith at NIGL for running isotopic analyses.

This project is indebted to Dr. Chu Guoqiang and Dr. Ivan Kalugin who have both provided core material and have shared their research findings. I thank them for their collaboration. Radiometric dating was conducted at Poznan Radiocarbon Laboratory and the Dating facility of the Unversity of Sussex.

On a more personal level I would like to thank my close family and friends, who have supported me to the bitter end. I couldn't have done it without you all. Thank you to my parents who have backed me 100% throughout and have shared interest in my research. Also to Oliver, who has had to live with *all* the ups and downs but has always inspired me to keep going, thank you. You can all relax now!

This project was funded by NERC Research Grant (NER/S/A/2006/14046) and is a Case Studentship with NERC Isotope Geoscience Laboratory. Funding was also received from the UCL Graduate Conference Fund and the Quaternary Research Association Conference Fund.

## Abstract

This project addresses the increasing need for high-resolution proxy studies of environmental change over the late Holocene from regions in northern Eurasia. The late Holocene has been identified as a key timeframe for investigating environmental change (e.g. PAGES Focus 2) due to the relatively small changes in boundary conditions. In particular, this project focuses on two sites; Lake Xiaolongwan, north east China, sensitive to changes in summer (EASM) and winter (EAWM) monsoonal intensity and Lake Arachlei, south east Siberia, sensitive to changes in Westerly transport and Siberian High intensity.

This project provides a detailed high-resolution reconstruction of diatoms and bulk organic isotopes from cores collected at each of these sites. The c. 2000 year record from Lake Xiaolongwan, has an age model derived from varve counting, $^{210}$Pb and SCPs. Ecological interpretations of diatom changes suggests a long term trend towards decreased lake water level and increased lake productivity (after c. 1650 years BP). Superimposed upon the trend are significant periods of assemblage changes thought to represent intensified EAWM intensity, occuring between c. 1450-1350 and 600-400 years BP, which are coincident with evidence of north Atlantic ice raft debris (IRD) events.

At Lake Arachlei, a similar trend of decreasing lake levels is also identified over the c. 3000 year record (based on a $^{14}$C and $^{210}$Pb age model). Significant assemblage changes are demonstrated between c. 3000-2800, 1450-1350 and 500-400 years BP, thought to indicate reduced Westerly transport to the region. These periods are coincident with Bond events 2, 1 and 0. This project demonstrates the role of teleconnections in the late Holocene, which may be responsible for environmental change. Nevertheless, the dramatic change identified in the Lake Xiaolongwan record after c. 1950 cannot be attributed to evidence of global warming in the region due to the demonstrated evidence of anthropogenic impacts (XRF and SCPs) in this otherwise perceived pristine region.

## Contents Pages

## List of Figures

**CHAPTER 5.**



**CHAPTER 6.**



**CHAPTER 7.**

## List of Tables

# CHAPTER 1. Introduction

## 1.1. Introduction

This study focuses on the recent environmental change over the late Holocene from two regions of northern Eurasia, which extends between 35 °N in central Asia to 78 °N and 20°E to 140°E (Shahgedanova 2002). The first region studied is in north eastern China, an area where the climate is dominated by the east Asian summer monsoon (EASM) and east Asian winter monsoon (EAWM) systems. The second site is located in central Transbaikalia, an ultracontinental region where the climate today is affected by variations in the Westerly wind system in the summer and the Siberian High (SH) in the winter. Variations in the atmospheric pressure systems (e.g. including The Siberian High, North Atlantic and Arctic Oscillation) over northern Eurasia are very important in influencing the trajectory and degree of penetration of the Westerlies and summer monsoonal wind systems.


*Figure 1.1. Map showing the location of the two sites in northern Eurasia. Lake Xiaolongwan in north east China and Lake Arachlei, south eastern Siberia. Latitude and longitude are shown on the figure (UNAVCO 2010).*

Indeed, there is a strong interplay between the climate systems in these two study regions, both responding to variations in dominant atmospheric pressure systems. Examples of the effect that these pressure systems have on climate in both regions will be discussed, especially with reference to the role teleconnections play on present day climate and over the late Holocene

period. Teleconnections can be defined as simultaneous variations in weather and climate over widely separated points on earth (Hurrell, 1996).

These two study sites (Lake Arachlei, south east Siberia and Lake Xiaolongwan, north eastern China; Figure 1.1) were selected due to their remote locations leading to minimal direct anthropogenic impact in recent history e.g. Lake Xiaolongwan is located in the protected Long Gang Volcanic Field (LGVF) National Park. Both lakes are deep, oligotrophic and dimictic lakes and Lake Xiaolongwan is also a maar crater lake. As a result, it is hypothesised that the lake sediments will be sensitive to recording the effects of climate change. This project will also act to directly test the hypothesis of minimal human impact upon such remote and pristine lakes, in order to place recent natural variability into context. This has not previously been conducted on either of the lakes discussed in this thesis and so will provide valuable information for future climate research.

The secondary rationale behind this project is linked to the climate dynamics in this region of northern Eurasia. Lake Arachlei and Lake Xiaolongwan (both oligotrophic, dimictic lakes) (Figure 1.1) are approximately equidistant from the EASM boundary (Figure 1.2), with the former not affected by monsoonal precipitation and the latter dependent upon it (Section 1.4). Both sites are however, affected by the intensity of the Siberian High (SH). While the climatic processes around Lake Arachlei are more strongly affected by the SH, changes in its intensity will also have an affect upon EAWM penetration and therefore the winter climate at Lake Xiaolongwan. Full details of the specific atmospheric controls at both sites will be provided below.

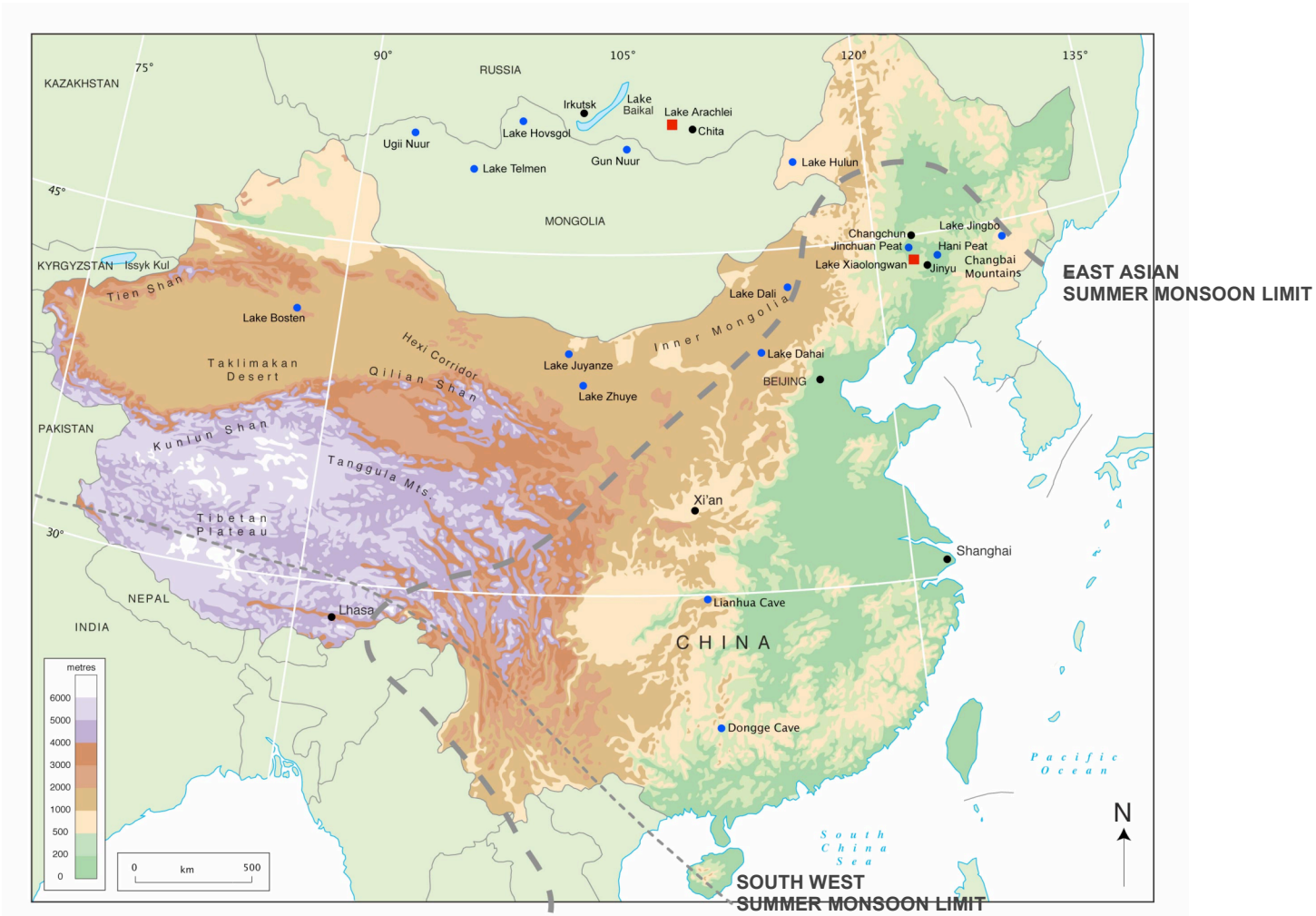


*Figure 1.2. Image displaying the approximate extension of the East Asian Summer Monsoon (EASM; thick dashed line) and South West Asian Monsoon (SWAM; fine dashed line) for present day southern Asia. The lines are adapted from Morrill et al (2003). The two sites studied in this project are outlined by red points. The studies mentioned in the thesis are shown as blue points and main cities are outlined by a black point. Adapted from a figure kindly provided by Prof. J.Holmes.*

## 1.2. Aims and objectives

The aim of this thesis is to develop high-resolution palaeoecological reconstructions from lake sediments in southern Siberia and north east China. In particular this study focuses on sediment cores taken from Lake Xiaolongwan, north east China, which is a site very sensitive to variation in the EASM due to its location close to the present day monsoonal boundary. The second site is Lake Arachlei, Transbaikalia, a site which is located in the ultracontinental region of southern Siberia and therefore very sensitive to variations in the SH and dominant Westerly systems. Both sites receive precipitation in summer months but from different sources providing a valuable reconstruction of how these systems have changed over the late Holocene and providing a discussion of teleconnection mechanisms between modes of variability.

This study has three main aims:
1) To examine evidence for teleconnections between the north Atlantic and northern Eurasia during the late Holocene by identifying climatic perturbations associated with ice rafted debris events (e.g. Bond events) superimposed upon the trend of late Holocene neo-glacial cooling.
2) To assess the sensitivity of proxies to variations in the east Asian summer/winter monsoons and Siberian High intensity as a result of Bond events and subsequent teleconnections.
3) To analyse the impacts of anthropogenic forcing over the recent past, in relation to natural variability. Multiproxy biotic proxies (diatoms, chrysophytes, organic isotopes) will be used to identify climatic events (e.g. changes in diatom assemblage and productivity) in response to local and global changes, while abiotic (geochemistry, lithological) proxies will be used to investigate more recent evidence of anthropogenic impacts.

Furthermore, the objectives of this project are to:

a) Analyse the isotopic composition of lake waters and catchment vegetation and soils in the LGVF, in order to investigate the modern day sensitivity of sites to the EASM, for the purpose of indirect downcore reconstructions of monsoonal variation. This objective was only conducted on Lake Xiaolongwan and its twelve neighbouring lakes as it was not possible to visit Lake Arachlei due to the limitation of fieldwork funding.
b) Provide a high-resolution (decadal to centennial scale) diatom reconstruction of assemblage changes. Through the knowledge of diatom ecology a palaeoecological reconstruction will be developed in order to investigate ecological changes over the past c. 3000 years.
c) Provide a high resolution bulk organic isotope reconstruction of $\delta^{13}C$ and of C/N ratios in order to investigate downcore changes in palaeoproductivity.
d) Conduct multivariate analyses (timeseries, SiZer) upon diatom and isotope data to summarise major trends in proxy data and investigate the presence of any periodicities. Data will be compared with other dominant climate indices for the region (e.g. EASM, SH).

e) Analyse sediments for fly-ash particle deposition in order to investigate anthropogenic impacts upon both these remote lakes. In addition, there was also the opportunity to conduct trace metal contamination analyses at Lake Xiaolongwan. However, insufficient material at Lake Arachlei prevented this.

## 1.3. Thesis structure

Chapter 1 will outline the dominant atmospheric controls at both sites. It will then provide detailed information upon external and internal forcing factors of climate and how they have affected climate change in the late Holocene. The chapter will finish with an outline of dominant environmental change in the late Holocene for these regions of northern Eurasia.

Chapter 2 will outline two aspects of the methodology used in this project. Firstly, a brief introduction will be given as to why the certain methodologies have been chosen to answer the project's research objectives. Secondly, the background to the techniques adopted will be outlined, in particular focussing on the theory behind the methods. The specific methods adopted are discussed in the relevant data chapters.

In Chapter 3 the contemporary isotopic composition of lake waters and dominant catchment vegetation and soil samples will be discussed. This data is only available for Lake Xiaolongwan and twelve other neighbouring lakes due to time and funding limitations to visit Lake Arachlei. These data are valuable in order to understand modern day lake processes and lake sensitivity to precipitation variations and therefore for palaeoreconstructions. Contempoarry climate in this region of NE China will also be outlined as well as detailed information on the limnology of each of the lakes. More detailed information is also provided for Lake Xiaologwan, including results of diatom sediment traps and temperature profiles of the lake throughout the year.

Chapter 4 outlines the methods and results of the chronology formation for the cores collected from Lake Xiaolongwan. Information on the different dating methods used is given and it also provides detail on the method of correlating the different cores.

In Chapter 5 the palaeoreconstruction for Lake Xiaolongwan is provided. Methods used and results are outlined. This chapter will present the palaeoenvironmental reconstruction derived from Lake Xiaolongwan. Bulk organic isotope reconstructions, as well as XRF data, will be discussed in order to look at the relevant importance of natural and anthropogenic driven changes. Qualitative interpretation of diatom ecologies will also be given. Timeseries and SiZer analyses will also be presented in order to tease out significant changes and trends in the data. The record will then be compared with other records from the region in order to discuss the context of environmental changes from the core.

In Chapter 6 the palaeoreconstruction for Lake Arachlei is provided. This will include qualitative interpretation of diatom ecologies and the changes in palaeoproductivity based on bulk organic isotope changes. Firstly an outline will be provided of the context of environmental change over the late Holocene in arid central Asia (ACA). Then, a quantitative interpretation based on multivariate analyses will also be used to compare the Lake Arachlei record with other studies from northern Eurasia. The effect of anthropogenic activity in the region within the context of such environmental change will also be discussed.

The final chapter, Chapter 7 provides a summary of the palaeoenvironmental reconstructions from both Lake Xiaolongwan and Arachlei. Comparisons of the data are made within a wider context of late Holocene environmental changes (in particular with indices of EASM intensity, solar insolation changes and north Atlantic ice raft events) in order to discuss teleconnections. Conclusions are made about the project and the importance of further work also presented.

## 1.4. Contemporary climate systems of northern Eurasia

In this section, the dominant atmospheric processes over both of the sites are outlined, in order to better contextualise regional climate change over the late Holocene. In the approach adopted it is necessary to understand how climate may have affected freshwater ecosystems in the past. To do this a solid understanding of the mechanisms in contemporary ecosystems (e.g. interaction between climate and lake ecology/processes) is mandatory. Full details of the context behind the methodology used, in order to investigate these relationships is provided in Chapter 2. The more detailed local climate at both of the sites (e.g. mean annual temperatures and precipitation) will be outlined in the relevant data chapters (north east China; Chapter 3 and southern Siberia; Chapter 6).

### 1.4.1. The east Asian summer monsoon (EASM)

The EASM domain can be defined as the region that covers 20° – 45° N and 110° – 140° E, encompassing eastern China, Korea, Japan and additional marginal seas (Yihui and Chan 2005). Figure 1.2 displays the approximate line of penetration of the EASM in China, as well as the south west Asian monsoon (SWAM). The atmospheric circulation in east Asia is determined by the interaction of the wind regime, which is forced by the seasonal temperature contrast between the Asian land mass and the subtropical Pacific Ocean. The superimposition of the zonal Westerlies show a seasonal shift of their trajectory from c. 28°N in January to c. 35°N in July, along with Walker and Hadley circulation (Schettler et al. 2006). The inter-tropical convergence zone (ITCZ) is defined as the convergence line of airflows in the air stream and has great seasonal variation, as outlined above (Ding 1994).

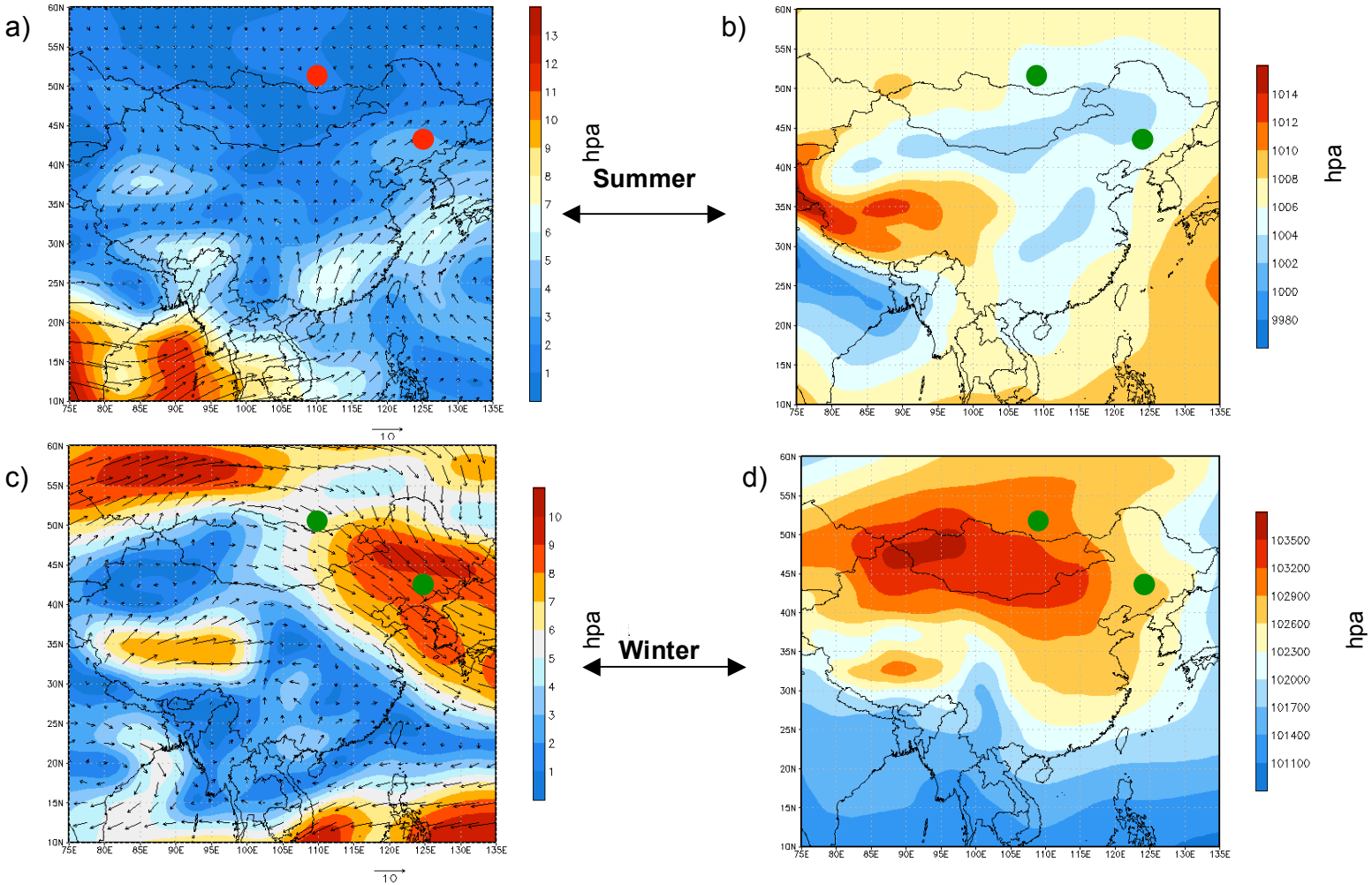


*Figure1.3a and b). Showing July 800 hpa (hectoPascal) wind vectors and sea level pressure (SLP) respectively. c) and d) display January wind vectors and sea level pressure (SLP) respectively. Images show the changing wind vectors in winter in a north westerly manner associated with the SH. Red (a) and green (b,c,d) marker points correspond to the two sites studied in this project. Image created 13/10/2009 and provided by the NOAA-NOMADS, National Weather Service(2010) (http://nomads.ncdc.noaa.gov/).*

As a result, the ITCZ has a significant impact upon weather and climate and circulation conditions in the western north Pacific and east Asia, especially affecting the activity of tropical cyclones and precipitation (Ding and Sikka 2006).

The pressure difference between the ocean and the landmass, as well as wind strength and direction, can clearly be seen in Figure 1.3a, b. During the northern boreal summer season, warm and humid air originating from the low latitude oceans migrates north along with the seasonal changes of planetary scale circulations, and is further driven by the east-west pressure gradient in east Asia (An 2000). The strength of the tropical Hadley circulation, which determines the subtropical high in south east China, depends on the sea surface temperatures (SSTs) of the tropical western Pacific which is, in addition to orbital forcing, strongly affected by sea water circulation on a global scale (Schettler et al. 2006). These effects will be discussed later in Section 1.5.2.

The summer rainy season (June, July and August, when the region receives up to 80% of annual precipitation) is closely associated with the retreat of the polar front and the accompanying advance of the summer monsoon of which the most northern position reaches north China and Mongolia in July – August (Zhang and Crowley 1989) (Figure 1.2). The temporal progression and the maximum extension of the summer monsoon front shows a distinct inter-annual variability which strongly affects agricultural production in China (Schettler et al. 2006).

### 1.4.2. The east Asian winter monsoon (EAWM)

In the northern winter season (December, January, February), cold air from high latitudes is controlled by the continental high-pressure system (SH) and propagates southward along the eastern margin of the Tibetan Plateau to form the strongest northerly dry and cold winter monsoon in the world (An 2000). During the winter months, it is these cold winds shifting southward from Siberia, which create favourable conditions for the development or intensification of cyclones and anticyclones resulting in the increase in surface wind speed and the occurrence of dust storms (Liu 1985).

This is demonstrated in Figure 1.3 (c,d). Here 800 hPa wind strength patterns show strong westerly trajectories across Siberia and Mongolia that migrate in a south westerly pattern across northern and eastern China. Indeed, strongest winds are seen in the Siberian region and north eastern region of China (Figure 1.3c). Figure 1.3d displays the sea level pressure (SLP) for the southern Asian region during the winter monsoon months. The SH is clearly defined in this region and the high pressure system to the south of the Tibetan Plateau can also be seen, the latter which deflects the westerlies around it (demonstrated in Figure 1.3c).

### 1.4.3. The Siberian High (SH)

The region of southern Eurasia extends from 35 °N and has two main differing characteristics, with low winter temperatures over most of the continent and a prominent aridity in southern parts (Shahgedanova 2002). Three main factors affect the climate for Russia; its northerly position, size and the arrangement of mountain regions. In winter months the SH develops due to strong radiational cooling of the earth's Northern Hemisphere surface. This is a semi-permanent centre of action dominating eastern and central Siberia between November and March (Figure 1.3c,d). The main position of the SH is over 90 – 110 ºE and 40 – 55 ºN. The presence of the SH ensures that winters remain cold and dry. Indeed, in the Transbaikalia region, only 10% of annual precipitation occurs between November and March, and snow cover is thin (c. 10 – 20 cm) (ibid.). Cold Arctic winds, which form due to the presence of the SH, are directed onto the continent during the winter, which become even colder after contact with the frozen snow covered land surface (Lydolph 1977). Transbaikalia is a region with an ultracontinental climate with extreme seasonal variations in temperature and moderate or small amounts of precipitation. It is the inner Asiatic depression that dominates in summer.

In order to understand the background of natural variability underlying anthropogenic climate change, it is important to analyse records of climate variability in the more recent past (Mayewski et al. 2004). For example Panagiotopoulos et al (2005) have outlined that between 1978 and 2001 there has been a decreasing trend in the SH index. Furthermore, that the teleconnection indices alone are not able to reproduce interannual variability in the SH index and this declining trend. An argument for the decline in the SH is that there is a concomitant decline in sea ice extent in the Arctic Seas associated with the upward trend in the Arctic/North Atlantic Oscillation (AO/NAO) (Desser et al. 2000). Jhun and Lee (2004) state that the SH is more strongly correlated with the AO/NAO than any other teleconnections pattern and that this correlation increases in interdecadal timescales. Todd and Mackay (2003) have also documented a trend to more positive phases of the AO since the mid 1970s, based on ice records from Lake Baikal. Having the ability to place recent climatic changes into the context of longer term variability is of significant importance in being able to establish the effects of anthropogenic forcing (Jones and Mann 2004). Any variation in climate observed over this time frame is likely to be representative of the natural climate variability that might be expected over the present century in the absence of any human influence, as a result of the principal boundary conditions on the climate (e.g. Earth's orbital geometry and global ice masses) not having changed significantly (Jones and Mann, 2004).

Increasingly, attention has been given to analysing high resolution proxy data over the past c. 2 millennia in order to further understand climatic variability on a local scale, to help understand better regional differences in timing, amplitude, duration and intensity of late Holocene climate perturbations. Indeed, while on very long-term time scales the variability of the EASM monsoon is understood (e.g. Tibetan Plateau uplift), over a period of decades to centuries that are much

more relevant to society, variability is less well understood (Black 2002). Evidence of late Holocene climate variability has been well documented in China via historical records (e.g. variations in snow cover anomalies and citrus tree distribution; Chu et al. 2008; Deer 1994 respectively). However due to the limitations of documentary evidence (e.g. user defined, missing data and qualitative interpretations) analysis of high resolution proxy records are of great significance and used in order to investigate climate variability.

## 1.5. Holocene climate forcing with special emphasis on the late Holocene

An understanding of the contemporary dynamics and relationships of the different climate systems of central Eurasia is important to understand how they have changed throughout the Holocene. This is important in order to place recent global warming into context and to provide an understanding of natural climate variability as a baseline for evaluating future climate changes (Jones et al. 1996).

As Imbrie et al (1992) outline, changes in the northern Atlantic region related to ice-sheet dynamics during the Quaternary are thought to control global climate change and that these are transmitted to remote regions via teleconnections. Indeed, in the extratropics, teleconnections link neighbouring regions mainly through the transient behavior of atmospheric planetary-scale waves (ibid.). Such links can be altered by changing boundary conditions forced by solar insolation variability, as well as internal feedbacks of the climate system (e.g. ocean and ice sheet changes) (Adams et al. 1999). Such forcing mechanisms will be discussed later in this section.

Traditionally most palaeoclimate reconstructions over the late glacial and Holocene have focused on neighbouring regions in the north Atlantic, so that well defined climatic events over this period appear synchronous. While there is now an increasing repository of such studies from other regions of the world, including northern Eurasia, there remains an increasing need for high resolution studies. This project attempts to address this issue. Such information is of vital importance in order to investigate further the role of teleconnections for the context of future climate change, a principal rationale behind PAGES Focus 2. Focus 2 has four themes, “Late Glacial”, “Holocene”, “2 Millennia” and “Reconstruction methods”. This project focuses on the “2 Millennia” theme, and in particular the “Asia 2ka” network. This research theme outlines the importance of identifying and understanding those aspects of past climate and environmental change that are of greatest significance for the future of human societies (PAGES-IGBP 2010). Focus 2 has two aims. Firstly, to gain a better understanding of past modes of climate variability and their teleconnections, and of rapid and extreme climate events at the regional scale (particularly in regions where low density data currently exists). Secondly,

to investigate regional scale information that builds the basis for global scale interactive studies with the remaining two foci in the research theme (ibid). Indeed, the late Holocene (e.g. the past 3000 years) is the most appropriate period in which to gauge the natural variability of modern and future climate, as the basic boundary conditions have not changed significantly over this interval.

As this thesis aims to look at environmental variability over the late Holocene (c. 3000 years) for the region of northern Eurasia, an introduction will first be given to the different mechanisms that are argued to be responsible for climatic variability. Bradley (2005) outlined that climate forcing can be considered on several time scales ranging from multi-millennial to interannual, and results from external and internal forcing factors. The IPCC (2007) defines external forcing factors as forcing agents outside of the climate system causing a change in it, for example due to changes in solar activity or orbital variations. Complex internal (within the climate system) negative and/or positive feedback mechanisms amplify these external forcing agents via the relationships of the atmosphere and ocean biosphere (e.g. changes in ocean circulation). The mechanisms by which external and internal climate forcing affects climate change in the study region, through the means of teleconnections are discussed below.

### 1.5.1. External forcing factors

#### 1.5.1.1. Orbital forcing

External forcing by changes in the distribution of insolation associated with orbital changes dominates climate variability on multi-millennial timescales (Jones and Mann, 2004). These orbital changes are described as Milankovitch cycles of which three dominate. Eccentricity occurs on a c. 100,000 and c. 400,000 year cycle, obliquity c. 41,000 year cycle, and precession every c. 19,000 c. 21,000 years. These cycles involve the significant re-distribution of energy both seasonally and latitudinally (Bradley 2005).

Eccentricity affects the amount of isolation that the earth receives. Obliquity and precession affect only the relative distribution of the solar radiation, with implications for the energy transport within the climate system (Beer and van Geel 2008). Reconstructions of insolation during the early Holocene in the northern Hemisphere have shown that it was higher with a decreasing trend (~ 10 %) over the past c. 12,000 years (Figure 1.4c) (Bradley 2005). At the onset of the Holocene interglacial, perihelion (the point of orbit nearest to the sun) was in July and northern hemisphere summer insolation was at its most recent maximum. Today however, the high northern latitudes receive less summer insolation and the discrepancy between this and the warm climate conditions in the north question why we are still in an interglacial (e.g. Broecker 1998; Müller and Pross 2007). Müller and Pross (2007) argue that the reason is a result of the c. 400,000 year envelope of the eccentricity of the earth's orbit that the influence of precession on insolation today is muted and most similar to the situation around 400,000 years

before present (BP) (the present day analogue of Marine Isotope Stage 11; MIS 11) (Loutre and Berger 2003). Figure 1.4 clearly shows that MIS 11 and the present day are analogous because of low eccentricity and similar phasing of precession, while insolation for the two periods differ significantly (Loutre and Berger, Crucifix 2008; 2003). All of the major climatic boundary conditions during the previous interglacials were similar to those found today: the major ice sheets had melted, sea level was high, boreal vegetation was in an interglacial state, tropical monsoon vegetation was in retreat, and insolation trends were similar (especially during MIS 11) (Ruddiman 2005). Ruddiman (2005) argues that the main difference between MIS 11 (and indeed MIS 5,7 and 9) and the present interglacial is that $CO_2$ and $CH_4$ have risen in the middle and late Holocene when they had previously always fallen, and that in fact, for those interglacials with stronger insolation forcing than the Holocene, the predicted $CO_2$ increases would probably be even larger than the Holocene rise. It is argued that this discrepancy is attributable to the onset of agriculture. Tzedakis (2010) also argue that the divergence between atmospheric methane concentrations and temperate tree populations in the late Holocene would appear to favour the view of Ruddiman (2003, 2007) that the $CH_4$ rise after 5 kyr BP reflects anthropogenic emissions. In addition, an assessment of the vegetation trends in MIS 1 and MIS 11 favours a precessional alignment of the two interglacials, which would support the notion that in the absence of anthropogenic interference, the Holocene should be nearing its natural completion.

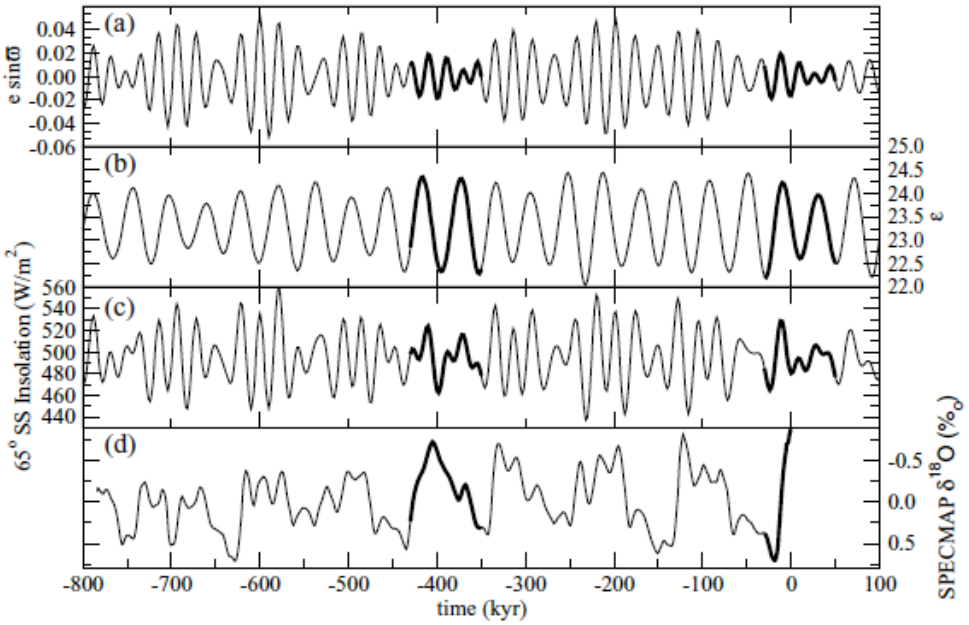


*Figure 1.4. Long term variations of (a) the climatic precession parameter, (b) obliquity, (c) summer solstice insolation at 65°N, and (d) ice volume reconstructed by Imbrie et al. (1984) Time zero corresponds to year 1950 AD. Portions corresponding to the periods [−430 to −350 kyr] and [−30 to +50 kyr] are in bold. (Figure from Crucifix et al. 2006).*

A general pattern of early to mid-Holocene warm conditions followed by neoglacial cooling is recognised throughout the Arctic areas of the North Atlantic (e.g. Jennings et al. 2002; Nesje and Dahl 1993; Wiiliams et al. 1995). Indeed, the neoglacial cooling period (after c. 6000 years BP), following from the Holocene optimum (between c. 8000 – 6000) is also argued to be a result of changes in solar insolation (Jennings et al. 2002; Wanner et al. 2008). In particular, Jennings (2002) argue that evidence for neoglacial cooling in North Atlantic sediments can be seen from an increase in ice rafted debris (IRD) which became pervasive after c. 6000 BP (Andrews et al. 1995; Andrews et al. 1997; Bond et al. 2001; Bond et al. 1997). They continue to argue that this evidence suggests an increase in sea-ice expansion in the north Atlantic during this time, as result of changes in atmospheric circulation patterns, driven by solar variability. The decreased trend in solar insolation forced the initiation of neoglacial cooling until a critical threshold was reached when internal mechanisms also became important in enhancing this trend e.g. changes in atmospheric circulation patterns like the North Atlantic Oscillation index (Andrews et al. 1997).

Changes in energy distribution as a result of variations in insolation are manifested through complex internal feedback mechanisms and ultimately climate, discussed below. Orbital parameters act as an important backdrop for such feedback mechanisms. Jones and Mann (2004) describe that orbital forcing is thought to act at too long timescales to be responsible for climate fluctuations limited to the late Holocene, therefore forcings that act on shorter timescales are most likely to represent the dominant forcings of climate variability. In the context of the late Holocene it is important to remember that orbital boundary conditions have not changed dramatically (in comparison to longer glacial-interglacial timescales) (Wanner et al. 2008).

#### 1.5.1.2. Solar forcing

The Sun is a variable star showing considerable cyclic changes in its magnetic activity, as expressed for example in the sunspot number (Beer and van Geel 2008). While orbital forcing involves the redistribution of solar energy, which may have differential affects on climate in the northern and southern hemispheres, changes in solar irradiance might be expected to affect all parts of the earth equally (Bradley 2005). There are many known cycles in solar activity, including the 11 year Schwabe, 22 year Hale, 88 year Geisberg, 211 year Suess and ~ 2200 year Hallstattzet cycles. The impacts of decadal to centennial scale solar variability on the climate system during the Holocene have been reported from mid to high northern latitudes to low latitude regimes including the EASM (Wang et al. 2005).

The total solar constant or total solar irradiance (TSI) is in phase with the magnetic activity of the sun (Beer and van Geel 2008). The TSI, that is integrated over all wave lengths, has been shown to vary by c. 0.08% over a Schwabe cycle with maximum values at times of maximum

solar activity (Bradley 2005). However, Lean (2000) argues that irradiance over short wavelengths (e.g. ultraviolet; UV) vary even more over a cycle. Changes in UV (the spectral solar irradiance; SSI) strongly influence the photochemistry in the upper atmosphere and in particular ozone concentrations. Haigh and Blackburn (2006) show that through dynamical coupling SSI can cause shifts in the tropospheric circulation systems and therefore a change in climate. As such, if irradiance changes in the past were greater and more persistent than solar cycle variability, the effects may have been quite significant (Bradley 2005).

TSI is thought to have ranged by c. 0.24% from the time of minimal solar variability at the end of the 17$^{th}$ Century (associated with the Maunder Minimum c. 1645-1715 AD; the coldest part of the "Little Ice Age"; LIA) to the present (the mean of the most recent solar cycle) (Bradley 2005). Indeed, the 70 year period which is known as the Maunder Minimum was a period of very little solar activity and may have accounted for the period of cold climate. Lean et al (1995) argue that a reduction in TSI of c. 0.24% was associated with a fall in mean annual temperature over the northern Hemisphere of 0.2-0.4$^{o}$C.

Beyond the period of historical records of solar activity, long term changes can be estimated from cosmogenic isotopes preserved in natural archives ($^{10}$Be and $^{14}$C). A clear link between solar activity and solar forcing based on physical processes is still missing, with direct observations of solar activity restricted to the period of the invention of the telescope (c. 1610 AD) (Wanner et al. 2008). During the last millennium, $^{10}$Be and $^{14}$C indicate that solar activity was high from c. 1100-1250 AD (coincident with the Medieval Warm Period; MWP), decreased to minima in the 15$^{th}$ (The Spörer Minimum) and the end of 17$^{th}$ Century, increasing once again in the 20$^{th}$ Century. Indeed, deviations of $^{14}$C from background levels reveal a large number of solar activity anomalies comparable to the Maunder Minimum as well as episodes of enhanced solar activity throughout the Holocene (Bradley 2005). Wanner et al (2008) argue that a characteristic feature of solar forcing is the occurrence of century-scale minima, corresponding to the so-called grand solar minima for example the Spörer Minimum. Indeed, power spectra of the solar activity conducted by Wanner et al (2008) agree well with previous spectral estimates of centennial-scale solar variability (e.g. Clemens 2005) including the distinct peaks at 208 and 87 years corresponding to the well known Suess and Gleissberg cycles. However, solar irradiance changes cannot alone explain the concurrent global warming (Wanner et al. 2008).

#### 1.5.1.3. Volcanic forcing

It is well established that volcanic eruptions can have a short term cooling effect on overall hemispheric or global mean temperatures. This is a result of direct radiative effects with volcanic aerosol reducing energy receipts at the surface, plus associated circulation changes that may result from such effects (Bradley 2005). If eruptions were more frequent in the past, or if they happened to occur in clusters of events, it is possible that the cumulative effect of

eruptions could have persisted for longer, resulting in decadal to multi-decadal scale impacts. What is more, that such effects would be enhanced if the initial cooling led to feedbacks within the climate system e.g. more persistant snow and sea ice cover, which would in turn raise surface albedo and alter atmospheric circulation (*ibid.*).

Sulphate aerosol forcing (from volcanic eruptions) results in cooling of most of the globe, with greater cooling in the northern hemisphere (NH) due to its higher aerosol loading (IPCC 2007). Volcanic sulphur dioxide emissions ejected into the stratosphere form sulphate aerosols, lead to a forcing that causes a surface and tropospheric cooling and a stratospheric warming that peak several months after a volcanic eruption and last for several years (ibid.). Volcanic forcing also likely leads to a response in the atmospheric circulation (e.g. changes in NAO) in boreal winter and a reduction in land precipitation (Broccoli 2003; Gillett et al. 2004; Robock and Liu 1994).

Records of sulphate from ice core records have been used to reconstruct volcanic activity over the Holocene. Zielinski (1994) argue that there were periods of more frequent volcanic events in the past, such as between 9500-11500 calibrated (cal) years BP. Evidence suggests that over the past 6000 years, a number of large “bipolar” tropical eruptions have been observed in both hemispheres and may represent large tropical eruptions affecting global climate (Crowley and Vinther In preparation). However their distribution over time varies. No fewer than 12 strong eruptions have been observed during the last 850 years with a large number of events during the LIA, with the 1256 AD event likely the strongest during the six millennia (Wanner et al. 2008). Shindell et al (2001) argue that cold conditions associated with the Maunder Minimum also coincide with an episode of exceptionally active explosive volcanism. Indeed, Salzer and Hughes (2007) have outlined how over the last millennium, the agreement between tree ring data and ice core data is high, with years of ring width minima matched with known volcanic eruptions or ice-core volcanic signals in 86% of cases. Over recent centuries it is suggested that explosive volcanism has contributed to the natural variability of hemispheric and global mean temperatures (e.g. Ammann et al. 2003a; Crowley 2000). Ammann and Naveau (2003b) suggested that the tropical explosive volcanic eruptions during the last 600 years followed a 60 year cycle, although there is no known mechanism for a cyclic behaviour of large volcanic eruptions (Wanner et al. 2008).

### 1.5.2. Internal forcing factors

#### 1.5.2.1. Variations in oceanic circulation

The thermohaline circulation (THC) has a very strong affect upon global atmospheric circulation patterns. As Figure 1.5 shows, warm, low saline surface currents of the north Atlantic are transferred north from the tropics to the northern latitudes where heat is released. This heat release gives off large amounts of energy. Following this, the water is cooled and salinity increases, water sinks to form north Atlantic deep water (NADW) and is transported back south

to the tropics before upwelling in the Pacific, becoming warmer and fresher. The outflowing undersea of cold and salty water from the Atlantic (Figure 1.5) makes the sea level (salinity) of the Atlantic slightly lower (higher) than the Pacific. The warmer fresher water from the Pacific flows up through the South Atlantic to Greenland, where it cools again (evaporative cooling) and sinks to the ocean floor providing a continuous thermohaline circulation (Gnanadesikan et al. 2005). The role of the Atlantic and Pacific oceans will be discussed further in Section 1.6 in relation to the modes of climate variability associated with them (e.g. North Atlantic Oscillation and El Nino Southern Oscillation respectively).

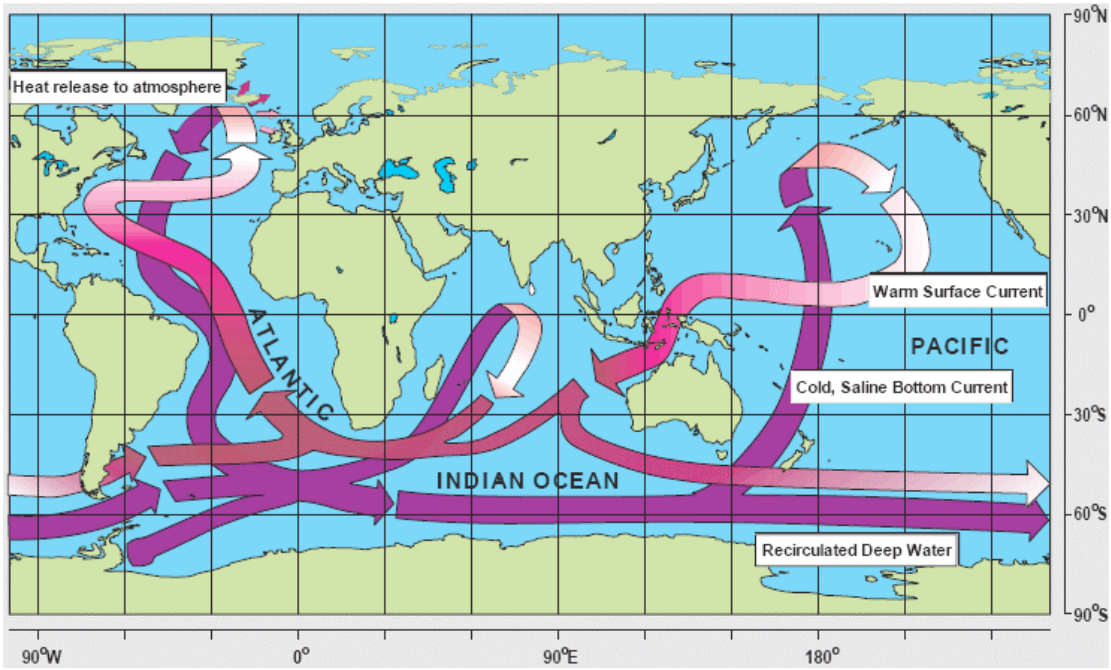


*Figure 1.5 Dominant currents of the oceans of the world. (From Russell, unpublished).*

The THC over the course of the Holocene has demonstrated considerable variation. The THC is the part of the ocean which is driven by density differences (Rahmstorf 2003), linked to the salinity and temperature differences which arise from heating/cooling at the surface and from the surface freshwater fluxes. For example, freshwater inputs into the north Atlantic are argued to reduce the density of the surface waters in the north Atlantic, lower salinity in the deep water formation area reduces the circulation and the circulation in turn transports lower salinity waters into the deep water formation regions (ibid.). These processes lead to a subsequent global cooling via teleconnections to weather systems. These freshwater inputs in the late Holocene result from the calving of ice sheets into the north Atlantic e.g. the attributable factor of Bond events (Bond et al, 1993). Bond et al (1997) outline that during the last glacial the pacing of Ice-Raft Debris (IRD) events in sediments of the north Atlantic and of abrupt climate shifts (e.g. changes in atmospheric circulation above Greenland) are statistically the same and follow a cyclicity close to 1470 +/- 500 years.

During the Holocene, such IRD events in sediments are therefore the most recent manifestation of these pervasive millennial scale climate cycles, which operate independently of the glacial-interglacial climate state (Bond et al, 1997). Later evidence states that surface winds and surface ocean hydrography in the sub-polar north Atlantic are influenced by variations in solar output throughout the entire Holocene, with such a solar forcing mechanism underlying at least the "1500 year" cycle present during the Holocene (Bond et al. 2001). As will be later outlined in section 1.7, during the Holocene it is argued that there are eight cooling events associated with changes in THC following IRD events, and that these occur on a c. 1500 year cycle (Bond and Lotti 1995; Bond et al. 1997). Solar activity is argued to be the attributable factor for this cycle and subsequently the IRD events. If solar activity is the main driver for changes in IRD, it is argued that the impact this freshwater input has on THC amplifies any climate change through teleconnection dynamics (Bond et al. 2001). Over the past 3000 years there is a distinct pacing of IRD events (based on increased deposition of Hematite stained grains in ocean sediment cores) on millennial scales, with peaks at c. 2800, 1400 and 500 cal years BP (Bond et al. 1997). These are known as Bond events 2,1 and 0 respectively.

The demise of the Laurentide Ice-Sheet (LIS) occurred after 6000 calendar years before present (cal years BP) and as a result changed the nature of freshwater inputs to the north Atantic (e.g. from ice sheets being the most dominant source to precipitation and glacier calving dominating). This changed the previous freshwater routing so that even at present it flows from the Arctic Ocean through the Fram Strait and the Canadian Arctic Archipelago, where it affects connective activity and hence the climate of the north Atlantic regions (Kaplan and Wolfe 2006). Within the context of the last c. 3000 years BP, the most recent Holocene cold event has been the LIA (concomitant with Bond event 0). Indeed, Broeker et al (1999) suggest that an oscillation in NADW formation led to a reduction of poleward heat transport with opposite conditions prevailing in the MWP (Cronin et al. 2003). More recent work by Seidenkrantz et al (2007; 2008) from c. 2000 to 1000 cal years BP, corresponding to the end of the "Roman Warm Period" the area of the Labrador Seas studied experienced stronger influx of Atlantic water and an increased fresh-water flux from land, probably related to increasing precipitation or to melt-water outflow from nearby inland ice. Furthermore, that during the "Dark Ages" (1500 to 1300 cal years BP) there was only a minor cooling of surface waters, while during the LIA (after 900 cal years BP) the area experienced a minor increase in sea-ice cover until c. 500 cal years BP after which it increased once again (ibid.). Cronin (2003) outlines that the NAO is also a major source of multi-decadal wintertime NH climate variability that has been associated with changes in the north Atlantic THC and therefore may have played a role during the MWP and LIA (Dickinson et al. 1996).

#### 1.5.2.2. Internal forcing of greenhouse gases

Greenhouse gas (GHG) concentrations are available from instrumental measurements back through the mid 20$^{th}$ century, and prior to that time they can be estimated from the relevant

trace gas concentrations (e.g. $CO_2$, $CH_4$, $N_2O$) trapped as bubbles in ice cores (Jones and Mann, 2004). Since the start of the Industrial Revolution the concentration of these gasses has shown a near exponential increase due to the burning of fossil fuels. For example, it is estimated that $CO_2$ concentrations have increased from c. 280 ppm (parts per million) during the pre-industrial period of the 18$^{th}$ century, to c. 379 ppm in 2005 (IPCC 2007).

As with solar radiative forcing, well mixed GHG within the atmosphere also act as a global radiative forcing, by affecting the balance between incoming and outgoing radiation at the top of the troposphere by trapping part of the outgoing infrared radiation (Reynaud et al. 2000). Unlike solar radiation, GHG concentrations can represent both a response to and a cause of climate variability, complicating the use of longer term GHG concentrations as a pure forcing of climate (Jones and Mann, 2004). Atmospheric $CO_2$ concentration increased by only 20 ppm over the c. 8000 years prior to industrialisation and multi-decadal to centennial-scale variations were less than 10 ppm and most likely due to natural processes (IPCC 2007) Both $CO_2$ and $CH_4$ show a generally positive trend over the last c. 6000 years, although a major increase in $CH_4$ is observed after only c. 3000 years, while $CO_2$ increases over the entire period (Wanner et al. 2008).

There are several competing hypotheses that have been put forward to explain the millennial trend in $CO_2$ (e.g. Broecker 2001; Indermuhle et al. 1999; Ridgwell et al. 2003; Ruddiman 2003). It is argued that prior to the Industrial Period, variations in the concentration of $CO_2$ and $CH_4$, rather than representing a forcing on temperature changes, instead reflected alterations in terrestrial carbon uptake due to temperature changes (Gerber et al. 2003; Jones and Mann, 2004). Wanner et al (2008) argue that a range of factors most likely contributed to the 20 ppmv $CO_2$ rise between c. 8000 cal years BP and the pre-Industrial Period including ocean calcite compensation, sea surface temperatures, coral reef build up and to a minor extent carbon uptake and release through changes in the terrestrial biosphere (e.g. Joos et al. 2004). They continue to outline that the low $CH_4$ concentrations in the mid Holocene were believed to be caused by gradual dessication in parts of the tropics (e.g. the Sahara and Sahel), and that the development of boreal wetlands are considered to be at least partly responsible for the $CH_4$ increases observed after c. 5000 cal years BP. This latter mechanism has been disputed as records of peatland development do not support a high northern Hemisphere origin of the observed $CH_4$ increase (MacDonald et al. 2006). Other literature has attributed this increase to early Holocene activity, e.g. through the advent of rice cultivation (Ruddiman and Thomson 2001). The range of $N_2O$ sources (oceanic and terrestrial) defies a simple interpretation of the record and a combination of additional measurements and modelling efforts is still required to understand the $N_2O$ evolution in the Holocene (Wanner et al. 2008).

A total direct aerosol radiative forcing (for example from biomass burning) was published for the first time in 2007 (IPCC 2007) stating that the total combined forcing, across all aerosol types, is

−0.5 ± 0.4 W $m^{-2}$. For biomass burning aerosols, the estimated direct radiative forcing is now revised from being negative to near zero due to the estimate being strongly influenced by the occurrence of these aerosols over clouds (ibid.). Between the mid-Holocene and the end of the pre-industrial period (c. 1750 AD) substantial anthropogenically driven land cover changes took place in temperate and subtropical Eurasia (Wanner et al. 2008). Evidence suggests that already in the early Holocene deforestation was recorded in the Middle East concurrent with the origin of Neolithic societies and by c. 6000 BP substantial Neolithic deforestation was recorded in Europe and southern and eastern Asia (ibid; Bar-Yosef 1998; Kirch 2005). The BIOME4 global vegetation model and the HYDE anthropogenic land use data set indicate that up to 2.5 x $10^6$ km of temperate and tropical forests had already been converted to cropland and pastures by 1700 AD (Kaplan et al. 2003; Klein Goldewijk and Ramankutty 2004) and Matthews et al (2004) argue that this may have affected climate globally.

## 1.6. Modes of climatic variability

As discussed above it is clear that there is a distinct relationship between the climate systems of central and southern Asia and southern Siberia. As displayed on Figure 1.3 (a-d) the climate of central Eurasia is dominated by the position of the SH, westerly jet streams and the summer and winter monsoons (Dodson and Liu 1995). However, there are a number of other mechanisms responsible for this complex relationship.

The mechanisms of climate in central Asia (the Westerlies, SH and EASM) have already been outlined in Section 1.4. This section will therefore discuss the effects of atmospheric indices upon them. The north Atlantic oscillation (NAO) and Arctic oscillation (AO) are the dominant patterns of atmospheric variability in the northern Hemisphere. Both the NAO and AO are regarded as related phenomena and generate much of the inter-annual and decadal variability in winter climate over Europe and the north Atlantic (Hurrell 1996; Jones and Briffa 2001). El Niño Southern Oscillation plays an important role of variability in SST of the Pacific ocean, which in turn have an affect upon EASM intensity via teleconnective mechanisms. As such it too will be discussed here.

### 1.6.1. The North Atlantic Oscillation (NAO)

The NAO has both positive and negative phases, which refer to the measured difference in sea-level pressure between the Azores and Iceland. When in a positive phase (high values) there is a mutual strengthening of the Icelandic low (65$^o$N) and Azores high (40$^o$N), so that south-westerly flow over Europe and north-western Asia is strong and displaced northwards and there are higher than normal temperatures in the north (Figure 1.6a; Hurrell 1996; Shahgedanova 2002). These winds bring enhanced moisture to higher latitudes, while the southern regions

(e.g. Turkey and Middle East) remain drier and colder (Cullen and deMenocal 2000). With a positive NAO strong positive temperature advection is seen and surface air temperature anomalies occur in central and northern Eurasia, including the Lake Baikal region, resulting in reduced ice cover and thickness (Todd and Mackay, 2003). The NAO has a strong influence upon snow cover depth over Eurasia, with the positive mode resulting in warmer temperatures, increased precipitation and therefore snow depth (Clark et al. 1999). Thompson and Wallace (2001) also outline that at the daily timescale there is a decrease in blocking events over northern Russia and a consequent decrease in cold air outbreaks over east Asia during the NAO/AO positive phase.

The NAO can have an impact on the location of the Westerlies and therefore the location of the SH, thereby affecting the northward extent of the EASM. During the negative phase of the NAO (Figure 1.6b) the relationships discussed above are reversed. In this case, the strength of the westerly jet flow decreases across northern Europe resulting in potentially much colder and drier conditions across these regions (Hurrell 1996). As discussed above, the extent of Eurasian snow cover, associated with the positive mode of the NAO, can have an impact on the penetration of the EASM monsoon. Due to the interplay between the EASM and surface albedo, high Eurasian snow cover can have a delayed affect upon the onset and penetration of the monsoon. This is due to the reduced solar radiation absorption of snow's high albedo and consummation of solar energy via snow melt and evaporation (Ye and Bao 2005).

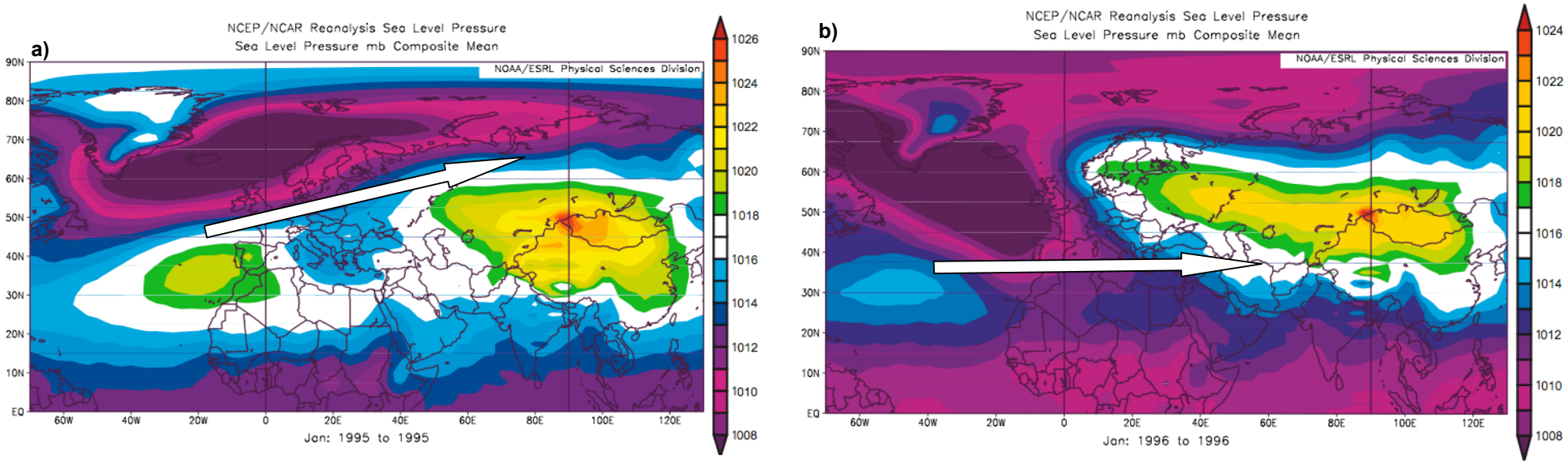


*Figure 1.6. Positive (left panel; a) and negative (right panel; b) phases of the NAO. Arrows show the migration in moisture and wind transport during the different phases. Measurements in sea level pressure (mb composite mean). Image created 3/11/2009 and provided by the NOAA-CIRES (2010) Climate Diagnostics Center, Boulder Colorado (http://www.cdc.noaa.gov/).*

The NAO may have played a prominent role in cold season extratropical northern hemisphere temperature changes in past centuries, potentially explaining (through a tendency for the negative phase), the enhanced regional winter cooling during the 17th Century (e.g. LIA) in Europe (Jones and Mann, 2004; Shindell et al. 2001). Wanner et al (2008) state the NAO dynamics are not very well understood in terms of Holocene NAO reconstruction or modelling. There is evidence that the NAO played a role in generating millennial scale SST trends in that the positive (negative) phase was accompanied by relatively mild (cold) winters over the northern Europe and a relatively cold (warm) climate over eastern Mediterranean and the middle East (Rimbu et al. 2003). Furthermore, Wanner (2008) continue to describe that based on this data the NAO index was likely subject to a trend from negative to positive values in the mid Holocene to negative ones in the late Holocene. However, Gladstone et al (2005) warn against jumping to conclusions about the role of the NAO in Holocene climate change, where results of PIMP2 model simulations suggest that there are only minor differences in NAO characteristics between the mid Holocene and pre-industrial climates and some tendency to more positive average NAO index during the mid Holocene.

### 1.6.2. El Niño-Southern Oscillation (ENSO)

The factors and processes that may produce changes in the Asian monsoons include fluctuations in the heating effect of the Tibetan Plateau, variations in snow cover on the European-Asian continent and the extent of the polar ice sheet, the thermal conditions of the Equatorial Pacific and Indian Oceans, changes in the West Pacific sub-tropical high, pressure and circulation and in the climatic state of the north Pacific Ocean, and in variations in solar radiation or volcanic activity. Shahgedanova (2002) describes that there is an increasing body of evidence pointing at the complex feedbacks between Eurasian surface processes, summer monsoon and sea surface temperature (SST) anomalies in which Eurasian snow cover and the monsoon play an active role as opposed to being controlled by El Niño-Southern Oscillation (ENSO) events that have been so far seen as pacemakers of interannual climate variability.

ENSO can be defined as coupled interannual (3 to 7 years) SST anomalies in the eastern tropical Pacific (Folland et al. 2002). Indeed, Diaz et al (2001) describes ENSO phenomenon as the most important branch of internal variability of the global climate system. Warm phases, known as El Niño are characterised by weakening of both trade winds and ocean upwelling and coincident increases in SSTs (ibid.). Changes between periods of El Niño and La Niña (the cold phases with opposite effect) have been shown to have large impacts upon the EASM. The mature phase of ENSO often occurs in boreal winter and is normally accompanied by a weaker than normal winter monsoon along the east Asian coast (Wang et al. 2001). Consequently, the climate in south-eastern China and Korea is warmer and wetter than normal during ENSO winter and the ensuing spring (ibid.). Wang et al (2003) found that an elongated anticyclonic ridge extending from the western Maritime Continent of the Indian Ocean to the Indian

subcontinent during the summer El Niño development leads to abnormal Westerlies creating frequent tropical storms on the West Pacific Ocean adjacent to Asia. Therefore, during the period from development to decay of an El Niño event, precipitation in the East Asian sector may be enhanced through frequent tropical storm activity in the West Pacific, a strengthening monsoon in the South China Sea and in particular, through increasing rainfall associated with the East Asian sub-tropical front (ibid).

Model simulations have shown the response of ENSO to solar and volcanic forcing and indicate a counterintuitive tendency towards El Niño conditions in response to negative radiative forcing (e.g. decrease in solar activity or increased volcanic activity) and a tendency for La Niña-like conditions in response to positive radiative forcing (Goosse et al. 2006; Mann et al. 2005). Evidence from tropical Pacific coral records has also supported this notion (Cobb et al. 2003). Furthermore, Adams (2003) also suggest that this relationship would potentially explain why evidence suggests that the tropical Pacific shows an El Niño phase during the LIA and La Niña phase during the MWP.

Bing et al (2006) argue that there may be similar interconnections between the Asian monsoon, ENSO and the north Atlantic Ocean climate during the c. 4000 and c. 8200 events both of which manifest as a reduction in EASM intensity. While for the c. “8.2 ka” event, reorganisation of the THC due to freshwater forcing is attributed as a main forcing factor (See Section 1.5.2), the same cannot be said for the c. 4000 event due to the different boundary conditions at the time. Bing et al (2006) therefore argue that a catastrophic fresh water input to the north Atlantic or an increase in drift ice caused by solar output would result in the reduction of the north Atlantic THC. The consequential events would contribute to an occurrence of the El Niño-like pattern in the tropical Pacific and the inverse phase variations on the EASM at c. 4000 years BP.

## 1.7. Holocene climate variability in northern Eurasia

As outlined in Section 1.3, according to PAGES Focus 2, there is an increasing need for high resolution regional climate reconstructions from current low density data regions of the world, in particular eastern Eurasia and covering the past c. 2000 years. Indeed, decadal to centennial scale variations in monsoonal precipitation, forced by solar activity and their relation with the north Atlantic climate have been described by many authors (Gupta et al. 2003a; Gupta et al. 2005; Liu et al. 2009; Wang et al. 2005; Wang et al. 2008). However, Liu et al (2009) argue that little information exists about decadal to centennial scale variations in the EASM and Westerlies. Chen et al (2008) also argue that Holocene climate patterns in arid regions of central Asia are poorly documented, a result of the complex interplay of competing forcing factors controlling regional climate: orographic influences of the Tibetan Plateau, low latitude

summer monsoonal circulation and the mid latitude westerlies. This project aims to address these issues through the use of lake sediment reconstructions, due to the absence of other high resolution proxy archives within the specific research regions of northern Eurasia discussed in this project (e.g. speleothems and ice cores). Furthermore, as Focus 2 states, the need for regional climate reconstructions is important in feeding into an integrative global scale interpretation, as such ocean sediments are inappropriate as they provide a more hemispheric reconstruction of climate.

Evidence shows that many lakes in northern Eurasia experienced maximum effective moisture between 8000 and 4000 years BP (Chen et al. 2008). Importantly the authors outline two distinctive regions of northern Eurasia, firstly monsoonal Asia which is that affected directly by precipitation derived from the EASM (e.g. Lake Xiaolongwan in this project) and the second is Arid Central Asia (ACA) which is dependent upon Westerlies for moisture transport in summer months (e.g. Lake Arachlei in this project) (Figure 1.2). The synthesis indicates that proxy records of EASM intensity (including speleothems, peat records, lake and ocean sediments) all show a strong monsoon, with high precipitation, during the early and mid Holocene (c. 11,000 to 5000 years BP) (Chen et al. 2008). They further argue that this general trend in the history of the monsoon in Asia during the Holocene is related to changes in solar insolation at low latitudes, with strong summer insolation in the early Holocene inducing strong land-ocean pressure and temperature gradients and therefore enhanced moisture flow. However, Chen et al (2008) outline that precipitation in regions of ACA depend mainly on the amount of water vapour transported by mid-latitude Westerlies from the north Atlantic Ocean, as well as inland seas and lakes along the westerly cyclonic storm tracks (Bohner 2006). As discussed in Section 1.4 the teleconnections across these regions are complex. When summer monsoon intensity is greater (e.g. the early Holocene) Chen et al (2008) argue that cold north Atlantic surfaces prevail (e.g. freshwater forcing) causing reduced evaporation, and that cold inland temperature conditions in the ACA region lead to weak cyclonic activity. In other words, increased winter SH intensity and a reduction in summer precipitation provided by Westerlies occurs (See Section 1.4).

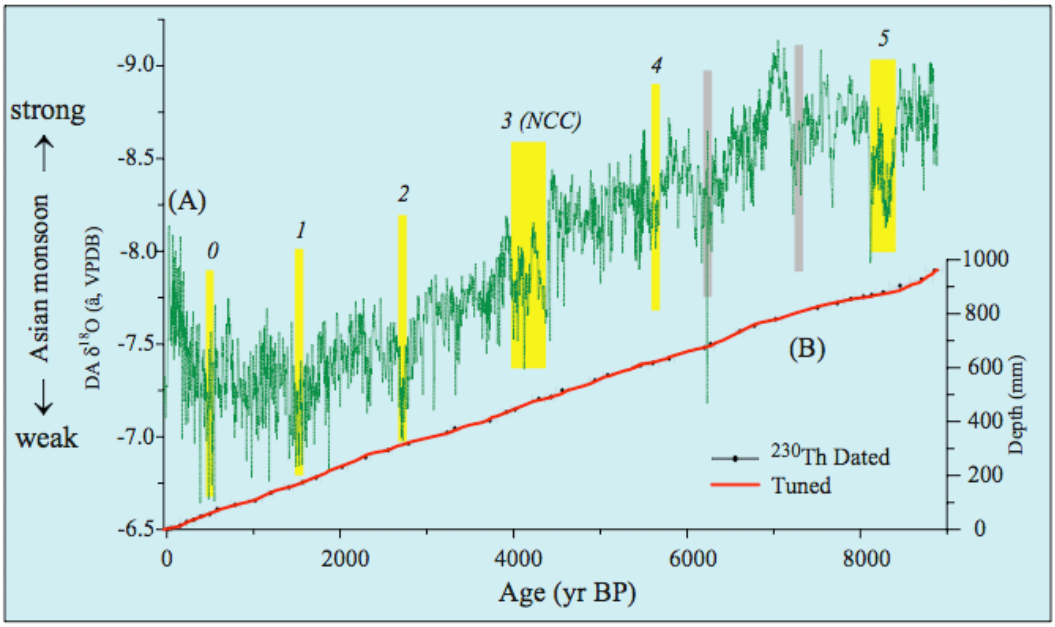


*Figure 1.7 (A) The Dongge Cave speleothem $\delta^{18}O$ record. Yellow bars correspond to IRD events corresponding to Bond et al (1997; 2001) in particular (3) is also coincident with other literature on the fall in Neolithic Chinese Culture and (5) the meltwater outburst from the Laurentide ice sheet ("8.2 event"). The two grey bars also correspond to weak EASM events that coincide with IRD events. Image from Wang et al (2005).*

The trend to declining monsoonal intensity after c. 5000 years BP follows the declining trend in solar insolation (Section 1.5.1). In the regions outside of the monsoonal boundary (ACA) an opposite trend is seen where effective moisture was lowest in the early Holocene, highest in the mid Holocene (c. 8000 to 5000 years BP) and lower again in the late Holocene (although greater than the early part of the Holocene) (ibid.). Marine records from the South China Sea have identified millennial-scale variations in the EASM, with significant changes in sea surface temperatures (a proxy for EASM intensity) at 775, 102 and 84 years (Gupta and Thomas 2003b; Holmes et al. 2009; Wang et al. 2001). As Figure 1.7 demonstrates, there is a total of 8 periods of weakened EASM intensity during the Holocene, at 8300, 7200, 6300, 5500, 4400, 2800, 1400 and 500 years BP, with five of these corresponding with north Atlantic events (Bond events) (Bond et al. 2001; Bond et al. 1997; Wang et al. 2005; Wang et al. 2008) (Figure 1.7). Long, continuous sequences from continental regions of northern Eurasia (e.g. Lakes Hovsgol and Baikal) have also noted centennial cooling events during the early to late Holocene, associated with millennial-scale cycles (e.g. Mackay 2007; Prokopenko et al. 2007). Similarly, peat records from north east China have also identified synchronous climate anomalies with the north Atlantic, with the most significant $\delta^{18}O$ peak seen at the same time as north Atlantic evidence of reductions in temperature (related to reduced solar activity between c. 8220 cal yrs BP) and freshwater forcing associated with the "8200" event (Hong et al. 2009). $\delta^{18}O$ records from speleothems from the caves Lianhua and Dongge (see Figure 1.2) have shown an overall increasing trend (coincident with trends in solar insolation) suggesting a weakening in summer

monsoonal circulation in response to diminishing insolation and a southward shift in the ICTZ (Cosford et al. 2008; Wang et al. 2005). The major excursions seen at c. 6100, 4000, 3300-3100, and 200 years BP, further corroborate those seen in regions of the north Atlantic (Cosford et al. 2008; Mayewski et al. 2004). Cosford et al (2008) continue to outline that these excursions in eastern Chinese record, are characterised by a strengthened SH system and enhanced winter monsoon circulation (Mayewski et al. 1997), drier tropical conditions (Haug et al. 2001) and increased ice-rafting in the north Atlantic (Bond et al. 2001). This emphasises the importance of teleconnections between the north Atlantic, the Pacific and across northern Eurasia. Evidence of a drier late Holocene is also seen in regions of Mongolia at Ugii Nuur basin after c. 4000 years BP, until c. 2800 years BP (Schwanghart et al. 2008; Schwanghart et al. 2009). This project aims to address this last point further, by looking at the climate variability at sites located in southern Siberia (affected by SH and Westerlies) and NE China (affected by the EASM and SH intensity), within the context of changes in these larger teleconnections over the late Holocene (north Atlantic and Pacific oceans).

## References

Adams J., Maslin M. and Thomas E. 1999. Sudden climate transitions during the Quaternary. Progress in Physical Geography 23: 1-36.

Adams J.B., Mann M.E. and Amman C.M. 2003. Proxy evidence for an El Nino like response to volcanic forcing. Nature 426: 274-278.

Ammann C.M., Meehl G.A., Washington W.M. and Zender C. 2003a. A monthly and latitudinally varying volcanic forcing dataset in simulations of 20th Century climate. Geophysical Research Letters 30: 1657.

Ammann C.M. and Naveau P. 2003b. Statistical analysis of tropical explosive volcanism occurences over the last 6 centuries. Geophysical Research Letters 30: 1210.

An Z. 2000. The history and variability of the East Asian paleomonsoon climate. Quaternary Science Reviews 19: 171-187.

Andrews J.T., Jennings A.E., Kerwin M., Kirby M., Manley W., Miller G.H., Bond G. and Maclean B. 1995. A Heinrich-Like Event, H-0 (Dc-0) - Source(S) for Detrital Carbonate in the North-Atlantic during the Younger Dryas Chronozone. Paleoceanography 10: 943-952.

Andrews J.T., Smith L.M., Preston R., Cooper T. and Jennings A.E. 1997. Spatial and temporal patterns of iceberg rafting (IRD) along the East Greenland margin, ca 68$^{o}$N, over the last 14 cal ka. Journal of Quaternary Science 12: 1-13.

Bar-Yosef O. 1998. The Natufian culture in the levant, threshold to the origins of agriculture. Evolutionary Athropology 6: 159-177.

Beer J. and van Geel B. 2008. Holocene climate change and the evidence of solar and other forcings. In: R. W. Battarbee and H. A. Binney (eds.), Natural Climate Variability and Global Warming. Blackwell Publishing, London, pp. 138-162.

Bing H., Quinghua L. and Yetang H. 2006. Interconnections between the Asian monsoon, ENSO and high northern latitude climate during the Holocene. Chinese Science Bulletin 51: 2169-2177.

Black D.E. 2002. The rains may be a-comin'. Science 297: 528-529.

Bohner J. 2006. General climatic controls and topoclimatic variations in Central and High Asia. Boreas 35: 279-295.

Bond G., Kromer B., Beer J., Muscheler R., Evans M.N., Showers W., Hoffmann S., Lotti-Bond R., Hajdas I. and Bonani G. 2001. Persistent solar influence on north Atlantic climate during the Holocene. Science 294: 2130-2136.

Bond G. and Lotti R. 1995. Iceberg discharges into the North Atlantic on millennial time scales during the last glaciation. Science 267: 1005-1010.

Bond G., Showers W., Cheseby M., Lotti R., Almasi P., deMenocal P., Priore P., Cullen H., Hajdas I. and Bonani G. 1997. A pervasive millennial-scale cycle in North Atlantic Holocene and glacial climates. Science 278: 1257-1266.

Bradley R.S. 2005. Climate forcing during the Holocene. In: A. W. Mackay, R. W. Battarbee, H. J. B. Birks and F. Oldfield (eds.), Global Change in the Holocene. Arnold, London, pp. 10-19.

Broccoli A.J. 2003. Twentieth century temperature and precipitation trends in ensemble climate simulations including natural and anthropogenic forcing. Journal of Geophysical Reasearch 108: 4798.

Broecker W. 1998. Paleocean circulation during the last deglaciation: a bipolar seesaw? Paleoceanography 13: 119-121.

Broecker W.S. 2001. Was the Medieval Warm Period Global? Science 291: 1497-1499.

Broeker W.S., Sutherland S. and Peng T.-H. 1999. A possible 20th Century slowdown of Southern Ocean deep water formation. Science 286: 1132-1135.

Chen F., Yu Z., Yang M., Ito E., Wang S., Madsen D., Huang X., Zhao Y., Sato T. and Birks H. 2008. Holocene moisture evolution in arid central Asia and its out-of-phase relationship with Asian monsoon history. Quaternary Science Reviews 27: 351-364.

Chu G., Qing S., Wang X. and Sun J. 2008. Snow anomaly events from historical documents in the eastern China during the past two millennia and implication for low-frequency variability of AO/NAO and PDO. Geophysical Research Letters 35: 1-4.

Clark M.P.M., Sierreze M.C. and Robinson D.A. 1999. Atmospheric controls on Eurasian snow extent. International Journal of Climate 19: 27-40.

Clemens S.C. 2005. Millennial-band climate spectrum resolved and linked to centennial-scale solar cycles. Quaternary Science Reviews 24: 521-531.

Cobb K.M., Charles C.D., Cheng H. and Edwards L.E. 2003. El Nino/Southern Oscillation and tropical Pacific climate during the last millennium. Nature 424: 271-276.

Cosford J., Qing H., Eglington B. and Mattey D. 2008. East Asian monsoon variability since the Mid-Holocene recorded in a high-resolution, absolute dated aragonite speleothem from eastern China. Earth and Planetary Science Letters 275: 296-307.

Cronin T.M., Dwyer G.S., Kamiya T., Schwede S. and Willard D.A. 2003. Medieval Warm Period, Little Ice Age and 20th century temperature variability from Chesapeake Bay. Global Planetary Change 36: 17-29.

Crowley T.J. 2000. Causes of climate change over the past 1000 years. Science 289: 270-277.

Crowley T.J. and Vinther B.M. In preparation. A plausible returned chronology for the GISP2 ice core for the last 6000 years.

Crucifix M. 2008. Global change: Climate's astronomical sensors. Nature 456: 47-48.

Crucifix M., Loutre M.F. and Berger A. 2006. The climate response to the astronomical forcing. Space Science Reviews 125: 213-226.

Cullen H. and deMenocal P.B. 2000. The possible role of climate in the collapse of the Akkadian Empire: evidence from the deep sea. Geology 28: 379-382.

Deer Z. 1994. Evidence for the Existence of the Medieval Warm Period in China. Climatic Change 26: 289-297.

Desser C., Walsh J.E. and Timlin M.S. 2000. Arctic sea ice variability in the context of recent atmospheric circulation trends. Journal of Climate 13: 617-633.

Diaz M., Hoerling M.P. and Eischeid J.K. 2001. ENSO variability, teleconnections and climate change. International Journal of Climatology 21: 1277-1293.

Dickinson R., Lazier J., Meincke J., Rhines P. and Swift J. 1996. Long term coordinated changes in the convective activity of the North Atlantic. Progress in Oceanography 38: 241-295.

Ding Y. 1994. Monsoon over China. Kluwer Academic, 419 pp.

Ding Y. and Sikka D.R. 2006. Synoptic systems and weather. Springer, New York, 781 pp.

Dodson J. and Liu T.S. 1995. PEP II: The Austral-Asian transect. Palaeoclimates of the northern and southern hemispheres. PAGES Report Series 95-1, pp. 43-64.

Folland C.K., Renwick J.A., Salinger M.J. and Mullan A.B. 2002. Relative influences of interdecadal Pacific oscillation and ENSO on the South Pacific convergence zone. Geophysical Research Letters 29: 1-4.

Gerber S.F., Joos P., Brugger T.F., Stocker T.F., Mann M.E., Stitch S. and Scholze M. 2003. Constraining temperature variations over the last millennium by comparing simulated and observed atmospheric $CO_2$. Climate Dynamics 20: 281-299.

Gillett N.P., Weaver F., Zwiers W. and Wehner M.F. 2004. Detection of volcanic influence on global precipitation. Journal of Geophysical Reasearch Letters 31: 12217.

Gladstone R.M., Ross I., Valdes P.J., Abe-Ouchi A., Braconnot P., Brewer S., Kageyama M., Kitoh A., Legrande A., Marti O., Ohgaito R., Otto-Bliesner B., Peltier W.R. and Vettoretti G. 2005. Mid-Holocene NAO: A PIMP2 model intercomparison. Geophysical Research Letters 32: 1-4.

Gnanadesikan A., Slater R.D., Swathi P.S. and Valiis G.K. 2005. The energetics of ocean heat transport. Journal of Climate 18: 2604-2616.

Goosse H., Arzel O., Luterbacher J., Mann M.E., Renssen H., Riedwyl.N., Timmermann A., Xoplaki E. and Wanner H. 2006. The origin of the European "Medieval Warm Period" . Climate of the Past 2: 99-113.

Gupta A.K., Anderson D.M. and Overpeck J.T. 2003a. Abrupt changes in the Asian southwest monsoon during the Holocene and their links to the North Atlantic Ocean. Nature 421: 354-357.

Gupta A.K., Das M. and Anderson D.M. 2005. Solar influence on the Indian summer monsoon during the Holocene. Geophysical Research Letters 32: 17703.

Gupta A.K. and Thomas E. 2003b. Initiation of Northern Hemisphere glaciation and strengthening of the northeast Indian monsoon: Ocean Drilling Program Site 758, eastern equatorial Indian Ocean. Geology 31: 47-50.

Haigh J.D. and Blackburn M. 2006. Solar influences on dynamical coupling between the stratosphere and troposphere. Space Science Reviews 125: 331-344.

Haug G.H., Hughen K.A., Sigman D.M., Peterson L.C. and Rohl U. 2001. Southward migration of the intertropical convergence zone through the Holocene. Science 293: 1304-1308.

Holmes J.A., Cook E.R. and Yang B. 2009. Climate change over the past 200 years in Western China Quaternary International 194: 91-107.

Hong B., Liu C., Lin Q., Yasuyuki S., Leng X., Wang Y., Zhu Y.T. and Hong Y. 2009. Temperature evolution from the d18O record of Hani peat, Northeast China, in the last 14,000 years. Science in China Series D-Earth Sciences 52: 952-964.

Hurrell J.W. 1996. Influence of variations in extratropical wintertime teleconnections on Northern Hemisphere tempertaure. Geophysical Research Letters 23: 665-668.

Imbrie J., Boyle E.A., Clemens S., Duffy A., Howard W.R., Kukla G., Kutzbach J., Martinson D.G., McIntyre A., Mix A.C., Molfino B., J.J. M., Peterson L.C., Pisias N.G., Prell W.L., Raymo M.E., Shackleton N.J. and Toggweiler J.R. 1992. On the structure and origin of the major glaciation cycles. 1. Linear responses to Milankovitch cycles. Paleoceanography 7: 701-738.

Indermuhle A., Stocker T.F., Joos F., Fischer H., Smith H.J., Wahlen M., Deck B., Masttroianni D., Blunier T., Meyer A. and Stauffer B. 1999. Holocene carbon cycle dynamics based on $CO_2$ trapped in ice at Taylor Dome, Antarctica. Nature 398: 121.

IPCC 2007. Contribution of Working Group I to the Fourth Assesment Report of the Intergovernmental Panel on Climate Change, 2007. In: S. D. Solomon, M. Qin, Z. Manning, M. Chen, K. B. Marquis, M. Averyt, Tignor and H. L. Miller (eds.), Cambridge.

Jennings A.E., Knudsen K.L., Hald M., Hansen C.V. and Andrews J.T. 2002. A mid-Holocene shift in Arctic sea-ice variability on the East Greenland Shelf. The Holocene 12: 49-58.

Jhun J.G. and Lee E.J. 2004. A new East Asian winter monsoon index and associated characteristics of the winter monsson. Journal of Climate 17: 711-726.

Jones P. and Mann M. 2004. Climate over past millennia. Review of Geophysics 42: 1–42.

Jones P.D., Bradley R.S. and Jones J. 1996. Climate variations and forcing mechanisms over the last 2000 years. Springer, New York.

Jones P.D. and Briffa T.G. 2001. The evolution of climate over the last millennium. Science 292: 662.

Joos F., Gerber I.C., Prentice B.L., Otto-Bliesner L. and Valdes P.J. 2004. Transient simulations of Holocene atmospheric carbon dioxide and terrestrial carbon since the Last Glacial Maximum. Global Biogeochemical Cycles 18: 1-18.

Kaplan J.O., Bigelow N.H., Prentice I.C., Harrison S.P., Bartlein P.J., Christensen T.R., Cramer W., Matveyva N.V., McGuire A.D., Murray D.F., Razzhivin V.Y., Smith B., Walker D.A., Anderson P.M., Andreev A., Brubaker E., Edwards M.E. and Lozhkin A.V. 2003. Climate change and Arctic ecosystems, Modelling paleo-data model comparisons and future projections. Journal of Geophysical Reasearch Atmospheres 108.

Kaplan M.R. and Wolfe A.P. 2006. Spatial and temporal variablilty of Holocene temperatures in the North Atlantic region. Quaternary Research 65: 223-231.

Kirch P.V. 2005. Archaeology and global change: the Holocene record. Annual review of Environment and Resources 30: 409-440.

Klein Goldewijk K. and Ramankutty N. 2004. Land cover change over the last three centuries due to human activities; the availability of new global data sets. Geojournal 61: 335-344.

Lean J. 2000. Evolution of the Sun's spectral irradiance since the Maunder Minimum. Geophysical Research Letters 27: 2425-2528.

Lean J.L., White O.R. and Skumanich A. 1995. On the Solar Ultraviolet Spectral Irradiance during the Maunder Minimum. Global Biogeochemical Cycles 9: 171-182.

Liu T. 1985. Loess and the Environment. Science Press of China, Beijing, 191 pp.

Liu Y., Linderholm H.W., Song H.M., Cai Q.F., Tian Q.H., Sun J.Y., Chen D.L., Simelton E., Seftigen K., Tian H., Wang R.Y., Bao G. and An Z. 2009. Temperature variations recorded in Pinus tabulaeformis tree rings from the southern and northern slopes of the central Qinling Mountains, central China. Boreas 38: 285-291.

Loutre M.F. and Berger A. 2003. Marine Isotope Stage 11 as an analogue for the present interglacial. Global and Planetary Change 36: 209-217.

Lydolph P.E. 1977. Geography of the USSR. Elsevier, The Hague.

MacDonald G.M., Beilman D.W., Kremenetski K.V., Sheng Y., Smith L.C. and Velichko A.A. 2006. Rapid early development of circumarctic peatlands and atmospheric $CH_4$ and $CO_2$ variations. Science 314: 285-288.

Mackay A. 2007. The paleoclimatology of Lake Baikal: A diatom synthesis and prospectus. Earth Science Reviews 82: 181-215.

Mann M.E., Cane M.A., Zebiak S.E. and Clement A. 2005. Volcanic and solar forcing of the tropical Pacific over the past 1000 years. Geophysical Research Letters 18: 447-456.

Matthews H.D., Weaver A.J., Meissner K.J., Gillett N.P. and Eby M. 2004. Natural and anthropogenic climate change: incorporating historical land cove change, vegetation dynamics and the global carbon cycle. Climate Dynamics 22: 461-479.

Mayewski P., Rohling E., Curt Stager J., Karlén W., Maasch K., David Meeker L., Meyerson E., Gasse F., van Kreveld S. and Holmgren K. 2004. Holocene climate variability. Quaternary Research 62: 243-255.

Mayewski P.A., Meeker L.D., Twickler M.S., Whitlow S., Yang Q., Lyons W.B. and Prentice M. 1997. Major features and forcing of high latitude northern hemisphere atmospheric circulation using a 110,000 year long glaciochemical series. Journal of Geophysical Reasearch 102: 26345-26366.

Morrill C., Overpeck J. and Cole J. 2003. A synthesis of abrupt changes in the Asian summer monsoon since the last deglaciation. The Holocene 13: 465-475.

Müller U.C. and Pross J. 2007. Lessons from the past: Present insolation minimum holds potential for glacial inception. Quaternary Science Reviews 26.

Nesje A. and Dahl S.O. 1993. The Greenland 8200 cal. yr event detected in loss-in-ignition profiles in Norwegian lacustrine sediment sequences Journal of Quaternary Science 16: 155-166.

NOAA-NCDC 2010. http://nomads.ncdc.noaa.gov/.

PAGES-IGBP 2010. http://www.pages-igbp.org/index.html.

Panagiotopoulos F., Shahgedanova M., Hannachi A. and Stephenson D. 2005. Observed trends and teleconnections of the Siberian high: A recently declining center of action. Journal of Climate 18: 1411-1422.

Prokopenko A., Khursevich G., Bezrukova E., Kuzmin M., Boes X., Williams D., Fedenya S., Kulagina N., Letunova P. and Abzaeva A. 2007. Paleoenvironmental proxy records from Lake Hovsgol, Mongolia, and a synthesis of Holocene climate change in the Lake Baikal watershed. Quaternary Research 68: 2-17.

Rahmstorf S. 2003. Thermohaline circulation: The current climate. Nature 421: 699.

Reynaud D., Barnola J.-M., Chappelaz J., Blunier T., Indermuhle A. and Stauffer B. 2000. The ice record of greenhouse gases: a view in the context of future changes. Quaternary Science Reviews 19: 9-17.

Ridgwell A.J., Watson A.J., Maslin M. and Kaplan J.O. 2003. Implications of coral reef build up for the controls on atmospheric $CO_2$ since the Last Gacial Maximum. Paleoceanography 18: 1083.

Rimbu N., Lohman G., Kim J.-H., Arz H.W. and Schneider P.R. 2003. Arctic/North Atlantic Oscillation signature in Holocene sea surface temperature trends as obtained from alkenone data. Geophysical Research Letters 30.

Robock A. and Liu Y. 1994. The volcanic signal in Goddard Institute for Space Studies three-dimensional model simulations. Journal of Climate 7: 44-55.

Ruddiman W.F. 2003. The anthropogenic greenhouse era began thousands of years ago. Climatic Change 61: 261-293.

Ruddiman W.F. 2005. Cold climate during the closest stage 11 analog to recent millenia. Quaternary Science Reviews 24: 1111-1121.

Ruddiman W.F. 2007. The early anthropogenic hypothesis: Challenges and responses. Reviews of Geophysics 45: 37.

Ruddiman W.F. and Thomson J.S. 2001. the case for human causes of increased atmospheric CH4 over the last 5000 years. Quaternary Science Reviews 20: 1769-1777.

Salzer M.W. and Hughes M.K. 2007. Bristlecone pine tree rings and volcanic eruptions over the last 5000 years. Quaternary Research 67: 57-68.

Schettler G., Liu Q., Mingram J. and Negendank J. 2006. Palaeovariations in the East-Asian monsoon regime geochemically recorded in varved sediments of Lake Sihailongwan (Northeast China, Jilin province). Part 1: Hydrological conditions and dust flux. Journal of Paleolimnology 35: 239-270.

Schwanghart W., Schutt B. and Walther M. 2008. Holocene climate evolution of the Ugii Nuur basin, Mongolia. Advances in Atmospheric Sciences 25: 986-998.

Schwanghart W., Schutt B. and Walther M. 2009. Holocene Climate Evolution of the Ugii Nuur Basin, Mongolia. Palaeogeography, Palaeoclimatology, Palaeoecology 279: 160-171.

Seidenkrantz M.-S., Aagaard-Sorensen S., Sulsbruck H., Kuijpers A., Jensen K.G. and Kunzendorf H. 2007. Hydrography and climate of the last 4400 years in a SW Greenland fjord: implications for Labrador Sea palaeoceanography. The Holocene 17: 387-401.

Seidenkrantz M.-S., Roncaglia I., Fischel A., Heilmann-Clausen C., Kuijpers A. and Moros M. 2008. Variable North ATlantic climate seesaw patterns documented by a later Holocene marine record from Disko Bugt, West Greeland. Marine Micropaleontology 68: 66-83.

Shahgedanova M. 2002. Climate at the present and in the historical past. In: M. Shahgedanova (ed.), The physical geography of northern Eurasia. Oxford University Press, Oxford. , pp. 70-103.

Shindell D., Schmidt G., Mann M., Rind D. and Waple A. 2001. Solar forcing of regional climate change during the Maunder Minimum. Science 294: 2149-2152.

Thompson D.J. and Wallace J.M. 2001. Regional climate impacts of the Northern Hemisphere annular mode. Science 293: 85-89.

Todd M.C. and Mackay A.W. 2003. Large-scale climatic controls on Lake Baikal ice cover. Journal of Climate 16: 3186-3199.

Tzedakis P.C. 2010. The MIS11-MIS1 analogy, southern European vegetation, atmospheric methane and the "early anthropogenic hypothesis". Climate of the Past 6: 131-144.

UNAVCO 2010. Jules Verne Voyager. http://jules.unavco.org/.

Wang B., Wu R. and Li T. 2003. Atmosphere warm ocean interaction and its impacts on Asian Australian monsoon variation. Journal of Climate 16: 1195-1211.

Wang Y., Cheng H., Edwards R., He Y., Kong X., An Z., Wu J., Kelly M., Dykoski C. and Li X. 2005. The Holocene Asian monsoon: links to solar changes and North Atlantic climate. Science 308: 854-857.

Wang Y., Cheng H., Edwards R.L., An Z.S., Wu J.Y., Chen C.-C. and Dorale J.A. 2001. A high reolution absolute dated late Pleistocne monsoon record from Hulu Cave, China. Science 14: 2345-2348.

Wang Y., Cheng H., Edwards R.L., Kong X. and Shao X. 2008. Millennial-and orbital-scale changes in the East Asian monsoon over the past 224,000 years. Nature 451: 1090-1093.

Wanner H., Beer J., Butikofer J., Crowley T.J., Cubasch U., Fluckiger J., Goosse H., Grosjean M., Joos F., Kaplan J.O., Kuttel M., Muller S.A., Prentice I.C., Solomina O., Stocker T.F., Tarasov P., Wagner M. and Widmann M. 2008. Mid- to Late Holocene climate change: an overview. Quaternary Science Reviews 27: 1791-1828.

Williams K.M., Andrews J.T., Jennings A.E., Short S.K., Mode W.N. and Syvitski J.P.M. 1995. The Eastern Canadian Arctic at c. 6 ka: a time of transition. Canadian Global Change Issue 49: 13-27.

Ye H. and Bao Z. 2005. Eurasian snow conditions and summer monsoon rainfall over south and southeast Asia: assesment and comparison. Advances in Atmospheric Sciences 6: 100-111.

Yihui D. and Chan J.C.L. 2005. The East Asian summer monsoon: an overview. Meteorology and Atmospheric Physics 89: 117-142.

Zhang J. and Crowley T.J. 1989. Historical climate records in China and reconstruction of past climates. Journal of Climate 2: 833-849.

Zielinski G.A., Mayewski P.A., Meeker L.D., Whitlow S., Twicker M.S., Morrison M., Meese D.A., Gow A.J. and Alley R.B. 1994. Record of volcanism since 7000 BC from the GISP2 Greenland ice core and implications for the volcano-climate system. Science 264: 948-952.

# CHAPTER 2. Theoretical background

## 2.1. Research design

The two dominant proxies used in this project as outlined in the objectives (Section 1.2), are bulk organic isotopes and diatoms. Based on the literature discussed in Chapter 1, it is argued that both Lakes Arachlei and Xiaolongwan will be susceptible to variations in precipitation (derived from differing sources) over the Holocene. Bulk organic isotopes have been chosen due to their ability to reconstruct catchment and lake productivity. It is therefore argued that changes in precipitation (and temperatures) over the late Holocene would change vegetation productivity and be recorded within lake sediments, particularly when a comprehensive understanding of contemporary linkages between systems is known. The method can be paired with analyses of the inorganic component of sediments to investigate inwash events linked to e.g. increased precipitation. Similarly, diatoms are a valuable method of reconstructing lake characteristics. They act, in this case, as an indirect record of environmental changes over the period. Diatoms are very sensitive to variations in lake stratification, water level and ice cover (among other factors) all of which are themselves very sensitive to changes in climate e.g. the link between increased SH intensity and ice cover duration (Todd and Mackay 2003). It is argued therefore that a multiproxy approach can be used to reconstruct the impacts of climate variability upon catchment and lake productivity and the ultimate effect it has upon lake characteristics. The use of inorganic proxies (trace metal contamination and fly ash particles) will also be adopted to analyse the importance of anthropogenic impacts upon these remote locations within the context of natural climate change.

## 2.2. Stable isotope geochemistry of water

Water isotopes ($^{18}O/^{16}O$ and $^{2}H/^{1}H$; $^{2}H$ is expressed here as D) in lake waters, precipitation and groundwaters are invaluable hydrological tracers. In limnology, water isotopes provide information about water sources and hydrological balance. The relative differences in isotopic ratios can be determined more precisely than absolute isotopic ratios (Sharp 2007). The delta ($\delta$) notation used to report stable isotope data was first introduced by (McKinney et al. 1950) and can be given by:

$$\delta = [(R_x - R_{std})/R_{std}] \times 1000$$

where $R$ is the ratio of the abundance of the heavy isotope to light isotope, $x$ denotes the sample, and std is an abbreviation for a given standard. Delta values are reported in per mil

(‰). The international standard used for water, Standard Mean Ocean Water (SMOW), has by definition $\delta^{18}O$ and $\delta D$ values of 0.0‰ (Sharp 2007).

Isotopic standards are different depending on which element is analysed, SMOW acts as the standard for both oxygen and hydrogen measurements of water and low temperature minerals (Craig 1961b); the ocean being the largest, most homogenous body of water in the world. Pee Dee Belemnite (PDB) from South Carolina (Craig 1957) was the standard for $^{12}C/^{13}C$ and $^{18}O/^{16}O$ measurements. However, the carbonates NBS-18 and 19 are now utilised originally calibrated to PDB, as PDB no longer exists.

### 2.2.1 Oxygen and hydrogen isotopes in precipitation

The isotopic composition of precipitation is primarily determined by the fractionation of water during the evaporation from the oceans and condensation to form precipitation. The lighter isotopologues of water preferentially escape from the surface of the liquid into the vapour phase upon evaporation, and the opposite occurs upon condensation (Sharp 2007).

Fractionation can be defined as the partitioning of isotopes between two substances or between two phases that results in the preferential uptake or release of one isotope (i.e. lighter or heavier respectively) relative to another (Leng et al. 2006b). Kinetic isotope effects are normally associated with fast, incomplete or unidirectional processes such as evaporation (Sharp 2007), while equilibrium fractionation between two phases is based on the differences in bond strength of the different isotopes of an element (ibid.).

As a result of these two processes, water vapour that evaporates from the oceans is isotopically lighter than the water from which it evaporates. The major controlling parameters are (Darling et al. 2006):

- Isotopic composition of the ocean surface
- Sea surface temperature
- Relative humidity of the atmosphere
- Wind regime

The main source water of continental water, including lakes, is precipitation. However, as marine moisture is transported further from source regions, the likelihood of rainout after cloud formation increases. Within the cloud, equilibrium fractionation between vapour and the condensing phases preferentially partitions $^{18}O$ and D into the rain or snow. Furthermore, along the trajectory of the air mass, the process of rainout distils the heavy isotopes of the vapour, becoming progressively depleted in $^{18}O$ and D according to a Rayleigh type distillation (Clark and Fritz 1997). Rainout is then an evolution towards cooler, isotopically lower precipitation due to the progressive rainout from a diminishing vapour mass. Clark and Fritz (1997) state that the

strong correlation between temperature and $\delta^{18}O$-$\delta D$ controls the position of precipitation on the meteoric water line. Isotope evolution during rainout can be modelled according to the relevant Rayleigh expression:

$$R/Ri = F^{\alpha-1}$$

Where *R* is the isotopic ratio of the vapour before condensation begins, *Ri* is the isotope ratio of the vapour remaining after a given amount of condensation, *F* is the fraction of the vapour remaining and $\alpha$ is the equilibrium isotope fractionation factor between liquid and vapour phases (ibid.).

The isotopic composition of rainfall collected at the ground surface appears to be close to the isotopic equilibrium with near-ground water vapour as a result of the raindrops re-equilibrating isotopically with the surrounding moisture on their way to the surface. This is controlled by the size of the raindrops, the actual height of the cloud base and the relative humidity of the atmosphere beneath the cloud (Darling et al. 2006). At sufficiently low condensation temperatures, the isotopic composition of snow is influenced by an additional kinetic effect, linked to supersaturation conditions around the forming of snow flakes (Jouzel and Merlivat 1984).

The isotopic composition of precipitation at a given location therefore depends on: the isotope composition of the ocean from which it evaporates, the temperature and relative humidity at which it evaporates and the amount of moisture recycling from the earth's surface (all dependent upon the trajectory of the airmass (Dansgaard 1964)), the degree of rainout of the air mass from which it condenses and of the atomospheric water vapour with which it re-equilibrates, and any evaporation that occurs as it falls. As a consequence of these observations, the average isotope composition of precipitation at a given location is often related to the temperature at the site of precipitation and Dansgaard (1964) quantified this relationship at mid- and high-latitude coastal stations, showing that:

$$\delta^{18}O_{ppt}(‰) = 0.695T\,(°C) - 13.6$$

Where $\delta^{18}O_{ppt}$ is the mean annual $\delta^{18}O$ of precipitation falling at a given site, and T is the mean annual temperature at that site in degrees Celsius. However, there are a number of factors that disrupt this relationship.

- Distance or continentality effect

Precipitation becomes isotopically lighter as the parent air masses move farther from their sources and over the continents, as they have undergone more cycles of precipitation and *F*

approaches ever-lower values (Sharp 2007). The continentality effect is associated with a number of physical controls on *F*, most notably the temperature decrease between the source of atmospheric vapour and the point of precipitation, and the continentality effect is greater during the colder months.

- Latitude effect

The gradual depletion in the D and $^{18}O$ content of precipitation from the tropics to the mid-latitudes can be understood as a result of the progressive removal of water from the moist air masses being transported from the tropical areas to the poles and the decrease in temperature with latitude (Darling et al. 2006; Sharp 2007) (Figure 2.1). This relationship is by no means linear as topographic and local meteorological conditions are operative as well in the process of rainout.

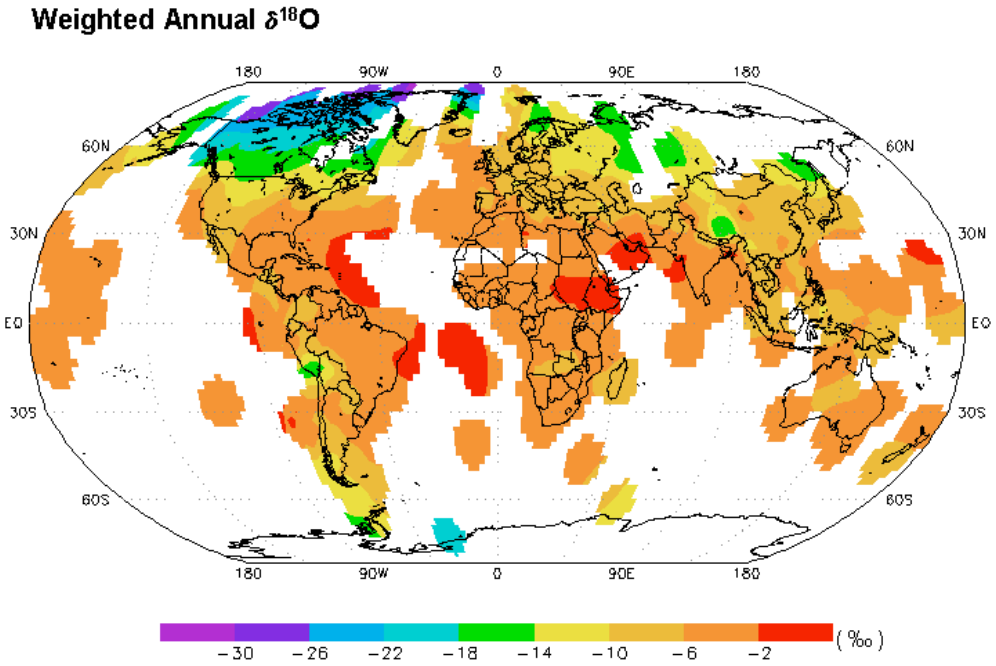


*Figure 2.1 Annual weighted $\delta^{18}O$ values of precipitation (‰ VSMOW) across the world (IAEA/WMO 2006).*

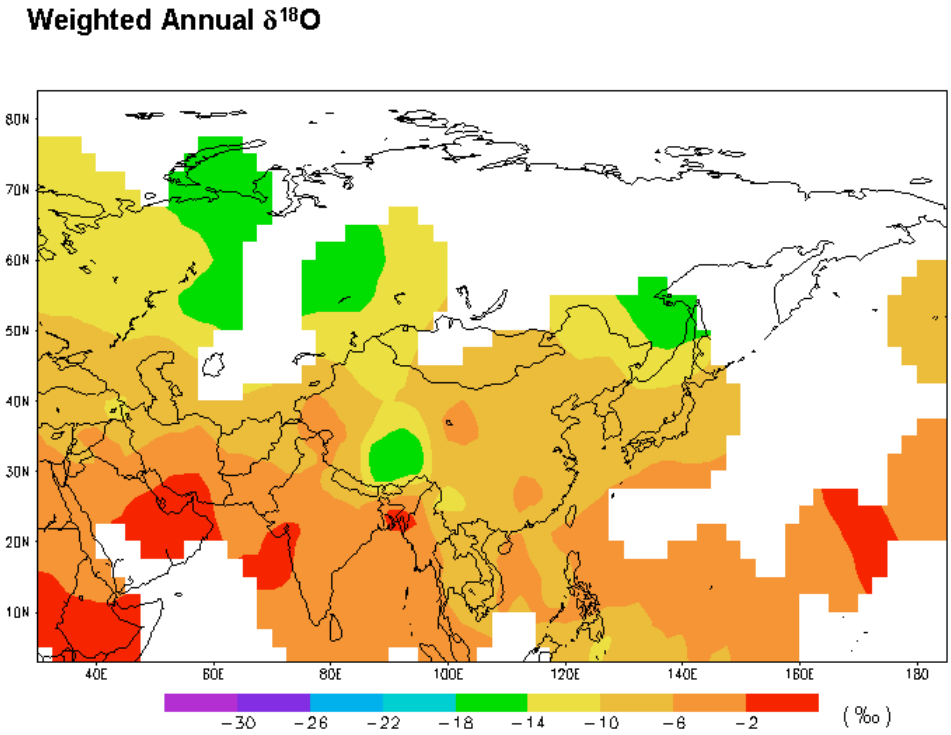


*Figure 2.2 Annual weighted $\delta^{18}O$ values of precipitation (‰ VSMOW) across Asia (IAEA/WMO 2006).*

- Altitude effect

The isotopic composition of water decreases with increasing altitude, again as it is colder at higher elevations and air masses hold less water when they are cooled (Sharp 2007). The isotopic evolution of the vapour reservoir and the resulting precipitation can be described by a modified Rayleigh process where only partial removal of the liquid phase from the vapour reservoir occurs (Clark and Fritz, 1997). As $\alpha$ values increase, so that the effect of Rayleigh fractionation is intensified. As an air mass is deflected upwards, it decompresses and cools pseudo-adiabatically where more rain out occurs (Sharp 2007). The percentage of remaining water vapour in the air mass will decrease rapidly if the relief is high. This is shown in Figure 2.1 and in 2.2 where the change in $\delta^{18}O$ can be seen above the Tibetan Plateau.

- Amount effect

There is a negative correlation between mean $\delta$ values and the amount of monthly precipitation which is more pronounced in tropical regions. For tropical regions, the $\delta$ values of rain at a given station are high in months with little rain and low during rainy seasons. Based on the principles discussed, the more rainout that occurs from a given air mass, the lower the delta value of

subsequent rainout. With regard to convecting air mass systems, four processes should be considered in order to understand the amount effect (ibid.):

- As air rises and cools to saturation, condensate falls through other droplets that formed below and the condensate can exchange with them.
- The droplets can grow larger by incorporating more vapour as they fall.
- Upon exiting the cloud, the droplets can evaporate into dry air.
- Droplets can exchange with vapour that is present in unsaturated air below the cloud.

$\delta^{18}O$ and $\delta D$ values of meteoric water are closely correlated, because both oxygen and hydrogen isotopes are fractionated in broadly the same way during the processes that determine the isotopic composition of precipitation (Friedman 1953). This relationship can be graphically displayed as the Global Meteoric Water Line (GMWL), a line on the $\delta^{18}O$-$\delta D$ plane formed when the $\delta^{18}O$ and $\delta D$ values of meteoric precipitation from all parts of the globe (e.g. different local meteoric water lines; LMWL) are plotted together (Figure 2.3) (Leng and Barker, 2006). Craig (1961a) suggested a best fit line (termed the GMWL), for the $\delta D$ and $\delta^{18}O$ contents of fresh water from around the world as:

$$\delta D = (8*\delta^{18}O) + 10$$

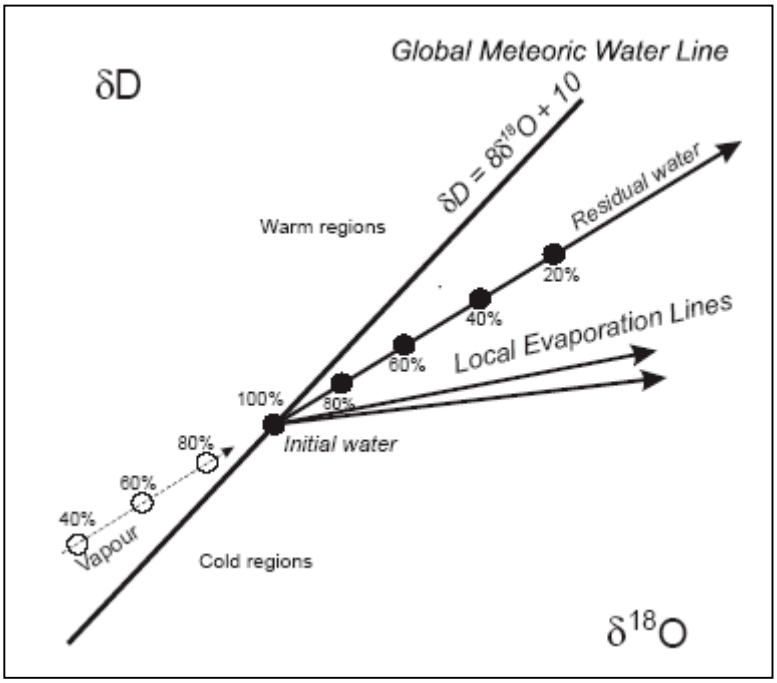


*Figure 2.3. Major controls on the $\delta^{18}O$ vs. $\delta D$ of precipitation and lake waters. The GMWL is plotted along with the local evaporation lines of lakes and vapour lines (Leng and Marshall 2004).*

LMWLs usually have a slope less than 8 (Sharp 2007). It has been demonstrated that the intercept of the GMWL (the *d*-excess) is controlled mainly by controls on the evaporation process in major source areas for atmospheric moisture (subtropical oceans), whereas the slope is determined, in the first instance, by the ratio of equilibrium isotope enrichments for D and $^{18}O$ respectively (Dansgaard 1964; Merlivat and Jouzel 1979). The slope of the meteoric relationship between D and $^{18}O$ in global precipitation is very close to 8, although it can be affected locally by evaporation that occurs after condensation (Clark and Fritz, 1997).

The deuterium excess parameter (*d*) is defined as (Dansgaard 1964; Darling et al. 2006):

$$d = \delta D - 8*\delta^{18}O$$

It is controlled predominantly by kinetic effects associated with the evaporation of water at the surface of the oceans or inland and increases with an increase in the moisture deficit, 1 – *h*, of the oceanic air masses, where *h* is the relative humidity at the surface temperature of the water (Merlivat and Jouzel, 1979). The effect of evaporation is to drive the remaining water to higher $\delta^{18}O$ and $\delta D$ values, with a $\delta D/\delta^{18}O$ slope of less than 8 (residual water line; Figure 2.3). The removal of water with isotopic compositions that lie to the right of the GMWL (evaporated water line) results in a vapour that lies to the left of the GMWL (vapour line; Figure 2.3) resulting in a deuterium excess (Sharp 2007). Regular seasonal variations of $\delta^{18}O$ and $\delta D$ in precipitation are observed at mid and high latitudes where the seasonal variations of $\delta^{18}O$ and $\delta D$ may result from the interplay of several factors (*ibid.*):

1. Seasonal changes of the temperature at the precipitation sites, leading to substantial changes of the total precipitable water in the atmosphere with season
2. Seasonal changes in the evapotranspiration flux on the continents, amplifying seasonal differences in total precipitable water
3. Seasonal changes of prevailing circulation patterns changing the origin of moisture

In continental regions e.g. Siberia, water recycling can occur. In the continental water cycle the water evaporated from oceans is transported by the atmosphere into the continental area, precipitates onto the surface and finally flows back to the oceans as river flow. Within this cycle some part of the water precipitated onto the continental surface evaporates again to the atmosphere and contributes to another precipitation event over surrounding continental regions (Numaguti 1999). Kurita et al (2004) argue that in Siberia, more than half of the moisture that forms summer precipitation originates from land surfaces; thus the isotopic content of precipitation in this region is controlled mainly by the contribution of recycled water. However, this recycling explains only 20% of the spatial variation of isotopic content in summer precipitation (ibid.). During summer months, it is argued that in regions of southern Eurasia (e.g. Transbaikalia region) the mean age of water in the precipitation from oceanic origin is one month or less, and the mean number of recycling events is less than one (Numaguti 1999). This

is much less compared to other regions of Eurasia, e.g. in northern inland Eurasia water has a mean age of three months or more. In winter on the other hand, water directly supplied from oceanic evaporation is dominant in the precipitating water over the Eurasian continent (Numaguti 1999).

### 2.2.2. Oxygen and hydrogen stable isotopes in lakes

Precipitation in warmer regions has a higher $\delta^{18}O$ and $\delta D$, while colder, polar precipitation has lower $\delta D$ and $\delta^{18}O$. Deviations of precipitation from the GMWL are found on a seasonal basis in many regions, mainly in the summer due to enhanced partial evaporation of raindrops below the cloud base and/or seasonal varying conditions in the source area for the vapour and these are responsible for the local evaporation lines (LEL) (Darling et al. 2006). Ratios of isotopes in lake waters increases after evaporation, along the LEL.

The $\delta^{18}O$ and $\delta D$ composition of lake water is determined by the isotope composition and volume of lake water inputs, and by the extent to which evaporation alters the composition of these inputs after they enter the water body. Lake waters plotting on or close to the GMWL are isotopically the same as precipitation, whereas lake waters that plot off the GMWL on a LEL have undergone kinetic fractionation. With evaporation, the isotopic composition of the residual water in the lake and the resulting water vapour become progressively enriched, in both cases the kinetic fractionation of $^{18}O$ exceeds that of D. Evaporating lakes will have $\delta^{18}O$ and $\delta D$ values which lie on a LEL with a slope determined by local climate (Clark and Fritz, 1997; Leng and Marshall, 2004) (Figure 2.3). The humidity is critical in determining the fraction of water lost by evaporation vs. outflow (Clark and Fritz. 1997). In cases where humidity is low, kinetic evaporation is maximised. During evaporative enrichment of water, the vapour will have a reciprocal depletion, and plot on the same evaporative line, but opposite the initial composition of the water (*ibid.*) (Figure 2.3).

A LEL may also be formed in a region where the atmospheric circulation regime of the given area varies seasonally (as is evident in north east China), bringing moisture to the precipitation site from two or more different sources which may differ in both absolute $\delta^{18}O$ and $\delta D$ values and the 'deuterium excess' value *d.*

### 2.2. 3. Dissolved inorganic carbon in water ($\delta^{13}C_{TDIC}$)

Inorganic carbon isotopes, mainly from TDIC (total dissolved inorganic carbon) in lake waters, are incorporated into the inorganic carbon within authigenic (formed in situ) and biogenic (formed from a biological component) carbonates (Leng and Barker, 2006; Leng and Marshall, 2004) (Figure 2.4).

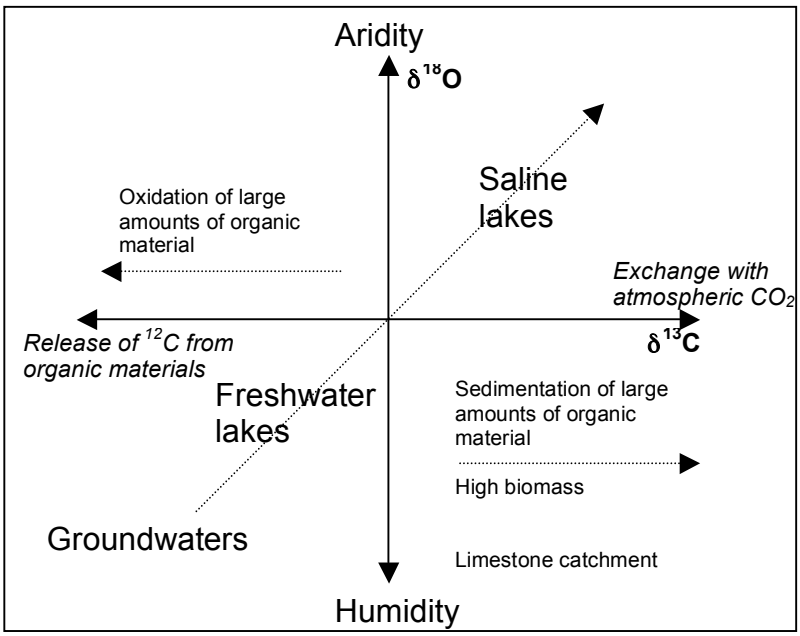


*Figure 2.4 The $\delta^{13}C$ vs. $\delta^{18}O$ of lake water. Hydrologically closed lakes often show $\delta^{13}C_{TDIC}$ vs. $\delta^{18}O$ covariance. High values reflect different degrees of equilibration of the TDIC with atmospheric $CO_2$ and the preferential evaporative loss of the $^{16}O$, respectively. Groundwaters and river waters have $\delta^{13}C_{TDIC}$ values that are typically low, values are generally between 20‰ and 30‰ from plant respiration and production of $CO_2$ in the catchment soils (Talbot 1990).*

Bicarbonate ($HCO_3^-$) is the main source of TDIC in lake waters and is derived from the interaction of groundwaters with rocks and soils in the catchment of a lake (Leng and Marshall, 2004). There are three main factors that control the inorganic carbon isotope composition of the TDIC: the isotopic composition of inflowing waters (including groundwaters); the $CO_2$ exchange between the atmosphere and water TDIC; and the photosynthesis/respiration of organisms within the lake water.

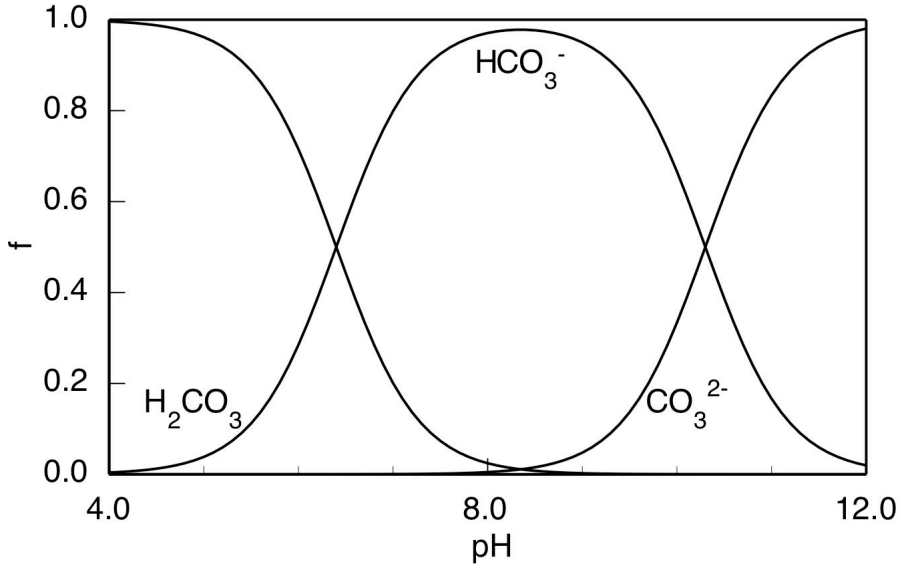


*Figure 2.5. The different carbon species of TDIC in lake waters along a pH range. Image provided by Prof. Jonathan Holmes.*

The carbon in groundwater and river waters in general has low $\delta^{13}C_{TDIC}$ values, so that a significant proportion of the carbon comes from plant respiration and production of $CO_2$ in the soils (*ibid*.). $\delta^{13}C$ depleted $CO_2$ liberated by the decay of terrestrial organic matter in the soil enters the soil waters and shallow groundwaters and when pH values lie between c. 7 – 10, $HCO_3^-$ is the dominant carbon species (Figure 2.5). $HCO_3^-$ in equilibrium with $CO_2$ gas has a $\delta^{13}C$ of c. 10‰ higher than $CO_2$, so that $HCO_3^-$ derived from soil $CO_2$ alone should have values of between -22‰ and -10‰ (Leng and Marshall, 2004).

Within-lake processes also modify the composition of the $\delta^{13}C_{TDIC}$ in lake waters. Dissolved inorganic carbon is made up of four species: $CO_{2\ (aq)}$, $H_2CO_3$, $HCO_3^-$ and $CO_3^{2-}$. The latter two contribute to the alkalinity of lake waters. Furthermore, their relative abundance is primarily determined by pH. Below pH 6.4 dissolved $CO_2$ dominates, between 6.4 and 10.3 bicarbonate is dominant and above 10.3 carbonate species are present (Figure 2.5) (Clark and Fritz, 1997). The pH of lake waters can therefore affect the $\delta^{13}C$ in lake waters due to altering the different species of inorganic carbon. Bicarbonate is isotopically heavier than other inorganic carbon species, with $\delta^{13}C$ values c. 9.5‰ higher than dissolved $CO_2$ and c. 1.8‰ higher than carbonate ions at 25˚C (Deines et al. 1974; Mook et al. 1974; Romanek et al. 1992; Turner 1982).

In hydrologically closed lakes, covariance of $\delta^{13}C_{TDIC}$ and $\delta^{18}O$ can occur. High values are likely to reflect the different degrees of equilibration of the TDIC with $CO_2$ and preferential evaporative loss of the $^{16}O$ (Figure 2.4) (Usdowski and Hoefs 1993). The extent to which the water body equilibrates with the atmospheric $CO_2$ depends on its residence time, which if sufficiently long, the $\delta^{13}C$ of lake water may approach a steady-state value determined by this process (Li and Ku 1997).

In lakes, the dissolved carbon pool is often changed by biological productivity, mainly by preferential uptake of $^{12}C$ by aquatic plants during photosynthesis. During periods of enhanced productivity or in lakes with a large biomass, the carbon pool in the water becomes enriched in $^{13}C$ and consequently has a higher $\delta^{13}C_{TDIC}$ (Leng and Marshall, 2004; Leng et al, 2006). The effect of lake stratification can also have an effect on the profile of TDIC through the water column. In this case with late spring and early summer turnover (before the onset of stratification) nutrients brought to the surface lead to phytoplankton blooms. $^{12}C$ is preferentially used up so that there is a significant increase in the $\delta^{13}C$ value of the TDIC in the surface waters while the bottom water TDIC drops to depleted values due to the respiration of sinking organic matter (Leng and Marshall, 2004). The decomposition of organic matter via methanogenesis can also affect the $\delta^{13}C_{DIC}$ of lake water (Rosenfeld and Silverman 1959). Methanogenesis can occur through two different forms of fermentation (carbon dioxide and acetate) and both pathways increase $\delta^{13}C_{DIC}$, as carbon dioxide reduction preferentially uses isotopically-light $CO_2$ which can escape from the system as gas, leaving the remaining DIC enriched in $^{13}C$ (Stiller and Magaritz 1974; Whiticar et al. 1986).

Following on from photosynthesis/respiration of organisms and their subsequent sedimentation, $^{12}C$ is removed from surface water DIC reservoirs. As this continues, the $\delta^{13}C$ values of the remaining inorganic carbon increases and produces a subsequent increase in the $\delta^{13}C$ values of newly produced organic matter (Meyers and Teranes 2001). Increased or decreased productivity therefore yields a respective increase or decrease in the $\delta^{13}C$ of organic matter that is produced in the lake and available for sedimentation (*ibid.*).

## 2.3. Stable isotope geochemistry of bulk organic matter

### 2.3.1. Total organic carbon, C/N ratios and carbon isotopes in lacustrine organic matter

The primary source of organic matter to lake sediments is from plants in and around the lake (Meyers and Teranes, 2001). The percentage of total organic carbon (%TOC) represents the amount of organic matter preserved after sedimentation, and so depends on both the initial production and degree of degradation (Meyers and Teranes, 2001). TOC is a bulk value that represents the fraction of organic matter that escaped re-mineralisation during sedimentation and it integrates the different origins of organic matter, delivery routes, depositional processes and amount of preservation. Meyers and Teranes (2001) state that TOC can be both diluted by addition of clastic sediment particles and concentrated by dissolution of carbonate minerals in sediment. Furthermore, that TOC concentrations commonly increase as sediment grain size decreases, so that concentrations can become larger in deeper parts of lake basins where fine grained sediments slowly settle than in shallower parts where coarse sediments rapidly accumulate.

The amount of sedimentary organic matter that originates from aquatic and terrestrial plants can be distinguished by C/N ratios (% total organic carbon versus % nitogen) (*ibid.*). Organic nitrogen occurs preferentially in proteins and nucleic acids, which are relatively abundant in lower plants such as aquatic phytoplankton (Talbot 1990; Talbot and Johannessen 1992). Organic matter derived solely from lacustrine phytoplankton therefore has a characteristically low C/N ratio, typically < 10 (Leng et al, 2006; Meyers and Teranes, 2001). Algae tend not to contain cellulose and lignin, while higher plants have lignocellulosic structural biopolymers which allows them to create standing chains and therefore they have higher C/N ratios (e.g. between 16 and 163) (Meyers and Teranes, 2001). However, decomposition can change the C/N ratio of organic matter through selective degradation of specific compounds. The C/N ratio of algal material often increases during decomposition as the nitrogen rich proteins are decomposed preferentially. The C/N ratio of terrestrial material can decrease due to immobilisation of N-rich compounds and remineralisation of carbon microbes (Meyers and Lallier-Vergès 1999). Bacterial growth in organic matter during decomposition can also reduce its average C/N ratio (Lehmann et al. 2002). However, these changes rarely outweigh the influence of plant type on C/N ratios (Meyers and Teranes, 2001).

Lacustrine algae preferentially use dissolved $CO_2$ as their source of carbon during photosynthesis, but some aquatic plants and cyanobacteria also use bicarbonate ions (Allen and Spence 1981; Miller and Colman 1980). Aquatic organisms tend to use bicarbonate as a source of DIC in conditions where $CO_2$ decreases, this in turn increases the average $\delta^{13}C$ values of aquatic organisms. The $\delta^{13}C$ values of both dissolved $CO_2$ and bicarbonate are influenced by a range of factors (as discussed in section 2.2.3) and the $\delta^{13}C$ of aquatic organisms therefore vary according to the isotope composition of DIC.

The carbon isotope signal ($\delta^{13}C$) from lacustrine organic matter acts as a tracer for past changes in the terrestrial and aquatic carbon cycles and is often used as a signal for changes in their productivity (Leng and Barker, 2006). Plant material has $\delta^{13}C$ values ranging from about −38 to −8‰, dividing into narrower ranges for each of the photosynthetic pathways: −38 to −22‰ for $C_3$ plants, −15 to −8‰ for $C_4$ plants and −30 to −13% for CAM plants (Crassulacean acid metabolism) (Darling et al. 2006).

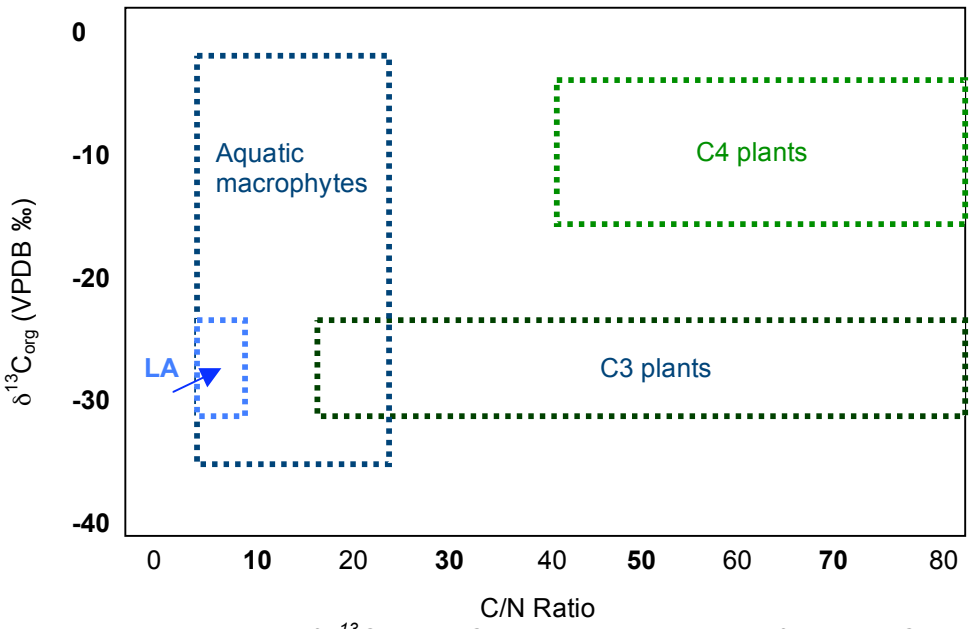


*Figure 2.6. A theoretical plot of $\delta^{13}C_{org}$ and C/N ratios. Plotting areas for where C4 land plants, C3 land plants, aquatic macrophytes and lacustrine algae (LA) occur are shown. Modified from Tyson (1995).*

$C_3$ photosynthesis is used by most trees, shrubs and aquatic plants. Most plants use the $C_3$ pathway of photosynthesis, also called the photosynthetic carbon reduction cycle (PCR). This means that $C_3$ plants have a single chloroplast type that performs all of the reactions that convert light energy into the chemical energy that is used to fix $CO_2$ and to synthesize the reduced carbon compounds upon which all life depends. Ribulose, 5-bisphosphate carboxylase oxygenase (RuBisCo) catalyzes primary carbon fixation, to a five carbon sugar phosphate, ribulose-l,5-bisphosphate (RuBP) (Fairbank and Taylor 1997).

The $C_4$ pathway is a more complex adaptation of the $C_3$ pathway. This pathway effectively suppresses photorespiration by elevating the $CO_2$ concentration at the site of RuBisCo using a biochemical $CO_2$ pump. These plants chemically fix carbon dioxide in cells in a reaction catalysed by the enzyme phospoenolpyruvate carboxylase (PEP carboxylase). $C_4$ plants have two chloroplast types and species mainly grow in hot climates with sporadic rainfall (e.g. low altitude grasses in regions with high growing season temperatures) (Fairbank and Taylor, 1997). CAM is mostly used by succulents and uses both RuBisCo and PEP carboxylase to fix carbon so that the photosynthetic products of this pathway therefore tend to have $\delta^{13}C$ values between those of $C_3$ and $C_4$ plants (O'Leary 1988).

Phytoplankton ($C_3$ algae) preferentially utilise $^{12}C$ to produce organic matter that averages 20‰ lighter than the $^{13}C/^{12}C$ ratio of their dissolved inorganic carbon (DIC) source (Wolfe et al. 2001). Cyanobacteria also use RuBisCo to fix carbon, but the form of the enzyme used by these organisms only fractionates carbon by c. 16-22‰ (Guy et al. 1993). The $\delta^{13}C$ of cyanobacteria using a specific source of inorganic carbon (reflecting their preference for neutral to alkaline

conditions) and their $\delta^{13}C$ values therefore often range between c. -10‰ and -20‰ (Sakata et al. 1997), although they can reach as high as -3‰ and as low as -27‰ (Tyson 1995) (Figure 2.6).

## 2.4. Inorganic proxies of environmental change

### 2.4.1. Sediment composition

As discussed in Section 2.3.1 TOC can be used as an indicator of the organic content of lake sediments. A number of other methods can also be adopted. The percentage Dry Weight (% DW) measured down core can act as a reference for changes in sediment water content. As a percentage, decreasing water content can imply an increase in sediment inwash to lake sediments and therefore can act as an indicator for catchment erosion (increased organic and/or inorganic material).

Sequential percentage Loss On Ignition (% LOI) is a common and widely used method to estimate the organic and carbonate content of sediments (e.g. Bengtsson and Enell 1986). Dean (1974) concluded that LOI provides a fast means of determining carbonate (LOI at 950$^{o}$C) and organic (LOI at 550$^{o}$C) contents of clay-poor, calcareous sediments and rocks. In the first reaction, organic matter is oxidised at 500-550$^{o}$C to carbon dioxide and ash. In a second reaction, carbon dioxide is evolved from carbonate at 900-1000$^{o}$C, leaving oxide. There are a number of considerations to take into account when conducting LOI analyses that have been outlined by Heiri et al (2001). These are essentially concerning the analytical methodology including exposure time, sediment sample size and the chance of other reactions other than burning taking place (e.g. dehydration of clay minerals). As a result, inter-comparisons should be conducted between laboratories taking these factors into consideration, or at least analysts should be aware of such biases when using the technique as a proxy for carbon content of sediment (LOI at 550$^{o}$C) (ibid.). It is also important to note that LOI tends to overestimate the actual amount of TOC.

### 2.4.2. Trace element analyses

A trace metal can be defined as a metal found in low concentration (fractions of ppm or less) in a specified source (Duffus 2002). A proper inventory of atmospheric emissions from natural sources is basic to our understanding of the atmospheric cycle of the trace metals, needed for assessing the extent of regional and global pollution by toxic metals (Nriagu 1989). Furthermore, it is generally presumed that the principal natural sources of trace metals in the atmosphere are wind-borne soil particles, volcanoes, sea salt spray and forest fires (ibid.). Accumulation rates for trace metals associated with fossil fuel combustion, smelting and vehicle emissions can be determined by analysis of accurately-dated sediments cores from lakes

(Norton and Kahl 1987). Absolute values vary from lake to lake depending largely on geographical location and basin morphology.

X-ray fluorescence (XRF) is used here to identify the characteristic elements present within sediment samples by accelerating electrons and measuring the rate of the emission from the sample (Boyle 2001). The emission is a function of the concentration of the element within the sample and absorption of the x-rays by the sample (Boyle 2000). The output of XRF analyses is a suite of trace elements, which can be adopted for the purpose of investigating atmospheric pollution signals in lake sediments.

The inorganic geochemical technique of XRF can provide valuable information on changes in lake (e.g. trophic status) and catchment environments (e.g. climate change, catchment erosion, sediment origin) as well as providing detailed information on the extent of atmospheric pollution at sites (Boyle 2001). For the purpose of this study these factors will all be discussed, although a greater emphasis will be placed on potential indicators of pollution in these remote regions.

The presence of allogenic metals in lake sediments can be attributed to four sets of factors:

1. A result of dry deposition of micro-sized particles, or wet deposition in which aerosols are scavenged from the atmosphere via precipitation.
2. Weathering of rocks and soils in the catchment.
3. Seepage from industrial sources, particularly sites in close proximity to mining and smelting operations.
4. Fluvial transport of trace metals in conjunction with suspended particulate matter.

Rognerud and Fjeld (2001) found that once these elements are in the water column, they are scavenged by particulate matter and deposited in the sediments.

2.4.2.1. Trace elements and pollution studies

The role of atmospheric pollution as a key factor in regional enrichment of surface sediments in Pb, Hg, Cd and Zn is widely known (Boyle 2001; Boyle and Birks 1999b). In pollution studies, the identification of the natural trace element contribution to lake sediments is essential if these archives are to be used as recorders of pollution (Norton and Kahl, 1987). As a result, Norton and Kahl (1987) apply a correction using $TiO_2$ ratios; the principle being that the natural trace element supply can be divided into two fractions; soil minerals with associated trace elements and the rest of the sediment lacking trace elements. As a result, unpolluted sediments will have trace element concentrations that vary with a soil mineral tracer, e.g. $TiO_2$ and the anthropogenic fraction can be found by subtracting the background fraction from the total concentration (Boyle 2001).

For example, in order to determine the anthropogenic component of lead the following equation can be adopted:

$$Pb_{a(x)} = Pb_{total,(x)} - \left[\frac{TiO_{2(x)}}{TiO_{2(b)}}\right]\left[Pb_b\right]$$

Norton and Kahl (1987); where $_a$ = anthropogenic, $_{(x)}$ is any depth and $_b$ = background.

This method is appropriate when total element concentrations are used as elements of Zn, Ni, Co and V are firmly bound in mineral lattices. For elements such as Hg, Cu, Ni and Pb, the labile fraction is generally greater and would reduce the value of the method (Boyle 2001).

There are a number of factors that must be considered when interpreting trace metal reconstructions in palaeolimnology. For example, it is important to distinguish whether there has been surface sediment enrichment or if a post depositional remobilisation of metals has taken place. The main factor contributing to the latter point is diagenesis. This results in dissolved ions of $Fe^{2+}$ and $Mn^{2+}$ being oxidised to a solid state in response to a gradient in dissolved metals within a sediment profile. At the same time other metals such as Cu, Co, Mo, Ni and Zn are removed either by absorption or co-precipitation (Boudreau 1999).

There are other considerations that must be taken into account when reconstructing atmospheric pollution from lake sediments using trace element methods. Firstly, there may be indirect effects due to acidification; Zn profiles in particular must be treated with great care as there is often an inconsistency between concentration profiles from the same lake (White and Gubala 1990). Furthermore, Boyle (2001) outlines that there may be diffusion within the sediment, particularly for As and that the potential impact of diffusion is greater at low sedimentation rates and is worse for elements that are mobile under reducing conditions (e.g. As, Co, Fe and Mn). Moreover, enrichment of the sediment surface in trace elements such as Cd, Cu, Zn and Ra is not uncommon (Boyle et al. 1998). This is often the result of ephemeral surface enrichment due to cycling in processes in the water column although this need not however have much impact on the longer term sediment record (Boyle 2001). Finally there is evidence for the direct diffusion of metals to lake sediments that potentially weakens the integrity of the temporal record, which again is worsened by circumstances of low accumulation rates. (Carignan and Tessier 1985).

Evidence of human impact through the use of trace element analyses has been shown by a number of studies. For example, Yang and Rose (2005) have demonstrated that relatively remote sites in the UK have experienced enhanced atmospheric deposition of anthropogenically-derived trace elements for over 100 years, possibly starting before industrialisation. Although a different model was adopted to calculate anthropogenic contamination to the one discussed here, they argue that Pb can be used as a tracer for

atmospheric pollution while the trace elements Ti, Zr,Si and Al were considered as possible passive tracers and therefore acting as background levels. Hammarlund et al (2008) also found high Pb concentrations (100-150 ug/g) in Sweden between the 16$^{th}$ and 18$^{th}$ centuries as a result of the proximity (c. 80 km) of the study site to a copper mine. Although evidence is also supported from other records for a regional atmospheric Pb pollution history for Sweden between the c. 13th and 20$^{th}$ century (ibid.).

Atmospheric contamination in areas remote to industrial activity (e.g. lakes Xiaolongwan and Arachlei) can be much harder to reconstruct. Furthermore, in circumstances of low sedimentation rates, the deposition of these elements in sediments and their concentration is also low. As a result, Boyle (2001) outlines that it is very important to pay very careful attention to estimation of natural concentrations (for example through the use of Norton and Kahl's $TiO_2$ normalisation method). Furthermore, that in such circumstances it is necessary to be far more critical of the data and to take full account of any natural processes, which might lead to surface enrichments. However, unambiguous indicators of anthropogenic contamination are spheroidal carbonaceous particles (SCPs) and I use this technique to complement trace element analyses.

### 2.4.3. Fly-ash particles

Spheroidal carbonaceous particles (SCPs) and inorganic ash spheres (IASs) are collectively known as fly-ash, the term used to describe the particulate matter within emitted flue-gases (Rose 2001). Fly-ash is the bi-product of fossil-fuel burning at high temperatures. The products from this combustion are porous spheroids of mainly elemental carbon (Goldberg 1985) and fused inorganic spheres formed from the mineral component of the original fuel (Raask 1984; Rose 2001).

Rose (2001) details three components of fly-ash, which are formed in different ways. First is non combustible material (IASs), second is combustible matter that was not burned (SCPs) and the third is matter that was formed during the combustion process. IASs are formed by the fusing of the minerals present within the fuel and SCPs are produced by the incomplete combustion of the fuel particle or oil droplet (Rose et al, 1999). These airborne particles with a diameter between 1 µm and 20 µm have finite settling velocities which are low with respect to normal windspeeds (Wark and Warner 1976) and so fly-ash particles are potentially able to travel long distances in air streams (Rose 1996a). Lake sediments store deposited fly-ash particles and consequently provide a record of anthropogenic atmospheric contamination (Rose 2001).

Despite the greater numbers of IASs emitted to the atmosphere, most palaeolimnological studies involving fly-ash particles have concentrated on SCPs (Rose 1996a). There are several reasons for this:

- SCPs are more chemically robust and therefore easier to extract and enumerate

- IAS from industrial sources are not easily separable from those produced naturally (e.g. they are morphologically and chemically similar to volcanic micospherules) while SCPs are solely from anthropogenic emissions

- SCPs can be used to identify potential origins of depositions as they can be characterised to fuel-type using energy dispersive spectroscopy (EDS) of the particle surface

2.4.3.1. Formation of SCPs

SCPs are formed when pulverised coal particles, heated rapidly in a combustion chamber, change from angular non-porous coal fragments to porous and often partitioned spheroids, which have a molten appearance (Lightman and Street 1968; Rose 1996b). In oil-droplet combustion, volatiles are produced as the droplets heat and it is in this expelled cloud of hydrocarbons that ignition first occurs (Rose 2001). Rose (2001) describes that as heat is given back to the droplet, burning of the volatiles on the particle surface takes place. As emission of volatiles decreases, the droplet collapses and becomes rigid forming the final SCP (Lightman and Street 1983). Oil SCPs are spheroidal, often more porous than coal SCPs due to the greater emission of hydrocarbons, and have a complex structure (Rose 2001). Images of SCPs (from previous studies) under scanning electron microscopy can be seen in Figure 2.7.

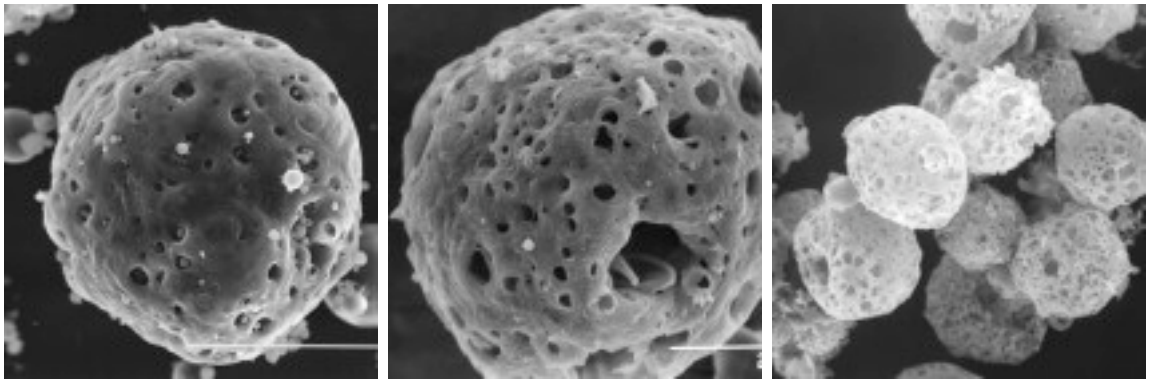

*Figure 2.7 Displaying images of SCPs in lake sediment cores. Images taken using SEM. (Images provided by Prof. Neil Rose).*

2.4.3.2. The application of SCPs in environmental change

As there are no natural sources of SCPs they consequently form an unambiguous record of the atmospheric deposition of industrial emissions in lake sediment records (Rose et al, 1999). Historically SCPs have been used in two ways. Firstly, as supporting the evidence for the acid deposition hypothesis in the surface water acidification debate of the 1980s in Europe and north America (Battarbee and Renberg 1990; Charles et al. 1990; Charles and Whitehead 1986). Through using a record of SCPs it has been shown that spatial distributions of these particulates are similar to those of other fossil-fuel derived pollutants, for example sulphur (Wik and Renberg 1991). However, unlike some deposited pollutants (e.g. sulphur, Zn, Cd) SCPs are inert to changes in water and sediment chemistry, and as a result these records are considered

as very robust (Rose et al, 1999). Secondly, SCP analyses are a relatively simple way of adding a few recent dates to sediment cores (Rose 2001). Indeed, the application of the technique was demonstrated by Rose and Appleby (2005) for the use of dating sediments in the UK, which will be discussed here.

Most palaeolimnological research studies involving fly-ash particles have produced down-core profiles of particle concentrations. Rose (2001) outlines three reasons for this:

- In order to correlate with other temporal trends (e.g. to attribute atmospheric deposition cause)
- To allocate dates to a core
- In order to determine the trends in particle concentrations through time (e.g. as indicators of impacts from atmospheric deposition)

There are three features that are identifiable on a SCP profile. Firstly, as SCPs are not produced by natural means the first major trend in a record if as a result of the beginning of high temperature fossil fuel combustion. In the UK, the start of the SCP record begins in c. 1850/1860 with the start of the Industrial Revolution (Rose et al. 1995). Similar situations occurred in every industrialised country as this new form of power generation was developed. As a result, the start of the SCP record occurs within a few decades (1850-1900) in most industrial countries (Rose 2001).

As meteorological phenomena will transport SCPs many thousands of kilometres from source regions to relatively clean areas, such particles may be detected in lake sediments of areas prior to the time of the first local or regional emissions (ibid.). Rose et al (1998) therefore outline that in these circumstances the detection limit of the technique may influence the date at which the presence of fly-ash in lake sediments records is first observed rather than first deposited. For example, Wu et al (2005) show that in central southern China, the beginning of the SCP record corresponds to the beginning of the Anhui Province's thermal power history in 1952. Furthermore, that for China after 1950 records detail the initiation of electricity and that after 1978 there is a rapid increase in generated power.

The second important consideration is the rapid increase seen in the SCP profile following the end of the Second World War (1939-1945). There was firstly a major expansion in the combustion of fossil-fuels at power stations which rapidly increased in size due to increased energy demands, and secondly, an increase in the availability of cheap fuel leading to the development of the first large-scale oil fired power stations (Laxen 1996; Rose 2001). While this rapid increase is seen throughout Europe and regions of north America, in regions of China and certain parts of Russia this increase is seen at a later date due to the differing industrial advances. It has been predicted that there will be a doubling in the global amount of coal used for electricity production by 2020 and most of this will be in China and India (ENDS 1999). While the same trends are seen from lake sediment records in different regions of the world, in terms

of using the rapid increase in SCP concentration as a dating feature, this is more useful in Europe (and to a certain extent in N. America).

The final diagnostic feature of the SCP profile is the particle concentration peak. The peak seen in SCP concentrations arises from movement from small, local power stations providing power to a limited area, to a smaller number of larger power stations located outside of urban areas. Rose (2001) also outlines that along side this movement, the efficiency of combustion also increased, as well as the introduction of particle arrestors at source and the implementation of successively more rigorous control legislation.

In the sediment record, these changes manifest as a movement away from the rapid increase in concentrations of the 1950/1960s to a particle concentration peak, followed by a decline to the surface. Although it is important to note that this peak occurs at different times in different regions, due to the national and regional changes in the processes outlined above (Rose 2001). As a result, despite the particle concentration peak being the least ambiguous and most clearly identifiable SCP profile feature, it is most probably the one most open to local variability.

Indeed, in the context of this study, SCP concentrations from south eastern China continue to show surface concentration maxima despite lakes having more rapid accumulation rates (Boyle et al. 1999a). Wu et al (2005) also outline that in regions of central eastern China and China as a whole generated thermal power emissions continued to increase, and SCP peaks continue to sediment surfaces.

Due to the scarcity of pollution data from remote regions of central Asia, this project identifies the importance of creating a high resolution investigation of recent pollution in these regions in order to investigate the effects of it and in order to provide a valuable comparison with such records from other regions of the world where implementation occurred earlier (e.g. UK and Europe).

## 2.5 Biological proxies of environmental change

### 2.5.1. Diatoms

Diatoms are unicellular, eukaryotic, micro-organisms (Round et al. 1990). They are of the class Bacillariophyceae and species numbers vary from $10^4$ to $10^5$ (Stoermer and Smol 1999). Diatoms are pigmented and photosynthetic, although some at least can live heterotrophically in the dark if supplied with a suitable source of carbon (Round et al. 1990). As a result they are found in all aquatic environments (ubiquitous) occupying different niches due to their short generation times and ability to respond quickly to changing ecological conditions (Battarbee et al. 2001). Some of these adaptations even include temporary exposure to the atmosphere (aerophilic) when not submerged.

Diatoms are well preserved in lake sediments as about 95% of their cell wall is impregnated with opaline silica (Brasier 1980). Although large numbers of different genera are found in all types of aquatic environments, irrespective of controlling variables such as salinity and temperature, many species are still subject to strict ecological constraints (Battarbee et al. 2001). As a result, a knowledge of diatom habitat requirements, survival strategies and their autoecology may be used to reconstruct past environments including climate variability (Bradbury 2002; Smol 1988). Quantitative techniques conducted upon diatom data have also been used to reconstruct Holocene climate variability, by both indirect and direct methods. Indirect methods reconstruct lake environmental characteristics that occur as a result of climate change. For example, numerous studies have employed sediment records to assess changes in lake salinity (e.g. Fritz 1990; Verschuren et al. 2000), pH (e.g. Koinig et al. 1998; Psenner and Schmidt 1992) and nutrients (e.g. Bennion 1994; Bennion et al. 1996), although other variables such as conductivity, lake ice cover, DOC and water level change have also been reconstructed. Direct methods are those that aim to reconstruct lake environmental change that is a direct result of climate change and both methods employ the technique of transfer functions (models based on modern calibration data sets applied to palaeodata) to do so. The most pioneering studies using direct techniques have reconstructed surface water temperatures (e.g. Bigler and Hall 2002; Rosén et al. 2000) and air temperatures (Korhola et al. 2000). However, Anderson (2000) highlights that we should be cautious of the application, over long time periods, of statistically significant diatom inferred water (and indeed air) temperature models, and furthermore, that these models do not perform as well as those that reconstruct climate using indirect techniques. More recently several palaeoecological studies have attempted to disentangle the effects of natural climate variability from those of climate change induced by anthropogenic activity, particularly in Arctic environments of the Northern Hemisphere (Hobbs et al. 2010; Ruhland et al. 2008; Smol et al. 2005).

While the use of diatoms in a quantitative way, as a means of climate reconstruction (direct or indirect), has often been disputed on the grounds of the robustness of models (e.g. Anderson, 2000) it cannot be denied that they are an important element of the proxy's application. Evidence for this is seen by the growing literature in this field and, in the context of this project, the recent publication of a surface sediment diatom calibration set from western Mongolia. Shinneman et al (2009) state that their diatom-based inference models show strong predictive capabilities and low prediction errors for salinity and total phosphorus. They argue that their data can be used to help identify and interpret historical and future disturbances to this sensitive and globally important eco-region.

For the purpose of this project however, the qualitative approach has been chosen. This is due to the logistic difficulty associated with developing my own training set for the two regions and the lack of an existing published training set north east China. Diatoms will be used in this study as a means of reconstructing lake ecological changes over the past c. 3000 years. These

organisms have rapid growth responses to both subtle and significant environmental changes, allowing high resolution reconstructions to be made here (Battarbee et al. 2001). Descriptions of diatom autoecology and the ecological interpretation of the palaeoecological record will be discussed in the relevant sections of this thesis for the purpose of reconstructing environmental change.

**References**

Allen E.D. and Spence D.H.N. 1981. The differential ability of aquatic plants to utilise the inorganic carbon supply in freshwaters. New Phytologist 87: 269-283.

Anderson N.J. 2000. Diatoms, temperature and climatic change. European Journal of Phycology 35: 307-314.

Battarbee R.W. and Renberg I. 1990. The Surface Water Acidification Project (SWAP) paleolimnology programe. Philosophical Transactions of the of the Royal Society London (Series B) 327: 227-232.

Battarbee R.W., Jones V.J., Cameron N.G., Bennion H., Carvahlo L. and Juggins S. 2001. Diatoms. In: J. P. Smol, H. J. B. Birks and W. M. Last (eds.), Tracking environmental change using lake sediments. Kluwer Academic Publishers, Dordrecht, pp. 155-203.

Bengtsson L. and Enell M. 1986. Chemical analysis. In: B. E. Berglund (ed.), Handbook of Holocene Palaeoecology and Palaeohydrology. Blackburn, New Jersey.

Bennion H. 1994. A diatom-phosphorous transfer function for shallow, eutrophic ponds in southest England. Hydrobiologia 275: 391-410.

Bennion H., Juggins S. and Anderson N.J. 1996. Predicting epilimnetic phosphorous concentrations using an improved diatom-based transfer function and its application of lake eutrophication management. Environmental Science & Technology 30: 2004-2007.

Bigler C. and Hall R.I. 2002. Diatoms as indicators of climatic and limnological change in Swedish Lapland: a 100-lake calibration set and its validation for paleoecological reconstructions. Journal of Paleolimnology 27: 97-115.

Boudreau B.P. 1999. Metals and models: diagenetic modelling in freshwater lacustrine sediments. Journal of Paleolimnology 22: 227-251.

Boyle J.F. 2000. Rapid elemental analysis of sediment samples by isotope source XRF. Journal of Paleolimnology 23: 213-221.

Boyle J.F. 2001. Inorganic geochemical methods in palaeolimnology. In: W. M. a. S. Last, J.P (ed.), Tracking environmental change using lake sediments: physical and geochemical techniques. Kluwer Academic, Dordrecht, pp. 83-143.

Boyle J.F. and Birks H.J.B. 1999b. Predicting heavy metal concentrations in the surface sediments of Norwegian headwater lakes from atmospheric deposition: an application of a simple sediment-water partitioning model. Water, Air and Soil Pollution 114: 27-51.

Boyle J.F., Mackay A.W., Rose N.L., Flower R.J. and Appleby P.G. 1998. Sediment heavy metal record in Lake Baikal: natural and anthropogenic sources. Journal of Paleolimnology 20: 135-150.

Boyle J., Rose N., Bennion H., Yang H. and Appleby P. 1999a. Environmental impacts in the Jianghan Plain: evidence from lake sediments. Water, Air, & Soil Pollution 112: 21-40.

Bradbury J.P. 2002. A 1500-year record of climatic and environmental change in Elk Lake Minnesota III, measures of past primary production. Journal of Paleolimnology 10: 213-252.

Brasier M.D. 1980. Microfossils. Unwin Hyman, London.

Carignan R. and Tessier A. 1985. Zinc deposition in acid lakes: the role of diffusion. Science 228: 1524-1526.

Charles D.F. and Whitehead D.R. 1986. Paleoecological investigation of recent lake acidification. Methods and project description. In: D. f. Charles and D. R. Whitehead (eds.), Report EA-4609. Electric Power Research Institute, Palo Alto; CA.

Charles D.F., Binford M.W., Furlong E.T., Hites R.A., Mitchell M.J., Norton S.A., Oldfield F., Paterson M.J., Smol J.P., Uutala A.J., White J.R., Whitehead D.R. and Wise R.J. 1990. Paleoecological investigation of recent lake acidification in the Adriondack Mountains, N.Y. Journal of Paleolimnology 3: 195-241.

Clark I. and Fritz P. 1997. Environmental isotopes in hydrogeology. Lewis Publishers, New York, 328 pp.

Craig H. 1957. Isotopic standards for carbon and oxygen and correction factors for mass spectrometric analysis of carbon dioxide. Geochemica Cosmochimica Acta 12: 133-149.

Craig H. 1961a. Isotopic variations in meteoric waters. Science 133: 1702-1703.

Craig H. 1961b. Standard for reporting concentrations of deuterium and oxygen-18 in natural waters. Science 133: 1833-1834.

Dansgaard W. 1964. Stable isotopes in precipitation. Tellus 16: 436-468.

Darling W.G., Bath A.H., Gibson J.J. and Rozanski K. 2006. Isotopes in water. In: M. J. Leng (ed.), Isotopes in palaeoenvironmental research. Springer, Amsterdam, p. 307.

Dean W.E.J. 1974. Determination of carbonates and organic matter in calcareous sediments and sedimentary rocks by loss on ignition: Comparison with other methods. Journal of Sedimentary Petrology 44: 242-248.

Deines P., Harmon R.S. and Langmuir D. 1974. Stable carbon isotope ratios and the existence of a gas phase in the evolution of carbonate ground waters. Geochimica et Cosmochimica Acta 38: 1147-1164.

Duffus J.H. 2002. Heavy Metals-a meaningless term? Pure Applied Chemistry 74: 793-807.

ENDS 1999. ENDS Daily, April 23, 1999. Environmental Data Services Ltd., London.

Fairbank R.T. and Taylor W.C. 1997. Regulation of photosynthesis in C3 and C4 plants: A molecular approach. The plant Cell 7: 797-807.

Friedman I. 1953. Deuterium content of natural water and other substances. Geochimica et Cosmochimica Acta 4: 89-103.

Fritz S.C. 1990. 20th-Century Salinity and Water-Level Fluctuations in Devils Lake, North-Dakota - Test of a Diatom-Based Transfer-Function. Limnology and Oceanography 35: 1771-1781.

Goldberg E.D. 1985. Black carbon in the environment: Properties and distribution. Wiley Interscience Publication, New York, 198 pp.

Guy R.D., Fogel M.L. and Berry J.A. 1993. Photosynthetic fractionation of the stable isotopes of oxygen and carbon. Plant Physiology 101: 37-47.

Hammarlund D., Mackay A., Fallon D., Pateman G., Tavio L., Leng M. and Rose N. 2008. A sedimentary record of the rise and fall of the metal industry in Bergslagen, south central Sweden. Journal of Paleolomnology: 463-475.

Heiri O., Lotter A. and Lemcke G. 2001. Loss on ignition as a method for estimating organic and carbonate content in sediments: reproducibility and comparability of results. Journal of Paleolimnology 25: 101-110.

Hobbs W.O., Telford R.J., Birks H.J.B., Saros J.E., Hazewinkel R.R.O., Perren B., Saulnier-Talbot E. and Wolfe A.P. 2010. Quantifying Recent Ecological Changes in Remote Lakes of North America and Greenland Using Sediment Diatom Assemblages. PLoS ONE 5: 1-12.

IAEA/WMO 2006. Global network of isotopes in precipitation. The GNIP Database. http://isohis.iaea.org.

Jouzel J. and Merlivat L. 1984. Deuterium and oxygen-18 in precipitation, modelling of the isotope effect during snow formation. Journal of Geophysical Research 89: 11749-11757.

Koinig K.A., Schmidt R., Sommaruga-Wograth S., Tessadri R. and Psenner R. 1998. Climate change as the primary cause for pH shifts in a high Alpine lake (vol 104, pg 167, 1998). Water Air and Soil Pollution 106: 505-505.

Korhola A., Weckstrom J., Holmstrom L. and Erasto P. 2000. A quantitative Holocene climatic record from diatoms in northern Fennoscandia. Quaternary Research 54: 284-294.

Kurita N., Yoshida N., Inoue G. and Chayanova E. 2004. Modern isotope climatology of Russia: A first assessment. Journal of Geophysical Reasearch-Atmospheres 109: 1-15.

Laxen D. 1996. Generating emissions? Studies of the local impact of gaseous power-station emissions. A National Power publication, p. 74.

Lehmann M.F., Bernasconi S.M., Barbieri A. and McKenzie J.A. 2002. Preservation of organic matter and alteration of its carbon and nitrogen isotope composition during simulated and in situ early sedimentary diagenesis. Geochimica et Cosmochimica Acta 66: 3573-3584.

Leng M. and Barker P. 2006a. A review of the oxygen isotope composition of lacustrine diatom silica for palaeoclimate reconstruction. Earth Science Reviews 75: 5-27.

Leng M. and Marshall J. 2004. Palaeoclimate interpretation of stable isotope data from lake sediment archives. Quaternary Science Reviews 23: 811-831.

Leng M.J., Lamb A.L., Heaton T.H.E., Marshall J.D., Wolfe B.B., Jones M.D., Holmes J.A. and Arrowsmith C. 2006b. Isotopes in lake sediments. In: M. J. Leng (ed.), Isotopes in palaeoenvironmetal research. Springer, Dordrecht, p. 307.

Li H.-C. and Ku T.-L. 1997. $\delta^{13}C$-$\delta^{13}C$ covariance as a paleohydrological indicator for closed-lake basin lakes. Palaeogeography, Palaeoclimatology, Palaeoecology 133: 69-80.

Lightman P. and Street P.J. 1968. Microscopical examination of heat treated pulverised coal particles. Fuel 47: 7-28.

Lightman P. and Street P.J. 1983. Single drop behaviour of heavy fuel oils and fuel oil fractions. Journal of the Institute of Energy 56: 3-11.

McKinney C.R., McCrea J.M., Epstein S., Allen H.A. and Urey H.C. 1950. Improvements in mass spectrometers for the measurement of small differences in isotope abundance ratios. Review of Scientific Instruments 21: 724-730.

Merlivat L. and Jouzel J. 1979. Global climate interpretation of the deuterium-oxygen 18 relationship for precipitation. Journal of Geophysical Research 84: 5029-5033.

Meyers P. and Lallier-Vergès E. 1999. Lacustrine sedimentary organic matter records of Late Quaternary paleoclimates. Journal of Paleolimnology 21: 345-372.

Meyers P.A. and Teranes J.L. 2001. Sediment organinc matter. In: W. M. Last and J. P. Smol (eds.), Tracking environmental change using lake sediments. Volume 2: Physical and Geochemical Methods. Kluwer Academic Publishers., London, pp. 239-269.

Miller A.G. and Colman B. 1980. Evidence for $HCO_3$- transport by the blue green alga (Cyanobacterium) *Coccochloris peniocystis.* Plant Physiology 65: 397-402.

Mook W.G., Brommerson J.C. and Staverman W.H. 1974. Carbon isotope fractionation between dissolved bicarbonate and gaseous carbon dioxide. Earth and Planetary Science Letters 22: 169-176.

Norton S.A. and Kahl J.S. 1987. A comparison of lake sediments and ombrotrophic peat deposits as long term monitors of atmospheric pollution. In: T. P. Boyle (ed.), New approaches to monitoring aquatic ecosystems (ASTM STP). American Society for Testing and Materials, Philadelphia, pp. 40-57.

Nriagu J.O. 1989. A global assessment of natural sources of atmospheric trace metals. Nature 338: 47-49.

Numaguti A. 1999. Origin and recycling processes of precipitating water over the Eurasian continent: Experiments using an atmospheric general circulation model. Journal of Geophysical Reasearch-Atmospheres: 1957-1972.

O'Leary M.H. 1988. Carbon isotopes in photosynthesis. Bioscience 38: 328-336.

Psenner R. and Schmidt R. 1992. Climate-Driven Ph Control of Remote Alpine Lakes and Effects of Acid Deposition. Nature 356: 781-783.

Raask E. 1984. Creation, capture and coalescence of mineral species on coal flames. Journal of Institutional Energy 57: 231-239.

Rognerud S. and Fjeld E. 2001. Trace element contamination of Norwegian lake sediments. Ambio 30: 11-19.

Romanek C.S., Grossman E.L. and Morse J.W. 1992. Carbon isotope fractionation in synthetic aragonaite and calcite: effects of temperature and precipitation rate. Geochimica et Cosmochimica Acta 56: 419-430.

Rose N. 1996a. Inorganic fly-ash spheres as pollution tracers. Environmental Pollution 91: 245-252.

Rose N. 2001. Fly ash particles. In: W. M. a. S. Last, J.P (ed.), Tracking environmental change using lake sediments volume 2: Physical and geochemical methods. Kluwer Academic Publishers, Dordrecht, pp. 319-351.

Rose N. and Appleby P. 2005. Regional applications of lake sediment dating by spheroidal carbonaceous particle analysis I: United Kingdom. Journal of Paleolimnology: 349-361.

Rose N.L., Appleby P.G., Boyle J.F., Mackay A.W. and Flower R.J. 1998. The spatial and temporal distribution of fossil-fuel derived pollutants in the sediment record of Lake Baikal, eastern Siberia. Journal of Paleolimnology 20: 151-162.

Rose N.L., Harlock S., Appleby P.G. and Battarbee R.W. 1995. The dating of recent lake sediments in the United Kingdom and Ireland using spheroidal carbonaceous particle concentration profiles. The Holocene 5: 328-335.

Rose N., Juggins, S., Watt, J 1996b. Fuel-type characterisation of carbonaceous fly-ash particles using EDS -derived surface chemistries and its application to particles extracted from lake sediments. Proceedings of the Royal Society of London (Series A) 452.

Rose N., Juggins, S., Watt, J 1999. The characterisation of carbonaceous fly-ash particles from major European fossil-fuel types and applications to environmental samples. Atmospheric Environment 33: 699-2713.

Rosén P., Hall R., Korsman T. and Renberg I. 2000. Diatom transfer-functions for quantifying past air temperature, pH and total organic carbon concentration from lakes in northern Sweden. Journal of Paleolimnology 24: 109-123.

Rosenfeld W.D. and Silverman S.R. 1959. Carbon isotope fractionation in bacterial production of methane. Science 130: 1658-1659.

Round F.E., Crawford R.M. and Mann D.G. 1990. The Diatoms: Biology and morphology of the genera. Cambridge University Press, Cambridge, 653 pp.

Ruhland K., Paterson A. and Smol J. 2008. Hemispheric-scale patterns of climate-related shifts in planktonic diatoms from North American and European lakes. Global Change Biology 14: 2740-2754.

Sakata S., Hayes J.M., McTaggart A.R., Evans R.A., Leckrone K.J. and Togasaki R.K. 1997. Carbon isotope fractionation associated with lipid biosynthesis by a cyanobacterium: relevance for interpretation of biomarker records. Geochimica et Cosmochimica Acta 61: 5379-5389.

Sharp Z. 2007. Principles of stable isotope geochemistry. Pearson Prentice Hall, New Jersey, 344 pp.

Shinneman A.L.C., Edlund M.B., Almendinger J.E. and Soninkhishig N. 2009. Diatoms as indicators of water quality in western Mongolian lakes: a 54 site calibration set. Journal of Paleolimnology 42: 373-389.

Smol J.P. 1988. Paleoclimate proxy data from freshwater arctic diatoms. Verh. Internat. Verein. Limnol. 23: 837-844.

Smol J., Wolfe A., Birks H., Douglas M., Jones V., Korhola A., Pienitz R., Ruhland K., Sorvari S., Antoniades D., Brooks S., Fallu M., Hughes M., Keatley B., Laing T., Michelutti N., Nazarova L., Nyman M., Paterson A., Perren B., Quinlan R., Rautio M., Saulnier-Talbot E., Siitoneni S., Solovieva N. and Weckstrom J. 2005. Climate-driven regime shifts in the biological communities of arctic lakes. Proceedings of the National Academy of Sciences of the United States of America: 4397-4402.

Stiller M. and Magaritz M. 1974. Carbon-13 enriched carbonate in intertial waters of Lake Kinneret sediments. Limnology and Oceanography 19: 849-853.

Stoermer E.F. and Smol J.P. 1999. The Diatoms: Applications for the environmental and earth sciences. Cambridge Unoversity Press, Cambridge, 469 pp.

Talbot M.R. 1990. A review of the palaeohydrological interpretation of carbon and oxygen isotopic ratios in primary lacustrine carbonates. Chemical Geology 80: 261-279.

Talbot M.R. and Johannessen T. 1992. A high resolution palaeoclimate record for the last 27,500 years in tropical west Africa from the carbon and nitrogen isotopic composition of lacustrine organic matter. Earth and Planetary Science Letters 110: 23-37.

Todd M.C. and Mackay A.W. 2003. Large-scale climatic controls on Lake Baikal ice cover. Journal of Climate 16: 3186-3199.

Turner J.V. 1982. Kinetic fractionation of carbon-13 during calcium carbonate precipitation. Geochimica et Cosmochimica Acta 46: 1183-1191.

Tyson R.V. 1995. Sedimentary organic matter: organic facies and palynofacies. Chapman and Hall, New Youk.

Usdowski E. and Hoefs J. 1993. Oxygen isotope exchange between carbonic acid, bicarbonate, carbonate and water: a re-examination of the data of McCrea (1950) and an expression for the overall partitioning of oxygen isotopes between the carbonate species and water. Geochimica et Cosmochimica Acta 57: 3815-3818.

Verschuren D., Laird K.R. and Cumming B.F. 2000. Rainfall and drought in equatorial east Africa during the past 1,100 years. Nature 403: 410-414.

Wark K. and Warner C.F. 1976. Air pollution: It's origin and control. Harper and Row, New York.

White J.R. and Gubala C.P. 1990. Sequentially extracted metals in Adirondack lake. Environmental Science and Technology 21: 211-216.

Whiticar M.J., Faber E. and Schoell M. 1986. Biogenic methane formation in marine and freshwater environments: $CO_2$ reduction vs. acetate fermentation- Isotopic evidnece. Geochimica et Cosmochimica Acta 50: 693-709.

Wik M. and Renberg I. 1991. Spheroidal carbonaceous particles as a marker for recent sediment distribution. Hydrobiologia 214: 85-90.

Wolfe B.B., Edwards T.W.D., Elgood R.J. and Beuning K.R.M. 2001. Carbon and oxygen isotope analysis of lake sediments. In: W. M. Last and J. P. Smol (eds.), Tracking environmental change using lake sediments: Physical and chemical Techniques. Kluwer Academic Publishers., Dordrecht.

Wu Y., Wang S., Xia W. and Liu J. 2005. Dating recent lake sediments using spheroidal carbonaceous particle (SCP). Chinese Science Bulletin 50: 1016-1020.

Yang H. and Rose N. 2005. Trace element pollution records in some UK lake sediments, their history, influence factors and regional differences. Environment International: 63-75.

# CHAPTER 3. Contemporary hydrology and limnology of the Long Gang Volcanic Field

## 3.1. Introduction

As outlined at the end of Chapter 2 contemporary analyses can improve the knowledge of modern day processes, providing valuable knowledge for palaeoreconstructions. Before a better understanding of palaeoenvironmental records derived from lacustrine sediments can be gained it is important to understand mechanisms that produce variation in isotope values of modern surface waters (Diefendorf and Patterson 2005). These data are very important for isotope reconstructions as they act as end members of contemporary isotopic compositions. For example, contemporary $\delta^{13}C_{(TDIC)}$ composition provides information on both the form of carbon used within the lake for photosynthesis and proportion of sources of carbon from catchments to the lakes. Furthermore, contemporary information on diatom assemblages from both littoral zones (e.g. epiphytes) and the central zone (e.g. diatom traps) of Lake Xiaolongwan (XLW) are of great importance in discussing issues of taphonomy and introductions of species through time (e.g. downcore) compared to the present.

Within the context of this project, contemporary analyses would have been conducted at both locations. However, due to funding limitations it was not possible to visit Lake Arachlei, to collect contemporary data. There are no published data available on present diatom communities in the lake or on the isotopic composition of the contemporary waters for any comments to be made on the site. As a result, this chapter only focuses on data collected from the NE China sites.

To begin, an introduction to the lake catchment characteristics of Lake Xiaolongwan will be given, discussing the limnology and vegetation community of the lake, acting as a context for the palaeoreconstruction in Chapter 5. This chapter will then focus on the contemporary regional climate and lake hydrology for lakes sampled in NE China. Contemporary climate, based on meteorological data, will be displayed and discussed in relation to the wider context of regional climatic processes. Furthermore, the modern day limnology of the Long Gang Volcanic Field (LGVF) and reservoir lakes will be discussed and the features of their catchment's outlined. Further to discussing the contemporary isotopic composition of precipitation, data will also be presented on the present day isotopic composition of lake waters ($\delta^{18}O$, $\delta D$, $\delta^{13}C$), catchment soils ($\delta^{13}C$, C/N) and vegetation ($\delta^{13}C$, C/N) for the LGVF lakes and the neighbouring reservoirs sampled. The data will be interpreted within the relevant sections although a brief discussion will be provided at the end to summarise the main trends before drawing conclusions on the Chapter.

## 3.2. Fieldwork methodology

### 3.2.1. Contemporary sampling from lake Xiaolongwan

All sampling sites discussed in this section were marked by the use of an e-Trex global positioning device (GPS). Refer to Table 3.1 for site names and codes. Three 25 ml (for $\delta^{18}O$ and $\delta D$ analyses) and three 100 ml (for $\delta^{13}C_{TDIC}$) water samples were collected in acid washed bottles from each of the 13 sites (Figure 3.2 and Figure 3.3). One of each was collected from the central regions of lakes (or in the case of the larger reservoirs, from one of the main basins). A hand held Plastimo echosounder was used in order to locate the deepest part of the lake basin. The remaining samples were collected from the littoral regions of each lake, although where present, a spring, inflow and/or an outflow was also sampled.

Three 500 ml acid washed bottles were also used to collect samples for measurement of pH, total phosphorus, nitrate, alkalinity and conductivity from each of the sites. For the deeper lakes (DALO, DONG, ERLO, SANJ, SIHAI) and the site XLW, a sample was collected from the central surface waters. pH was analysed immediately in the field on filtered samples with a Hi8424 pH meter (Hanna instrument). Alkalinity was later measured by Gran titration using the same device on return to Beijing. All bottles were sealed under the water surface, lids wrapped with Parafilm and then sealed with electrical tape. Samples were stored in a dark cool box (<4°C) before shipping back to the UK.

Around 2 g of soil sediment was collected from each lake catchment, from < 10 cm depth. A collection of the most representative vegetation (leaves) from each catchment was also sampled to act as end members of carbon content to compare with downcore $\delta^{13}C$ analyses. Both soil and vegetation samples were stored in a dark and cold (<4°C) environment until further analyses were conducted on return to the UK.

Six contemporary diatom samples were collected from the littoral margins of the lake XLW from dominant littoral macrophytes (*Equisetum, Phragmites, Typha* and *Trapa natans)*. A few drops of Lugol's iodine were added for preservation and the Sterilin® tubes used were sealed with electrical tape and stored in a dark cool box.

### 3.2.2. Diatom traps

These methods were conducted by Drs. Chu Guoqiang and Patrick Rioual (Chinese Academy of Sciences; CAS) and only for Lake Xiaolongwan. Cylindrical sediment traps were built according to the recommendations of Blomqvist and Håkanson (1981) and Håkanson and Jansson (1983). The sediment trap consisted of three individual, non-transparent, polyethylene tubes (diameter: 15 cm, height: 78 cm) (Chu et al. 2005). The trap site is shown in Figure 3.2.

Chu et al (2008) detail that after settling for 38 hours and removing the excess water, the residues were freeze dried. No preservatives were added. The traps were collected monthly from August 2003 to November 2003 then left under ice-cover from November 2003 to April 2004.

Dinoflagellate analyses were conducted by Chu et al (2008) for the purpose of varve counting (refer to Chapter 4). For this study the diatom species were identified to provide a contemporary context of different species blooms and abundances throughout the year, which are of significance in diatom reconstructions and subsequent interpretation. Discussion of these results and their interpretation will be given in detail in Section 3.5.

### 3.2.3. Water chemistry analyses

Water chemistry analyses were only conducted on the contemporary samples collected from the Long Gang Volcanic fieldwork. Methods adopted for total phosphorous (TP) determination described below follow those outlined in Washbourne (2003). To each water sample (10 ml) a drop of concentrated HCl (5.6 N) was added so that pH dropped to 1. Then 0.25 ml of potassium persulfate (0.05 g/ml) was added to each sample and well mixed in a vortex after which they were tightly capped with a Teflon lined phenolic cap and placed into an autoclave at 105 $^{o}$C for 90 minutes.

A standard stock solution was made by adding dried $KH_2PO_4$ (1.36 g) to a one litre volumetric flask of distilled water. A series of dilutions derived from this stock solution were made. 2 reagents were also made, the first a 100 ml solution of 35 ml sulphuric acid solution to 50 ml of 10 g/50 ml ascorbic acid solution and distilled water. The second reagent was a 50 ml solution made from 35 ml of sulphuric acid solution to 12.5 ml of ammonium heptamolybdate tetrahydrate solution and 2 ml of potassium antimonyl tartrate solution. After digestion of the standards and samples, 200 μl of reagent 1 was added to each standard and well mixed. Reagent 2 was then added to each standard, mixed and left for colour to develop. Standards were run on the spectrometer at 885 nm to detect TP concentrations. These standards were used to develop a standard curve. Samples were run in the same way as the standards. Samples were run twice as were standards. The digested blanks were also run after every 10 samples in order to act as a control.

Total Nitrogen (TN) was analysed by Dr. Patrick Rioual (CAS) following the methodology outline in Bronk et al (2000) and data provided for the purpose of this thesis.

### 3.2.4. Isotope methodology

All isotopic analyses were conducted at NERC Isotope Geosciences Laboratory, Keyworth. The following techniques were only adopted for the contemporary samples from the Long Gang Volcanic field. Water samples collected for measuring total dissolved inorganic carbon (TDIC)

were precipitated using 30ml of barium chloride ($BaCl_2$) added to each sample. Samples were left overnight for the crystals to grow, after which they were washed 4 times with de-ionised water through silica filter papers. Once clean, samples were dried and reacted with anhydrous phosphoric acid in vacuum overnight, at a constant 25°C (McCrea 1950). Measurements of the evolved $CO_2$ were made on a VG Optima mass spectrometer. Isotopic results for carbonates from TDIC are reported in the $\delta^{13}C$ notation in per mil (‰) versus the international Vienna Pee Dee Belemnite (VPDB) standard based on calibration of the laboratory standards against NBS-18 and NBS-19. Analytical reproducibility is normally better than 0.1‰ (2 sigma) for the TDIC.

Water samples collected for $^{18}O/^{16}O$ analyses were equilibrated with $CO_2$ using an ISOPREP 18 device. Mass spectrometry was performed on a VG SIRA (Zn $\delta^2H$ and $\delta^{18}O$) and MICROMASS IsoPrime (Cr $\delta^2H$) in conjunction with laboratory standards calibrated against NBS standards. Results are reported in the usual notation in per mil (‰) versus V-SMOW. Analytical errors are estimated as 0.5‰ for $\delta^{18}O$, 2‰ for $\delta^2H$ and 1‰ (Zn) for $\delta^2H$ (Cr).

## 3.3. Regional climate of NE China

This section presents data from the nearest GNIP station to Lake Xiaolongwan, at Changchun (refer to Figure 1.2).

### 3.3.1. Temperature and precipitation at Changchun

Changchun is a meterological station located to the north-west of the Long Gang Volcanic Field (refer to Figure 3.1). Isotopic, precipitation and temperature data are available for this site from the ISOHIS website and presented here.

Mean annual temperature for the region, based on the data above, is +5.9°C, with temperatures falling below a mean monthly value of 0°C from November to the end of March (Figure 3.1). The rain between the monsoon peak months (June, July, August) is greater than the rest of the year at 63, 78 and 157 mm respectively. Total mean precipitation for the years 1999-2001 inclusive was 444 mm. Based on the data displayed above, highest mean precipitation is seen in August, lowest in February (2 mm), highest mean temperatures are in July (+25.5°C) and lowest in January (−16.7°C). Mean temperatures for the coldest month, December, are −16.7°C.

### 3.3.2. Isotopic composition of precipitation at Changchun

The isotopic composition of rainfall from Changchun shows a seasonal variation throughout the year (Figure 3.1). During November, January, February and March, $\delta^{18}O$ weighted mean values are lower than the remainder of the year at −10.2‰, −19.5‰, −16.9‰ and −12.2‰ respectively. Although values are not available for December, it is assumed that data would follow this trend as the presence of lower isotopic values corresponds with the fall in precipitation and presence of cold temperatures (Figure 3.1). For the remainder of the year, $\delta^{18}O$ values fluctuate between

−9.4‰ and +3.6‰. δD demonstrates a similar trend as the $\delta^{18}O$ data for Changchun. Once again, with lower values seen during the winter months in the region (November to February inclusive) after which values are higher. The highest δD is again seen for the months July and August, a reflection of the increased temperatures at this time.

There is a clear seasonal variation of precipitation amount across north east China as shown by the monitoring data from Changchun. Results show that precipitation during winter months has lower $\delta^{18}O$ and δD values than summer precipitation. This is a result of the change in wind direction, source of precipitation and temperatures associated with the EAWM (refer to Chapter 1.4). During winter months the prevailing wind direction to north eastern China originates from the north west. Strength and penetration of these winds is associated with intensity of the Siberian High. The continentality of this region, with very low temperatures and precipitation (mainly snow or hail), results in the low $\delta^{18}O$ and δD.

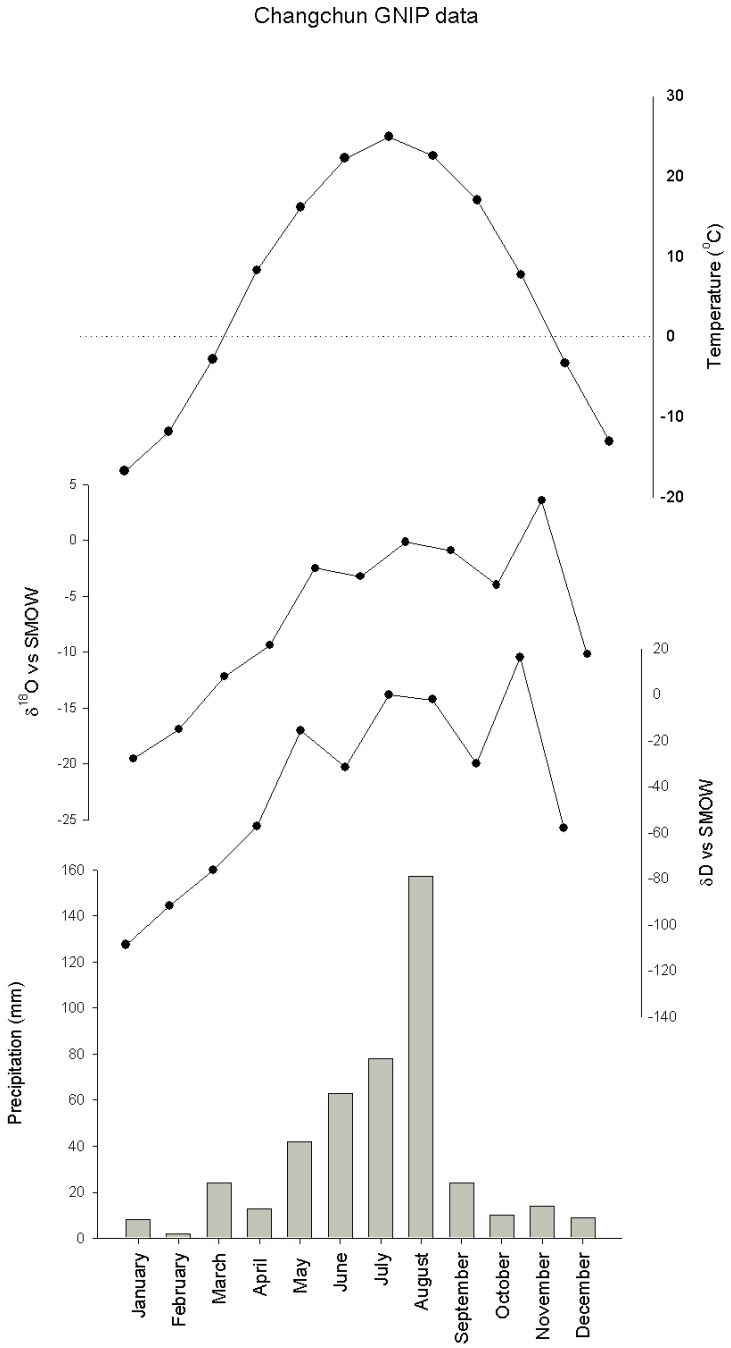


*Figure 3.1. Monthly mean temperature (°C), mean precipitation (mm), weighted monthly mean δD (‰), weighted monthly mean $\delta^{18}O$ (‰) at Changchun for the years 1999 - 2001 (refer to Figure 3.2A for location). Please note that the $\delta^{18}O$ and δD weighted means are missing for the month December. Data from IAEA/WMO (2006).*

During summer months, however, the EASM dominates, bringing the moist, warmer air from south east China. Due to the shorter transport distance and warmer temperatures, the $\delta^{18}O$ and $\delta D$ values of precipitation are higher, compared to the westerly cold, continental air prevailing in winter months. In this case, during summer months the $\delta^{18}O$ and $\delta D$ of rainfall is lower (Ye et al. 2007; Zhenlong and Xiangyang 2008). As the greatest amount of precipitation falls here within the summer months the location of the weighted average annual precipitation plots close to the summer samples.

## 3.4. Present day limnology of lakes

Lake Xiaolongwan (XLW) is one of the 8 maar (low relief volcanic crater lake) lakes present in the LGVF, Jilin Province, NE China (Figure 3.2). Along with the Long Gang lakes, five more reservoir lakes were also sampled from the surrounding region, for the purpose of this project. The location of these sites, in relation to the LGVF can be seen in Figure 3.3. The main catchment characteristics of the 8 Long Gang lakes is shown in Table 3.1 (Mingram et al. 2004). Unfortunately, there is no published information on the reservoirs.

| Lake name | Location | Elevation (m.a.s.l.) | Lake area ($km^2$) | Catchment area ($km^2$) | Max water depth (m) | Rim height (m) |
|---|---|---|---|---|---|---|
| Dalongwan (DALO) | 42°20'N, 126°22'E | 635 | 0.8 | 1.0 | 85 | 20 |
| Donglongwan (DONG) | 42°26'N, 126°31'E | 599 | 0.4 | 0.5 | 127 | 50 |
| Erlongwan (ERLO) | 42°18'N, 126°21'E | 724 | 0.3 | 0.4 | 36 | 30 |
| Longwan (LONG) | 42°25'N, 126°36'E | 618 | 0.85 | 1.0 | 115 | 10 |
| Nanlongwan (NANG) | 42°25'N, 126°28'E | 655 | 0.3 | 2.0 | 69 | 20 |
| Sanjialongwan (SANJ) | 42°22'N, 126°25'E | 730 | 0.7 | 0.9 | 76 | 40 |
| Sihailongwan (SIHAI) | 42°17'N, 126°36'E | 797 | 0.5 | 0.7 | 50 | 20 |
| Xiaolongwan (XLW) | 42°18'N, 126°19'E | 655 | 0.1 | 0.15 | 15 | 20 |

*Table 3.1. The main catchment and lake characteristics for the 8 crater lakes in the LGVF, from Mingram et al (2004).*

The geology of the lake region is complex (Figure 3.2), mostly composed of alkali basaltic rocks of Quaternary age (Liu et al. 2009). Covering around 1700 $km^2$ of this is the upper Archaen volcanic basement (Figure 3.2) (Chu et al. 2008; Liu et al. 2009). The main difference between the Long Gang and reservoir lakes is based on the change in this geology, with the volcanic lakes located on the Archean basement. However, not all of the Long Gang lakes are located within this more recently deposited geology (including SANG, NANG, LONG; Figure 3.2). Carbonate rocks do not occur in this region.

Other differences between the two groups of lakes (e.g. Long Gang and reservoirs) include the presence of inflows and outflows. Some reservoirs had an inflow and outflow, in particular QING has a spring inflow, LWXH and JIAN both have outflows. All of these waters were sampled and discussed in Section 3.6. The Long Gang lakes are all natural and closed systems.

The context of such differences between the different lakes will be discussed in this chapter with reference to the contemporary isotopic composition of lake waters.

### 3.4.1. Lake water chemistry

Table 3.1 shows the lake sampling locations, site altitudes and lake water characteristics of the 13 sites visited in August 2007. The lakes vary between 300 and c. 750 m.a.s.l (as measured based on barometric pressure) with pH varying between 6.4 and 8.6 units. Other lake characteristics show that surface water temperatures (at the time of sampling) were between c. +22 and +27°C and secchi disk depths between 0.3 – 0.85 m for the reservoirs and c. 6 – 8 m for the Long Gang lakes. The reservoirs are the shallowest of the 13 lakes, varying in depth from 3.7 – 6.6 m while the Long Gang lakes are deeper, varying between 16 and 105 m in depth.

DALO has the highest alkalinity of the 13 lakes sampled (2743 mEq/l) while ERLO has the lowest (265 mEq/l). In the case of conductivity, HUAN has the highest values at 415.5 µS at the surface while ERLO also has the lowest values at 38.5 µS at the surface of the water. For TP however, it is the reservoir JIAN that has the highest values (171.1 µg/l) as do all of the reservoirs compared to the Long Gang lakes and DALO has the lowest values at the surface (1.1 µg/l). Again the values of TP increase when depth down the water column increases (based on profiling data), although this is not the case for SIHAI. TN values are generally highest for the resevoir lakes HUAN, JIAN and LWXH. Lake LONG however has the highest values at 2208 µg/l and SIHAI the fourth highest at 1013 µg/l.

DOC values are the highest for XLW (12.3 mg/l) while the remaining of the lakes are below 10 mg/l, apart from the resevoir (LWXH). Interestingly, XLW has the lowest, or among the lowest, values for the remaining lake water chemistry (Cl, $NO_3$, $SO_4$, Mg, Na). The resevoirs have the highest values generally for many parameters, although in particular $SO_4$ values, DOC values (besides XLW) and Si values (besides lake DALO).

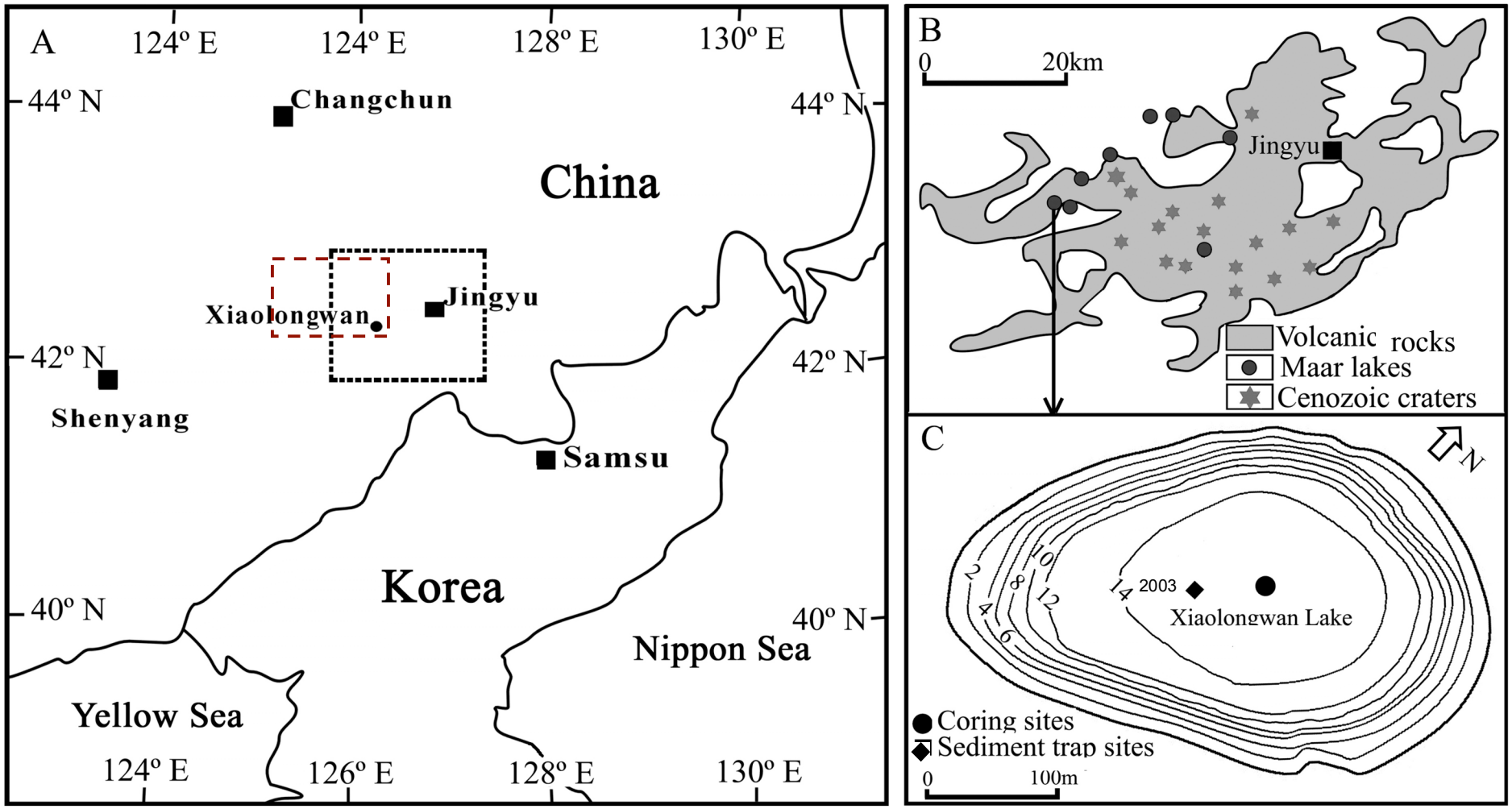


*Figure 3.2(A) The location (black dotted line) of the LGVF in NE China. The red dashed line corresponds to the area shown in Figure 3.2 (B) location of the LGVF lakes and their dominant geology of the upper Archaen basement, (C) the XLW lake basin. Lake bathymetry in meters is also shown. The location of core collection in 2007 is shown and the diamond corresponds to the location of the 2003 diatom trap, which was analysed for the purpose of this project. Image taken from (Chu et al. 2008).*

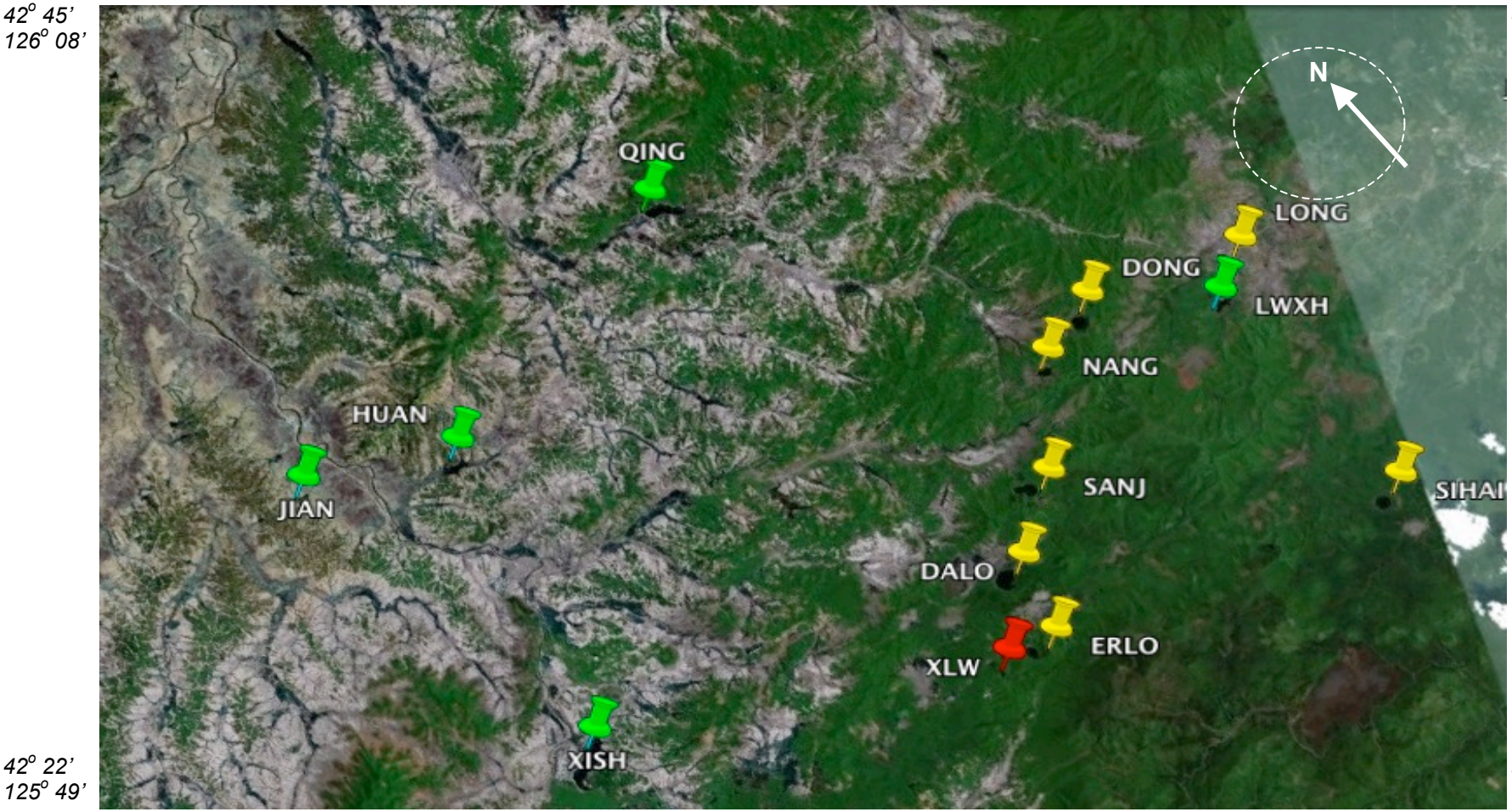


*Figure 3.3 Location map of lakes sampled for the purpose of this study. The seven LGVF lakes are displayed in yellow, five reservoir lakes in green. Lake XLW is outlined by a red point. Longitude and latitude are also shown. (Google 2010).*

| | Xiaolongwan (XLW) | Dalongwan (DALO) | Donglonwan (DONG) | Erlongwan (ERLO) | Longquan (LONG) | Nanlongwan (NANG) | Sanjialongwan (SANJ) | Sihailongwan (SIHAI) | Huangnihe shuiku (HUAN) | Jiangjiajie shuiku (JIAN) | Longwan Xihu (LWXH) | Qingdingzi Shiku (QING) | Xiaoqishan Shiku (XISH) |
|---|---|---|---|---|---|---|---|---|---|---|---|---|---|
| Sampling location at central region of lake (for following analyses) | 42° 17'59.8"N | 42° 20.281'N | 42° 27.753'N | 42° 18.136'N | 42° 25.015'N | 42° 24.859'N | 42° 21.975'N | 42° 17.149'N | 42° 30.172'N | 42° 31.32'N | 42° 24.173'N | 42° 33.838'N | 42° 21.569'N |
| | 126° 21'34.3"E | 126° 23.458'E | 126° 30.631'E | 126° 22.820'E | 126° 36.150'E | 126° 28.549'E | 126° 25.863'E | 126° 36'.171'E | 126° 9.267'E | 126° 4.20'E | 126° 35.355'E | 126° 20.425'E | 126° 8.092'E |
| Max measured depth | 16.2 | 79.0 | 27.1 | 35.5 | 105.0 | 67.4 | 39.0 | 51.3 | 3.7 | - | 6.6 | 6.3 | - |
| pH | 6.7 | 8.6 | 8.1 | 6.9 | 7.4 | 8.3 | 7.7 | 7.4 | 7.2 | 6.4 | 7.1 | 7.5 | 7.7 |
| Water surface temperature (°C) | +22.3 | +24.6 | - | +23.4 | +23.2 | +26.0 | +22.4 | +23.4 | +26.9 | - | +24.7 | +25.6 | +25.5 |
| Secchi depth (m) | 2.6 | 8.1 | 7.8 | 6.1 | 2.6 but low light | 7.7 | 7 | 7.6 | 0.3 | - | 0.9 | 0.6 | 0.7 |
| Alkalinity (mEq/l) | 387.7 | 2743.9 | 1120.4 | 264.7 | 668.1 | 1280.5 | 699.5 | 420 | 3365.3 | 578.7 | 1008.4 | 1257.2 | 1268.2 |
| Conductivity (µS) | 51.6 | 238.5 | 113.9 | 38.5 | 77.8 | 134.2 | 71.4 | 55.6 | 425 | 97.6 | 95.0 | 146.7 | 143.7 |
| TP (µg/l) | 3.9 | 1.1 | 8.8 | 11.1 | 15.9 | 6.0 | 3.9 | 6.2 | 102.8 | 171.1 | 62.2 | 60.9 | 60.5 |
| TN (µg/l) | 784 | 331 | 599 | 471 | 2208 | 503 | 200 | 1013 | 1663 | 1235 | 955 | 451 | 394 |
| DOC (mg/l) | 12.3 | 5.2 | 2.6 | 3.1 | 6.3 | 3.5 | 2.5 | 4.2 | 7.7 | 9.3 | 11.4 | 7.5 | 7.3 |
| Cl (mg/l) | 1.0 | 3.5 | 1.9 | 1.1 | 1.3 | 1.7 | 1.4 | 3.0 | 16.8 | 6.1 | 2.0 | 4.4 | 3.1 |
| $NO_3$ (mg/l) | 0.0 | 0.4 | 1.0 | 0.3 | 0.04 | 1.4 | 0.1 | 0.0 | 1.5 | 0.4 | 0.1 | 0.1 | 0.2 |
| $SO_4$ (mg/l) | 3.1 | 9.9 | 4.6 | 4.7 | 4.1 | 5.7 | 3.9 | 4.2 | 57.1 | 8.3 | 5.5 | 9.4 | 9.2 |
| Ca (mg/l) | 8.2 | 15.6 | 15.6 | 5.4 | 10.7 | 20.0 | 7.9 | 7.1 | 44.8 | 11.4 | 17.2 | 2536 | 13.1 |
| K (mg/l) | 2.6 | 8.5 | 4.3 | 2.0 | 2.6 | 4.7 | 3.4 | 4.4 | 5.9 | 2.5 | 2.9 | 2.9 | 3.6 |
| Mg (mg/l) | 1.8 | 23.2 | 3.6 | 1.8 | 4.6 | 5.9 | 3.0 | 2.9 | 23.9 | 3.4 | 6.4 | 6.2 | 12.3 |
| Na (mg/l) | 1.4 | 14.3 | 10.2 | 1.6 | 3.3 | 8.7 | 5.9 | 3.1 | 31.6 | 6.1 | 4.4 | 5.2 | 6.8 |
| Si (mg/l) | 0.3 | 0.5 | 4.2 | 0.1 | 0.2 | 0.2 | 0.2 | 0.05 | 2.2 | 2.8 | 2.1 | 3.2 | 3.3 |

*Table3.2. Total alkalinity, conductivity and total phosphorous (TP) for the 13 sites (August 2007). Lakes considered as oligotrophic (based on TP) are shaded white, mesotrophic shaded in pale orange and eutrophic in dark orange. Other chemical parameters measured are also shown including dissolved organic carbon (DOC), chloride ions (Cl), nitrates (NO3), sulphates (SO4), calcium ion (Ca), potassium ions (K), magnesium ions (Mg), sodium ions (Na) and silica (Si). Water temperature, pH, secchi disk depth and samples collected for contemporary isotope analyses are also shown. The first lake is XLW. The 8 LGVF lakes are shown in white and the 5 reservoirs in grey.*

## 3.5. Lake Xiaolongwan

### 3.5.1. Characteristics of Lake Xiaolongwan

Lake Xiaolongwan itself is the smallest of the 8 lakes in the LGVF (maximum water depth 16.2 m in August 2007, area of 0.1 $km^2$) and is a closed basin (Table 3.1). The catchment of XLW is covered with typical broadleaf (predominantly *Betula costata; $C_3$*) and mixed conifer vegetation (Figures 3.4a,b).

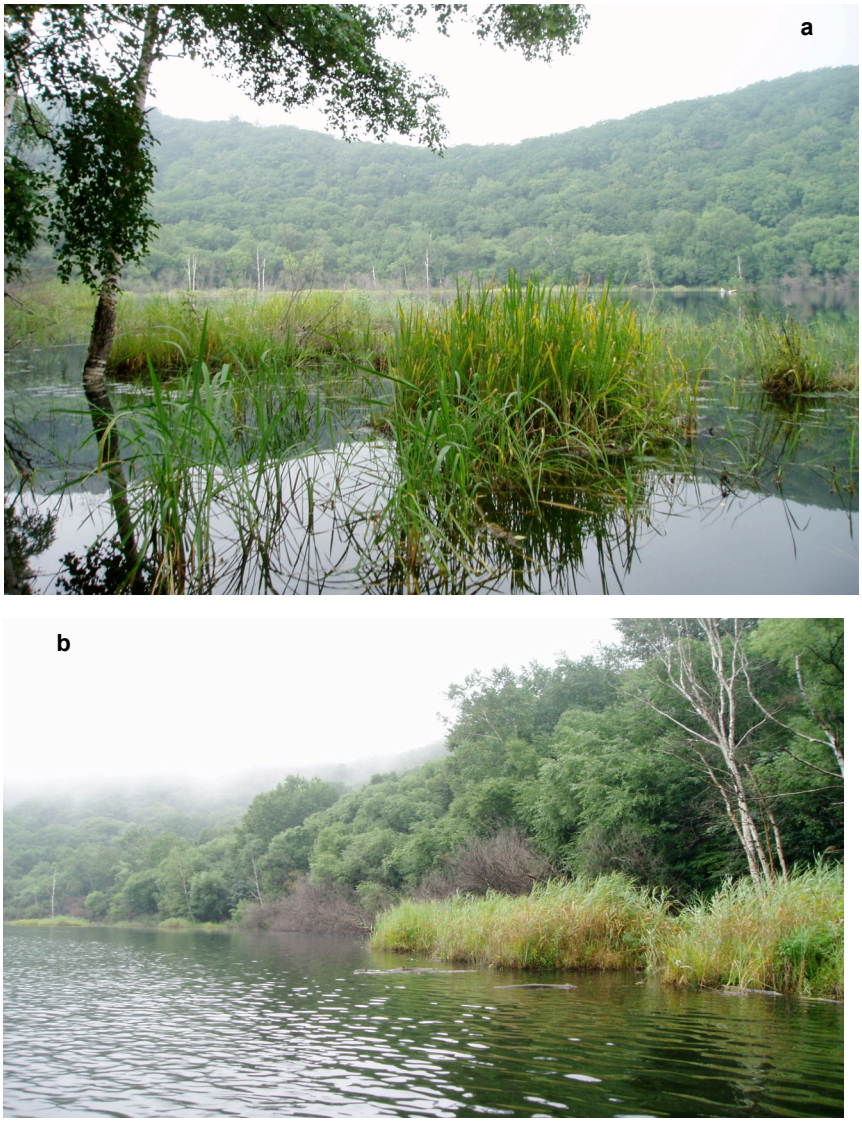


*Figure 3.4. Photographs of Lake Xiaolongwan taken in August 2007 during summer fieldwork. a)Dominant emergent vegetation (Phragmites; $C_3$) and vegetation seen as looking along the western shore; b) and as looking along the south western shore from the launching site including Phragmites and Typha ($C_3$) emergents.*

Current climatic conditions, discussed earlier in this chapter (Figure 3.1) affect the limnology of XLW, which is dimictic with a period of ice cover between November and April when regional temperatures are at their lowest (Figure 3.5).

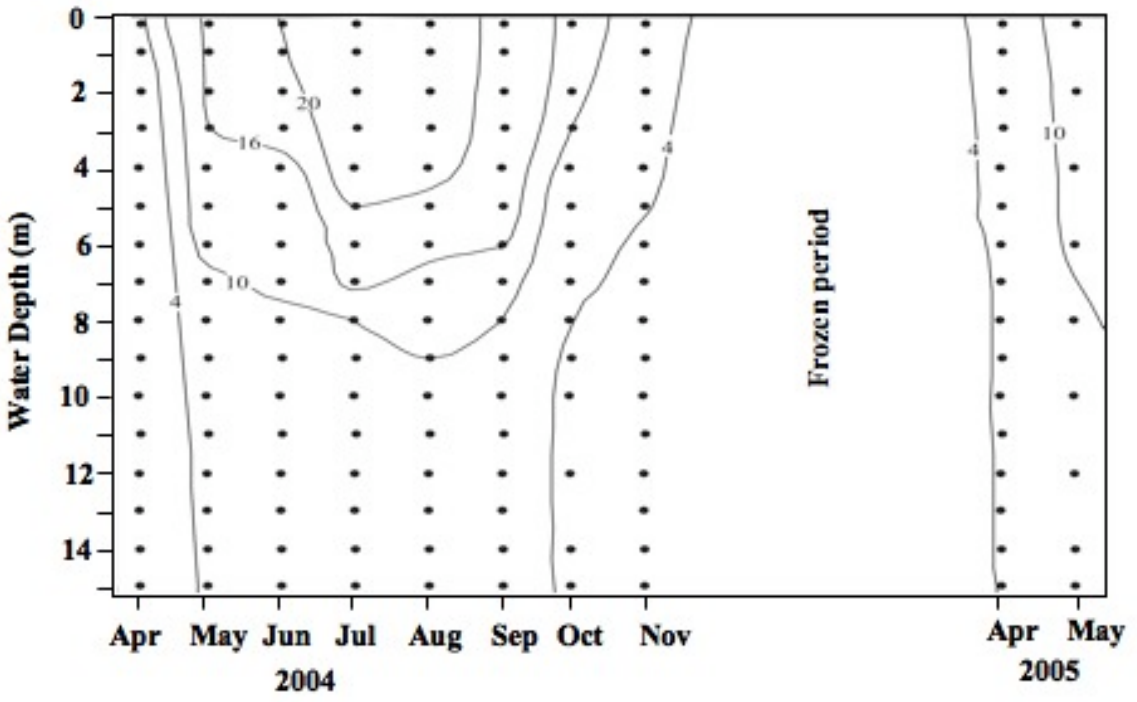


*Figure 3.5. Variation in lake water temperatures (°C) at the different depths of XLW demonstrating the changing stratification of the lake for the year April 2004 to May 2005. (From Chu pers. comm.).*

There are two periods of overturn in spring (April-May) and autumn (late September to October). A period of lake stratification occurs between May and mid September. Data shows that different diatom species blooms are associated with spring and autumn overturn (Figure 3.6). An understanding of this relationship is of importance for the interpretation of past diatom species abundances down core.

### 3.5.2. Contemporary sediment trap data

Figure 3.6 shows the seasonal changes in diatom community structure at Lake Xiaolongwan (refer to Figure 3.2 for trap location) (analyses conducted by Dr. Patrick Rioual). *Discotella woltereckii, Achnanthidium minutissimum* and *Encyonopsis subminuta* were the dominant species found in the trap between August 2003 and November 2004. During the period of summer stratification in 2003 these three species, as well as *Brachysira neoexilis,* were the most abundant. Overall, the percentage of planktonic species decline while the percentage of benthic species increased, between August 2003 and October 2003. With turnover, after summer stratification, the abundances of chrysophyte stomatocysts increased also.

During ice cover trap collection was not conducted and therefore no samples were counted. However, on ice out in April 2004 (and spring overturn) planktonic species were the most abundant within the diatom assemblage. This corresponds in particular to *Puncticulata praetermissa* and *D. woltereckii.* With the onset of lake stratification in May 2004 percentage planktonic species fall and benthic concentrations increased, in particular an increase was seen in *A. minutissimum* and later *E. subminuta* and *B. neoexilis.* Between July and September concentrations of benthic, planktonic and stomatocysts all declined only to increase once more with autumn turnover in October, when there was an increase in *D. woltereckii, Fragilaria cf. nanoides* and *A. minutissimum.*

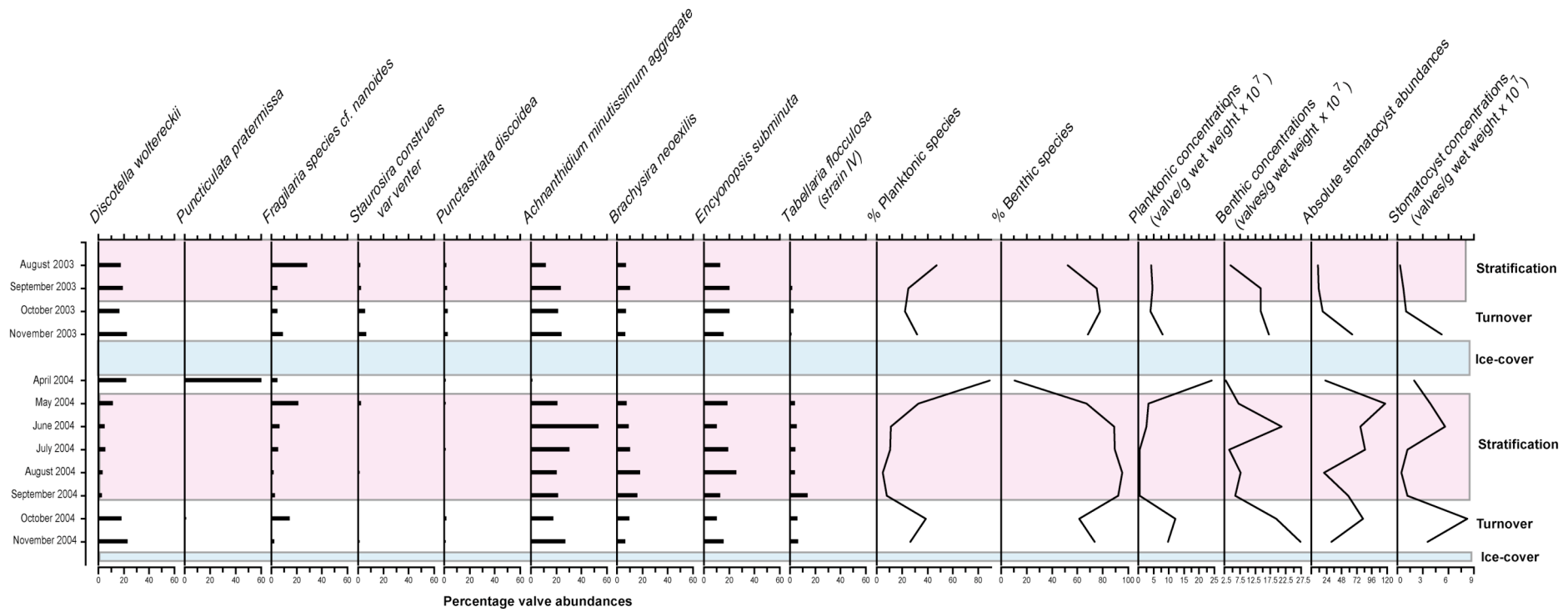


*Figure 3.6. Contemporary diatom communities from Lake Xiaolongwan based on sediment trap data collected between August 2003 and November 2004. Dominant species counted are shown as well as % planktonic, % benthic species, planktonic concentrations, benthic concentrations. Chrysophyte stomatocycsts relative abundances and concentrations are also shown. Periods of lake stratification (pink), ice cover (blue) and turnover (white) are also displayed. All analyses were conducted by Dr. Patrick Rioual.*

### 3.5.3. Epiphytic diatom assemblage

Figure 3.7 shows the epiphytic diatom sampling conducted during fieldwork in August 2007. Only the dominant species are shown here, of which *B. neoexilis* is the most abundant at the sites. The sites 1 to 6 are different littoral plants around Lake Xiaolongwan and they are identified in Table 3.3.

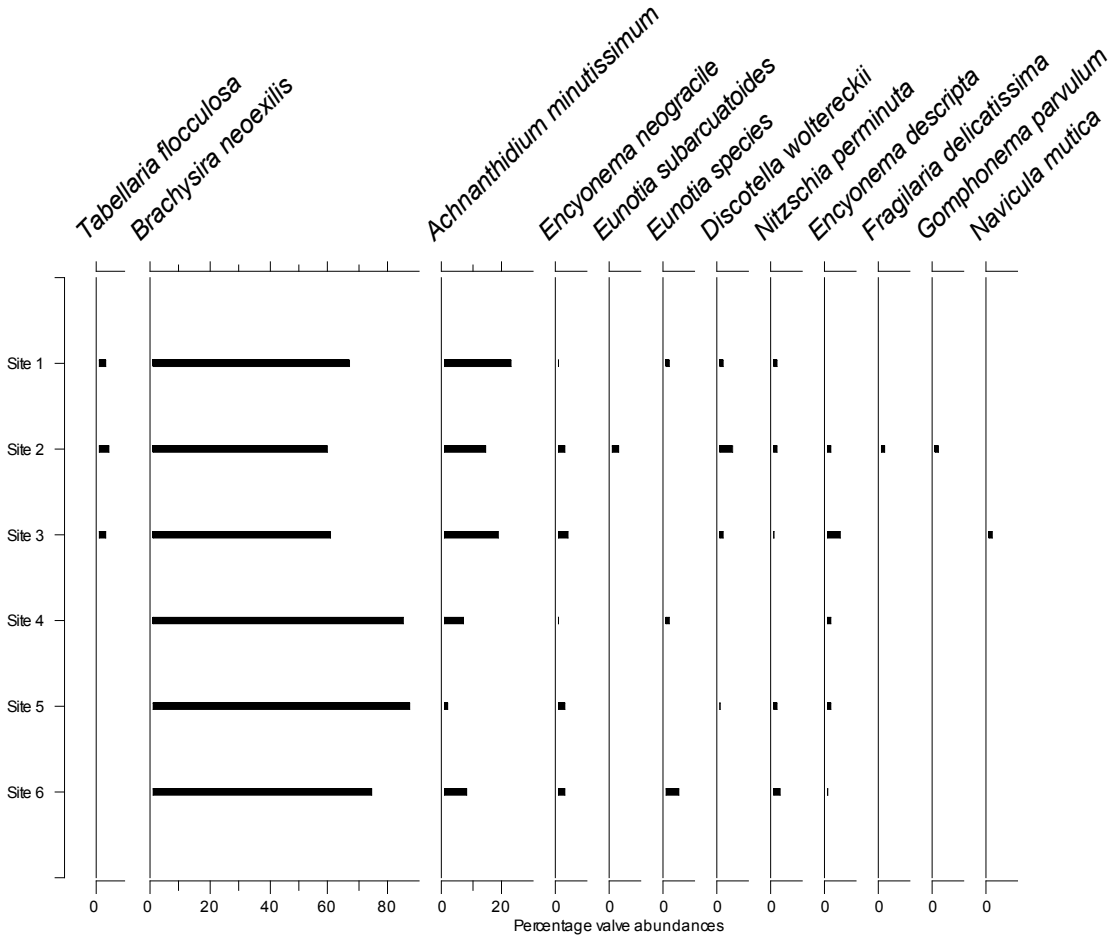


*Figure 3.7. Dominant contemporary epiphytic diatom species. Table 3.2 below lists the species that were sampled at each site. Sampling was conducted in August 2007.*

| Site Number | Longitude | Latitude | Macrophyte Name |
|---|---|---|---|
| 1 | 42° 18'00.9" N | 126 ° 21'35.3" E | *Equisetum* spp. |
| 2 | 42 ° 17'56.3" N | 126 ° 21'32.5" E | *Phragmites* spp. |
| 3 | " | " | *Phragmites australis* |
| 4 | " | " | *Typha* spp. |
| 5 | 42 ° 18'03.0" N | 126 ° 21'33.0" E | *Utricularia* spp. |
| 6 | 42 ° 18'03.2" N | 126 ° 21'35.8" E | *Trapa natans* |

*Table 3.3 Summary of the location and name of macrophytes sampled for epiphytic diatom communities during August 2007 fieldwork. All macrophytes have the $C_3$ photosynthetic pathway.*

Results from the contemporary epiphyte sampling shows that the diatom communities from the dominant vegetation sampled are very similar (Figure 3.7). *B. neoexilis* is found in high percentage abundances upon all plant macrophytes sampled, with values *c.* 80% for *Typha* and *Utricularia*. *A. minutissimum* is found in higher abundances on *Phragmites* and *Equisetum* macrophytes, in particular the former, while *Tabellaria flocculosa* is only found on *Phragmites* and *Equisetum*. *Phragmites australis* and *Typha spp.* can form dense stands in littoral regions of lakes of deeper water, which is consistent with the steep lake shelf of XLW as displayed in Figure 3.2c (Preston and Croft 1997). Examination of macrophytes during fieldwork also supports this argument with large macrophyte communities, floating, in littoral regions. *Trapa natans* is abundant in lakes which are nutrient rich, although circumneutral (c. pH 6.7-7.3) (Methe et al. 1993) consistent with present day limnology at XLW (Table 3.2).

When comparing epiphytic sampling and trap data, the presence of *B. neoexilis,* abundant on epiphytes, is also represented in the trap data and therefore central regions of the lake. This shows that the presence of the species in trap data is indeed a representation of littoral and epiphytic assemblages. It can be argued therefore that there are limited issues with taphonomy at the lake. *A. minutissimum* and *D. woltereckii* from epiphytic assemblages are also seen in trap data. As *D. woltereckii* is more abundant in the trap data it is assumed to represent a plankton assemblage here (Rioual pers. comm.) rather than epiphytic assemblages, where its abundances are much lower. The epiphytic taxa e.g. *A. minutissimum* at Lake Xiaolongwan are generally at their most abundant in the sediment trap in autumn periods when macrophytes are transported to the central regions of the lake with wind transport (the east Asian winter monsoon) (Rioual pers. comm.). This is also the time of lake turnover and increased wind stress on the lake surface. Macrophytes die at this time so that epiphytic species are deposited in sediments at the central region of the lake and account for these higher abundances. There are also high abundances of epiphytic species in the sediment trap at the end of lake stratification although the mechanisms responsible for this are not yet fully understood (Figure 3.6). Concentrations of planktonic taxa at Lake Xiaolongwan (e.g. *Discotella* and *Puncticulata* species) are more abundant during spring and autumn overturn while have low abundances during summer.

### 3.5.4. Annual lamination formation

Lake Xiaolongwan is a lake with varved sediments. Chu et al (2008) describe in depth the formation of these laminations, on the basis of analyses of sediment trap data and micrographs of cores collected from the central regions of the lake. Laminations from Lake Xiaolongwan are formed of distinct layers of dinocysts, chrysophyte stomatocysts and diatoms. Dinocyst layers are strongly associated with November overturn in the lake, when the dinocyst flux at this time accounts for up to 57% of annual flux in 2004. At this time of year, there are strong winds in the area and therefore lake mixing occurs causing the re-suspension of nutrients from the bottom of the lake and mature dinocysts (ibid.). Diatoms also show a peak in fluxes at this time as well as chrysophytes, although the latter is also shown to peak after ice off in April-May. Chu et al

(2008) argue that on the basis of the strong relationship between dinocysts and November overturn, they can be used for the purpose of lamination counting, later adopted for the chronology of X00/X06. A more detailed description of this method is given in Chu et al (2008). Further information on the chronology, and its associated problems, will be discussed in Chapter 4.

### 3.6. $\delta^{18}O$ and $\delta D$ of contemporary lake waters

These data are useful for understanding the hydrology of the lakes in and surrounding the LGVF, which is essential for palaeoreconstructions. A $\delta^{18}O$ reconstruction was however not carried out for Lake Xiaolongwan due to the absence of carbonates in the system and the known problems with clay contamination when analysing $\delta^{18}O$ from diatom silica (Brewer et al. 2008). The data are therefore used in this thesis to emphasise the sensitivity of these sites to variations in precipitation.

Figures 3.8 and 3.9 show the relationship between $\delta^{18}O$ and $\delta D$ composition of lake waters collected in August 2007. The global meteoric water line (GMWL) and calculated local evaporation line (LEL) are also displayed. Figure 3.8 shows the composition of monthly precipitation collected at Changchun, based on GNIP data. The LMWL is parallel to the LEL, based on theory (as discussed in Section 2.2) the isotope composition of the lake waters is expected to derive from the composition of precipitation in the region, with different lakes composed of waters with varying amounts of evaporative enrichment. Isotopes can be used as a way of assessing the magnitude of evaporation loss where they have been used to estimate the amount of lake water lost via evaporation as a proportion of the annual water budget (e.g. in northern Canada; Gibson et al. 1996).

As discussed in Section 2.2.1 there are a few main assumptions which can be drawn between the relationship between the GMWL, LMWL and LEL in this region of NE China:

1. The LEL should intercept the LMWL close to the point of the weighted average annual precipitation.
2. Spring water should plot close to the weighted average annual precipitation.

As Figure 3.8 shows, these two expectations are not met. Firstly, the LEL intercepts the GMWL before intercepting the LMWL. Should the LEL and LMWL meet on Figure 3.8, it would be where both $\delta^{18}O$ and $\delta D$ are very low. This suggests that the lake waters receive most of their recharge during the coldest months (when the composition of rainfall is isotopically very low).

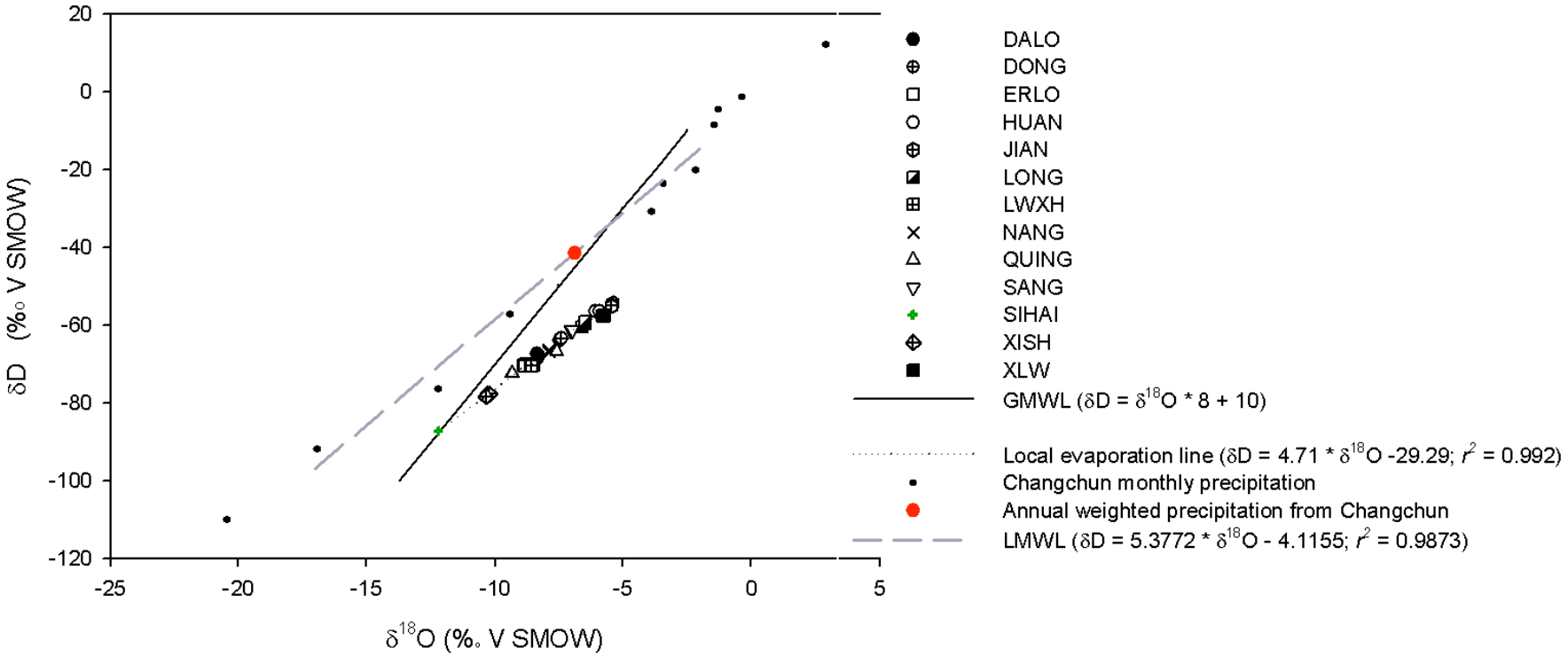


*Figure 3.8 $\delta^{18}O$ and $\delta D$ composition of lake waters. Changchun monthly precipitation values are also displayed along with the weighted annual precipitation composition (red) and local meteoric water line (LMWL). The global meteoric water line (GMWL) and local evaporation line (LEL) for the lakes are shown. A summary composition of these sites (mean of the 3 sampled waters for each site) are given in Table 3.4. Data for the GMWL and LMWL are derived from the IAEA/WMO (IAEA/WMO 2006).*

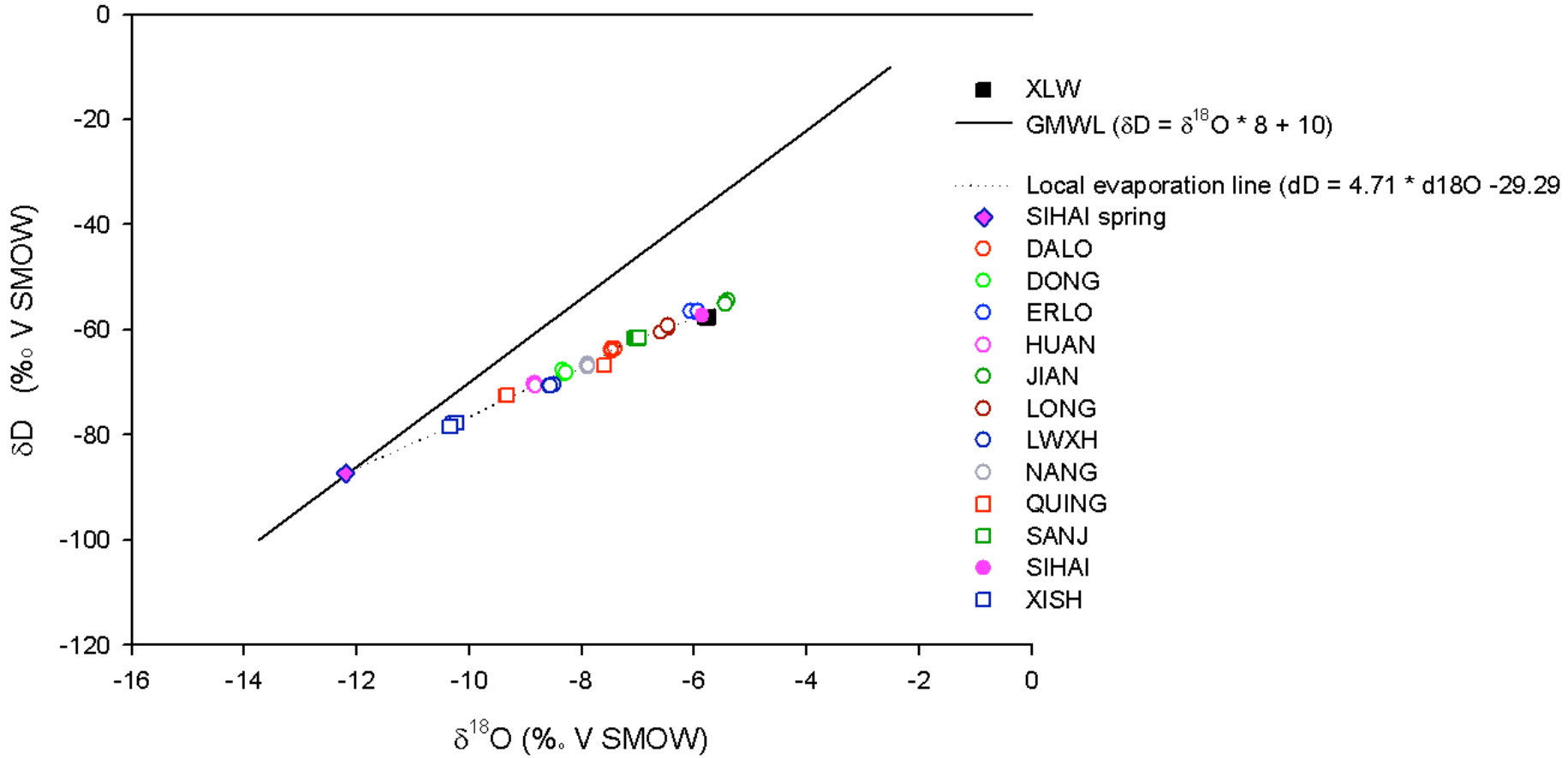


*Figure 3.9. $\delta^{18}O$ vs $\delta D$ of lake waters sampled in August 2007, showing only the LEL and GMWL. Three samples were collected at each site and are displayed, each site in different colours. Values define the local evaporation line (LEL dashed line; $\delta D=4.71*\delta^{18}O$ -29.29; $r^2$ = 0.992). Solid line represents the global meteoric water line (GMWL).Sites are redrawn in colour to make relationship between them clearer. (Agency 2006; Chu et al. 2008).*

A second interpretation could be that the lakes are fed predominantly by groundwaters, which were recharged during colder periods e.g. during the last glacial. However, not all of the lakes sampled in this region are closed basins, for which this hypothesis may hold. When examining Figure 3.9 the four largest of the five reservoirs sampled (see Table 3.4) all plot closest to the GMWL. While the eight LGVF lakes are all closed, these reservoir lakes are artificial so that they have inflows and outflows. They therefore receive a considerable amount of surface run-off from the catchment. Based on theory, it could be argued that they should have a lake water composition closest to the GMWL, and therefore the least evaporative enrichment. As these lakes also do not intercept the LMWL it could be argued that the precipitation data from the ISOHIS website are incorrect.

There are a number of possible factors that can account for the possible inaccuracy of this precipitation data used to create a LMWL. The first possible reason relates to the limited amount of data points collected. The data from Changchun are based over only 3 years (1999-2001 inclusive). In order to obtain a representative sampling of monthly precipitation for the region, ideally an average of more years should be used, particularly as the data are to be compared with isotopic data of the composition of lake waters, which as discussed in Chapter 2.2.2 represent a well mixed isotopic composition of source precipitation. Furthermore, data for the month December are not available for any of the three years, which may also affect the calculation of the LMWL. A second, and possibly more important reason, relates to the laboratory methods used when analysing the isotopic composition of precipitation. When analysing this composition, it is common (and often assumed) that laboratories calibrate at both the higher end and the lower end of the $\delta^{18}O$ and $\delta D$ scales. However, based on the nature of the plot in Figure 3.8 it could well be that this has not been the case (Leng, pers. comm.). Here, the GNIP precipitation data and LMWL are not discussed further and the lake water composition is only discussed in relation to the GMWL.

A summary of the ranking of the different sites, based on their $\delta^{18}O$ composition is shown in Table 3.4. The reservoirs (in particular XISH) plot close to the GMWL (Table 3.4, Figure 3.9), suggesting they contain the least evaporated water. These lakes have both inflows and outflows, have the greatest catchment area and so therefore proportionately receive more catchment inwash compared to the Long Gang lakes. The spring sample collected from SIHAI (Figure 3.9) also plots at the intercept of the LEL with the GMWL, suggesting it represents mean weighted precipitation and that the spring water (and therefore ground water feeding the lakes) is closely allied to modern day precipitation in the region.

| Name of site | Type of lake | $\delta^{18}O$ (‰ V SMOW) | $\delta D$ (‰V SMOW) | Lake area ($km^2$) | Max Lake depth (m) |
|---|---|---|---|---|---|
| JIAN | Reservoir | −5.43 | −54.8 | (smallest) | - |
| XLW | LGVF | −5.76 | −57.6 | 0.1 | 15 |
| ERLO | LGVF | −5.99 | −56.6 | 0.3 | 36 |
| LONG | LGVF | −6.50 | −60.0 | 0.85 | 115 |
| SANJ | LGVF | −7.02 | −61.5 | 0.7 | 76 |
| DALO | LGVF | −7.45 | −63.7 | 0.8 | 85 |
| NANG | LGVF | −7.98 | −66.8 | 0.3 | 69 |
| SIHAI | LGVF | −7.96 | −67.4 | 0.5 | 50 |
| DONG | LGVF | −8.32 | −68.1 | 0.4 | 127 |
| LWXH | Reservoir | −8.54 | −70.6 | ($4^{th}$ largest) | - |
| QUING | Reservoir | −8.76 | −70.6 | ($2^{nd}$ largest) | - |
| HUAN | Reservoir | −8.84 | −70.4 | ($3^{rd}$ largest) | - |
| XISH | Reservoir | −10.28 | −78.0 | (largest) | - |

*Table 3.4. A summary list of the average isotopic composition of contemporary lake waters sampled. The sites are sorted based on $\delta^{18}O$(‰) values (less negative to more negative). $\delta D$ is also shown for each site, again ranked based on the $\delta^{18}O$ composition. In order to look at the relationship between lake characteristics and their isotopic composition, lake area ($km^2$) and depth (m) is also shown (Mingram et al. 2004). Based on looking at the satellite imagery in Figure 3.1 a rough estimate is made of the size of the reservoirs as this data was not measured in the field. The reservoirs are ranked based on this data. "-" refers to the absence of lake depth data.*

The location of the LGVF lake waters along the LEL displays the effect of annual evaporation from these lakes, which all lack surface inflows and outflows (Mingram et al. 2004). The lowest $\delta^{18}O$ and $\delta D$ values of the crater lakes from the LGVF are lakes XLW and DONG. There appears to be no clear relationship between the isotopic composition of the LGVF lake waters with either the respective lake area or depth (Table 3.4). Measurements of the lake area and depth are not available for the reservoirs. However, an approximate estimate of the area of the reservoirs is given based on looking at satellite imagery (Figure 3.3). Based on this, a trend can be seen between the decreasing size in the reservoir basins and the increasing evaporative enrichment (Figure 3.9). Again, this is most likely a result of the decreasing catchment run-off associated with the smaller reservoir lakes. XISH is visibly the largest of the reservoirs and has a different lake water composition compared to HUAN, QUING and LWXH, which themselves all have a composition of c. −8‰ ($\delta^{18}O$) and c. −70‰ ($\delta D$) (Table 3.4). Interestingly, JIAN is the only reservoir which plots at the end of the LEL, suggesting that it is the most evaporatively enriched of the lakes sampled and that there is less catchment run-off compared to the other lakes.

## 3.7. Carbon isotope composition of TDIC

### 3.7.1. Results of TDIC analyses

There is often a very close relationship between the $\delta^{18}O$ and $\delta^{13}C_{TDIC}$ values of lake waters in hydrologically closed lakes (Chapter 2, Section 2.2.3). There is however no correlation between the $\delta^{18}O$ and $\delta^{13}C_{TDIC}$ of the thirteen lakes sampled for the purpose of this project ($r^2$=0.017) (Figure 3.10). Most of the lake waters sampled had $\delta^{13}C$ that fall within the range −20‰ to −5‰ and there is no correlation between the size of the lakes and measured $\delta^{13}C$ (Figure 3.10). Lake DALO has the highest $\delta^{13}C_{TDIC}$ at c. 0‰ and ERLO has the lowest at − 16.2‰ (Figure 3.10).

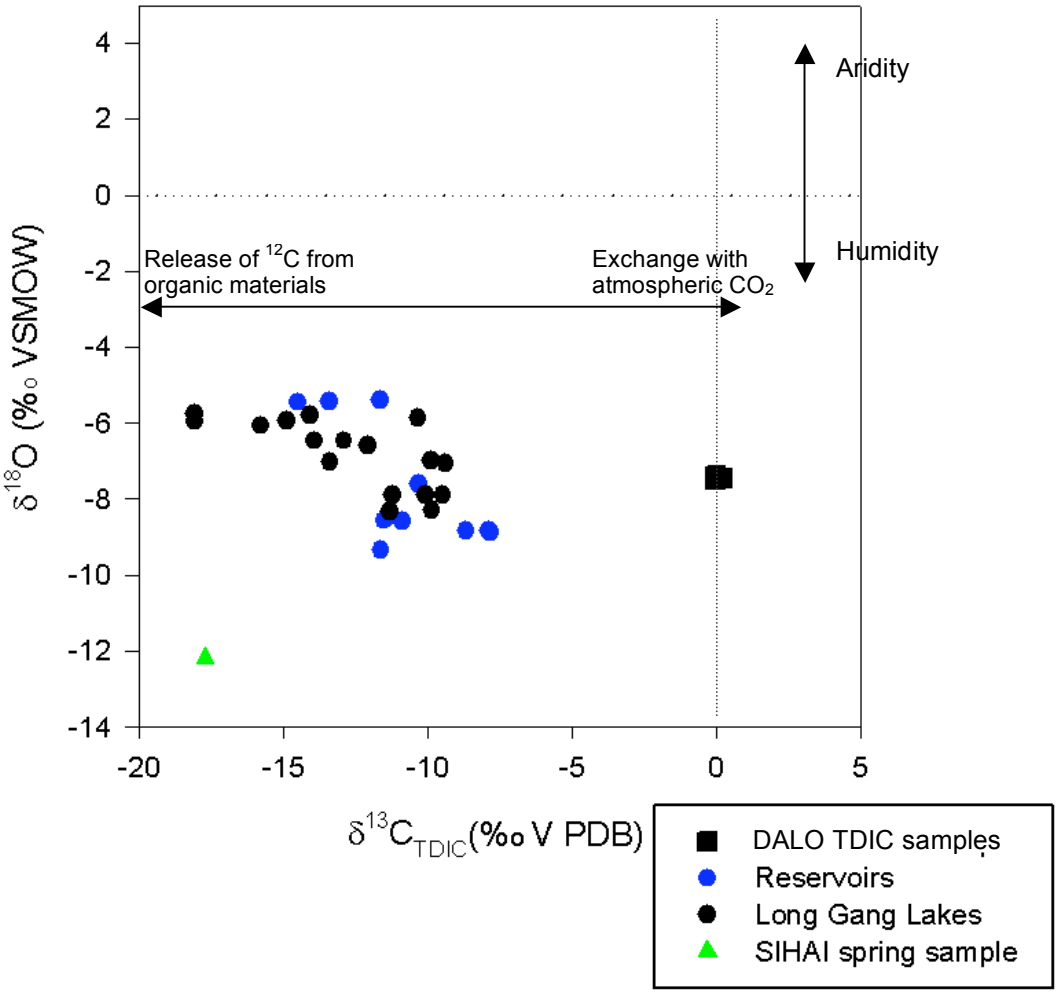


*Figure 3.10. $\delta^{18}O$ vs $\delta^{13}C_{TDIC}$ of modern lake waters. The arrows signify the general trend for the interpretation of TDIC composition of lake waters (based on Leng and Marshall 2004).*

The range of $\delta^{13}C_{TDIC}$ values for all sites suggests that there are a variety of processes affecting the TDIC composition of the lakes (Figure 3.10). The spring sample from lake SIHAI plots outside of the general cluster with a $\delta^{13}C$ of −17.7‰.

### 3.7.2. TDIC Interpretation

There appears to be no distinct or discreet clustering of the samples from the Long Gang lakes and the reservoir lakes (Figure 3.10). All the lake waters where $\delta^{13}C$ was sampled have pH which falls between c. 6.4 and 10.3 (Table 3.2) suggesting that the dominant species of TDIC in the lakes is from the bicarbonate ion ($HCO_3^-$) (Clark and Fritz 1997) (refer to Figure 2.5). In general, the composition of groundwater $\delta^{13}C_{TDIC}$ lies between c. −20 to −0‰ (ibid.) similar infact to the lakes sampled here. In general, $\delta^{13}C_{TDIC}$ in shallow groundwater (in this case as $HCO_3^-$) entering lakes is lower in $^{13}C$ due to the presence of isotopically light carbon derived from organic matter in soils (Leng and Anderson 2003). In hydrologically simple lakes, waters with low $\delta^{13}C$ also tend to have low $\delta^{18}O$ (ibid.). The spring sample from SIHAI plots as one of the lowest ($\delta^{13}C$) samples suggesting that the groundwater has carbon derived from soils in the catchment. However, when groundwater inflows into a lake it will exchange with atmospheric $CO_2$, which when in equilibrium with $HCO_3^-$, has a $\delta^{13}C$ value of less than 0‰. All the lakes measured here have $\delta^{13}C$ values that fall between the spring water value ($\delta^{13}C$; −17.7‰) and −7‰ (non have reached equilibrium with atmospheric $CO_2$).

Lake productivity can also have an effect upon the $\delta^{13}C_{TDIC}$ composition of lake waters and phytoplankton preferentially utilise $^{12}C$ to produce organic matter that averages 20‰ lower than the $\delta^{13}C$ of the TDIC (Leng and Anderson, 2003). However, as most of the lakes sampled here are oligotrophic (apart from the reservoir sites; Table 3.2) it is assumed that productivity effects upon the TDIC pool of lake waters are low. During periods of increased productivity the carbon pool will become enriched in $\delta^{13}C_{TDIC}$ so that $^{13}C$ values are increased. As Figure 3.10 displays, values for the sites remain low therby suggesting that productivity effects are minimal and that catchment inwash plays a large role in changing the TDIC of the lakes.

DALO is the lake with the highest conductivity, although the lowest TP values (see Table 3.2). The higher $\delta^{13}C$ composition of TDIC in lake waters occurs by a number of processes, for example groundwaters may have an isotopically heavier carbon isotope source (Leng and Anderson, 2003). The geology of DALO does not differ from the other Long Gang lakes; the upper Archaen basement (volcanic) geology. Therefore the source of bicarbonate is not derived from a different geology. The $\delta^{13}C_{TDIC}$ composition of DALO lake waters are the highest of all the sites. The data suggests that there may be a minimal inflow of groundwaters and/or a higher amount of atmospheric $CO_2$ exchange with the lake waters. Therefore it can be concluded that

atmospheric $CO_2$ exchange must be responsible for the higher $\delta^{13}C_{TDIC}$ values of this lake compared to the others. As equilibration with atmospheric $CO_2$ is a slow process this also implies a reasonably long residence time for the lakes. This is consistent with the evidence of the evaporative enrichment of the lakes along the LEL (Figure 3.9).

## 3.8. $\delta^{13}C$ and C/N composition of contemporary vegetation and soil samples

### 3.8.1. Results of $\delta^{13}C$ and C/N analyses

$\delta^{13}C$ and C/N ratios of contemporary vegetation and soil samples were measured from samples collected from the sites in August 2007 (Figure 3.11).

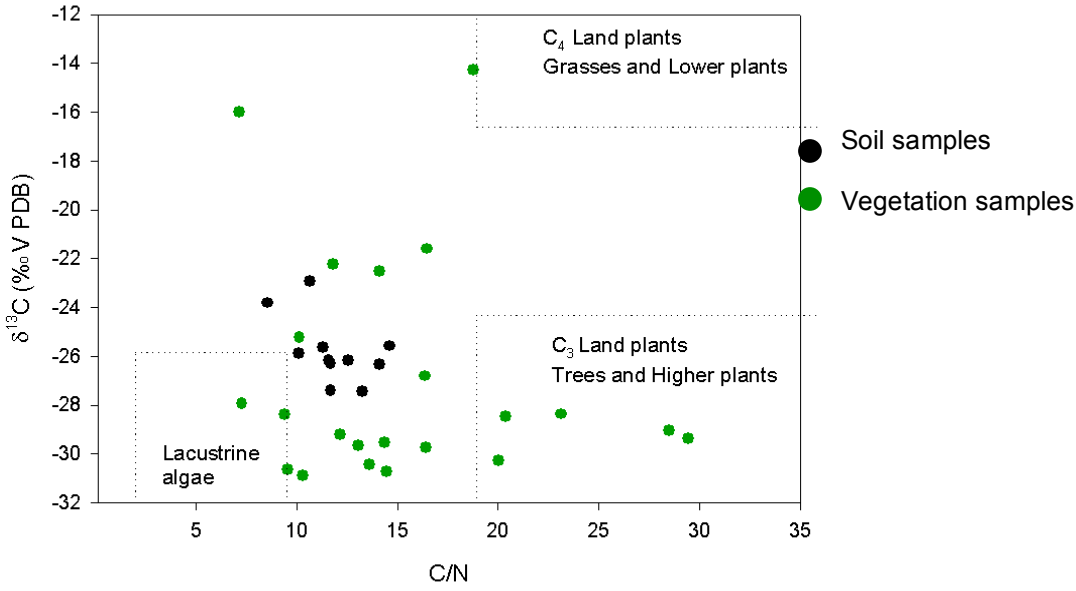


*Figure 3.11 Bi-plot of $\delta^{13}C$ vs C/N for the dominant vegetation and soil from each of the 13 sites sampled in August 2007. The dotted squares act as a reference to the fields of data are globally defined C/N vs $\delta^{13}C$ for average algae, $C_3$ and $C_4$ terrestrial plants (Meyers and Lallier-Vergès 1999; Tyson 1995).*

The relationship shows that contemporary vegetation at the sites is composed of plants mainly utilising the $C_3$ photosynthetic pathways. Soil organic matter is derived from a similar origin, which would follow if vegetation within the catchment were the same. $C_3$ plants employ the Calvin pathway of photosynthesis, which occurs in higher plants and algae, although there are additional considerations that govern the $\delta^{13}C$ composition of algae (Leng and Barker 2006). These plants strongly discriminate (20‰) against $^{13}C$ during carbon incorporation (*ibid.).* The two points plotting near the $C_4$ band are grasses found within the NANG and XISH catchments. However, the predominant vegetation in the region is that of $C_3$ plants (Figure 3.11).

### 3.8.2. $\delta^{13}C$ and C/N ratio interpretation

The presence of some $C_4$ plants is demonstrated, although these are only found in the NANG and XISH catchments. Soil composition in the region shows a strong component of carbon sourced from $C_3$ plants and macrophytes. The presence of carbon sourced from macrophytes maybe due to the sampling location. While samples were dug down to c. 10 cm prior to collection and the selected location was away from the shores of the lake, the composition of samples shows a mixed macrophyte source (Figure 3.11). This could be suggesting that the lakes at times experience variations in water levels, attributing for this composition.

## 3.9 Conclusions

A number of conclusions can be drawn for this chapter, emphasising the addition that this data provides to the ongoing research conducted in the region (Chu et al. 2008; Chu et al. 2009a; Chu et al. 2009b; Mingram et al. 2004; Schettler et al. 2006a; Schettler et al. 2006b).

1. The data described here present the first detailed contemporary diatom trap data for Lake Xiaolongwan. Results show the distinct changes of diatom productivity (blooms) throughout the year associated with spring and autumn overturn, lake stratification, ice cover, wind stress and macrophyte transport. These characteristics of lake stratification and turnover also play an important role in varve formation within the lake (dinoflagellate and chrysophyte blooms). The understanding of the peaks in productivity of biotic organisms with in the lake (through trap data) is of indispensable value when varve counting and age model formation.

2. Contemporary epiphyte diatom assemblages are also presented for the first time outlining the minimal impacts of lake taphonomy. It is as a result of this extensive contemporary data from Lake Xiaolongwan, that sediment cores were collected in order to look at the relative affects of climate change or human impacts upon the productivity and limnology of the lake.

3. Measured contemporary isotopic composition of lake waters in the Long Gang lakes and five neighbouring reservoirs is also presented here for the first time. The results have also highlighted possible problems associated with laboratory calibration procedures. Data demonstrates that the lakes plot along a regional LEL, with source water derived from weighted average precipitation. The reservoirs (apart from JIAN) have the lowest isotopic water composition, as a result of the greater catchment inwash the lakes receive from their river inflows (compared to the hydrologically closed Long Gang lakes).

4. $\delta^{13}C_{TDIC}$ analyses also demonstrate the input of shallow groundwater source to the lakes, as shown by the intercept of the spring sample (SIHAI) with the LEL and GMWL. While TDIC results show the input of groundwater inflow to the lakes sampled in this project.

5. Results from catchment vegetation ($\delta^{13}C$ and C/N analyses) demonstrate that the dominant photosynthetic pathway of vegetation in this region is that of $C_3$ plants. $C_3$ plants are at a competitive advantage in regions where temperature and sunlight are moderate, while $C_4$ in regions of drought and high temperature. The findings strongly corroborate contemporary records of precipitation and temperature (Figure 3.1).

6. Analyses from contemporary isotopic data show that the lakes are sensitive to variations in precipitation amount as they fall along a local evaporation line, supporting their use for palaeoenvironmental reconstructions.

## References

Blomqvist S. and Hakanson L. 1981. A review on sedimentt traps in aquatic environments. Arch. Hydrobiologia 91: 101-132.

Brewer T.S., Leng M.J., Mackay A.W., Lamb A.L., Tyler J.J. and Marsh N.G. 2008. Unravelling contamination during MIS-10 to 12: Implications for atmospheric CO2. Climate of the Past 4: 333-344.

Bronk D.A., Lomas M.W., Gilbert P.M., Schukert K.J. and Sanderson M.P. 2000. Total dissolved nitrogen analysis: comparisons between the persulfate, UV and high temperature oxydation methods. Marine Chemistry 69: 163-178.

Chu G., Liu J., Schettler G., Li.J., Sun Q., Gu Z., Lu H.Y., Liu Q. and Liu T. 2005. Sediment fluxes and varve formation in Sihailongwan, a maar lake from northeastern China. Journal of Paleolimnology 34: 311-324.

Chu G., Sun Q., Rioual P., Boltovskoy A., Liu Q., Sun P., Han J. and Liu J. 2008. Dinocyst microlaminations and freshwater "red tides" recorded in Lake Xiaolongwan, northeastern China. Journal of Paleolimnology 39: 319-333.

Chu G., Sun Q., Wang X., Li D., Rioual P., Qiang L., Han J. and Liu J. 2009a. A 1600 year multiproxy record of paleoclimatic change from varved sediments in lake Xiaolongwan, northeastern China. Journal of Geophysical Reasearch-Atmospheres 114: 1-10.

Chu G., Sun Q., Zhaoyan G., Rioual P., Qiang L., Kaijun W., Han J. and Liu J. 2009b. Dust records from varved lacustrine sediments of two neighboring lakes in northeastern China over the last 1400 years. Quaternary International 194: 108-118.

Clark I. and Fritz P. 1997. Environmental isotopes in hydrogeology. Lewis Publishers, New York, 328 pp.

Diefendorf A. and Patterson W. 2005. Survey of stable isotope values in Irish surface waters. Journal of Paleolimnology: 257-269.

Gibson J.J., Edwards T.W.D. and Prowse T.D. 1996. Development and validatiob of an isotopic method for estimating lake evaporation. Hydrological Processes 10: 1369-1382.

Google 2010. Google Earth Map Application.

Hakanson L. and Jansson M. 1983. Principles of lake sedimentology. Springer Verlag, Heidelberg, 316 pp.

IAEA/WMO 2006. Global network of isotopes in precipitation. The GNIP Database. http://isohis.iaea.org.

Leng M. and Anderson N. 2003. Isotopic variation in modern lake waters from western Greenland. The Holocene 13: 605-611.

Leng M. and Barker P. 2006. A review of the oxygen isotope composition of lacustrine diatom silica for palaeoclimate reconstruction. Earth Science Reviews 75: 5-27.

Leng M. and Marshall J. 2004. Palaeoclimate interpretation of stable isotope data from lake sediment archives. Quaternary Science Reviews 23: 811-831.

Liu J., Chu G., Han J., Rioual P., Jiao W. and Wang K. 2009. Volcanic eruptions in the Longgang volcanic field, northeastern China, during the past 15,000 years. Journal of Asian Earth Sciences 34: 645-654.

McCrea J.M. 1950. On the isotope chemistry of carbonates and paleotemperature scale. Journal of Chemical Physics 18: 849-857.

Methe B.A., Soracco R.J., Madsen J.D. and Boylen C.W. 1993. Seed production and growth of waterchestnut as influenced by cutting. Journal of Aquatic Plant Management 31: 154-157.

Meyers P. and Lallier-Vergès E. 1999. Lacustrine sedimentary organic matter records of Late Quaternary paleoclimates. Journal of Paleolimnology 21: 345-372.

Mingram J., Allen J., Brüchmann C., Liu J., Luo X., Negendank J., Nowaczyk N. and Schettler G. 2004. Maar-and crater lakes of the Long Gang Volcanic Field (NE China)—overview, laminated sediments, and vegetation history of the last 900 years. Quaternary International 123: 135-147.

Preston C.D. and Croft J.M. 1997. Aquatic plants in Britain and Ireland. Harley, Colchester.

Schettler G., Liu Q., Mingram J. and Negendank J. 2006a. Palaeovariations in the East-Asian monsoon regime geochemically recorded in varved sediments of Lake Sihailongwan (Northeast China, Jilin province). Part 1: Hydrological conditions and dust flux. Journal of Paleolimnology 35: 239-270.

Schettler G., Liu Q., Mingram J., Stebich M. and Dulski P. 2006b. East-Asian monsoon variability between 15,000 and 2000 cal. yr BP recorded in varved sediments of Lake Sihailongwan (northeastern China, Long Gang volcanic field). The Holocene 16: 1043-1057.

Tyson R.V. 1995. Sedimentary organic matter: organic facies and palynofacies. Chapman and Hall, New York.

Washbourne I. 2003. Total phosphorous determination-Acid persulfate method. Marine Biological Laboratory.

Ye W., Yao T.D., Tian L.D., Ma Y.Z., Kurita N., Ichiyanagi K., Wang Y. and Sun W.Z. 2007. Stable isotope variations in precipitation and moisture trajectories on the Western Tibetan Plateau, China. Arctic, Antarctic and Alpine Research 39: 688-693.

Zhenlong Z. and Xiangyang L. 2008. Correlation between $\delta^{18}O$ in precipitation and surface air temperatures on different time scales in China. Nuclear Techniques 9.

# CHAPTER 4: Chronologies for Lake Xiaolongwan

## 4.1. Introduction

Work on Lake Xiaolongwan has been done in collaboration with Dr. Chu Guoqiang (CAS). A number of previous analyses have been conducted upon cores from the lake. Most notably these have focused on the nature of lamination formation and formation of varve chronologies (Chu et al. 2008). Further work has also discussed the nature of dust deposition at lake Xiaolongwan (XLW) and neighbouring Lake Sihailongwan in the late Holocene (Chu et al. 2009b). More recently work has been published on productivity changes in the lake ($\delta^{13}C$, $\delta^{15}N$) over the past 1600 years (Chu et al. 2009a). This project aims to build further on this work by conducting diatom analyses in order to look at changes in lake ecology and productivity over the late Holocene. The cores X00 and X06 were subsampled by Dr. Chu Guoqiang for this project, and the latter of these is the same core used for isotopic analyses described in Chu et al (Chu et al. 2009a). A further core (XLW2) was also collected and isotope analyses ($\delta^{13}C$) were conducted at a much higher resolution to Chu et al (2009a). This core was radiometrically dated and analyses of atmospheric pollution (SCPs) were also conducted.

This chapter will outline the chronology formation for the cores X00/X06 and XLW2. The reasons why methods were chosen and the errors associated with them will also be outlined. The initial rationale behind the project was to provide a high resolution diatom reconstruction from XLW, with a chronology that was derived from varve counting. As cores X00 and X06 had not been independently radiometrically dated and therefore the varve chronology was floating, a further core was collected (XLW2) in order to correlate diatom species abundance changes between the two records. This core would also be used to conduct high resolution organic isotope analyses. Discrepancies between the floating chronology and radiometrically dated XLW2 were later highlighted and SCP analyses were also conducted to demonstrate the more recent age of the samples.

## 4.2. Varve counting for cores X00 and X06

Varve chronologies for cores X00 and X06 were all counted through the use of thin-section analyses, carried out by Dr. Chu Guoqiang (CAS). The methodology described here follows those outlined in Chu et al (2008). Sediment slabs (6 x 2 x 1.5 cm) were sampled using aluminium trays, shock-freezing using liquid nitrogen, and then vacuum-dried. The freeze dried slabs were penetrated with synthetic resin and manufactured into thin sections (Lamoureux 2001). Thin sections were observed at different (x 20 – x 630) magnifications under a Leitz light microscope. Magnetic susceptibility was used as a method of correlating the two cores X00 and

X06 once again by Dr. Chu Guoqiang. The amalgamation of both sets of data (X00 and X06) forming a composite core was used to construct the varve chronology. The cores X00 and X06 were then sub-sampled by Dr. Chu Guoqiang for the purpose of this project.

Zolitschka (1996, 2006) described three common errors that occur in varve chronologies. These are errors related to technical problems (e.g. incomplete recovery of a core), errors related to depositional events (e.g. turbidites) and errors related to sediment processes (e.g. very high or low sedimentation rates). In order to estimate these errors a number of techniques can be adopted, including replicate counts. However, this does not provide any indication about the chronological error of the record, which can only be obtained through independent dating methods (Zolitschka 1996). Both X00 and X06 cores have not been independently and radiometrically dated however in order to corroborate the varve chronology. As a result, the varve counting years derived (from thin section analyses) for the cores analysed here cannot be correlated with the numerous cores collected from Lake Xiaolongwan.

Figure 4.1 displays the number of different cores collected from Lake Xiaolongwan and used for this project. Due to differential compression of each of the cores (X00 and X06) collected by Dr. Chu Guoqiang, prior to the thin section analyses, not all of the cores can be correlated by the varve chronologies alone. Furthermore, cores X00 and X06 remain uncorrelated with any of the other cores collected and chronologies published by Dr. Chu Guoqiang the latter which have had methods of independent dating (e.g. Chu et al. 2008; Chu et al. 2009a; Chu et al. 2009b). The short core X00 and the long core X06 therefore both have a floating chronology.

$^{210}$Pb, $^{137}$Cs or $^{14}$C dating was not conducted by Dr. Chu Guoqiang when creating the varve chronology. Insufficient material was subsampled in order for this to be done at UCL. This necessitated the collection of a second short core for such further analyses (XLW2). SCP analyses were conducted on the core XLW2 in order to cross-correlate it with the cores X00 and X06, in conjunction with the relative timings of the notable appearance of the diatom species *Discotella woltereckii* (Figure 4.1). A summary of the different analyses conducted on each of the cores is seen in Table 4.1 below. $^{14}$C dating was also not conducted on the bottom sediments of core X06 so that these varve ages may have large errors associated with them.

| Core name | Year of core collection | Analyses conducted | Analyst name |
|---|---|---|---|
| **X00** | **2006** | Diatom counting | V.N.P |
| | **(Dr.C.G)** | Varve counting | Dr. C.G. |
| | | Magnetic susceptibility | Dr. C.G |
| **X06** | **2006** | Diatom counting | V.N.P |
| | **(Dr. C.G)** | Varve counting | Dr. C.G |
| | | Magnetic susceptibility | Dr. C.G |
| **XLW1** | **2007 (V.N.P et al)** | DW, LOI 550 $^{o}$C, LOI 905 $^{o}$C | V.N.P |
| **XLW2** | **2007** | DW, LOI 550 $^{o}$C, LOI 905 $^{o}$C | V.N.P |
| | **(V.N.P et al)** | Diatom counting for core chronology | V.N.P |
| | | $^{210}$Pb and $^{137}$Cs | Dr. Andy Cundy and Handong Yang pers. comm. |
| | | SCP analyses | Prof. Neil Rose |
| | | XRF analyses | V.N.P |
| | | Bulk organic isotopes | V.N.P + N.I.G.L |

*Table 4.1. A summary of the different analyses conducted upon the 3 cores used in this study. XLW1 is shown as it was collected on the same fieldwork as XLW2 in 2007, although the analyses are not discussed in this project. Year of collection and by whom is also shown. The analyst conducting the relevant methods is also shown (V.N.P; Virginia Panizzo and Dr. C.G; Dr. Chu Guoqiang). Refer to Figure 4.1 to see how the cores correlate.*

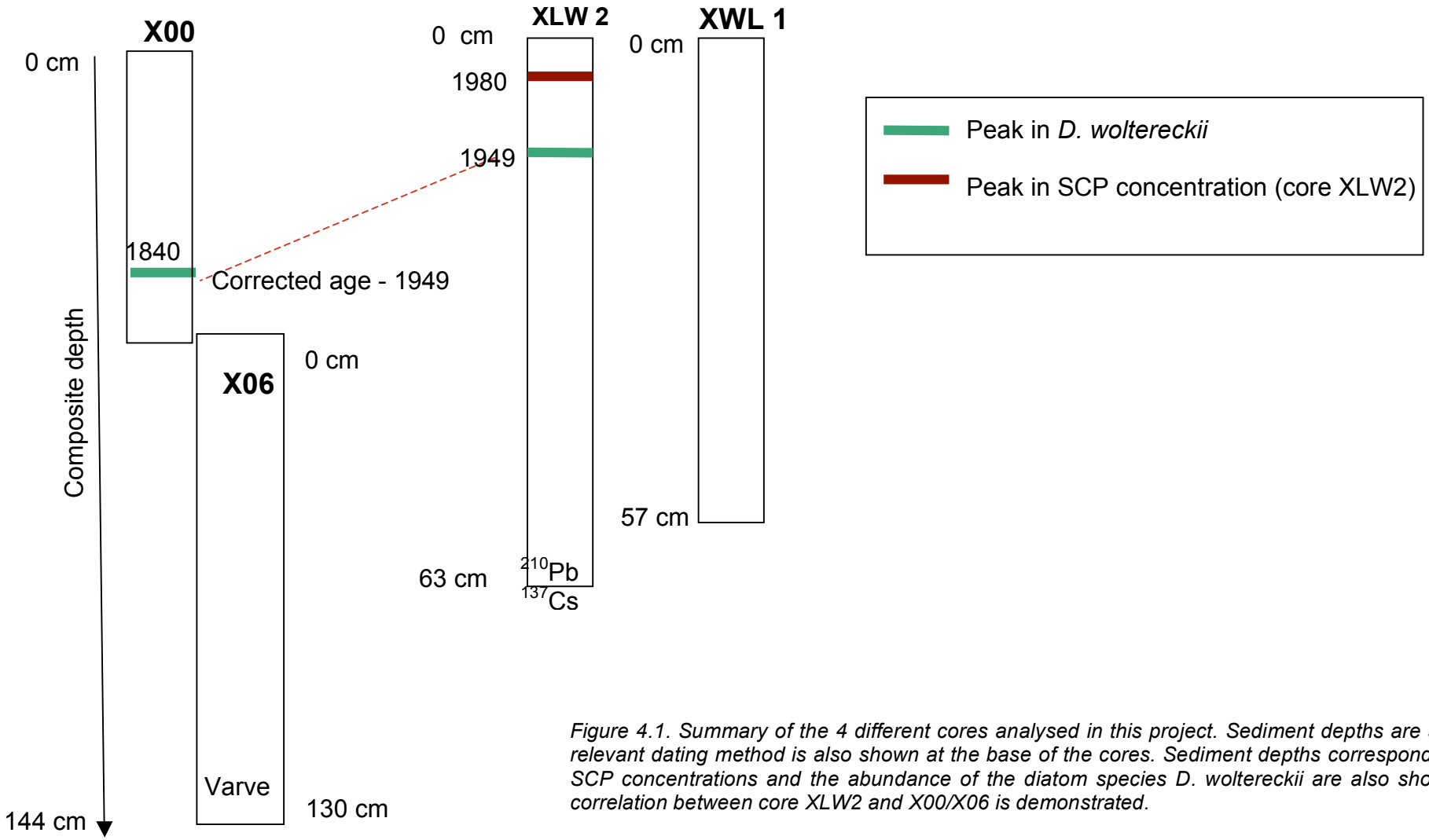


*Figure 4.1. Summary of the 4 different cores analysed in this project. Sediment depths are shown in cm. The relevant dating method is also shown at the base of the cores. Sediment depths corresponding to the peak in SCP concentrations and the abundance of the diatom species D. woltereckii are also shown. Their use for correlation between core XLW2 and X00/X06 is demonstrated.*

## 4.3. Xiaolongwan (XLW) sediment core sampling

A total of 4 cores were collected over the course of this study. Table 4.1 summarises the analyses conducted on each of the cores, the core lengths and composite depths for the cores collected in 2006 which have been cross correlated.

X00 and X06 were collected from the central region of XLW in 2006. A modified piston corer, designed by Dr. Chu Guoqiang, was used, operated with metallic rods (instead of ropes). A revised method of coring was also used due to the high gas content in the core sediment (Chu et al. 2008). As such, coring was conducted in October when the lake was ice covered and ambient temperatures were the same as lake water temperatures (c. 4°C). This reduced the chance of gas bubbles escaping the core tube and thereby affecting the integrity of the core. The corer was carefully operated so as to penetrate the sediments slowly and once brought to the surface, the top water was removed with a syringe and dried by inserting paper towels. Cores were transported back vertically to the lab in Beijing after which they were further dried by paper towels. Cores were cut open longitudinally and photographed (Chu et al. 2008). On one half of the core-sections, overlapping 10-cm long sediment slabs were cut and impregnated with resin for making thin-sections. The other half of the core sections were then sliced at 1 cm intervals. Correlation between the core sections is based on thin section analyses of varves and magnetic susceptibility (MS). Eventually, a composite record with a length of 143 cm, was developed and used for all diatom-based reconstructions discussed in this project. All core correlations (X00/X06) were conducted by Dr. Chu Guoqiang and later provided for this study.

As outlined in Section 2.3 contemporary isotope analyses and bulk organic isotope analyses of sediment cores were conducted in order to help quantify changes in lake productivity, as an addition to diatom analyses. Furthermore, as discussed here, independent dating was also needed to corroborate the varve chronology for cores X00/X06. As such, more material was needed to do this and as a result, on 18$^{th}$ August 2007, 2 further cores (XLW1 and XLW2) were collected from the central region of XLW (42°17'59.8"N and 126°21'34.3"E) using a UWITEC-gravity corer. A Plastimo hand-held echosounder was used in order to locate the deepest position for coring, 16.2 m. Surface sediments were carefully sampled using a syringe and placed into a labelled Whirlpack bag. The 2 cores collected were extruded in the field after a number of unsuccessful attempts to extrude other cores due to gas bubbles deforming sediments. Core XLW1 was extruded at 0.5 cm until 10 cm and thereafter every 1 cm until 57 cm. Core XLW2 was extruded every 0.5 cm until 20 cm and thereafter every 1 cm until 64 cm. Samples were then stored in a dark cool box (<4 °C) and transported to the UK for later analyses. XLW2 is used for bulk organic isotope reconstructions discussed here. Samples (0 – 20 cm) were also analysed for diatoms for the use of cross correlation with X00 and X06.

## 4.4. Chronology formation for core XLW2

Radiometric techniques ($^{210}$Pb and $^{137}$Cs) were used to date XLW2. These techniques were adopted to date the recent sediments and to independently corroborate SCP analyses conducted on the same core. $^{210}$Pb is removed from the atmosphere by precipitation and dry deposition, falling onto the earth's surface (e.g. lakes and oceans) (Appleby 2001). Total activity in lake sediments has two components, supported activity resulting from the *in situ* decay of the natural $^{226}$Ra in sediments, and unsupported $^{210}$Pb, which arises from atmospheric fallout. This decays in accordance with the radioactive decay law (Appleby 2008). It is the modelling and quantifying of this excess that is used in the development of reliable methods for calculating dates (Appleby 2001). As outlined previously, it is important to corroborate dating methods with independent means. When using $^{210}$Pb the most widely used independent dating technique is from sediment records of artificial radionuclides such as $^{137}$Cs and $^{241}$Am. Indeed fallout on a global scale began in 1954 following thermonuclear weapons testing and reached a peak in 1963. More recently, fallout from the Chernobyl reactor accident has been used to identify the 1986 depth (Appleby 2001).

Sediment samples were dated by non-destructive gamma spectrometry (Appleby and Oldfield, 1992) at the Centre for Environmental Research, University of Sussex. Ten core sub-samples were counted for at least 8 hours on a Canberra well-type ultra-low background HPGe gamma ray spectrometer to determine the activities of $^{137}$Cs, $^{210}$Pb and other gamma emitters.

| Sample depth (cm) | $^{210}$Pb activity (Bq/kg) | Counting error (Bq/kg) | $^{137}$Cs activity (Bq/kg) | Counting error (Bq/kg) | $^{214}$Pb activity (Bq/kg) | Counting error (Bq/kg) | Year (AD) | Error (Year) |
|---|---|---|---|---|---|---|---|---|
| -0.75 | 1608 | 95 | 37 | 5 | BLD | - | 2006 | 2 |
| -1.5 | 1585 | 89 | 36 | 3 | BLD | - | 2004 | 2 |
| -3 | 1922 | 98 | 51 | 2 | 74 | 2 | 1995 | 2 |
| -4.5 | 1041 | 61 | 112 | 5 | BLD | - | 1989 | 3 |
| -6.5 | 719 | 49 | 150 | 7 | 49 | 4 | 1979 | 4 |
| -8.5 | 1235 | 82 | 823 | 25 | 67 | 7 | 1963 | 8 |
| -10.5 | 950 | 55 | 115 | 5 | 72 | 4 | 1947 | 9 |
| -12.5 | 521 | 32 | 24 | 2 | 73 | 3 | 1928 | 11 |
| -14.5 | 327 | 18 | 21 | 1 | 69 | 2 | 1909 | 15 |
| -16.5 | 240 | 14 | 18 | 1 | 76 | 2 | 1892 | 22 |

*Table 4.2. Displaying the $^{210}$Pb, $^{137}$Cs, $^{214}$Pb activity and respective errors for the sample depths displayed in core XLW2. Year based on the CRS model is also displayed along with errors.*

Sediment accumulation rates were determined using the 'simple model' of $^{210}$Pb dating (e.g. Robbins 1978), where the sedimentation rate is given by the slope of the least squares fit for the natural log of the $^{210}Pb_{excess}$ activity versus depth. This model was chosen due to the near exponential decline in $^{210}Pb_{excess}$ activity with depth (Figure 4.2) and the close fit with $^{137}$Cs-derived accumulation rates (Appleby and Oldfield 1992).

**Figure 4.2**

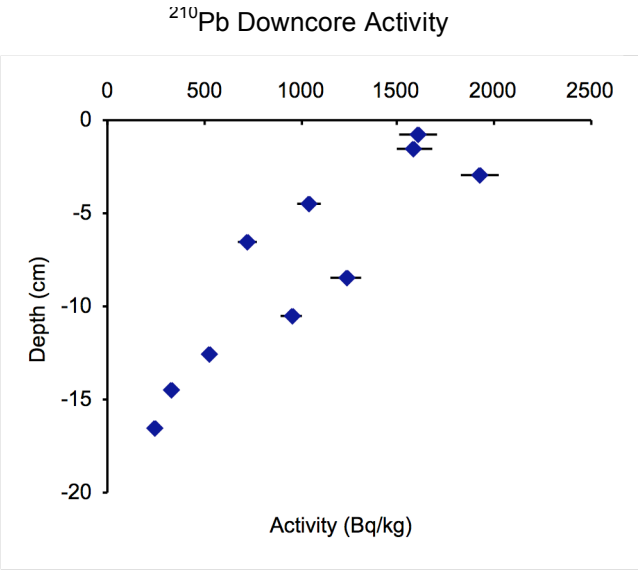


**Figure 4.3**

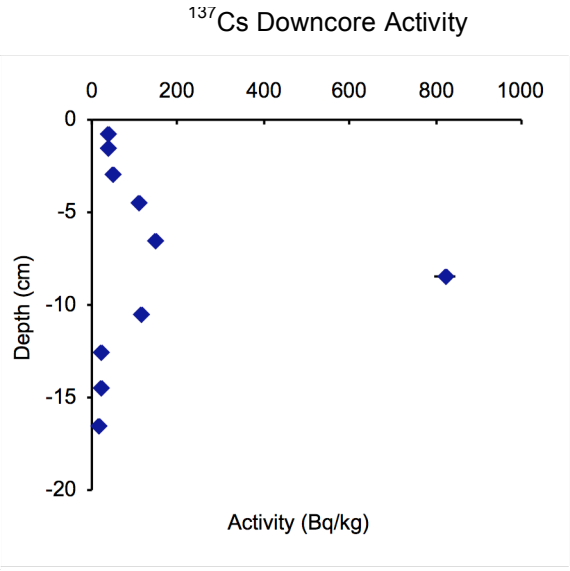


*Figure. 4.2. The $^{210}$Pb downcore activity (Bq/kg) for the core XLW2 against depth. Figure 4.3. The $^{137}$Cs activity (Bq/kg) for the core XLW2 against depth*

Slightly lower activities are present at and around 5 cm, which cause the $^{210}$Pb profile to deviate from the near-exponential decline with depth typically observed in uniformly accreting lacustrine sediments (Appleby and Oldfield 1992). These lower activities are most likely a consequence of an increase in grain size at this depth horizon, as indicated by a coincident decrease in $^{214}$Pb activity, which is a naturally-occurring radionuclide dominantly associated with the fine silt / clay fraction of sediments (Cundy, pers. comm.).

The chronology of the core is calculated by using the CRS model and corrected by the $^{137}$Cs peak, in this case which occurs at 8.5 cm (Figure 4.3). The chronology can be seen in Figure 4.4. The sedimentation rates are also displayed in this figure, showing how they have changed over time (Handong Yang, pers. comm.). The finalised chronology for the core XLW2 has been applied for the purpose of the $\delta^{13}C_{organic}$ reconstruction.

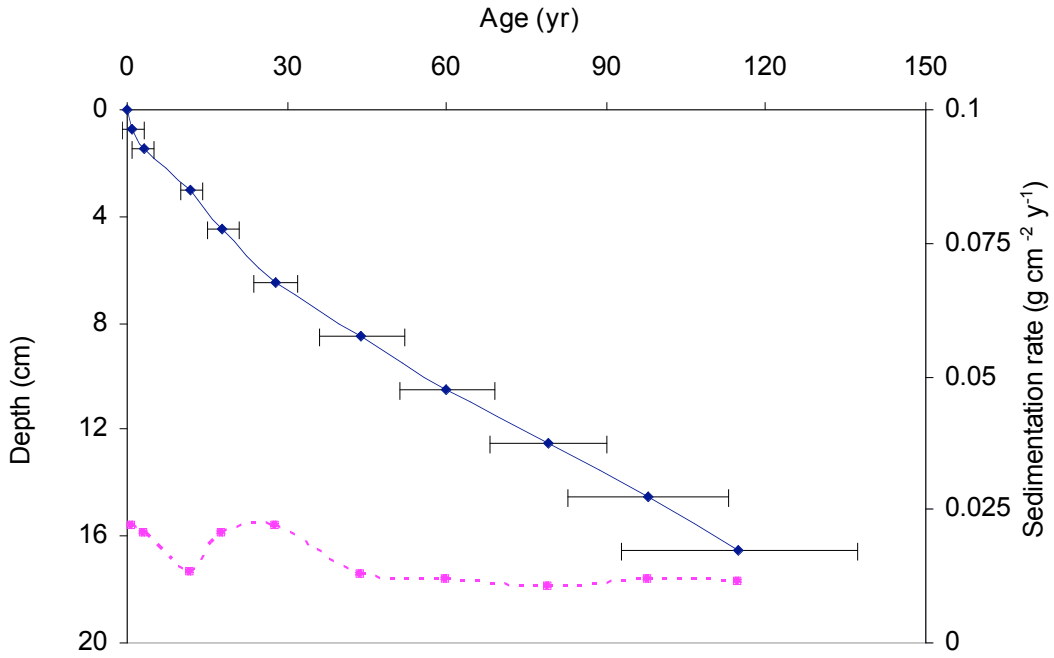


*Figure 4.4. The derived chronology (age against depth) for the core XLW2 with the respective errors associated with the CRS model. Sedimentation rates (g/cm$^2$/yr) for the XLW2 core are also displayed by a pink line against depth. The age scale is in years BP (before 2007).*

In order to aid with the correlation of the XLW2, X00 and X06 cores, by independent means, the top 20 cm of core XLW2 was also counted for diatoms. This technique was adopted due to the high percentage abundance of *D. woltereckii* in the top samples of the latter cores, which shows a distinct peak at c.12.5 cm in the composite X00/X06 record (estimated c. 1840 AD based on the varve chronology) (refer to Figure 5.14b).

## 4.5. Summary of the correlation of XLW cores

A summary of the correlations conducted between the cores adopted in this thesis (XLW2, X00 and X06) is displayed in Figure 4.1.

Initially, the introduction of *D. woltereckii* in both the core XLW2 (radiometrically dated) and cores X00, X06 (varve dated) was to be used as a marker and for the correlation between the two data sets. On closer inspection of the timing of this introduction, based on the respective chronologies of the cores, it was seen that there was a c. 100 year discrepancy between them (Table 4.3). It was for this reason that further independent analyses were conducted using SCP analysis. Unfortunately this was only possible for the XLW2 core due to the limited material left in cores X00 and X06. As SCPs are linked with anthropogenic activity, they would help to corroborate the $^{210}$Pb dating of XLW2 and define if the peak in *D. woltereckii* did indeed occur at c. 1840 AD as based on the varve chronology of X00, X06 or at c. 1950 AD

as based upon the $^{210}$Pb derived chronology. The methods of SCP techniques will be outlined in Chapter 5. The resolving of the differences in both the records will also be discussed later.

### 4.5.1. SCP results from core XLW2

SCP analyses therefore have also been conducted on XLW2 as a means to assist in the correlation of XLW2, X00 and X06 cores. Analyses were conducted by Prof. Neil Rose, UCL, and are displayed below. The dating shown for the cores is based on the $^{210}$Pb and $^{137}$Cs of XLW2 (Figure 4.4).

**Figure 4.5**

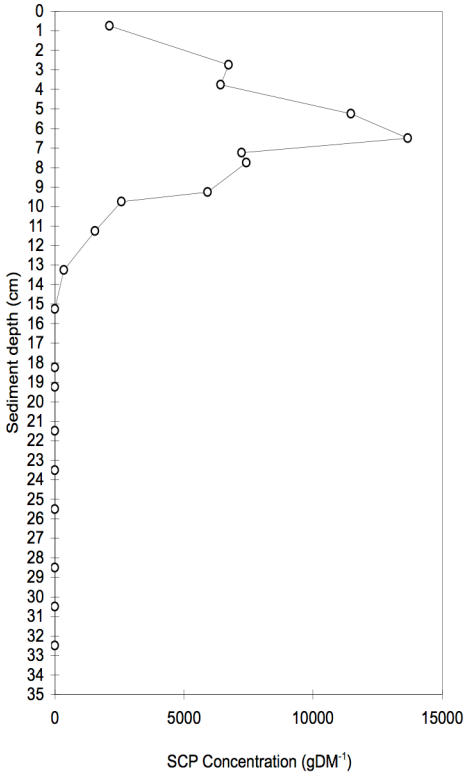


**Figure 4.6**

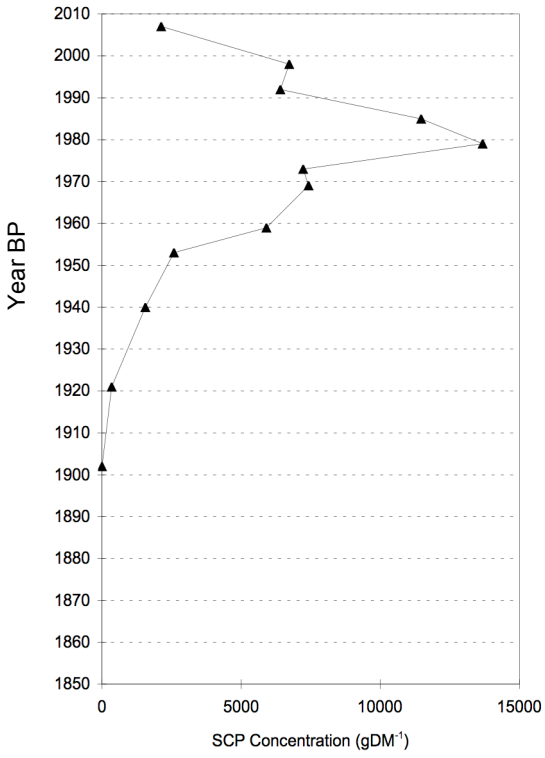


*Figure 4.5 SCP concentration (g/DM) against depth (cm) for XLW2 and Figure 4.6. SCP concentration for the core XLW2, plotted against the age model created based on the CRS method applied to $^{210}$Pb dating. Age scale is in years AD.*

SCP analyses show a distinct increase in concentrations after c. 1950 AD. The highest values are seen at c. 1980 AD, when concentrations reach 13674 (g/DM). Following this time, values begin to fall once again towards the surface sediments. As little literature exists on the initiation of coal combustion in this region of north east China (Chapter 5.4.4), thereby providing an independent means of dating the SCP record from XLW2, the $^{210}$Pb chronology has been applied.

## 4.6. Discussion

On the basis of the data above, the peak in *D. woltereckii* is argued to be more likely dated in core XLW2 at c. 1949 AD rather than 1840 AD (see Table 4.3). Based on this argument a correction factor has been applied to the X00/X06 record on a basis of the peak in *D. woltereckii*.

| Core name | Technique | Composite depth | Original date AD (chronology method) | Corrected Age AD |
|---|---|---|---|---|
| XLW2 | *D. woltereckii* peak | 10.25 cm | 1949 ($^{210}$Pb) | 1949 |
| XLW2 | Peak in SCP concentration | 6.5 cm | 1980 ($^{210}$Pb) | - |
| X00/X06 | *D. woltereckii* peak | 12.5 cm | 1840 (Varve-floating) | 1949 |

*Table 4.3. The original date for the respective cores of the peak in D. woltereckii and SCP concentrations. The corrected age, based on interpretation of the SCP analyses is also displayed. This corrected age is used here for the composite core record of X00 and X06.*

While this is not the optimal method of correlating the cores, without further independent dating of the X00/X06 record, for the purpose of this project it was the only possible solution. As a result, due to the corroboration of the SCP and $^{210}$Pb analyses and peak in *D. woltereckii,* we assume that the floating chronology for the varve dated X00/X06 cores is c. 100 years too old. As the *D. woltereckii* peak is so distinct and the presence of SCPs is evident in the same samples we can argue that these dates are likely to be correct. The difference between the occurrences of *D. woltereckii* in the different cores analysed (c.100 years) is therefore used to correct the age model. This new age model will be used from hereon for the X00/X06 cores.

As Table 4.2 shows, the errors associated with the $^{210}$Pb age model fall between 2 and 22 years. Furthermore, the errors associated with the corrected chronology for the cores X00 and X06 are displayed in Figure 4.8.

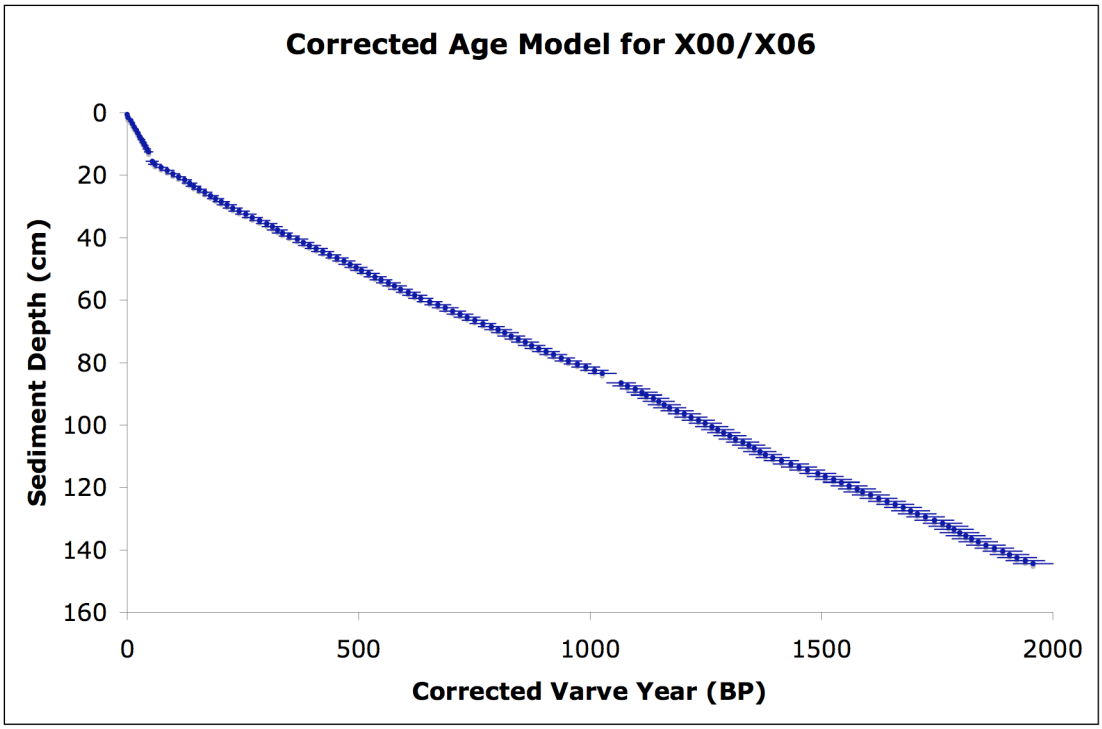


*Figure 4.8. The corrected age-depth varve model for the cores X00/X06. The corrections are based on the agreement between the $^{210}$Pb and SCP age-depth models (Table 4.3). Errors (based on varve counting errors) are also displayed. Year is before present at the time of coring, 2006.*

As Figure 4.8 shows, the errors associated with the corrected age model of X00/X06 are a maximum of c. 45 years at the base of the core. While the calculated errors are small (compared to those associated with other dating methods e.g. $^{14}$C) there will be an error also associated with the correction of this model, although this remains unquantifiable. Sample resolution falls between c. 1 and 44 corrected varve years for the diatom reconstruction of cores X00/X06. The age model is presented in years BP (present being the time of coring, 2006).

## 4.7. Conclusions

Based on the results drawn from this chapter there are a number of conclusions that can be made. It is clear that there are many limitations associated with the chronologies developed for Lake Xiaolongwan. However, this project aims to remain aware of this when discussing environmental reconstructions, particularly when comparing this record with other regional indices. Nevertheless, it is argued that a robust $^{210}$Pb and $^{137}$Cs derived chronology has been created for the short core XLW2. This is also further corroborated by the SCP profile from the same core. The results of both chronologies have been adopted in order to correct the varve dated cores X00 and X06. It is this chronology, which is referred to for these cores for the remainder of the project.

## References

Appleby P. 2001. Chronostratigraphic techniques in recent sediment In: W. M. Last and J. P. Smol (eds.), Tracking environmental change using lake sediments volume 1: Basin analysis, coring and chronological techniques. Kluwer Academic Publishers, London, pp. 171-204.

Appleby P. 2008. Three decades of dating recent sediments by fallout radionuclides: a review. The Holocene: 83-93.

Appleby P. and Oldfield F. 1992. Application of $^{210}$Pb to sedimentation studies: . In: M. Ivanovich and R. S. Harmon (eds.), Uranium-series disequiibrium: Applications to earth, marine and environmental sciences. Oxford University Press, Oxford, pp. 731-778.

Chu G., Sun Q., Rioual P., Boltovskoy A., Liu Q., Sun P., Han J. and Liu J. 2008. Dinocyst microlaminations and freshwater "red tides" recorded in Lake Xiaolongwan, northeastern China. Journal of Paleolimnology 39: 319-333.

Chu G., Sun Q., Wang X., Li D., Rioual P., Qiang L., Han J. and Liu J. 2009a. A 1600 year multiproxy record of paleoclimatic change from varved sediments in lake Xiaolongwan, northeastern China. Journal of Geophysical Research-Atmospheres 114: 1-10.

Chu G., Sun Q., Zhaoyan G., Rioual P., Qiang L., Kaijun W., Han J. and Liu J. 2009b. Dust records from varved lacustrine sediments of two neighboring lakes in northeastern China over the last 1400 years. Quaternary International 194: 108-118.

Lamoureux S. 2001. Varve chronology techniques. In: W. M. Last and J. P. Smol (eds.), Tracking environmental change using lake sediments volume 1: Basin analysis, coring and chronological techniques. Kluwer Academic Publishers, London, pp. 247-260.

Robbins J.A. 1978. Geochemical and geophysical applications of radioactive lead. In: J. O. Nriagu (ed.), Biogeochemistry of lead in the environment Elsevier, Amsterdam, pp. 285-393.

Zolitschka B. 1996. Recent sedimentation in a high arctic lake, northern Ellesmere Island, Canada. Journal of Paleolimnology 16: 169-186.

Zolitschka B. 2006. Varved lake sediments. In: S. A. Elias (ed.), Encyclopedia of Quaternary Science. Elsevier, Amsterdam, pp. 3105-3114.

# CHAPTER 5. Palaeoenvironmental reconstruction from Lake Xiaolongwan

## 5.1. Introduction

### 5.1.1. Late Holocene environmental change in northern China

During the period between 3800 and 3000 calibrated (cal) years BP, evidence has demonstrated a phase of slightly reduced total amount of summer rainfall, indicated by a decline in Lake Juyanze (north west China) water levels and changes in Artemisia/Chenopodiaceae (A/C) pollen ratios (Figure 1.2) (Hartmann and Wunnemann 2009). The record from Lake Juyanze also identifies a short term dry interval between 2600 and 2400 cal yr BP when increased aeolian deposits are seen across many lakes in dryland China (*ibid*.). One consideration outlined with pollen reconstructions is the effect of anthropogenic clearance over the late Holocene. For example, Li et al (2009) document a decline in *Pinus* and *Quercus* between 2000 and 680 cal years BP, and an increase in herbs including *Artemisia,* indicating an extensive human impact on vegetation in the southeastern Heilongjiang Province, NE China. Makohonienko et al (2008) do however outline that it is possible to distinguish between pollen derived from anthropogenic impact, so that a climatic signal can be derived. Nevertheless, as this region of NE China is affected by the east Asian summer monsoon (EASM), the interpretation of Li et al (2009) here suggests that this was a period of reduced summer monsoonal intensity. Other evidence also suggests a wide interval of weak EASM intensity and consequent lake desiccation between c. 4500 to c. 2100 years BP, which has been linked to cold events e.g. the ice raft debris (IRD) events 1, 2 and 3 (Section 1.7), concomitant with the cultural collapse of the Chinese Neolithic populations (Figure 1.7) (Selvaraj et al. 2007; Wang et al. 2005).

Late Holocene records from Lake Zhuye, NW China, which is in the marginal area of the EASM demonstrate a period of strong aridification after c. 1600 years BP which the authors attribute to the interplay of Westerlies and the EASM in summer months, suggesting that the arid conditions might be affected by the decreased moisture content of the Westerlies (other evidence of aridification in the Westerly domain after c. 1500 years BP supports this) (Li et al. 2009). Evidence published from Lake Xiaolongwan (low $\delta^{13}C$ values) also suggests a period of increased aridity centred at c. 1500 years BP, lasting c. 50 years, which is concomitant with a solar minimum (Chu et al. 2009a). In the northern Tibetan Plateau, Liu et al (2009b) also argue that periods of intensified (weakened) east Asian winter monsoon (EASM) are concomitant with Bond events 0 to 2. Furthermore, Mischke and Zhang (2010) outline that in regions of the Tibetan Plateau, the cold events between c. 1700 and 1300 cal years BP (e.g. Bond event 1) and later between 600 and 100 cal BP (e.g. Bond event 0) are coeval with the decline and establishment of Chinese Dynasties implying a remarkable impact on the social systems in eastern China.

Evidence of the medieval warm period (MWP) and Little Ice Age (LIA) has been demonstrated in sediments from Jinchuan peat bog, north east China, with the latter of these events being punctuated by several warmer episodes (Hong et al. 2000). Furthermore, Hong et al (2009) also argue that evidence from the Hani peat record, between c. 450 and 250 cal years BP, demonstrates two cold events both corresponding to the LIA, with the latter being the most prominent. As highlighted, speleothem records have also identified such perturbations over this time period, with the LIA identified as Bond event 0, with the most cold conditions coincident with the Maunder Minimum (Wang et al. 2005; Wang et al. 2008b). Chu et al (2009a) once again show evidence of severe drought conditions lasting c. 100 years after c. 350 years BP with a decline in $\delta^{13}C$ values and increase in dust events (Chu et al. 2009b) corresponding to the LIA and also documented after c. 200 years BP.

Nevertheless, contradictory evidence exists as to the nature, timing and impact of well-defined perturbations such as the Medieval Warm Period (MWP; AD 900-1300), Little Ice Age (LIA; AD 1350-1850) and recent warming (Morrill et al. 2003; Osborn and Briffa 2006). Indeed, while the LIA is identified as a cold and dry period in central and eastern regions of China, Chen et al (2008) argue that in arid central Asia (ACA) it is presented in lake sediment records from Bosten Lake, as humid and warm (Figure 1.2). Other literature based on climatic modelling suggests that such events should be most pronounced in continental areas (Shindell et al. 2001).

Evidence of more recent warming has been widely documented from the sensitive, remote regions of the Arctic which is argued to be primarily driven by climate warming through lengthening of the summer growing season and related limnological changes (Smol et al. 2005). Ruhland et al (2008) provide a coherent picture that climate-driven, diatom taxon-specific changes are now evident across large regions of the Northern Hemisphere representing a wide spectrum of lake ecosystems. Furthermore, these lake ecosystems have crossed ecological thresholds with changing climate that initiated in the 19th Century in Arctic and alpine regions, but typically only occurred in the mid-20th Century in lakes from mid-latitude regions of North America (ibid). Most evidence has indeed focused on the sensitivity of these remote Arctic regions. There is an increasing need to asses the degree to which anthropogenically induced climate change is seen in other remote regions of the world, and in particular continental regions. In regions of the Tibetan Plateau You et al (2009) describe the clear weakened effect found in diurnal temperature ranges (important in regulating precipitation and circulation) due to anthropogenic emissions.

## 5.2. Methods

### 5.2.1. Sediment analyses

The following analyses in the sections 5.2.1 to 5.2.3 were conducted on cores XLW2. Refer to Table 4.1 in order to identify the different analyses conducted on each of the cores. Please refer to Chapter 4 for information on sediment chronologies.

5.2.1.1. % Dry weight analyses

% Dry weight was calculated by measuring between 0.1 and 0.2 g of wet sediment into sub-sampled, pre-weighed crucibles. Sediments were dried overnight in a Gallenkamp oven at 105°C. Once dried sediments were re-weighed in order to calculate loss on drying and therefore % dry weight (%DW) using the following equation from Bengtsson and Enell (1986):

*%DW = (weight after drying/wet weight) x 100*

5.2.1.2. % Loss on ignition at 550°C

After conducting dry weight analyses, sediments were placed in a Carbolite oven at 550°C for 2 hours. Once removed from the furnace, samples were allowed to cool in a dessicator and re-weighed. % loss on ignition (%LOI) was calculated using the following equation from Bengtsson and Enell (1986):

*% LOI = [(weight after drying – LOI 550 $^{o}$C weight)/weight after drying ] x 100%*

%total organic carbon (TOC), a bi-product of $\delta^{13}$C laboratory analyses is also displayed in the results section and acts as an indicator, like %LOI, of the organic content of cores.

5.2.1.3. % LOI at 950$^{o}$C

Following %LOI, sediment samples were placed in Carbolite oven at 950$^{o}$C for 4 hours in order to calculate approximate carbonate content of sediment samples. Samples were then allowed to cool overnight in the furnace after which they were weighed. Carbonate content was then calculated using the following equation (Heiri et al. 2001):

*% Carbonate content = [(weight after LOI 550$^{o}$C – weight after 950$^{o}$C)/weight after drying] x 100%*

### 5.2.2. Organic isotope analyses

Vegetation samples, collected from the Long Gang Volcanic field sites, were left to dry overnight in a drying cabinet at c. 40°C. Once dried they were frozen and milled to a fine powder. Bulk carbon samples for core XLW2 were prepared by placing 2 g of wet sediment in 5 ml of 5% HCl overnight in order to remove carbonates. Samples were next washed 4 times with de-ionised water through Whatman's 41 filter papers using manifolds and dried overnight at 40°C. Once vegetation and bulk sediment samples were ground to a fine powder using a marble pestle and mortar, $^{13}C/^{12}C$ analyses were performed by combustion using a Carlo Erba NA1500 on-line to a VG TripleTap and Optima dual-inlet mass spectrometer. $\delta^{13}C_{organic}$ values were calculated to the VPDB scale using within-run laboratory standards calibrated against NBS-18 and NBS-19. %C and %N, from which C/N is calculated, were determined simultaneously by reference to an Acetanilide standard. Replicate analyses of well mixed samples for both $\delta^{13}C$ and C/N were conducted in order to obtain a precision of +/- 0.1‰ and 0.1 respectively

### 5.2.3. X-ray fluorescence (XRF) spectrometry analysis

Up to 2 g of freeze dried sediment were finely ground and compressed into 25 mm deep polythene sample pots for XRF analysis. A total of 50 samples were analysed throughout the 64 cm core. Due to the limited amount of sediment, after earlier subsampling, certain samples were amalgamated where needed while at other intervals sampling was not possible. Samples were subjected to gamma photons from a silicon (lithium) semi-conductor detector for 240 s each using a Spectro Xlab 2000 energy dispersive X-ray fluorescence spectrometer. Calibration was conducted with two known sediment standards of Buffalo River Sediment. The Norton and Kahl equation (Section 2.4.2.1) was then adopted to calculate the anthropogenic contamination of sediments in order to discuss pollution in the area.

### 5.2.4. Diatom sample preparation

The following methodology was adopted for all three sediment cores (XLW2, X00, X06) (Table 4.1). Procedures followed those outlined in Renberg(1990) where approximately 0.1 g of wet sediment (for core XLW2) and 0.01 g of dry sediment (for cores X00 and X06) were digested in 5 ml 5% $H_2O_2$ using the water bath technique (Battarbee et al. 2001). A total of 144 samples were analysed for cores X00/X06 and for 20 samples XLW2. Once all samples had finished reacting they were washed with distilled water 4 times before adding DVB (divinylbenzene) microspheres at a known concentration of 2.47 x $10^7$ (to reach a ratio of approximately 1:1 with microspheres and diatoms) in order to calculate diatom concentrations (Battarbee and Kneen 1982). Around 1ml of diluted, well mixed solution was pipetted onto a 15 mm diameter wide coverslip and left to dry overnight in a clean laboratory before being mounted onto slides on a 70°C hot plate using Naphrax. Concentrations of the microsphere solution were adapted for each of the cores on the basis of abundances of diatoms on test slides.

Diatom counting was conducted using a Zeiss light microscope at x1000 magnification under oil immersion and phase contrast. A minimum of 300 valves were counted per slide and microspheres were also counted. Diatom preservation was good for the cores XLW2, X00 and X06, with little issues with diatom frustule dissolution. Diatom taxonomy followed Krammer and Lange-Bertalot (1986, 1988, 1991a, b). For further information of newer species of the genera *Navicula* and *Pinnularia* the following literature was consulted: Krammer (1992) and Lange-Bertalot (1996, 1999, 2001). Haworth and Hurley (1986) was consulted to aid in the identification of *Discotella woltereckii*. Other literature also includes Lange-Bertalot and Moser (1994) and Vyverman (1991). For the identification of the species *Punctastriata disoidea,* from the newly identified *Punctastriata glubokoensis* both Williams et al (2009) and Flower (Flower 2005) were consulted. Please consult the appendices for further information on diatom taxonomy of dominant species.

Photographs were taken using a Nikon CoolPix 5000, attached to the microscope, to help with diatom harmonisation with Dr. Patrick Rioual at the Chinese Academy of Sciences. To further ensure that diatom taxa were correctly identified, scanning electron microscopy (SEM) was conducted. A Jeol JSM-6480LV high-performance, Variable Pressure Analytical Scanning Electron Microscope was used (UCL, Earth Science Department). The machine has a resolution of 3.0 nm, along with an EDS (Energy Dispersive System) and EBSD (Electron Backscatter Diffraction). The preparation procedure follows those outlined above, with the settling out of diatoms overnight on 8 mm diameter round coverslips, before being mounted on SEM stubs and gold spatter coated.

The counting of microspheres allows diatom species concentrations to be calculated using the following equation from Battarbee (1986). They are measured as valves/g dry weight depending on the nature of the core sediment at sub-sampling.

*Diatom concentrations = [(Microspheres introduced x valves counted)/microspheres counted] x sediment dry weight (g)*

*Microspheres introduced = microsphere concentration x weight added (g)*

The ratio of diatom to chrysophyte cysts was also calculated using the following equation from Pinewoods (2005):

*D:C = [diatoms / (diatoms + chrysophyte cysts)] x 100%*

The simple ratio of comparing the chrysophyte cysts to diatom frustules preserved in lake sediments provides an approximate measure of the relative abundances of these two important algal groups (Smol 1983, 1985).

### 5.2.5. SCP analysis

All SCP laboratory methods and counting were conducted by Prof. Neil Rose, at University College London, for the purpose of this project.

Between 0.1 and 0.2 g wet weight material was sampled from core XLW2. This was added to 1.5 ml of concentrated nitric acid overnight, to remove organic matter. 1.5 ml of concentrated nitric acid was added once again c. 12 hrs later and samples were placed in a water bath at 80°C for 2 hours. Samples were then washed using distilled water, centrifuged, and the supernatant nitric acid removed. Once clean, 3 ml hydrofluoric acid was added to each sample tube and they were returned to the water bath at 80°C for 2 hours, in order to remove all minerogenic matter. After this time, samples were removed from the waterbath, topped with distilled water and left in a fume cupboard overnight.

Once settled, samples were centrifuged at 1500 rpm for 5 minutes and supernatant removed. 3 ml 6M HCl was added and samples placed in a water bath for 2 hours at 80°C. Once the time had elapsed, samples were topped with distilled water and centrifuged at 1500 rpm for 5 minutes. Once done, supernatant was removed and the procedure repeated 2 more times. Once cleaned, sample vials were weighed, the sample residue added and then weighed again.

One or two drops of the cleaned sample were added to cover slips and left to dry overnight. Vials were weighed once more. Once dried, cover slips were mounted on slides using the mountant Naphrax (refractive index 1.7).

SCPs were counted at x 400 magnification ensuring that the entire cover slip was counted. SCP concentration was calculated using the following equation:

$$SCP\ concentration = 1000N/E*M$$

Where N is the number of SCPs counted, E is the percentage of the final suspension evaporated onto the coverslip and M is the initial mass of the sediment. E was calculated using the following equation:

$$E = 100*(VS - V_{SUB})/(VS - VE)$$

Where VS is mass of the sample and the sample vial, $V_{SUB}$ is the weight of the vial after subsampling and VE is the empty vial. SCP concentration is in the units gDM-1 (numbers of particles per gram mass of sediment).

### 5.2.6. Multivariate analyses

5.2.6.1. Diatom data

Diatom taxa are expressed as percentage data and relative abundances were calculated for each species. The data were reduced so that only species with a percentage > 2% (the most

dominant species) were retained, using the software C2 v. 1.4.3 (Juggins 2007). This new spreadsheet was adopted for all multivariate analyses explained below. Species above a percentage of 5% were then selected using C2 in order to reduce the data set to 21 species (in order to pick out dominant trends) for X00/X06.

5.2.6.2. Ordinations

The software program Canoco v. 4.5 (ter Braak and Šmilauer 2002) was used for all ordination analyses. Detrended correspondence analysis (DCA) was conducted upon each of the reduced diatom data sets of >2% species abundance. Here, detrending by segments was selected in order to remove the presence of an arch effect in plots. Downweighting of rare species and square root transformation was also selected in order to dampen the effects of dominant species and pick out trends in all the data. Results show an Axis 1 gradient length was 1.409 (refer to Table 5.2). For data with low beta diversity, a linear method of ordination was performed (Leps and Šmilauer 2003).

Principal components analysis (PCA) was therefore conducted due to the linear response of data. Square root transformation of data was selected due to the more favourable plotting of the data in the samples biplot (see Figure 5.3). Centering by species was selected in order to calculate a covariance matrix (Kent and Coker 1992).

5.2.6.3. Cluster analysis

The program R v. 2.7.1 (2008) was used to run cluster analyses on a standardised diatom species spreadsheet. A total of seven cluster strategies were run which used different methods to determine the dissimilarity between a sample and a cluster, or two clusters (Simpson 2008). These strategies include single link, complete link, average link, Ward's minimum variance clustering, weighted average link, *k*-means and fuzzy clustering. Dendrograms for all techniques (apart from the latter two for which they are not generated) were consulted and compared. The resulting classification was applied to all ordinations to summarise distinct groupings of the data and therefore the dominant species assemblages (see Figures 5.3 and 5.4).

*k*-means clustering was chosen to apply to species data from cores X00 and X06, due to the optimal groupings that were created, compared to the other techniques. *K*-means is a non-hierarchical technique, which relocates objects/samples until a local minimum of the sum of squares is reached, that is when none of the movements being considered will further reduce the sum of squares (Gordon 1981). In the hierarchical methods, once clusters have been formed, they cannot be changed even if it would be sensible to. Due to the more robust algorithms adopted by *k*-means and the optimal groups it forms, a total of 3 groups (renamed as classes in Canoco 4.5) were chosen to classify diatom species in cores X00 and X06.

5.2.6.4. Diatom zonation

The program Zone v 1.2 (Juggins 1992) was adopted to apply zonation techniques to the Xiaolongwan diatom species data (cores X00 and X06). This was in order to summarise main sections in data where changes have occurred and therefore provide a simpler method to discuss these changes.

This included the techniques of Constrained Single Link (CONSLINK), Constrained Sum of Squares (CONISS), binary division using Sum of Squares criteria (SPLITLSQ) and Constrained Optimal divisive analysis (OPTIMAL). These different techniques use different methods of partitioning the data. For both binary and optimal splitting, the "best" location for a maker is the location that results in the greatest reduction in variance over the data set as a whole, determined by minimising either sum-of-squares or information content (Bennett 1996). Results from all methods were similar with same split being defined. Binary division using information statistic criteria (SPLITINF) was adopted in order to split the stratigraphic data into 5 main zones for the cores X00, X06. The chosen zones were displayed on the stratigraphy using C2.

5.2.6.5. Timeseries techniques

Timeseries analyses have been conducted in order to look at the main trends in PCA axis scores, as well as bulk organic isotope data from Lake Xiaolongwan. Generalised Additive Models (GAMs) are used here in order to summarise main trends. GAMs are a non-parametric tool, which can model changes and detect trends in data. Additive models are a generalisation of linear models that replace the sum of regression coefficients x covariates by the sum of smooth functions of the covariates (Simpson 2008). GAMs are data driven models so that the resulting fitted values do not come from a priori model (as with generalised linear model; GLMs). As such, GAMs allow the data to determine the shape of the response curves, a useful tool for data exploration (Yee and Mitchell 1991).

A mixed-effects model (GAMM) is one that contains both fixed and random effects (Simpson and Anderson 2009). Indeed, fixed effects are the standard representation of variables in a linear model, such as the effects of a treatment variable or explanatory variable on the response. The GAMMs used in this project allow for a smooth function of co-variates so that likelihood ratio tests and AIC (An Information Criterion) can be used to compare the models.

Two models were run for each of the variables (PCA axes scores, $\delta^{13}C$ and C/N), GAMM1 and GAMM2 using the software R (v.2.7.1 2008). GAMM1 is the general additive model, while GAMM2 has another element that looks at the autocorrelation structure between the data. This is an important element to consider in palaeodata as samples that are close together in time are likely to be more similar than samples further apart in time. The model with the lowest AIC value was selected and plots were made. 95% confidence levels were shown for each variable.

5.2.6.6. Significant ZERo crossing of derivatives (SiZer)

As discussed above, smoothing for curve estimation in statistics is a useful tool for discovering features in data (Chadhuri and Marron 1997). The variable *h* is a window that can be applied to data, to control the amount of smoothing. There are often problems with choosing the correct size of this window in order to make sure that there is no over or under-fitting of a curve to the data. Chadhuri and Marron (1997) devised the method of SiZer (Significant ZERo crossing of derivatives) to overcome this and provide a means of making inferences about which features are really present in data. The method helps to assess which features in a smoothed time-series are statistically significant and hence which features may represent "signal" (Birks pers. comm.). The program R (v.2.7.1 2008) was used in order to conduct SiZer analyses on diatom data.

## 5.3. Results

Please note that the constant rate of sedimentation method was used to extend the $^{210}$Pb age model to the base of the XLW2 core, after 1892 AD (0.116 cm/yr). Furthermore, that for the remainder of this thesis $\delta^{13}$C refers to isotopes of bulk organic matter (otherwise $\delta^{13}C_{org}$).

### 5.3.1. Bulk organic isotope reconstruction and core lithology

Core lithology (%DW, %LOI 550$^{o}$C and %LOI 950$^{o}$C) and bulk organic isotope results analysed from core XLW2 are displayed below (Figure 5.1). Please refer to Chapter 4 for details of age uncertainties associated with core XLW2 (Table 4.2).

%DW shows a decreasing trend after increasing between c. 1695 and 1720 AD (up to c. 15%). %DW oscillates between c. 7 and 10% for the remainder of the record and at c. 1980 values fall until the surface sediments. %LOI decreases at the beginning of the record from 65% and varies between 57 and 48% until c. 1750 AD. %LOI then shows an increasing trend of c. 10% until c. 1880 AD. By c. 1975 AD %LOI falls until the present day. %LOI at 950$^{o}$C displays very little variation for the XLW2 record (between c. 0.8 and 1.8%) as a result it will not be discussed in detail.

%TOC shows an increasing trend after c. 1710 AD to some of the highest values in the record, after a decrease in values between c. 1700 and 1710 AD to c. 18%. After this, %TOC shows little change, oscillating around the mean for the record (Table 5.1). However, at c. 1985 AD an increase in values is seen once more.

| | % TOC | $\delta^{13}C$ (‰) | C/N |
|---|---|---|---|
| **Mean** | 23.3 | -29.06 | 12.63 |
| **S.D** | 5.59 | 0.63 | 1.15 |

*Table 5.1. Summary of the mean and standard deviation of %TOC, $\delta^{13}C$(‰) and C/N for the XLW2 core.*

$\delta^{13}C$ decreases after the beginning of the record and then increases at c. 1700 AD. The values fall once more at c. 1725 AD. $\delta^{13}C$ shows an overall increasing trend with values increasing up core, this is an overall change greater than the standard deviation of 2 % (Table 5.1) (between c. -30 to -28‰). Increases in values are again seen between c. 1900 to 1945 AD (to c. -27‰) and later between c. 1945 and c. 1985 AD (to c. -27‰), after which a decreasing trend is prominent. C/N oscillates between c. 11.5 and 14.5 between c. 1675 and 1850 AD, a change just greater than the standard deviation (3 units) and predominantly greater than 12 (refer to Chapter 2.3.1). After c. 1850 AD, while changes in C/N remain small (c. 2 ‰) a shift is seen to values <12 between c. 1920 and 1965 AD and a rapid increase to higher values occurs in surface sediments of the core.

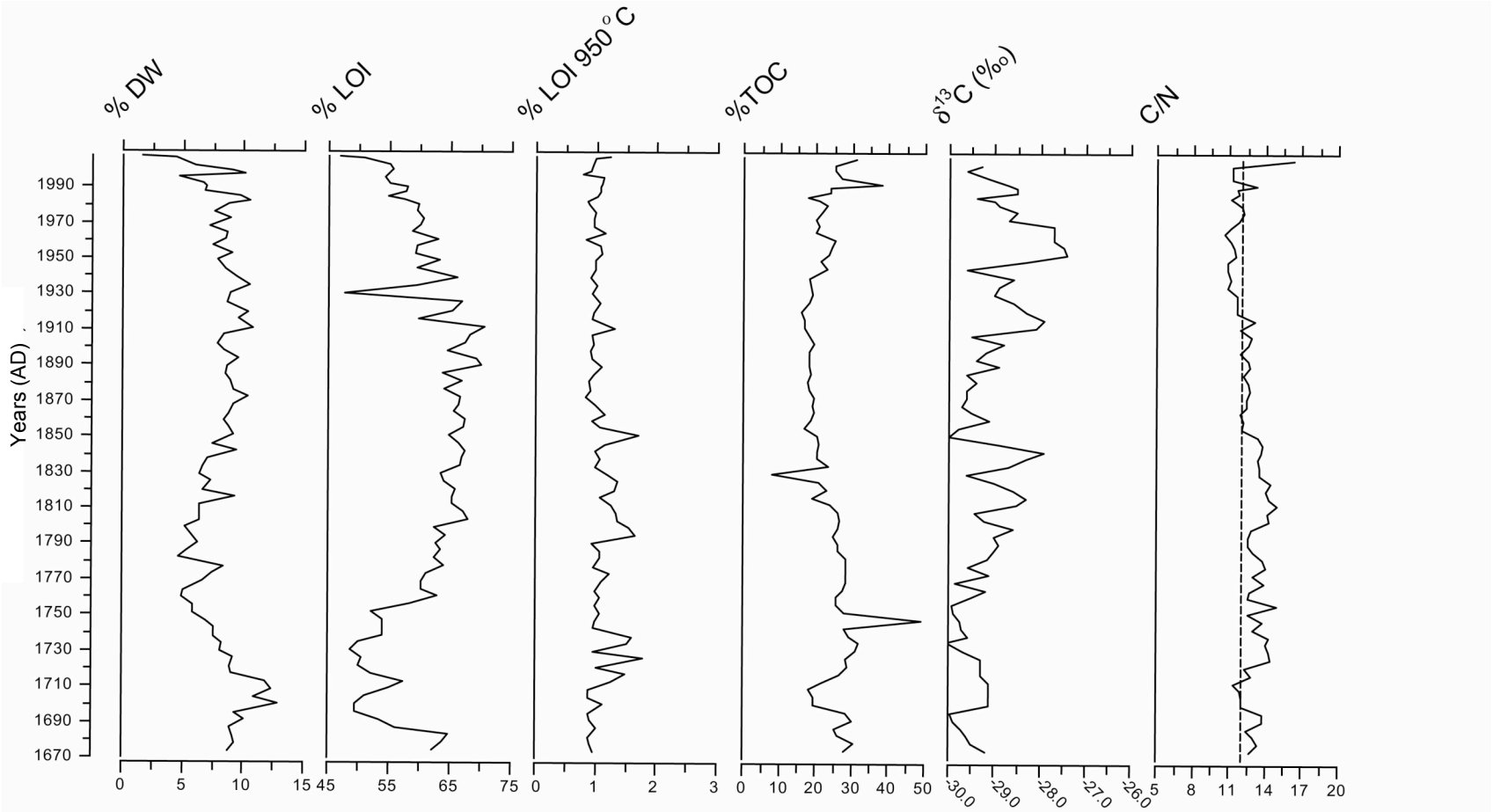


*Figure 5.1. The results of organic isotope analyses conducted on XLW2. The age model is derived from $^{210}$Pb analyses conducted on the core and is therefore in AD (before 2007). %DW, %TOC, %LOI 950$^{o}$C are displayed as well as $\delta^{13}$C (‰) and C/N ratios for the core. The dotted line on the C/N plot corresponds to the reference line for an aquatic source of carbon to the lake system (< 12) and mixed macrophytes (> 12 and < 20).*

### 5.3.2 XRF analyses from core XLW2

All elements (apart from Pb and Pb/Ti) are at high levels at the beginning of the record, c. 1670 AD after which they decrease again after c. 1690 AD (including Fe, Ti, Zn, Cu and Ni) (Figure 5.2). The pollution indices also show a decline, in particular, Cu/Ti Zn/Ti and Ni/Ti. Values for all elements (apart from Pb and Pb/Ti) all increase once again after c. 1715 AD. Fe increases to 6%, Ti to 0.6%. Zn, Cu and Ni also increase to between c. 165 and 215 (µg/g), between c. 55 and 73 (µg/g) and c. 50 and 60% respectively. Two peaks are seen in Cu/Ti at c. 1735 (1.2) and c. 1770 (1.09). These elements all show a decreasing trend once again at c. 1810 AD.

After 1810 AD there is little change shown by the elements. An increase is shown in Zn at c. 1875 to 136 (µg/g). A similar peak is shown by the ratio Zn/Ti at the same time to values of 0.8. Cu/Ti and Ni/Ti also increase at c. 1850 (to 0.98) and between c. 1840-1856 (between 0.96 and 0.98) respectively. After c. 1970 AD, a distinct increase is seen by many of the variables in Figure 5.2. The elements Pb and Zn all increase to the greatest values in the record at 162 and 217 µg/g respectively. Pb/Ti, Zn/Ti and Ni/Ti also demonstrate this change. Cu/Ti also shows an increase in values, although this occurs at c. 1970. All these values decline at the top of the core, after c. 2000 AD.

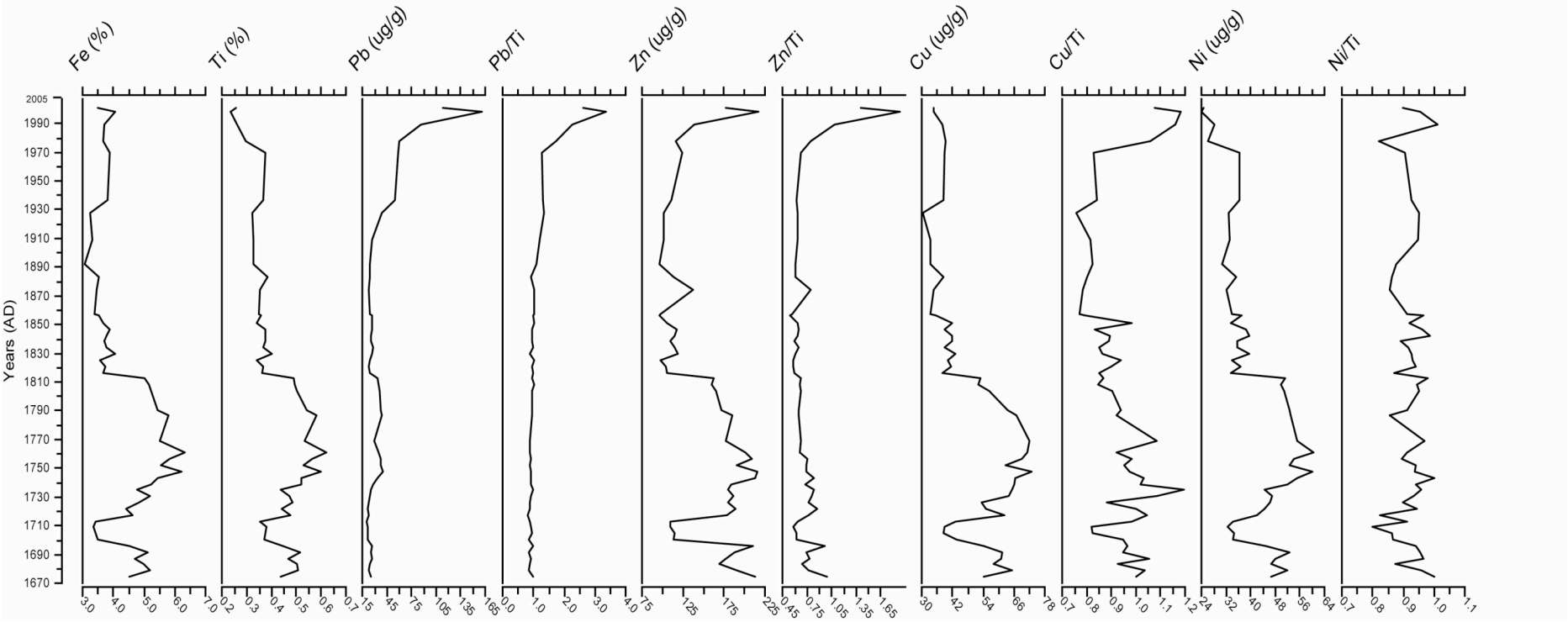


*Figure 5.2 Trace element results from XRF analyses on core XLW2. The age scale is in AD as it is derived from the $^{210}$Pb derived model. The pollution indices are also shown (Pb/Ti, Zn/Ti, Cu/Ti, Ni/Ti). Relevant units are shown on the figure.*

### 5.3.3. Results of multivariate analyses on X00-X06

5.3.3.1. DCA

Ordinations were carried out on species data > 2% in any one sample. DCA analyses resulted in a first axis eigenvalue of 0.152 (Table 5.2). A first axis gradient length of 1.409 (less than 2.0) suggests a linear response of the species data and as a result PCA analyses were conducted.

| DCA | 1 | 2 | 3 | 4 | Inertia |
|---|---|---|---|---|---|
| Eigenvalues | 0.152 | 0.054 | 0.032 | 0.020 | |
| Length of gradient | 1.409 | 1.433 | 1.020 | 0.921 | |
| Cumulative % variance of species data | 20.9 | 28.4 | 32.8 | 35.6 | |
| Sum of all eigenvalues | | | | | 0.726 |

*Table 5.2. DCA eigenvalues and gradient length results for axes 1 to 4, for cores X00 and X06.*

5.3.3.2. PCA

PCA analyses with centering by species and square root transformation, resulted in a first axis and second axis eigenvalue of 0.248 and 0.155 respectively. The first two axes therefore capture 40.4% of the variation in species data, with axis 1 capturing over half of this (c. 25%) (Table 5.3).

| PCA | 1 | 2 | 3 | 4 | Total Variance |
|---|---|---|---|---|---|
| Eigenvalues | 0.248 | 0.155 | 0.080 | 0.060 | |
| Cumulative % variance of species data | 24.8 | 40.4 | 48.4 | 54.4 | |
| Sum of all eigenvalues | | | | | 1.000 |

*Table 5.3. PCA eigenvalues and cumulative percentage variance of species data results for axes 1 to 4, for cores X00 and X06.*

The results of *K-means* cluster analyses was applied to the PCA samples biplot for the cores X00 and X06 (Figure 5.3). A total of 3 groups were selected (Table 5.4). In order to reduce label crowding on the species biplot, only species of N>5 were displayed (Figure 5.4).

| Class number | Samples |
|---|---|
| 1 | 1 to 13 |
| 2 | 14 to 48 and 50, 51, 52 |
| 3 | 49, 53 to 144 |

*Table 5.4. Sample classification of the three chosen groups after K-means cluster analysis. The classification is adopted in Figure 5.3.*

Figures 5.3 and 5.4 display the sample plot and diatom species vector plot respectively. The sample plot shows the clear transition from the bottom core samples (class 3) dominated by *A. minutissimum* to class 2 along axis 1 (Table 5.5). Other species associated with this group include *Fragilaria tenera, Eunotia subarcuatoides, Eunotia bilunaris* and *Nupela vitiosa.* Along the transition between class 3 and 2 the assemblage changes, being composed of *Eunotia, Navicula* and *Neidium* species. Class 2 sees a composition derived of *Punctastriata discoidea, Naviculadicta raederiae, Staurosira construens var venter, Pinnularia subcapitata* and *Cymbopleura subcuspidata.* A movement along axis 2 is then shown, driven by the appearance of *Discotella woltereckii, Eolimna minima, Tabellaria flocculosa* and *Fragilaria nanana.*

As Table 5.5 displays, the species *S. construens var venter* and *A. minutissimum* are closely associated with axis 1 with values of -0.8372 and 0.8853 respectively which is also clearly demonstrated in Figure 5.4. *D. woltereckii* and *E. subarcuatoides* are on the other hand closely associated with axis 2 with values of 0.7221 and 0.8505 respectively.

| Species name | Axis 1 Score | Axis 2 Score |
|---|---|---|
| *Staurosira construens* var *venter* | -0.8372 | -0.1222 |
| *Achnanthidium minutissimum* | 0.8853 | 0.3474 |
| *Discotella woltereckii* | -0.0908 | 0.7221 |
| *Eunotia subarcuatoides* | 0.3235 | -0.8505 |

*Table 5.5. PCA axis 1 and 2 scores for the dominant species shown in Figure 5.4, from the core X00 and X06.*

**Figure 5.3**

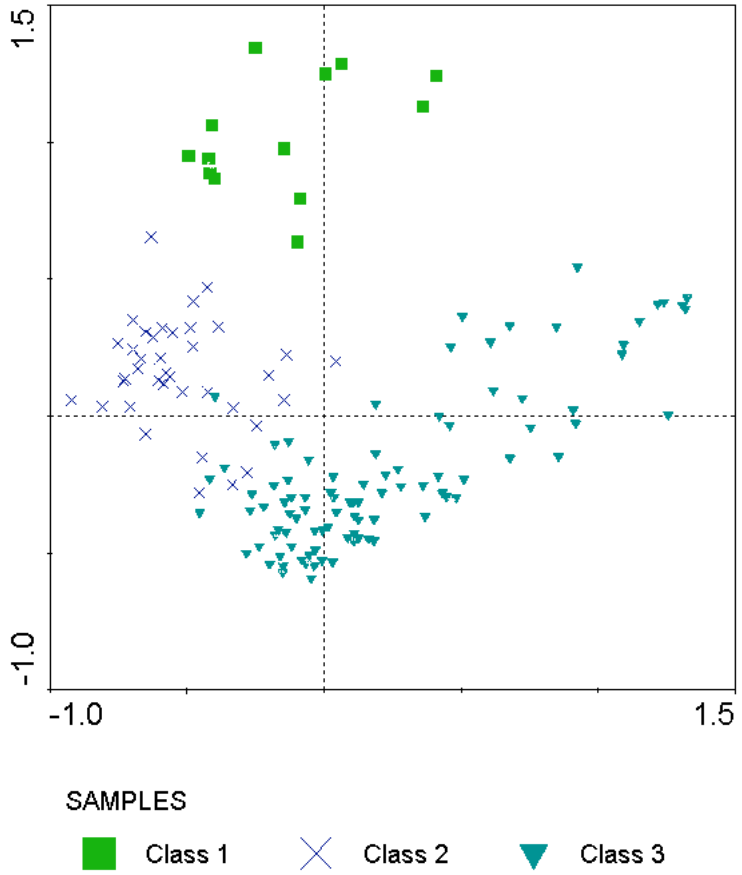


**Figure 5.4**

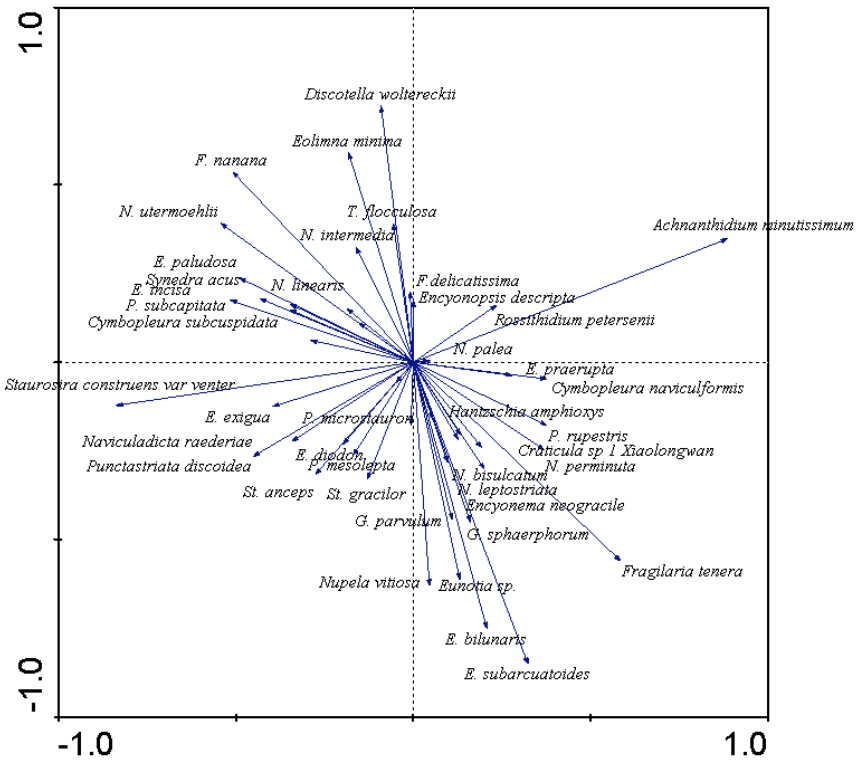


*Figure 5.3 Samples biplot from the cores X00 and X06. K-means cluster analysis results are displayed on the stratigraphy to identify the three main zones of change in the core. Class one refers to core top. Figure 5.4 Species vector biplot for the core X00 and X06. Species N>5% are only displayed for visual purposes.*

### 5.3.4. Results from diatom stratigraphy of core X00/X06

Please refer to Figure 5.5 for the diatom stratigraphy.

5.3.4.1. Zone 1 (c. 2000 ± 45 to c. 1675 ± 40 years BP)

*A. minutissimum* is the dominant species in zone 1 and this is also reflected by PCA axis 1 score (refer to Table 5.4). The abundance of *A. minutissimum* declines after c. 1760 years BP which is concomitant with an increase in *S. construens var venter*. The presence of other species in the zone is also seen including *Eunotia bilunaris, E. subarcuatoides, G. parvulum, N. leptostriata* and *P. discoidea.* Values of D:C increase during the zone between c. 1840 and 1760 years BP after decreasing after 1920 years BP. These increases also coincide with an increase in valve concentrations (4 x $10^7$ and 3 x $10^7$ valves/g dry weight).

5.3.4.2. Zone 2 (c. 1675 ± 40 to c. 920 ± 30 years BP)

Percentage abundances of *A. minutissimum* remain in general at lower values through this zone while percentages of *S. construens* var *venter* increase, reaching values as high as c. 60% by c. 1635 years BP. A peak is seen in *A. minutissimum* between c. 1450 and 1395 years BP. The abundances of other species show little change although an increase is seen between the start of zone 2 and c. 1470 years BP and later after 1250 years BP (e.g. *E. subarcuatoides*, *P. disoidea*).

A small increasing trend is seen in diatom concentrations with a peak of 5 x $10^7$ valves/g dry weight between c. 1450 and 1395 years BP, which is coincident with the increase in *A. minutissimum* abundances. D:C show an increase in values to c. 70% after entering zone 2 until c. 1265 years BP. PCA axis 1 increase concomitant with the increase in *A. minutissimum* after which they fluctuate at c. 0. PCA axis 2 scores show an overall decreasing trend apart from an increase concomitant with increases in D:C and valve concentrations.

5.3.4.3. Zone 3 (c. 920 ± 30 to c. 495 ± 25 years BP)

Values for *A. minutissimum* fall to the lowest in the sequence on entering zone 3 while abundances of *S. construens var venter* continue to fluctuate between c. 20 and 50%. Percentage abundances of *E. subarcuatoides* remain between 0 and 15%. Small increases are also seen in *Punctastriata discoidea* throughout zone 3 and in particular towards the end of the zone c. 495 years BP. At this time the presence of *Synedra acus var angustissima* is seen although percentage abundances are low (below 10%). *Navicula utermoehlii* makes an appearance in the record towards the end of zone 3 and percentage abundances of *N. leptostriata* make an appearance once more. D:C also show an increasing trend after c. 730 years BP although fluctuating. Diatom concentrations also fluctuate with values showing a small increasing trend.

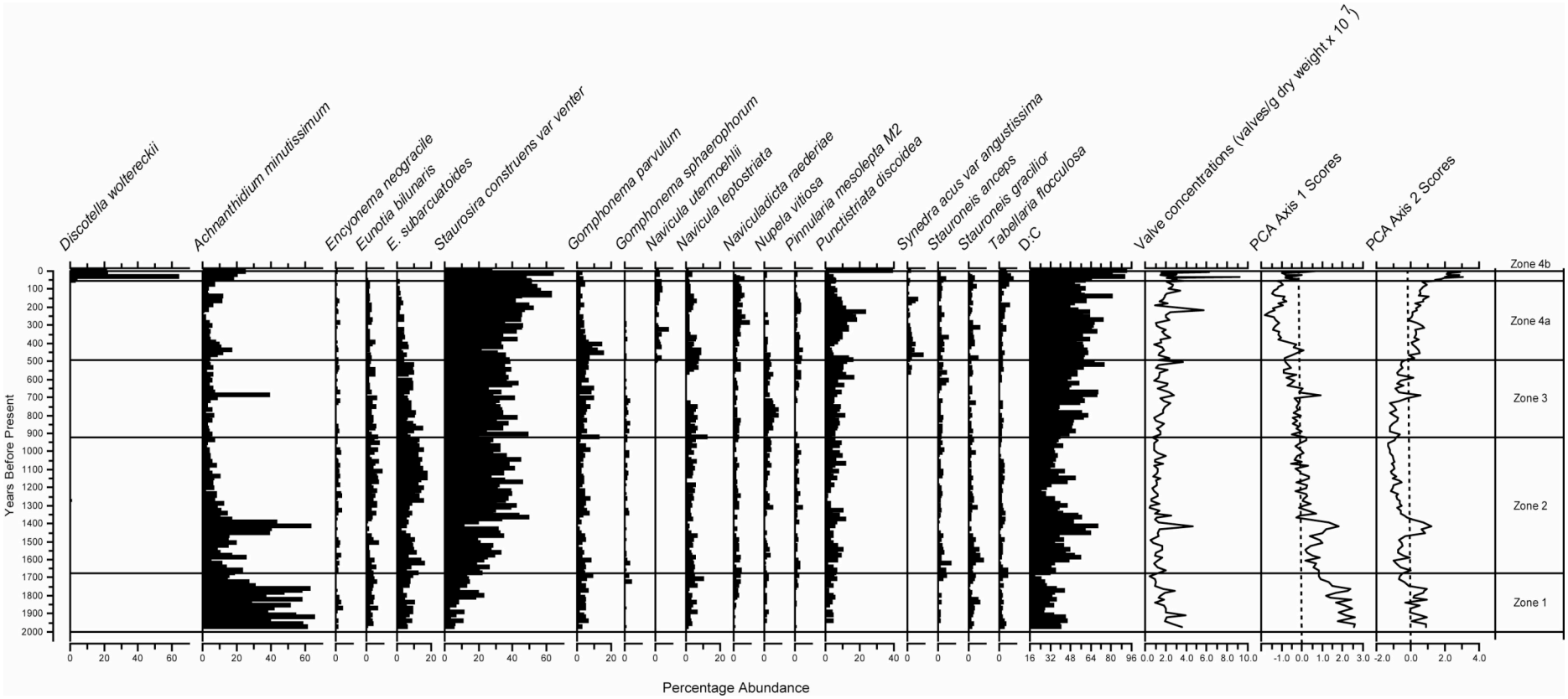


*Figure 5.5. The diatom species reconstruction from cores X00 and X06. The corrected age chronology is used here, so that years are in years before present, 2006 when the core was collected (BP). D:C, valve concentration and PCA axis 1 and 2 scores are also shown. The 5 zones are applied to the data, based on results from zoning techniques.*

5.3.4.4. Zone 4a (c. 495 ± 25 to c. 55 ± 10 years BP)

*A. minutissimum* percentages increase on entering zone 4a although percentage abundances remain below 30%. Percentages of *S. construens* var *venter* decrease after the end of zone 3 but by c. 395 years BP they begin to increase once again. Abundances of *E. subarcuatoides, E. bilunaris* and *N. vitiosa* show a decreasing trend as do *G. parvulum* although the latter after increasing between 495 and 400 years BP. *P. discoidea* also increases on entering zone 4a until c. 230 years BP after which it declines. *S. acus* var *angustissima* appear in the stratigraphy prior to zone 4a (at c. 565 years BP) and decline after c. 155 years BP.

Peaks are seen in diatom concentrations and D:C, reaching the highest values in the record for both proxies. A peak is seen in concentrations (c. 5.5 x $10^7$ g/dry weight) at c. 215 years BP. The decreasing (increasing) trend in PCA axis 1 (axis 2) scores is still seen in zone 4a, reflecting the decline in *A. minutissimum* and fall in *S. construens var venter* respectively.

5.3.4.5. Zone 4b (c. 55 ± 10 to c. 0 years BP)

Zone 4b sees the introduction of *D. woltereckii* to the stratigraphy. Abundances reach a peak at c. 65% at c. 35 years BP, after which values fall and oscillate around 20% abundance. Abundances of *A. minutissimum* also increase on entering the zone which is reflected by the increase in PCA axis 1 scores. *S. construens* var *venter* declines in the zone apart from the surface sample, the same trend is shown by *P. discoidea*. Valve concentrations increase in zone 4b on two occasions (c. 35 and 10 years BP) corresponding to the increase in *D. woltereckii* and *S. construens* var *venter, P. discoidea* respectively. D:C also increase in this zone again reflecting the abundances of these species.

**5.3.5. Timeseries results from bulk organic isotopes**

As outlined in Section 5.2.6.5, timeseries analyses were used in order to outline the major trends in the data from both X00 and X06 cores as well as XLW2. The fitting of GAMM models, with 95% confidence levels outlined, permits the identification of significant changes in the records.

Figure 5.6

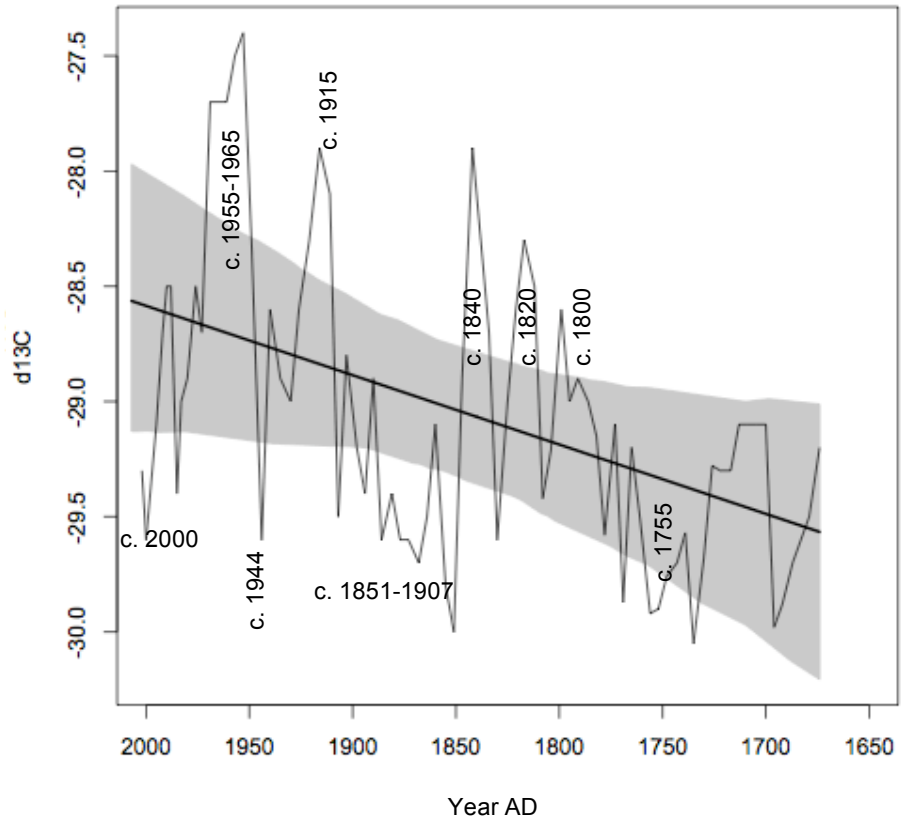


Figure 5.7

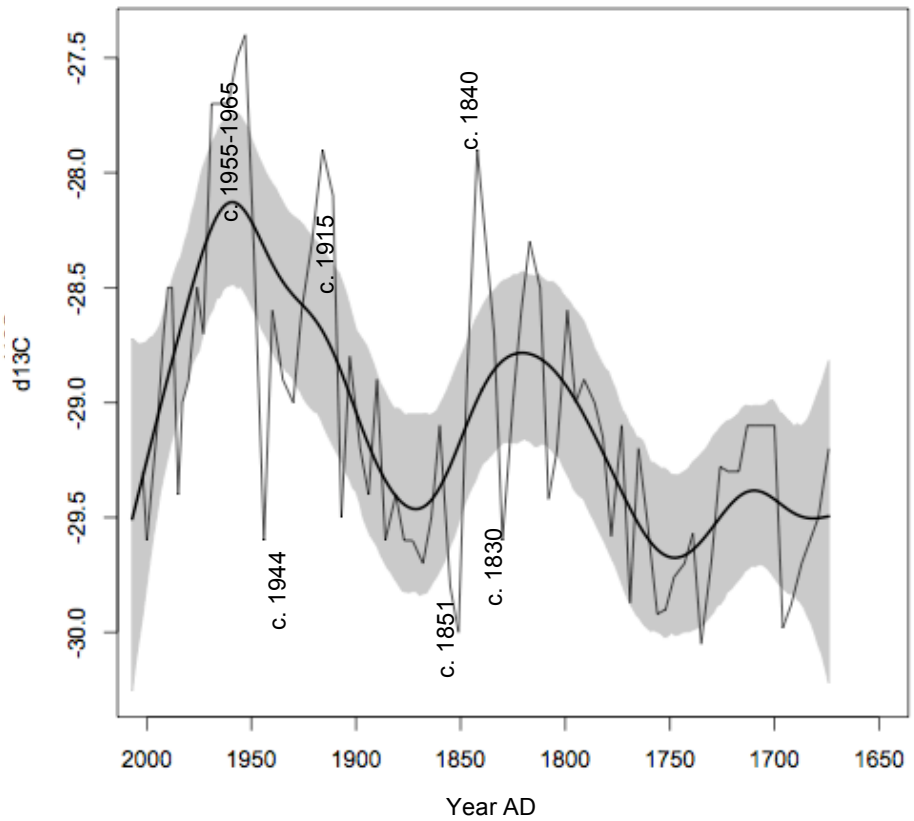


*Figure 5.6. Timeseries analyses on $\delta^{13}C$ (‰) data from core XLW2. GAMM2 model (with auto-correlation structure) was chosen. Figure 5.7. Timeseries analyses on $\delta^{13}C$ (‰) data from core XLW2. GAMM1 model is shown here. The black line corresponds to the fitted model and grey shaded area the 95% confidence intervals associated with the model. Year AD is based on the derived $^{210}Pb$ age model. Dates corresponding to significant changes in the data are highlighted.*

Timeseries analyses were conducted upon the bulk organic isotope data from XLW2. Both GAMM1 and GAMM2 models were applied to the data. On the basis of AIC scores, GAMM2 was chosen as the best model to apply to the $\delta^{13}C$ data. However, when looking at Figure 5.6 the fitted model does not pick out any distinct features of the data (e.g. compared to Figure 5.7). This can often occur when applying a model with auto-correlation structure, when a data set has a relatively short length (in this case 83 samples) (Simpson, pers. comm.). The model has trouble distinguishing cases of auto-correlation between actual (significant) changes which occur close (temporal scale) to each other due to the length of the record sampled (ibid.). As a result, the results from the fitting of the GAMM1 model are also displayed.

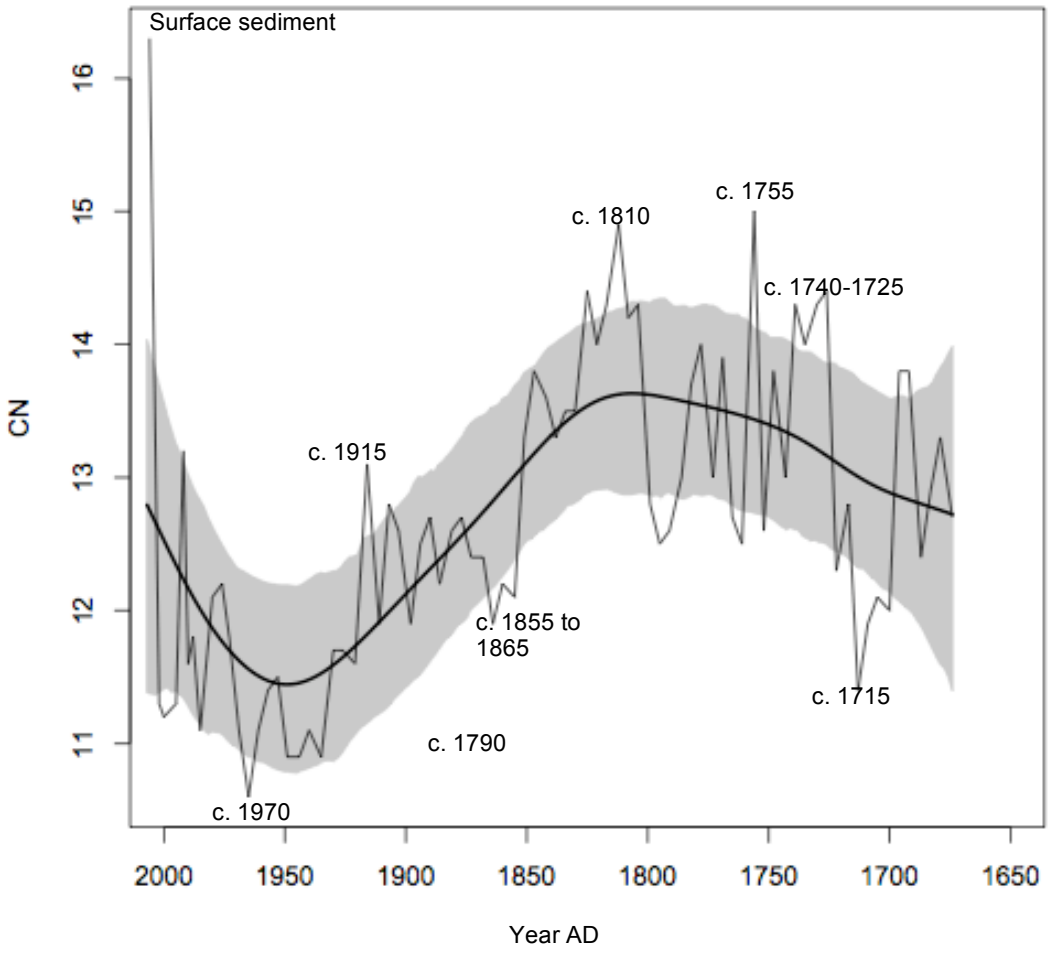


*Figure 5.8. Timeseries analyses on C/N data from core XLW2. GAMM2 model (with auto-correlation structure) is shown here. The black line corresponds to the fitted model and grey shaded area the 95% confidence intervals associated with the model. Year AD is based on the derived $^{210}Pb$ age model. Dates corresponding to significant changes in the data are highlighted.*

Both GAMM2 (Figure 5.6) and GAMM1 (Figure 5.7) show a general increasing trend in the $\delta^{13}C$ data. Significant changes are outlined in both of the records, although as model GAMM1 is more fitted to the data (as it is without auto-correlation structure) fewer changes are seen as

significant. Instances of significant changes are seen in both models at the following times; c. 1842, c. 1850, c. 1915, c. 1945 and between c. 1955 and 1965 AD.

C/N show an increasing trend according to the GAMM1 model until c. 1800 AD, after which a decreasing trend is seen (Figure 5.8). This continues until c. 1965 AD after which values increase once more to present day. It is important to note that the overall changes are around 3 units for the whole record. However, significant peaks are seen at the following times: c. 1715, between c. 1740-1725, c. 1755 and c. 1810 AD. The increase in surface sediments (2007) is also seen, where C/N values are greater than 12.

### 5.3.6. Timeseries results from diatom PCA axes scores

Timeseries results show that there are a number of significant shifts in axes scores from cores 00/06. For PCA axis 1 and 2, the GAMM2 (with autocorrelation structure) was found to be the significant model (with lower AIC than GAMM1).

Overall the model demonstrates a decreasing trend in axis 1 scores over the past 2000 years BP (Figure 5.9). After c. 215 years BP this trend shifts to an increasing one. When looking at specific changes in the data, any points that are outside of the 95% confidence intervals are regarded as significant. As a result, the following shifts in the axis 1 scores are significant: between c. 1825-1775, c. 1450-1380, at c. 685, between c. 435-420 years BP and in surface sediments. As Table 5.5 demonstrates, *A. minutissimum* is strongly associated with axis 1. As a result, these significant changes most likely reflect increases in this species as seen in Figure 5.5. changes in this species down-core. A decline in *A. minutissimum* and increase in *Staurosira construens* var *venter* is seen at c. 1760 years BP. At the start of the PCA axis 2 record a decreasing trend in is seen until c. 920 years BP after which the trend changes to an increasing one (Figure 5.10). Axis 2 is most strongly associated with the species *Eunotia subarcuatoides* and *Discotella woltereckii,* although this latter species is only introduced after 55 years BP (Table 5.5). PCA axis 2 has fewer changes that are considered as significant, on the basis of the selected GAMM2 model. These occur between c. 1450-1395 and at c. 685 years BP and are a result of the decreases in *E. subarcuatoides*. The timings of these events are mirrored in timeseries results from axis 1. Significant reductions in *E. subarcuatoides* are seen at c. 1700 and 1600 years BP. The introduction of *D. woltereckii* is identified after c. 55 years BP and is also a significant change in the axis scores.

Figure 5.9

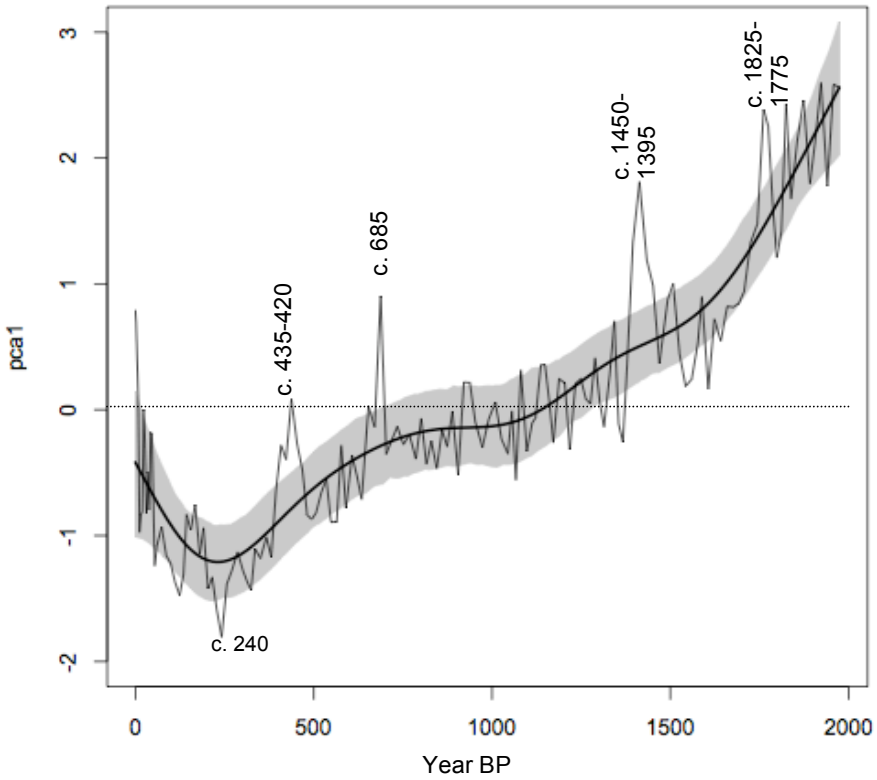


Figure 5.10

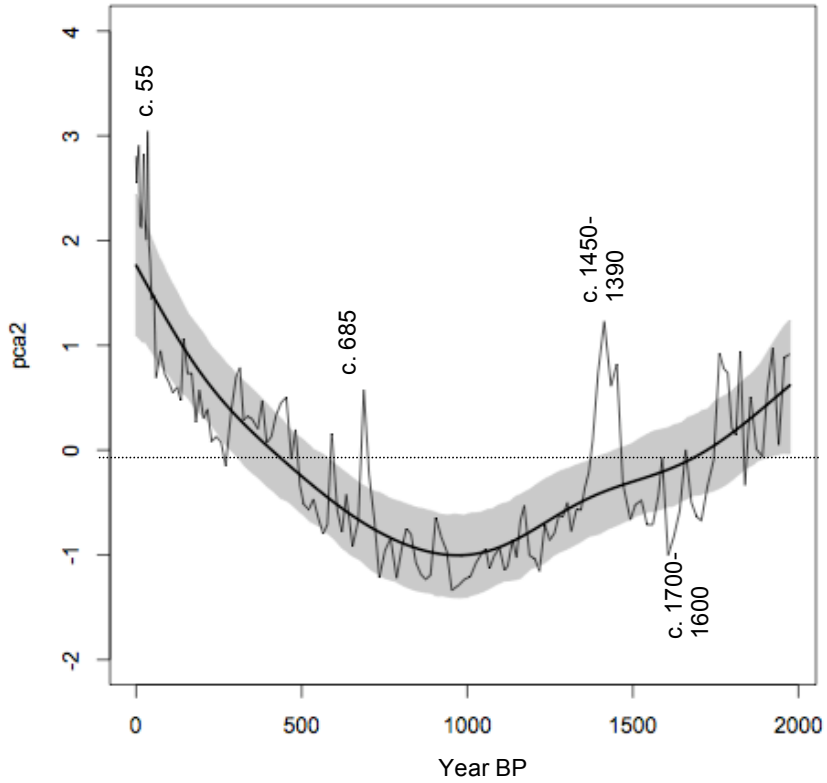


*Figure 5.9. Timeseries analyses of PCA axis 1 scores. Figure 5.10. Timeseries analyses in PCA axis 2 scores. A GAMM2 model (with auto-correlation structure) was chosen. The black line corresponds to fitted model and grey shaded area the 95% confidence intervals associated with the model. Dashed line corresponds to the reference line of 0 for the axes scores. Years BP (2006), based on the corrected varve age model are shown. Dates correspond to significant events.*

### 5.3.7. Results of Significant ZERo crossing of the derivatives (SiZer)

Results from SiZer analyses can be adopted as a means to identify which features in data are significant and which features may be due to spurious sampling artefacts (Rondonotti et al. 2007). SiZer goes further to visually display the statistical significance of features over both location *t* and scale *h* (the bandwidth or level of data resolution) (ibid.). SiZer considers a wide range of bandwidths, which avoids the classical problem of bandwidth (*h*) selection. In this project, the bandwidth *h* has also been changed into equivalent years. These do not correspond to the length of the data set. At each point in scale space (therefore at each location, and also at each bandwidth), a confidence interval for derivatives is constructed and when that confidence interval is completely above (below) 0, there is a statistically significant increase (decrease), and that location on the surface is shaded red (blue). When the confidence interval for the derivative contains 0, the intermediate colour of purple is used and grey is shown when the data are too sparse to do meaningful inference (Rondonotti et al. 2007).

As discussed in Section 5.3.6, over the period of the record (c. 2000 years) a downward trend is seen in PCA axis 1 scores (reflected by a decrease in the species *Achnanthidium minutissimum*) then increasing after c. 350 years BP. Axis 2 scores show a decreasing trend after 1000 years BP after which axis 2 scores increase. Based on timeseries analyses significant changes are seen between c. 1775-1760, 1450-1395, 685, 435-420 and 55 years BP. SiZer results show that for the majority of the PCA axis 1 record and across many bandwidths higher than c. 300 years, a significant decreasing trend in data is seen but that the later increasing trend identified by timeseries results is not significant (Figure 5.11). For bandwidths less than c. 300 years this increase is significant.

On a smaller bandwidth, c. 400 years, this is seen as a significant increase. When looking at the results within the smaller bandwidths e.g. between 100 and 32 years, significant decreases in the axes scores are seen at c. 1700-1650, 1350, 600, 500-350 and an increase at c. 50 years BP. These coincide with the significant shifts in axes scores displayed by the timeseries, suggesting that these are significant within the decadal to centennial bandwidth.

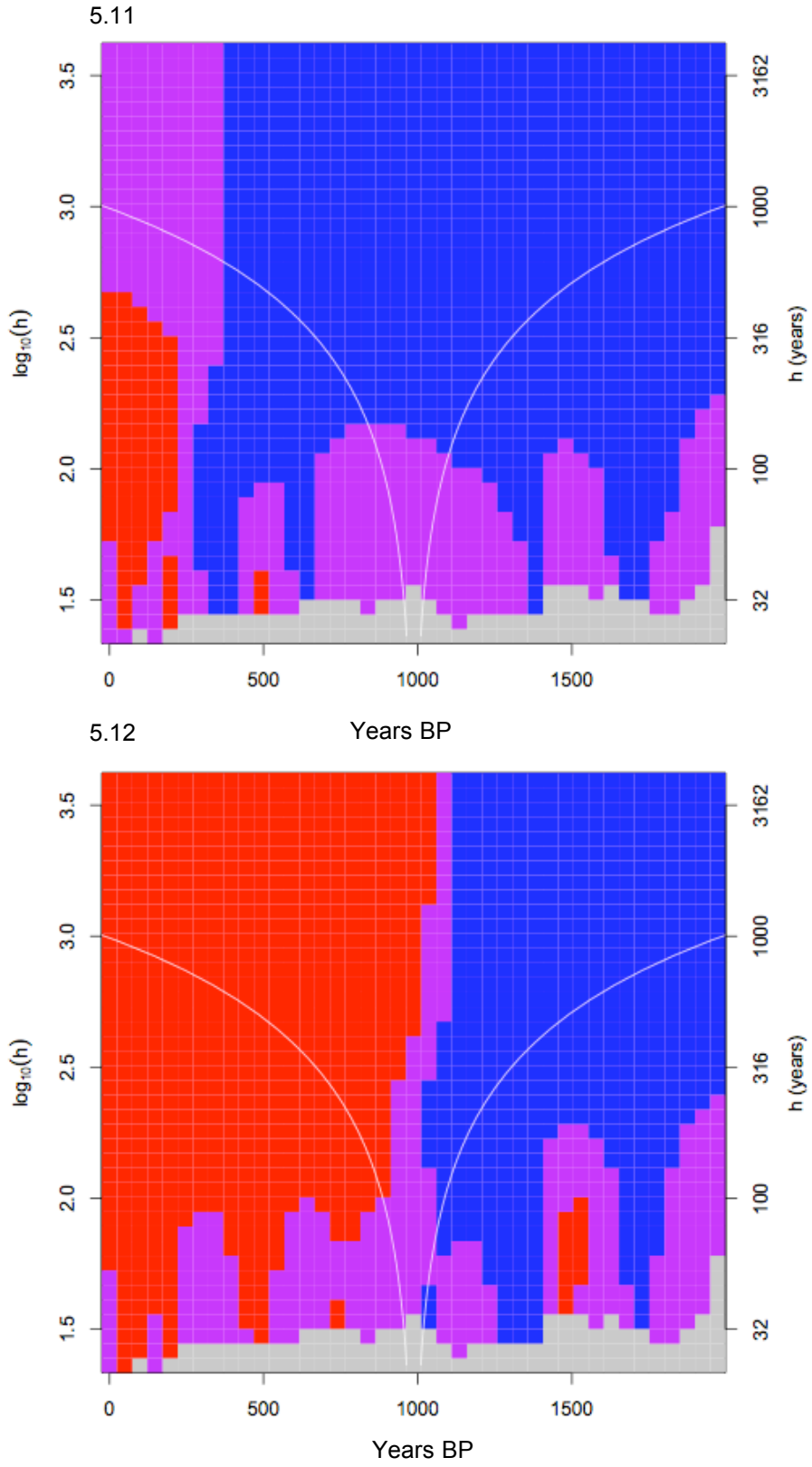


*Figures 5.11. SiZer results from PCA axis 1 scores and 5.12. PCA axis 2 scores of lake Xiaolongwan. Y-axis represents the bandwidth applied to the data (h) and right hand y-axis the equivalent bandwidth in years. Blue (red) corresponds to decreasing (increasing) trend in data. The age scale is in years BP (present is 2006).*

PCA axis 2 scores show that a decreasing trend is seen until c. 1100 years BP and that this is significant until a bandwidth of 310 years is reached (Figure 5.12). The increasing trend is seen after c. 1050 years BP that is significant across a greater number of bandwidths (e.g. up to 85 years). Significant increases and decreases are also seen within smaller bandwidths (between 100 and 50 years) at c. 1750-1650, 1400-1250, 600-400 and 25-5 years BP. These correspond with the changes in axis 1 scores (Figure 5.11), again demonstrating significant variability at centennial to decadal timescales.

For the Xiaolongwan record, superimposed upon the PCA axes score trends are intervals of significant change between centennial and decadal bandwidths (Figures 5.11 and 5.12). Although the exact timing of these events varies depending on the different smoothing methods used (e.g. timeseries or SiZer) the main changes from SiZer analyses occur between the periods c. 1775-1650, 1450-1350, 600-350, 50 and after 25 years BP for the whole Xiaolongwan (XLW) record. These results will be adopted to discuss the periods of significant change from the XLW record in order to compare with regional indices.

## 5.4. Discussion

As discussed in Section 5.2.6.3, *k-means* cluster analyses were conducted on diatom data in order to classify principal assemblage changes. In order to summarise main trends in PCA sample biplots, the cluster analysis was adopted to apply different classes to the data (Table 5.4). These class divisions will be adopted here in order divide palaeoenvironmental data into three different timing intervals. Although sample 49 is grouped in Class 3, for ease it will be grouped with Class 2. This is so that age boundaries associated with the classes can be applied for the discussion. Classification rather than zonation techniques were decided to divide the diatom data presented in Section 5.3.4 for the purpose of the discussion as some zonation techniques can find artificial zones in data (Birks, pers. comm.). Some reference however will still be made to the zones in Figure 5.5 to emphasise further significant stratigraphical changes in the data. The discussion will be divided into two sections; firstly an ecological interpretation of the diatom reconstruction from Lake Xiaolongwan will be provided after which comparisons with other records of environmental change will be carried out.

### 5.4.1. Ecological interpretation of diatom ecology at Lake Xiaolongwan

*A. minutissimum* is regarded as an opportunistic species that is cosmopolitan and can tolerate a broad range of nutrient and disturbance conditions (Table 5.6) (Van Dam et al. 1994; Watchorn et al. 2008). It is an epiphytic species on macrophytes (e.g. Phragmites; Karosienė and Kasperovičienė 2008) found at the outer edges of the lake, and at Lake Xiaolongwan is also an epiphyte of the macrophyte *Equisetum* (Figure 3.6, Table 3.3). At the end of summer

stratification the macrophytes die and some remain that are transported to the central regions of the lake, associated with autumnal wind transport. This is the most likely process accounting for the presence of *A. minutissimum* in the sediment trap at these times (Figure 3.6). The strength of these autumnal winds is associated with the intensity of the east Asian winter monsoon (EAWM), so that increases in the species abundance may be reflecting its increased intensity. However, the mechanism behind presence of the species in sediment traps during stratification is not clear. Other literature has also suggested that the species, while normally periphytic, can also have tychoplanktonic abilities with increased turbulence (Kuhn et al. 1981) (Table 5.6). Based on the ecology of the species it suggests that the lake environment at Lake Xioalongwan was more dynamic when this opportunistic species dominated the assemblage. This could be an indirect reflection of stronger turnover at the lake, increasing oxygen saturation in the lake, which is another ecological preference of the species.

The Lake Xiaolongwan record shows a progressional decline in *A. minutissimum* and increase in the species *Staurosira construens* var *venter.* This benthic/epiphytic species also has a high oxygen demand although cannot tolerate as wide a trophic status as *A. minutissimum* (Table 5.6). Evidence has also shown that this species is abundant in littoral regions where water is shallow. As such, the competitive advantage of this species, compared to *A. minutissimum* may be reflecting a decline in lake water level. Abundances of *P. discoidea,* often an indication of shallow regions and present today in the phytobenthos, also increases at the same time as *S. construens* var *venter,* as well as *Eunotia subarcuatoides* (Figure 5.5), a species whose habitat is sometimes located in wet/moist places outside of the water body (Van Dam et al. 1994). Both of these species further indicate a possible shallowing of lake levels (Table 5.6; Figure 5.5). *S. construens* var *venter* is also regarded a species that is more competitive in nutrient-rich waters while *E. subarcuatoides* is an indicator of lower pH. *Navicula utermohlii,* which is introduced after c. 500 years BP, is a species argued to have a trophic status optimum of mesotrophic waters, further supporting a move to more nutrient rich waters at Lake Xiaolongwan (Van Dam et al. 1994).

Later, the introduction of *Discotella woltereckii* and an increase in *Tabellaria flocculosa* is seen after c. 60 years BP. Contemporary trap data from Lake Xiaolongwan shows that *D. woltereckii* is most abundant during spring and autumn overturn while *T. flocculosa* is more abundant at the end of lake stratification and overturn (Figure 3.6). These species suggest that there is an increase in lake turnover. *T. flocculosa* is also a species which has a high oxygen demand, possibly further supporting the evidence of enhanced (a longer period of) lake turnover.

| Species name | Ecology | References |
|---|---|---|
| *Achnanthidium minutissimum* var *minutissimum* | Benthic/epiphytic, sometimes tychoplanktonic. Oxygen loving, pioneer species, phosphorous specialist. pH circumneutral and also at pH < 5.5. Abundant at the beginning of stratification and autumn turnover at XLW following macrophyte decay. Opportunistic species with wide tolearance of trophic state, high oxygen requirement. | (Brown et al. 2008; Cholonky 1968; Kuhn et al. 1981; Reavie and Smol 1998; Van Dam et al. 1994; Watchorn et al. 2008) See Figure 3.5; Rioual pers.comm. |
| *Gomphonema parvulum* | Epiphytic. Best development in nutrient rich waters and low pH < 5.5. Can occur on moist/wet places. | (Patrick and Reimer 1966; Round 1990; Van Dam et al. 1994) |
| *Navicula leptostriata* | Oligo-mesotrophic status and can occur in moist/wet places outside of water bodies | (Van Dam et al. 1994) |
| *Pinnularia mesolepta* | Fresh water of low mineral content, usually circumneutral to slightly acidic. High oxygen saturation and mesoeutrophic to eutrophic status. | (Patrick and Reimer 1975; Van Dam et al. 1994) |
| *Fragilaria species* | Species from Xiaolongwan, tychoplanktonic | Rioual pers. comm. |
| *Discotella woltereckii* | Abundant in spring and autumn overturn and summer stratification | Figure 3.5; Rioual pers. comm.. |
| *Staurosira construens* var *venter* | Shallow, standing water, non-alkaline. Mesoeutrophic to eutrophic or oligotrophic to eutrophic(Patrick et al. 1966). 75% oxygen saturation in water. Epiphytic/littoral assembage. | (Bradbury 1971; Haberzettl et al. 2005; Metcalfe et al. 1997; Patrick et al. 1966; Van Dam et al. 1994) |
| *Synedra acus* | Can indicate shallow enriched, turbid waters. Planktonic. | (Padisak et al. 2009) |
| *Eunotia subarcuatoides* | Can tolerate high and an abrupt variation in pH. Also found at pH < 5.5. Likes metal rich waters, oligotrophic. Epiphytic. Can be found in wet/moist places. | (Alles et al. 1991; Razjigaeva et al. 2004; Van Dam et al. 1994) |
| *Punctastriata discoidea* | Phytobenthos, benthic, epiphytic. Shallow lakes and lake environments. | (Kingston 2003) Rioual, pers. comm. |

*Table 5.6 Summary of main ecological characteristics of dominant species from cores X00 and X06. Respective references are provided.*

### 5.4.2. Environmental reconstruction between c. 2000 to c. 550 years BP

At Lake Xiolongwan an increase in the abundance of the species *S. construens* var *venter* is seen after c. 2000 years BP suggesting a trend to more shallow lake waters over this period (up to c. 350 years BP based on axis 1 species scores; Figure 5.5, Tables 5.5 and 5.6). This is most likely a reflection of the weakening east Asian summer monsoon (EASM) intensity over the late Holocene in response to changes in insolation and a southward shift in the Intertropical Convergence Zone (ITCZ) (e.g.Cosford et al. 2008; Wang et al. 2005). The Xiaolongwan data is concomitant with regional indices demonstrating a regional cooling and drying trend after c. 2000 years BP (Hong et al. 2000; Hong et al. 2001; Makohonienko et al. 2008). Palaeoenvironmental evidence of $\delta^{18}O$ and $\delta^{13}C$ records, collected from a swamp in Jinchuan (north of Dalongwan lake; Figure 1.2), indicate that between c. 2800 and 1800 years BP there is a decrease in mean air temperatures and frequent fluctuations in soil moisture and precipitation

(Hong et al. 2000; Hong et al. 2001; Makohonienko et al. 2008). Makohonienko (2008) argue that after c. 2000 years BP a second expansion of pine is seen in the Changbai region indicating a cooler period and one with low evapotransipration potential. Li et al (2010) also argue that between 2200 and 1800 cal years BP the record from Jingbo Lake suggests a weakening of the EASM, correlating evidence from other regions of eastern China (e.g. Dongge cave; Section 1.7). Other evidence suggests a high drought index over the period with reconstructed air temperatures at their highest and a decline of Korean pine in the Changbai mountain region close to Lake Xiaolongwan, reflecting a concurrent drop in precipitation (ibid.; Makohonienko et al. 2008).

Based on timeseries and SiZer analyses events of change are identified between the periods c. 1775-1650, 1450-1350, 600-350, 50 and after 25 years BP for the whole Xiaolongwan record. Cosford et al (2008) demonstrate that punctuating the drying trend seen in the region are abrupt millennial- to decadal-scale fluctuations, supporting the evidence from Lake Xiaolongwan. During the time period c. 2000 to c. 500 years BP, two of these events are reflected by fluctuations in PCA axis 1 scores (Figure 5.9), representing significant increases in *A. minutissimum.* As outlined in Section 5.4.1, this signifies a dynamic lake environment and may be suggesting an increase in autumn winds in the region (e.g. EAWM intensity), transporting macrophytes to the central region of the lake. Largest changes in axes scores correspond to the interval c. 1450-1350 years BP (refer to Figures 5.9 and 5.10), which coincides with evidence of a significant decrease in EASM intensity, associated with fresh water forcing of the North Atlantic Ocean in response to solar forcing, Bond event 1 (at c. 1400 years BP) (Bond et al. 2001; Bond et al. 1999; Wang et al. 2005). In the Xialongwan record a significant increase in *A. minutissimum* as demonstrated in PCA axis 1 scores*,* a species that at Lake Xiaolongwan is associated with wave energy, is coincident with Bond event 1 (Table 5.6). In light of recent discussion, it is possible that the increase in *A. minutissimum* reflects periods of increased wave energy, lake turnover (and/or possible shorter lake stratification period), a response to increased EAWM intensity. Bond et al (1997) argue that during cool type events, a negative North Atlantic Oscillation (NAO) regime may be a key feature and as such similar responses may have happened with other fresh water forcing events in the Holocene (Wanner et al. 2008). The negative NAO index leads to cold (and dry) winters over northern Europe, indicative of a stronger Siberian High (SH) intensity (Chapter 1. 6). Wu and Wang (2002) show strong correlation ($r$ = 0.8) between the SH and the EAWM and that when the SH is intensified so is the penetration of the EAWM. As a result, if the independent record from Lake Xiaolongwan is displaying a period of increased lake turnover attributed to increased EAWM, concomitant with Bond event 1, results suggest the interplay of teleconnection mechanisms (negative NAO, positive SH) leading to this intensification. This argument is also supported by Liu et al (2009b) who argue that between c. 1600 and 1300 cal years BP a decrease is seen in warm demanding pollen taxa in Lake Jingbo records which is consistent, they state, with indications of weakened monsoon intensity seen in the Dongge Cave record (Wang et al. 2005). Other evidence of

drought was documented in China during the 4th and 5th centuries AD by Gong and Hameed (1991) based on historical records of which the period with the lowest moisture index, that they calculated, occurred at c. 350 AD (c. 1600 years BP). As such the record at Lake Xiaolongwan displays EAWM rather than EASM intensity. A decline in $\delta^{13}C$ and increase in dust deposition from Xiaolongwan itself between c. 1500-1350 years BP also suggests an arid period, although C/N ratios continue to reflect a mixed macrophyte assemblage (Chu et al. 2009a).

The commencement of zone 3 (Figure 5.5) occurs at c. 920 years BP and so may be concomitant with evidence from Jichuan peat bog (an increase in $\delta^{18}O$ records) suggesting another later warm period between c. 1100 and 1200 AD (c. 1000 to 850 years BP), which is argued to be associated with the Medieval Warm Period and warm epoch of Europe (Hong et al. 2000). In the context of Lake Xiaolongwan, abundances of *P. discoidea* continue to increase, possibly reflecting a shallowing of the lake (Table 5.6).

### 5.4.3. Environmental reconstruction between c. 550 to c. 55 years BP

The second large significant change in PCA axes scores is seen between c. 600 and 400 years BP at Lake Xiaolongwan (based on SiZer results; Section 5.3.7, Figure 5.11) between the centennial and decadal bandwidths, coincident with Bond event 0 (or the LIA). For PCA axis 1 timeseries results, this is again due to an increase in *A. minutissimum* (at c. 685 and 420-435 years BP) and for PCA axis 2 an increase in *E. subarcuatoides* (at c. 685 years BP). As for the earlier period this may suggest an increase in EAWM intensity. Other records of increased EAWM intensity are published by Chu et al (2009b) from Lake Xiaolongwan and neighbouring Sihailongwan. They argue that increased minerogenic clastic material was deposited between c. 1690 and 1590 AD, once again coincident with the increase in PCA axis 1 and 2 scores presented here. Increased dust storms may occur when there is less snow cover in source regions of north west China and the Tibetan Plateau, associated with intensified SH (cold and dry climate).

The Little Ice Age (LIA) is argued to be concurrent with Bond event 0 and dated to c. 500 ka years BP (Bond et al. 2001; Bond et al. 1997; Wang et al. 2005). This is concurrent with the commencement of zone 4a at Lake Xiaolongwan and the division of Class 2. Wang et al (2005) argue that this was a period of reduced summer monsoonal intensity. Chu et al (2009b) also identify evidence of drought periods between c. 1590 and 1690 AD (c. 360-300 years BP), arguing that increased minerogenic input in lake sediments occurs in drought periods due to such drier conditions in source regions. Both are coincident with the timing of the Sporer minimum e.g the LIA (Liu et al. 2009a).

Although the record from XLW2 does not extend as far as the X00/X06 diatom record, some discussion can be made comparing the reconstructions derived from them. XRF data (Figure

5.2) shows that after c. 1700 AD until c. 1870 AD elements increase. Similar trends are seen in the bulk organic isotope data (Figure 5.5; Figures 5.6 and 5.8). In this case, higher $\delta^{13}C$ values are seen until c. 1850 and C/N ratios also reflect a trend to higher values until c. 1850. The data suggest a change in the source of organic matter, displayed by the higher $\delta^{13}C$ values (a mixed macrophyte source). XRF results also indicate a period of increased surface inwash to the lake.

The dominant macrophytes at the lake are *Phragmites*, *Equisetum, Typha* and *Trapa natans*. These are all emergent vegetation. The submerged species *Utricularia* is also present. Little literature exists that looks explicitly at the preferential carbon uptake of emergent macrophytes (e.g. atmospheric $CO_2$ versus DIC, or a mixture of both in limiting environments), which has important implications when interpreting the $\delta^{13}C$ record from Lake Xiaolongwan. Literature does suggest that *Phragmites* utilises atmospheric $CO_2$ which would suggest that the traditional interpretation of higher $\delta^{13}C$ with more lake productivity cannot be assumed (Section 2.3.1) (Brix 1990; Edwards et al. 2007). A full examination of submerged lake macrophytes should be conducted for Lake Xiaolongwan in order to understand the representation of both types of macrophytes, the dominant form of carbon uptake and therefore the interpretation of the $\delta^{13}C$ record (e.g. changes in atmospheric carbon versus changes in DIC and lake productivity). As the mean for C/N is close to 12 (12.63; Table 5.1), the values are close to the aquatic carbon C/N boundary and we therefore propose that the traditional interpretation can be adopted for now (Section 2.3.1). Nevertheless, it cannot be denied that factors affecting the composition of atmospheric $CO_2$ over the duration of the record may be important. Indeed, Keeling et al (1979) have documented that after c. 1900 there is a 1.5‰ fall in atmospheric carbon composition, known as the Suess effect. Such changes may be important in interpreting the part of the Lake Xiaolongwan record after c. 1900. Nevertheless, C/N ratios after 1900 AD suggest an aquatic source of carbon and therefore dependence on DIC in lake waters, so that implications of the Suess effect may not be as clear as with emergent vegetation (e.g. *Phragmites*).

### 5.4.4. Environmental reconstruction between c. 55 years BP to present

The period after c. 1950 shows that times of enhanced drought periods are more pronounced in duration than the historical drought periods discussed above (Hong et al. 2000). This warming trend is also demonstrated by the meteorological data plotted from Changchun meteorological station (Figure 5.13). While these earlier historical drought events are attributed to variations in solar activity (as inferred from $^{14}C$ activity) the 20$^{th}$ century warming is believed to be a result of anthropogenic activity (Hong et al. 2000).

After c. 55 years BP abundances of *S. construens* var *venter* and *P. discoidea* show a decline (although a trend that began at c. 150 years BP) towards the surface sediments while values of *A. minutissimum* begin to increase once more. Abundances of the species *Tabellaria flocculosa* and later the planktonic *Discotella woltereckii* also increase with the latter making its first

appearance in the record. As timeseries results demonstrate there is a significant increase in $\delta^{13}C$ after c. 1955 AD, which is concomitant with the introduction of *D. woltereckii.* The trend in C/N ratios also falls after this time, demonstrating a movement to increased algal productivity. After c. 1970 AD C/N rapidly increase, $\delta^{13}C$ declines and the species *S. construens* var *venter* and *P. discoidea* increase once again.

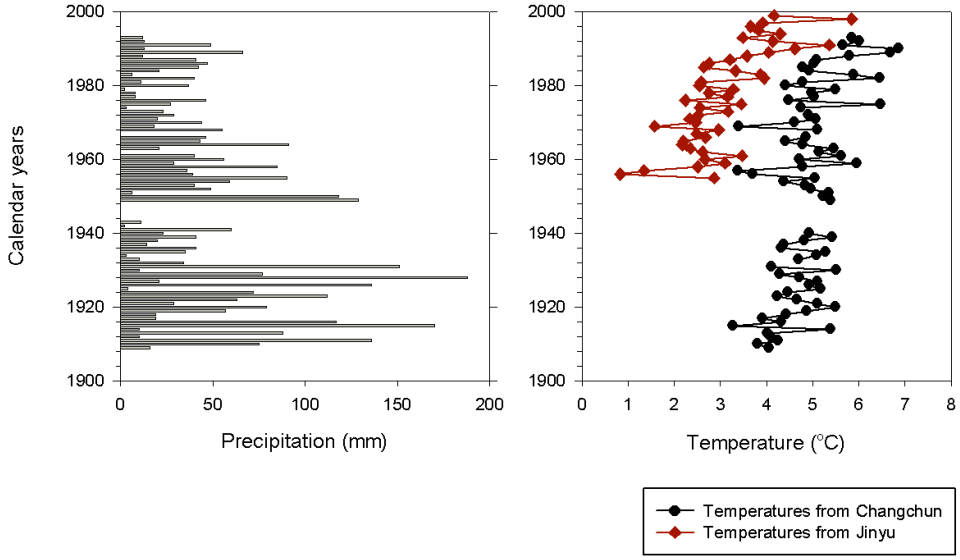


*Figure 5.13. Mean annual precipitation (mm) from Changchun city and mean annual temperatures (°C) from Changchun and Jinyu cities. Precipitation data is not available from Jinyu in order to plot. Data received from the China Meteorological Data Sharing Service System.*

The appearance of *D. woltereckii*, and temporary increase in productivity, at Lake Xiaolongwan is at least coincident with a recent warming (and decreased precipitation) trend seen at Changchun and Jinyu (refer to Figure 1.2 for location). As discussed in Section 5.1. detailed evidence has been provided for the effects of warming over recent decades in regions of the Arctic. Most notable is the increase in planktonic species such a *Cyclotella* due to the relative increase in the ice-free period and warmer lake temperatures (Ruhland et al. 2008; Smol et al. 2005). In the context of the regional climate indices for Lake Xiaolongwan, evidence from southern China has also demonstrated an increase in *Cyclotella stelligera* species associated with warm lake waters and reduced EAWM wind intensity (Wang et al. 2008a). These conclusions may suggest that the appearance of *D. woltereckii* corresponds to increased summer temperatures and reduced winter monsoon intensity. Independent evidence of increased temperatures and reduced summer monsoon precipitation occurs at the same time (Figure 5.13). Organic isotope data show a temporary increase in productivity (higher $\delta^{13}C$ values; Section 2.3.1) after c. 1850 AD and decrease once again after c. 1960 AD. Over this time, meteorological records at Changchun from c. 1920 (Figure 5.13) show an increasing trend in mean annual temperatures with mean annual precipitation showing a decreasing trend. At

around 1950 AD, C/N ratios move to lower values demonstrating a move to a phytoplanktonic carbon source in the lake, which is increasing in productivity (e.g. the introduction of *D. woltereckii*).

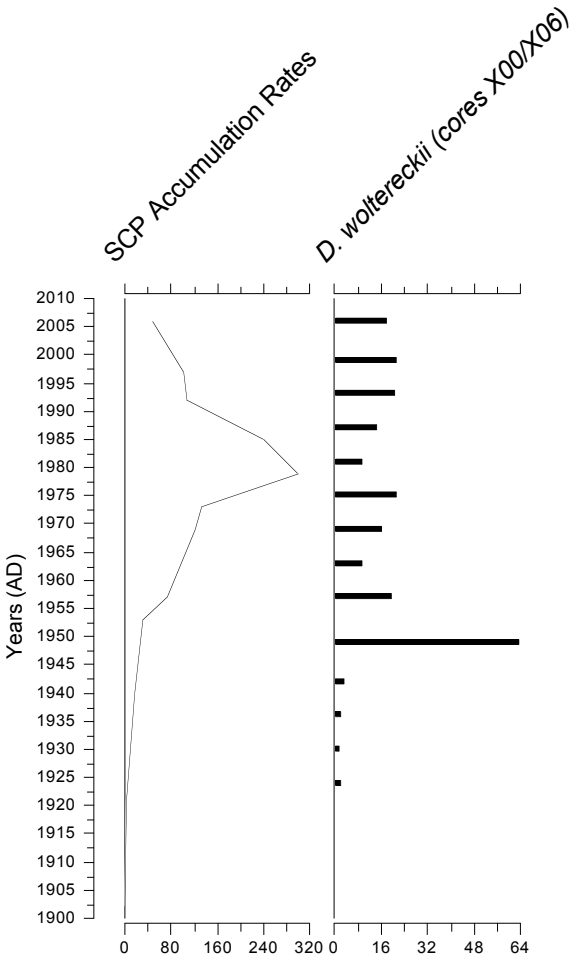


*Figure 5.14a) SCP accumulation (no. cm$^2$ yr$^{-1}$) rates for core XLW2. Chronology is in Year AD based on formulated $^{210}$Pb derived age model. b) Percentage abundance of Discotella woltereckii in cores X00/X06. Chronology is based on the corrected varve chronology but displayed in AD for comparisons with 5.14.*

As discussed in Chapter 3, SCP analyses conducted on the XLW2 core show an increase in atmospheric contamination at this otherwise pristine lake from 1950 AD. SCP accumulation rates presented in Figure 5.14a) further demonstrate the increase in SCP deposition after 1950 AD. Very little literature documents the industrialisation increase in this region of China for the corroboration of this data (and its derived chronology). However, one source does state that after 1945 and with the reign of the Chinese leader Mao, Jillin Province became the “industrial heartland of China”, with coal-fired power stations rapidly increasing in number (Hays 2009). The increase in SCPs continued to a peak at c. 1980 AD after which concentrations decline once more to present day. Furthermore XRF data demonstrate an increase in metal deposition after c. 1970 AD. Based on these data, the appearance of *D. woltereckii* in the last c. 50 years

may not be solely attributable to the observed recent increase in temperatures (and decrease in precipitation); air pollution as provided by SCP evidence, could also be an important factor. After c. 1920 pollution indices (Figure 5.2) increase although the peak is seen after c. 1970. The introduction is before the appearance of *D. woltereckii* and so they can be considered a trigger factor for the species presence. After c. 30 years BP a decline is seen in *D. woltereckii* concomitant with this increase in pollution indices (Figure 5.14b). Evidence from regions of Canada have demonstrated that increased metal contamination to lake environments (e.g. Zn and Cu) can lead to the decrease in planktonic assemblages (e.g. *Cyclotella stelligera*) and increase in D:C ratios (as demonstrated in Figure 5.5) argued to be a result of the competitive advantage of littoral assemblages under the stress conditions that contamination causes (Cattaneo et al. 2008). However, it should be noted that the level of contamination in this example was 40 x for Zn and 280 x for Cu, greater in magnitude than the metals in core XLW2.

## 5.5. Conclusions

1. A decrease in *A. minutissimum* and increase in *S. construens* var *venter* from c. 2000 to c. 350 years BP most likely reflects a reduction in lake water level over this period

2. Significant changes in the diatom records were identified at c. 1775-1650, 1450-1350, 600-350, 50 and after 25 years BP, the most significant occurring at c. 1450-1350, c. 600-350 and after c. 50 years BP. These events correspond to the temporary increase in *A. minutissimum* reflecting periods of increased autumnal lake turnover.

3. The events at c. 1450-1350 and c. 600-350 are concomitant with other regional and North Atlantic evidence of IRD events, in particular Bond events 1 and 0. The Lake Xiaologwan record is, therefore, reflecting sensitivity to enhanced EAWM (reduced EASM) intensity, with periods of increased lake turnover, in response to North Atlantic perturbations.

4. Bulk organic isotope analyses covering the period from c. 1675 AD (past c. 330 years BP) to present exhibit a general trend to higher values, outside of the range of natural variability. After c. 1970 AD a change to decreasing $\delta^{13}C$ is seen, suggesting decreasing productivity in mixed macrophyte communities at this time.

5. The species *D. woltereckii* appears in Lake Xiaolongwan after c. 55 (± 10) years BP, which is coincident with a recent warming (and decreased precipitation) trend. This is also highlighted as a significant perturbation in timeseries and SiZer analyses.

6. There is evidence of anthropogenic impact in the more recent sediments of XLW, as shown by SCP and XRF records. XRF values increase rapidly after c. 1970 AD and SCP

concentrations increase after c. 1970 AD and peak at c. 1980 AD suggesting a degree of air pollution from industrial sources. Hence, the recent change in diatom assemblages at Lake Xiaolongwan may not be attributed to climatic changes alone.

## References

Alles E., Norpel-Schempp M. and Lange-Bertalot H. 1991. Zur systematik und okologie charakterischer *Eunotia* Arten in elektrolytarmen Bachoberlaufen. Nova Hedwigia 53: 171-213.

Battarbee R.W. 1986. Diatom Analysis. In: B. E. Berglund (ed.), Handbook of Holocene Palaeoecology and Palaeohydrology. Wiley, Chicester, pp. 527-570.

Battarbee R.W. and Kneen M. 1982. The use of electronically counted microspheres in absolute diatom analysis. Limnology and Oceanography 27: 184-188.

Battarbee R.W., Jones V.J., Cameron N.G., Bennion H., Carvahlo L. and Juggins S. 2001. Diatoms. In: J. P. Smol, H. J. B. Birks and W. M. Last (eds.), Tracking environmental change using lake sediments. Kluwer Academic Publishers, Dordrecht, pp. 155-203.

Bengtsson L. and Enell M. 1986. Chemical analysis. In: B. E. Berglund (ed.), Handbook of Holocene Palaeoecology and Palaeohydrology. Blackburn, New Jersey.

Bennett K. 1996. Determination of the number of zones in a biostratigraphical sequence. New Phytologist: 155-170.

Bond G., Kromer B., Beer J., Muscheler R., Evans M.N., Showers W., Hoffmann S., Lotti-Bond R., Hajdas I. and Bonani G. 2001. Persistent solar influence on north Atlantic climate during the Holocene. Science 294: 2130-2136.

Bond G., Showers W., Cheseby M., Lotti R., Almasi P., deMenocal P., Priore P., Cullen H., Hajdas I. and Bonani G. 1997. A pervasive millennial-scale cycle in North Atlantic Holocene and glacial climates. Science 278: 1257-1266.

Bond G.C., Showers W., Elliot M., Evans M., Lotti R., Hajdas I., Bonani G. and Johnson S. 1999. The North Atlantic's 1-2 kyr climate rythm: relation to Heinrich events, Dansgarrd/Oeschger cycles and Little Ice Age In: P. U. Clark, R. S. Webb and L. D. Keigwin (eds.), Mechanisms of Global Climate Change at Millenial Time Scales. American Geophysical Union, Washington.

Bradbury J.P. 1971. Paleolimnology of lake Texoco Mexico: Evidence from diatoms. Limnology and Oceanography 16: 180-200.

Brix H. 1990. Uptake and photosynthetic utilisation of sediment-derived carbon by *Phragmites australis* (Cav.) Trin. ex Steudel. Aquatic Botany 38: 377-389.

Brown L., May J. and Hunsaker C. 2008. Species composition and habitat associations of benthic algal assemblages in headwater streams of the Sierra Nevada, California. Western North American Naturalist 68: 194-209.

Cattaneo A., Couillard Y. and Wunsam S. 2008. Sedimentary diatoms along a temporal and spatial gradient of metal contamination. Journal of Paleolimnology 40: 115-127.

Chadhuri P. and Marron J.S. 1997. SiZer for exploration of structures in curves. Journal of the American Statistical Association 94: 807-823.

Cholonky B.J. 1968. Die Okologie der Diatomeen in Binnengewasser. J. Cramer, Lehre, 699 pp.

Chu G., Sun Q., Wang X., Li D., Rioual P., Qiang L., Han J. and Liu J. 2009a. A 1600 year multiproxy record of paleoclimatic change from varved sediments in lake Xiaolongwan, northeastern China. Journal of Geophysical Reasearch-Atmospheres 114: 1-10.

Chu G., Sun Q., Zhaoyan G., Rioual P., Qiang L., Kaijun W., Han J. and Liu J. 2009b. Dust records from varved lacustrine sediments of two neighboring lakes in northeastern China over the last 1400 years. Quaternary International 194: 108-118.

Cosford J., Qing H., Eglington B. and Mattey D. 2008. East Asian monsoon variability since the Mid-Holocene recorded in a high-resolution, absolute dated aragonite speleothem from eastern China. Earth and Planetary Science Letters 275: 296-307.

Edwards E.J., Still C.J. and Donoghue M.J. 2007. The relevance of phylogeny to studies of global change. Trends in Ecology and Evolution 22: 243-249.

Flower R.J. 2005. A taxonomic and ecological study of diatoms from freshwater habitats in the Falkland Islands, South Atlantic. Diatom Research 20: 23-96.

Gong G. and Hameed S. 1991. The variation of moisture conditions in China during the last 2000 years. International Journal of Climatology 11: 271-283.

Gordon A.D. 1981. Classification. University Press, Cambridge, 193 pp.

Haberzettl T., Fey M., Lucke A., Maidana N., Mayr C., Ohlendorf C., Schabitz F., Schelser G.H., Wille M. and Zolitschka B. 2005. Climatically driven lake level changes during the last two millennia as reflected in sediments of Laguna Potrok Aike, southern Patagonia (Santa Cruz, Argentina). Journal of Paleolimnology 33: 283-302.

Hartmann K. and Wunnemann B. 2009. Hydrological changes and Holocene climate variations in NW China, inferred from lake sediments of Juyanze palaeolake by factor analyses. Quaternary International 194: 28-44.

Haworth E.Y. and Hurley M.A. 1986. Comparison of the stelligeroid taxa of centric diatom genus Cyclotella. In: M. Ricard (ed.), Proceedings of the 8th International Diatom Symposium. Koeltz Scientific Books, Koenigstein, pp. 43-53.

Hays J. 2009. Facts and Details: Jilin Province. http://factsanddetails.com/china.php?itemid=451&catid=15&subcatid=98.

Heiri O., Lotter A. and Lemcke G. 2001. Loss on ignition as a method for estimating organic and carbonate content in sediments: reproducibility and comparability of results. Journal of Paleolimnology 25: 101-110.

Hong B., Liu C., Lin Q., Yasuyuki S., Leng X., Wang Y., Zhu Y.T. and Hong Y. 2009. Temperature evolution from the d18O record of Hani peat, Northeast China, in the last 14,000 years. Science in China Series D-Earth Sciences 52: 952-964.

Hong Y., Jiang H., Liu T., Zhou L., Beer J., Li H., leng X., Hong B. and Qin X. 2000. Response of climate to solar forcing recorded in a 6000-year $\delta^{18}O$ time-series of Chinese peat cellulose. The Holocene 10: 1-7.

Hong Y., Wang Z., Jiang H., Lin Q., Hong B., Zhu Y., Wang Y., Xu L., leng X. and Li H. 2001. A 6000-year record of changes in drought and precipitation in northeastern China based on a $\delta^{13}C$ time series from peat cellulose. Earth and Planetary Science Letters 185: 111-119.

Juggins S. 1992. Zone v 1.2. Environmental Change Research Centre.

Juggins S. 2007. C2 v.1.5.2. Environmental Change Research Centre.

Karosienė J. and Kasperovičienė J. 2008. Seasonal succession of epiphyton algal communities on Phragmites australis (Cav.) Trin. ex Stend. in a mesoeutrophic lake. Ekologija 54: 32-39.

Keeling C.D. 1979. The Suess effect: $^{13}$Carbon- $^{14}$Carbon interrelations. Environmental International 2: 229-300.

Kent M. and Coker P. 1992. Vegetation description and analysis: a practical approach,. Wiley, Chichester.

Kingston J.C. 2003. Araphid diatoms and monoraphid diatoms. In: J. D. Wehr and R. G. Sheath (eds.), Freshwater algae of North America: ecology and classification. Elesvier Science, San Diego, pp. 595-636.

Krammer K. 1992. Pinnularia: eine Monographie der europäischen taxa., Bibliotecha Diatomologica. Cramer., Stuttgart.

Krammer K. and Lange-Bertalot H. 1986. Bacillariophycea. I. Teil. Naviculaceae. Gustav Fisher Verlag, Stuttgart.

Krammer K. and Lange-Bertalot H. 1988. Bacillariophyceae 2. Tiel. Bacillariaceae, Epithemiaceae, Surirellaceae. Gustav Fisher Verlag., Stuttgart.

Krammer K. and Lange-Bertalot H. 1991a. Bacillariophyceae. 3. Tiel. Zentrische Diatomeen, Diatoma, Meridion, Asterionellla, Tabellaria, Fragilaria, Eunotia und Verwandte, Peronia und Actinella. Gustav Fisher Verlag., Stuttgart.

Krammer K. and Lange-Bertalot H. 1991b. Bacillariophyceae. 4. Tiel. Achnanthes, Navicula, Gomphonema, Kritsche Nachtraege, Literatur. Gustav Fisher Verlag., Stuttgart.

Kuhn D.L., Plafkin J.L., Cairns J. and Lowe R.L. 1981. Quantitative characterisation of aquatic environments using diatom life-form strategies. Transactions of the American Microscopial Society 100: 165-182.

Lange-Bertalot H. 1996. Annotated Diatom Monographs. Koeltz Scientific Books, Königstein.

Lange-Bertalot H. 1999. Annotated Diatom Monographs. In: H. Lange-Bertalot (ed.), Iconographica Diatomologica. Koeltz Scientific Books, Königstein.

Lange-Bertalot H. 2001. Navicula senso stricto. 10 Genera seperated from Navicula sensu lato Frustulia. Koeltz Scientific Books., Königstein.

Lange-Bertalot H. and Moser G. 1994. Brachysira: Monographie der Gattung und *Naviculadicta* nov. genus. Cramer, Stuttgart, 212 pp.

Leps J. and Šmilauer P. 2003. Multivariate analysis of ecological data using CANOCO. University Press, Cambridge, 269 pp.

Li C., Wu Y. and Hou X. 2010. Holocene vegetation and climate in northeast China revealed from Jingbo lake sediment. Quaternary International In press.

Li Y., Wang N., Cheng H.Y., Long H. and Zhao Q. 2009. Holocene environmental change in the marginal area of the Asian monsoon: a record from Zhuye Lake, NW China. Boreas 38: 349-361.

Liu J., Chu G., Han J., Rioual P., Jiao W. and Wang K. 2009a. Volcanic eruptions in the Longgang volcanic field, northeastern China, during the past 15,000 years. Journal of Asian Earth Sciences 34: 645-654.

Liu Y., Linderholm H.W., Song H.M., Cai Q.F., Tian Q.H., Sun J.Y., Chen D.L., Simelton E., Seftigen K., Tian H., Wang R.Y., Bao G. and An Z. 2009b. Temperature variations recorded in Pinus tabulaeformis tree rings from the southern and northern slopes of the central Qinling Mountains, central China. Boreas 38: 285-291.

Makohonienko M., Kitagawa H., Fujiki T. and Liu X. 2008. Late Holocene vegetation changes and human impact in the Changbai Mountains area, Northeast China. Quaternary International 184: 94-108.

Metcalfe S.E., Bimpson A., Courtice A.J., O'Hara S.L. and Taylor D.M. 1997. Climate change at the monsoon/Westerly boundary in northern Mexico. Journal of Paleolimnology 17: 155-171.

Mischke S. and Zhang C. 2010. Holocene cold events on the Tibetan Plateau. Global and Planetary Change In press.

Morrill C., Overpeck J. and Cole J. 2003. A synthesis of abrupt changes in the Asian summer monsoon since the last deglaciation. The Holocene 13: 465-475.

Osborn T.J. and Briffa K.R. 2006. The spatial extent of 20th century warmth in the context of the past 1200 years. Science 311: 841-844.

Padisak J., Crossetti L.O. and Naselli-Flores L. 2009. Use and misuse in the application of the phytoplankton functional classification: a critical review. Hydrobiologia 621: 1-19.

Patrick R. and Reimer C.W. 1966. The diatoms of the United States. The Academy of Natural Sciences, Philadelphia.

Patrick R. and Reimer C.W. 1975. The diatoms of the United States. The Academy of Natural Sciences, Philadelphia. Second Edition.

Pinewoods T. 2005. Fossil diatoms and chrysophycae cysts as indicators of palaeoecological change in lake Ostrowite. Oceanological and Hydrobiological Studies 34: 269-286.

Razjigaeva N.G., Grebennikova T.A., Ganzey L.A., Mokhova L.M. and Bazarova V.B. 2004. The role of global and local factors in determining the middle to late Holocene environmental history of the South Kurile and Komandar islands, northwestern Pacific. Palaeogeography, Palaeoclimatology, Palaeoecology 209: 313-333.

Reavie E.D. and Smol J.P. 1998. Epilithic diatoms of the St. Lawrence river and their relationships to water quality. Canadian Journal of Botany 76: 251-257.

Renberg I. 1990. A procedure for preparing large sets of diatom slides from sediment cores. Journal of Paleolimnology 4: 87-90.

Rondonotti V., Marron J.S. and Park C. 2007. SiZer for time series: A new approach to the analysis of trends. Electronic journal of statistics 1: 268-289.

Round F.E. 1990. Diatom communities, their response to changes in acidity. Philosophical Transactions of the Royal Society: Series B, Biological Sciences 327: 243-249.

Ruhland K., Paterson A. and Smol J. 2008. Hemispheric-scale patterns of climate-related shifts in planktonic diatoms from North American and European lakes. Global Change Biology 14: 2740-2754.

Selvaraj K., Chen C. and Lou J. 2007. Holocene East Asian monsoon variability: Links to solar and tropical Pacific forcing. Geophysical Research Letters 34: 1-5.

Shindell D., Schmidt G., Mann M., Rind D. and Waple A. 2001. Solar forcing of regional climate change during the Maunder Minimum. Science 294: 2149-2152.

Simpson G. 2008. "Numerical analysis of biological and environmental data". Environmental Change Research Centre, University College London.

Simpson G.L. and Anderson N.J. 2009. Deciphering the effect of climate change and separating the influence of confounding factors in sediment core records using additive models. Limnology and Oceanography 54: 2529-2541.

Smol J. 1983. Paleophycology of a high Arctic lake near Cape Herschel, Ellesmere Island. Canadian Journal of Botany 58: 458-465.

Smol J. 1985. The ratio of diatom frustules to chrysophycean statospores: a useful paleolimnological index Hydrobiologia 123: 2195-2204.

Smol J., Wolfe A., Birks H., Douglas M., Jones V., Korhola A., Pienitz R., Ruhland K., Sorvari S., Antoniades D., Brooks S., Fallu M., Hughes M., Keatley B., Laing T., Michelutti N., Nazarova L., Nyman M., Paterson A., Perren B., Quinlan R., Rautio M., Saulnier-Talbot E., Siitoneni S., Solovieva N. and Weckstrom J. 2005. Climate-driven regime shifts in the biological communities of arctic lakes. Proceedings of the National Academy of Sciences of the United States of America: 4397-4402.

ter Braak C.J.F. and Šmilauer P. 2002. Canoco v. 4.5. Ithaca.

R. v.2.7.1 R. 2008. R Develpoment Team. Vienna.

Van Dam H., Mertens A. and Sinkeldam J. 1994. A coded checklist and ecological indicator values of freshwater diatoms from the Netherlands. Netherlands Journal of Aquatic Ecology 28: 117-133.

Vyverman W. 1991. Diatoms from Papua New Guinea. Cramer, Berlin, 224 pp.

Wang L., Lu H., Liu J., Gu Z., Mingram J., Chu G. and Li J. 2008a. Diatom-based inference of variations in the strength of Asian winter monsoon winds between 17,500 and 6000 calendar years BP. Journal of Geophysical Research-Atmospheres 113: 1-9.

Wang Y., Cheng H., Edwards R., He Y., Kong X., An Z., Wu J., Kelly M., Dykoski C. and Li X. 2005. The Holocene Asian monsoon: links to solar changes and North Atlantic climate. Science 308: 854-857.

Wang Y., Cheng H., Edwards R.L., Kong X. and Shao X. 2008b. Millennial-and orbital-scale changes in the East Asian monsoon over the past 224,000 years. Nature 451: 1090-1093.

Wanner H., Beer J., Butikofer J., Crowley T.J., Cubasch U., Fluckiger J., Goosse H., Grosjean M., Joos F., Kaplan J.O., Kuttel M., Muller S.A., Prentice I.C., Solomina O., Stocker T.F., Tarasov P., Wagner M. and Widmann M. 2008. Mid- to Late Holocene climate change: an overview. Quaternary Science Reviews 27: 1791-1828.

Watchorn M., Hamilton P., Anderson T., Roe H. and Patterson R. 2008. Diatoms and pollen as indicators of water quality and land-use change: a case study from the Oak Ridges Moraine, Southern Ontario, Canada. Journal of Paleolimnology 39: 491-509.

Williams D.M., Chudaev D.A. and Gololobova M.A. 2009. *Punctastriata glubokoensis* spec. nov., a new species of "fragilarioid" diatom from Lake Glubokoe, Russia. Diatom Research 24: 479-485.

Wu B. and Wang J. 2002. Winter Arctic oscillation, Siberian high and East Asian winter monsoon. Geophys. Res. Lett. 29: 1-3.

Yee T.W. and Mitchell N.D. 1991. Generalised additive models in plant ecology. Journal of Vegetation Science 2: 577-586.

You Q., Kang S., Flugel W.-A., Sanchez-Lorenzo A., Yan Y., Xu Y. and Huang J. 2009. Does a weakend effect in diurnal temperature range exist in the eastern and central Tibetan Plateau? Environmental Research Letters 4: 045202.

# CHAPTER 6. Palaeoenvironmental reconstruction from Lake Arachlei

## 6.1. Introduction

### 6.1.1. Late Holocene environmental change in arid central Asia

Evidence from Lake Telmen, north central Mongolia, has suggested that after c. 4500 calibrated (cal) years BP, a period of humidity was seen, with increasing humidity suggesting increased lake level stands. In particular, conditions were most humid between c. 3000 and 1600 cal years BP when they infer cooler summer temperatures decreased evaporation and increased moisture availability in the Telmen basin (Fowell et al. 2003). Indeed, evidence from Lake Baikal (Figure 1.2), between c. 3300 cal years BP to c. 2000 cal years BP suggests increasing warm summer temperatures, based on known ecologies of diatom taxa, and a concomitant increase in precipitation-fed river input to the lake (Mackay et al. In review). Further evidence of a humid late Holocene is interpreted from many Mongolian records but the time varies from place to place (An et al. 2006). As these reconstructions suggest, due to the location of these sites they may reflect changes in effective moisture related to summer precipitation amount and therefore increased Westerly strength. This is of great significance for this project, as Lake Arachlei is located in the ultra continental region of southern Siberia and therefore also argued to be sensitive to such changes (Figures 1.3d).

However, Prokopenko et al (2007) argue that between c. 4000 and 2500 cal years BP there was a period of regional warming in arid central Asia (ACA). They highlight that the expansion of *Picea obovata* and *Pinus sylvestris* is time transgressive, occurring 1000-2000 years earlier around Lake Hovsgol than around the central basin of Lake Baikal, in response to change in precipitation and temperature across these regions (Prokopenko et al. 2007). Furthermore, at Lake Hovsgol, lithological records indicate lower P/E between 4000 to 2500 cal years BP, an indication of evaporative loss of moisture. This data corroborates the general circulation model (GCM) evidence published by Bush et al (2005) of elevated summer mean and annual temperatures and increased aridity at the time.

At Lake Ugii Nuur, central Mongolia, high lake level stands indicating enhanced moisture supply were seen from 2800 years BP to present. However, Schwanghart et al (2009) argue that this could be explained by changes in rainfall patterns intensifying runoff and allogenic material transport to the lake. They go further to note that changes in lake sediments may also be reflecting human impact of the ecosystem, with pollen evidence identifying woodland clearance (Rosch et al. 2005). As such, drivers of environmental change beyond natural forcing should be considered to understand the environmental evolution in this region (Schwanghart et al. 2009). In Mongolia, sediments from Lake Telmen later suggest a decline in effective moisture between

c. 1400 and 1260 cal years BP (Fowell et al. 2003; Peck et al. 2002). This is then followed by an increase in humidity until c. 400 cal years BP (ibid.).

While the LIA is identified as a cold and dry period in central and eastern regions of China, Chen et al (2008) argue that in ACA it is presented in lake sediment records from Bosten Lake as humid and warm (Figure 1.2). Other literature based on climatic modelling suggests that such events should be most pronounced in continental areas (Shindell et al. 2001). However, records from Lake Baikal, Siberia, the MWP is argued to occur between c. 880-1180 AD and the LIA from 1180-1840 AD (expressed as cold, increased lake ice cover and a decline in precipitation-fed rivers; Mackay et al. 2005; Mackay et al. In review). Severe drought episodes are indicated by tree ring data from northern Mongolia during the early 18$^{th}$ and 19$^{th}$ Centuries e.g. LIA (Mackay et al. 2005).

## 6.2. Climate characteristics for the region

Irkutsk is the closest meteorological station to Chita and Lake Arachlei. The location of the site can be seen in Figure 1.2.

### 6.2.1. Temperature and precipitation

Mean annual precipitation at Irkutsk meteorological station for the year 2008 was 460 mm (Figure 6.1). The greatest amount of precipitation falls in July and August with 125 and 75 mm respectively. Mean annual temperatures for the year 2008 were 0$^{o}$C. Temperatures are below 0$^{o}$C for 5 months of the year, after which they increase above 0$^{o}$C between the months April to October. Highest temperatures are in the months June, July and August at +15, 17 and 14$^{o}$C respectively. The climate of this region of southern Siberia is ultra continental as these results show, with low mean precipitation, cold dry winters and low summer temperatures as based on the data presented.

### 6.2.2. Isotopic composition of precipitation

At Irkutsk, the isotopic composition of rainfall shows a distinct seasonality. The lowest $\delta^{18}$O and $\delta$D values are during the winter months (although values for December are not available). $\delta^{18}$O values between the months May and September range between –9.9 and –13.3‰, greater than the remaining months of the year. $\delta^{18}$O values are at their lowest for the months October to April (between –14 to – 25‰). $\delta$D values show a similar trend, with lowest values (less than –104‰) in winter months (between October to April). Highest $\delta$D values fall between May to September, ranging between –85 and –74‰, although fall in August to –105‰. These higher values fall in the months with greatest precipitation and temperature.

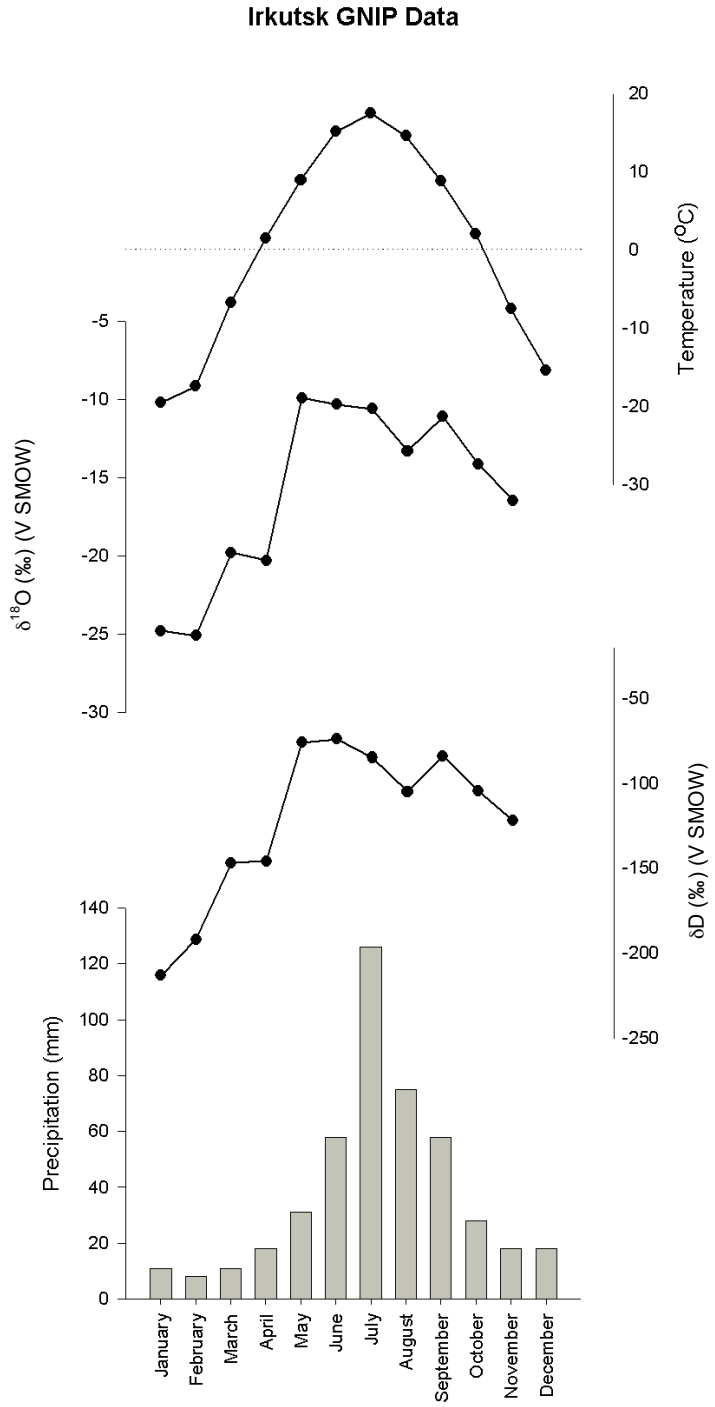


*Figure 6.1. Monthly mean temperature ($^{o}$C), mean precipitation (mm), weighted monthly mean $\delta$D (‰), weighted monthly mean $\delta^{18}$O (‰) at Irkutsk for the year 2008 (refer to Figure 1.2). Please note that the $\delta^{18}$O and $\delta$D weighted means are missing for the month December. Data from IAEA/WMO (2006).*

### 6.2.3. Interpretation

To summarise the main trends in the mean weighted isotope record from Irkutsk, it is clear that there is a distinct annual seasonality. Winter months have low precipitation and cold temperatures, both associated with the winter monsoonal westerly winds across north east Eurasia (Chapter 1; Figures 1.3). Indeed, this is associated with the presence of the SH of which the main core is located near Lake Baikal (Lydolph 1977). As a result, $\delta^{18}O$ and $\delta D$ values are low, associated with this changing air mass trajectory and change in precipitation type dominating (e.g. snow fall).

In summer months, the isotopic composition of rainfall at Irkutsk is higher compared to winter precipitation. In summer months, moisture is provided by the westerly wind systems. Lydolph (1977) states that precipitation which falls in the Transbaikalia region falls primarily from cyclones along the Mongolian sector of the Polar Front, and move east-northeastwards. Precipitation and temperatures are low and there is an increased proportion of snow-melt as a result of its ultra-continental climate thereby accounting for the lower isotopic values (Shahgedanova 2002).

## 6.3. Introduction to Lake Arachlei

Lake Arachlei (52°15'N, 112°54'E; Figure 1.2) is located in the southeastern part of Russia (eastern Transbaikalia region), near the town of Chita. The lake is classified as being part of the Ivan-Arakhley group of lakes located in an intermountain depression at a height of c. 1000 m.a.s.l., in the southern Vitim Plateau (Bazarova and Itigilova 2006; Shishkin 1973).

The catchment of the lake is covered with a birch/larch forest and steppe/pine forest. Sedge grasses are present on the lake shores (Figure 6.2). Lake macrophyte vegetation present in 2000, as discussed in Bazarova and Itigilova (2006) includes *Ceratophyllum demersum* ($C_3$ pathway; Best 2006), *Lemna trisulca, Persicaria amphibia, Cladophora* ($C_3$ pathway; Cheney and Hough 1983), *Chara arcuatofolia, Bryophyta* ($C_3$ pathway; Hamana and Matsuzaki 1985) *and Potamogeton perfoliatus* ($C_3$ pathway; Frost-Christensen and Sand-Jensen 1995) the last of which covered a total area of c. 816 ha (Figure 6.2).

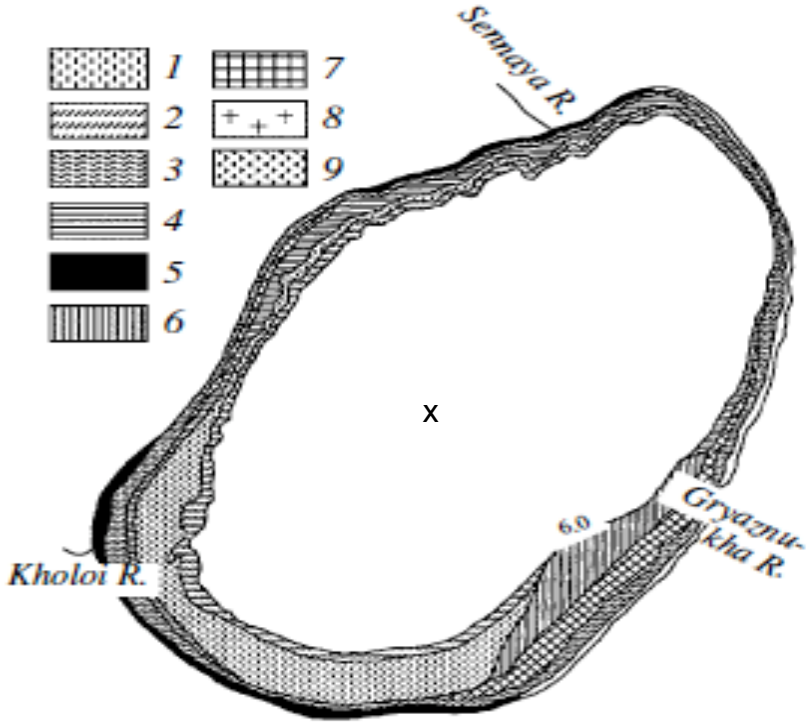


*Figure 6.2. The mapping of aquatic vegetation structure in Lake Arachlei in 2000 and the coring location (x). Vegetation key is as follows: 1.Ceratophyllum demersum ; 2, Potamogeton praelongus; 3, P. perfoliatus ; 4, Lemna trisulca ; 5, Persicaria amphibia ; 6, Cladophora aegagropila ; 7, Chara arcuatopholiae ; 8, Nitella opacae ; 9, Bryophyta (Bazarova et al. 2006).*

### 6.3.1. Lake Arachlei limnology

Lake Arachlei is located at an altitude of c. 965 m above sea level, has a maximum depth of 17 m (mean 10.2 m) and has a lake surface area of 59 $km^2$ (Bazarova et al. 2006). The three main tributaries of Lake Arachlei are the Kholoi River (outflow) and inflow rivers Sennaya and Gryanznukha (Matafonov et al. 2005). It is not clear where the source region of the lake inflows is located. It is quite possible that some source water originates from northern Mongolian tributaries (based on cartographic evidence). As a result, this would mean that down core reconstructions may be displaying more regional climatic change as a result. While it has not been possible to resolve this issue, it is important to bear it in mind during detailed environmental reconstructions conducted for the purpose of this study.

The lake hydrological regime shows that evaporation from the lake is c. 80%, the outflow c. 20%, surface inflows represent c. 20% and precipitation c. 52% (Kalugin, pers. comm.). As a result, in years of high water levels the outflow is weak and in years of low lake level there is no

superficial outflow (Kalugin, pers. comm.). Lake Arachlei is classified as a mesotrophic, polymictic lake (Kalugin pers. comm.). During winter months the lake is ice covered with up to 180 cm thick ice (Shishkin 1973). Indeed, due to the low amount of solid precipitation in winter months (c. 31 mm) there is a great amount of solar radiation penetration to the lake underneath, which is likely to have an important affect upon the growth of aquatic species. Shishkin (1973) highlights that the heating of the water by solar radiation begins as early as December at Lake Arachlei. As a result the photosynthesis of dominant macrophytes e.g. *Potamogeton* species can take place even under ice cover. Development of phytoplankton species also occurs and chrysophytes appear as early as February after which their growth season is completed after ice off (ibid.).

## 6.4. Methodology

### 6.4.1. Fieldwork methodology

The sediment core Ar-2005 was collected in July 2005 by the use of a box corer in the central region of the lake at a water depth of 15 m (52°12'44.2" N and 112°53'16.8" E). Core collection and sub-sampling the 35 cm core at a resolution of 0.25 cm was conducted by Dr. Ivan Kalugin.

### 6.4.2. Sediment analyses

6.4.2.1. % Dry weight analyses

% Dry weight was calculated by measuring between 0.1 and 0.2 g of wet sediment into sub-sampled, pre-weighed crucibles. Sediments were dried overnight in a Gallenkamp oven at 105°C. Once dried sediments were re-weighed in order to calculate loss on drying and therefore % dry weight (%DW) using the following equation from Bengtsson and Enell (1986):

$$\%DW = (\text{weight after drying}/\text{wet weight}) \times 100$$

6.4.2.2. % Loss on ignition at 550°C and 950°C

After conducting dry weight analyses, methodology for % Loss on ignition at 550°C and 950°C followed those outlined in Section 5.2.1.

### 6.4.3. Bulk organic isotope analyses

Bulk carbon samples for core Ar-2005 were prepared by placing 2 g of wet sediment and follow the methodology presented in Section 5.2.2.

### 6.4.4. Diatom sample preparation

Procedures once again follow those outlined in Renberg (1990) (Section 5.2.4). A minimum of 300 valves were counted per slide (total of 100 slides) although this number was sometimes

revised for the core Ar-2005 due to the low concentration of valves. Some diatom valves demonstrated evidence of dissolution (e.g. *Ellerbeckia arenaria* and *Puncticulata* species) although this was not common and not the reason for the low counts. Low counts were mainly due to high amounts of clastic material in slides (despite increased cleaning methods of the samples) leading to low concentration of diatom valves. Overall, diatom preservation was good for the core. Diatom taxonomy followed Krammer and Lange-Bertalot (1986, 1988, 1991a, b). Other literature also includes Khursevich (1976) and Nikulina (2008) for the identification of the Arachlei taxonomy. SEM and light microscope photographs were conducted as outlined in Chapter 5, Section 5.2.4. Photographs were taken using a Nikon CoolPix 5000, attached to the microscope, in order to conduct diatom harmonisation with Dr. Patrick Rioual at the Chinese Academy of Sciences. To further ensure that diatom taxa were correctly identified, scanning electron microscopy (SEM) was conducted. The preparation procedure follows those outlined above, with the settling out of diatoms overnight on 8 mm coverslips, before being mounted on SEM stubs and gold spatter coated. Please consult the appendices for further taxonomic information on dominant species.

#### 6.4.5. SCP analysis

Between 0.1 and 0.2 g wet weight material was sampled from core Ar_2005. The methodology used for SCP analyses follows those outlined in Section 5.2.5.

## 6.5. Multivariate analyses

#### 6.5.1. Diatom data

Diatom taxa were expressed as percentage data and relative abundances were calculated for each species. The data were reduced so that only species with a percentage > 2% were retained, using the software C2 v. 1.4.3 (Juggins 2007). This new spreadsheet was adopted for all multivariate analyses explained below. Species above a percentage of 5% were then selected using C2 in order to reduce the data set to 21 species for Ar-2005.

#### 6.5.2. Ordinations

The software program Canoco v. 4.5 (ter Braak and Šmilauer 2002) was used for all ordination analyses. Detrended correspondence analysis (DCA) was conducted upon each of the reduced diatom data sets of >2% species abundance. Here, detrending by segments was selected in order to remove the presence of an arch effect in plots. Downweighting of rare species was also selected in order to dampen the effects of rare species and pick out trends in all the data and square root transformation. Results show an Axis 1 gradient length was 1.898 (refer to Table 6.4) thus data were responding in a linear fashion. The data are relatively homogenous and so a linear method of PCA has been chosen (Leps and Šmilauer 2003). Centering by species was selected in order to calculate a covariance matrix (Kent and Coker 1992).

### 6.5.3. Cluster analysis

Cluster analyses was conducted in order to pick out the main trends in the species down-core data using the program R v. 2.7.1 (2008). Results were applied to sample biplots to summarise distinct groupings of the data and therefore the dominant species assemblages (see Figures 6.10 and 6.11). The method of average link was adopted for the core Ar-2005. While this method is hierarchical, it resulted in the optimal grouping of samples for the basis of displaying on the PCA biplots. Average link calculates the dissimilarity between samples based on the average distance between them and acts as an intermediate between single and complete link (Simpson 2008). Three groups were chosen as displayed on the PCA biplots.

### 6.5.4. Diatom zonation

The program Zone v 1.2 (Juggins 1992) was adopted to apply zonation techniques to the Arachlei diatom species data. This was in order to summarise main sections in data where changes have occurred and therefore provide a simpler method to discuss these changes. SPLITINF was again selected in order to split the stratigraphic data into four zones. The zones were displayed on the stratigraphy using C2.

### 6.5.5. Timeseries and SiZer techniques

Two models were run for each of the variables (PCA axes scores, $\delta^{13}C$ and C/N), GAMM1 and GAMM2. GAMM1 is the general additive model, while GAMM2 has another element that looks at the autocorrelation structure between the data. The program R (v.2.7.1 2008) was then used in order to conduct SiZer analyses on data as discussed in Sections 5.2.6.5 and 5.2.6.6.

## 6.6. Core chronologies for Lake Arachlei (Ar-2005)

### 6.6.1. $^{210}$Pb dating for core Ar-2005

Radiometric dating was carried out on core Ar-2005 in March 2006 at Novosibirsk University, Russia. The low background gamma-spectrometer FP-6300B was used and counting based on germanium detector EGPC-192-P21.

The Constant Rate of Sedimentation (CRS) model was chosen for the formulation of the $^{210}$Pb chronology of Ar-2005 and the extrapolation of dates. It is argued that the sediment at the depths 2.5 and 7.5 mm is mixed due to the similar $^{210}$Pb excess values seen at these depths (Figure 6.3, Table 6.1). Furthermore, values for the $^{137}$Cs are also similar for the depths 2.5 and 7.5 mm. While the result at 12.5 mm appears to reflect the $^{137}$Cs 1963 peak, it is argued that the peak may in fact be dated between any of the three upper samples as $^{137}$Cs activity is high in all cases, probably reflecting sediment mixing (Kalugin, pers. comm.).

| Sediment depth (mm) | $^{210}$Pb (excess) (Bq/kg) | $^{210}$Pb error (Bq/kg) | $^{137}$Cs (Bq/kg) | $^{137}$Cs error (Bq/kg) | Derived chronology (AD) | Error (Year) |
|---|---|---|---|---|---|---|
| 2.5 | 899.4 | 89.9 | 208.7 | 31.3 | 1991 | - |
| 7.5 | 897.6 | 89.8 | 221.2 | 33.2 | 1963 | - |
| 12.5 | 847.8 | 84.8 | 268.1 | 40.2 | 1935 | 2 |
| 17.5 | 490.2 | 49.0 | 172.0 | 25.8 | 1908 | 1 |
| 22.5 | 254.1 | 38.1 | 88.8 | 17.8 | 1880 | 1 |
| 27.5 | 128.8 | 19.3 | 41.6 | 8.3 | 1825 | 2 |
| 37.5 | 31.4 | 6.3 | 16.1 | 4.0 | 1770 | 2 |
| 47.5 | 2.1 | >0.6 | 3.9 | >1.3 | 1714 | 2 |
| 57.5 | 31.4 | 6.3 | 4.4 | >1.3 | 1632 | 2 |
| 72.5 | 26.2 | 5.2 | 2.1 | >0.6 | 1494 | 4 |
| 97.5 | 27.9 | 5.6 | 1.0 | >0.3 | 1176 | 9 |

*Table 6.1 $^{210}$Pb and $^{137}$Cs activity and respective errors for the sample depths displayed in core Ar-2005. The depths for which the model is created are shaded in grey. Year based on CRS model are also displayed along with errors.*

As a result, the calculations of the sediment accumulation rate (SAR) are based on the $^{210}$Pb activity of the sample depths 12.5 to 47.5 mm only (Kalugin, pers. comm.). Results of the $^{137}$Cs activity (e.g. 1963 peak) are therefore not used for the purpose of corroborating this model, for the reasons outlined above. After 47.5 mm the activity of both $^{210}$Pb and $^{137}$Cs is low and therefore these samples are not used for the chronology formulation. Due to the reasons outlined, the year 1963 displayed in Table 6.1 is calculated based on the $^{210}$Pb age model.

A sediment accumulation rate (SAR) of 0.181 mm/year is calculated between the depths 12.5 and 47.5 mm. The derived chronology is displayed in Figure 6.5.

Figure 6.3

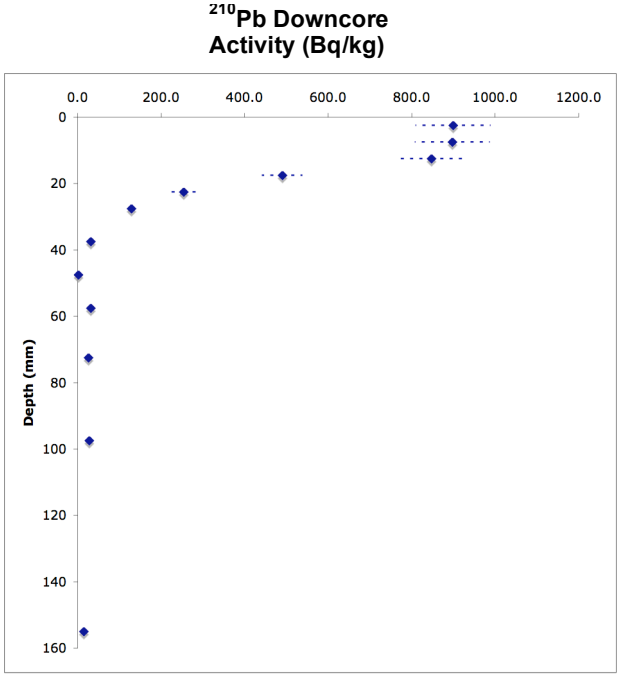


Figure 6.4

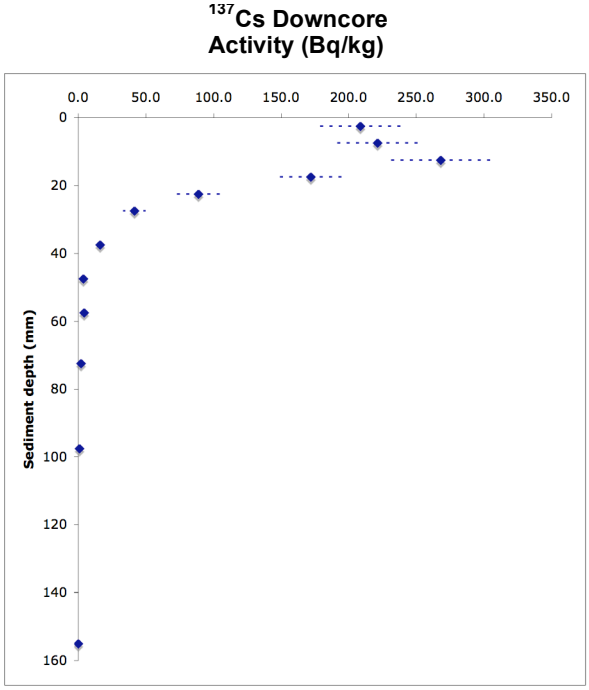


*Figure 6.3. The $^{210}$Pb downcore activity (Bg/kg) for the core Ar-2005 against depth (mm). Figure 6.4. The $^{137}$Cs downcore activity (Bq/kg) for the core AR-2005 against depth (mm). Note that the first two samples are mixed, as a result the peak that is shown in 12.5 mm does not correspond with the peak in $^{137}$Cs activity seen at 1963.*

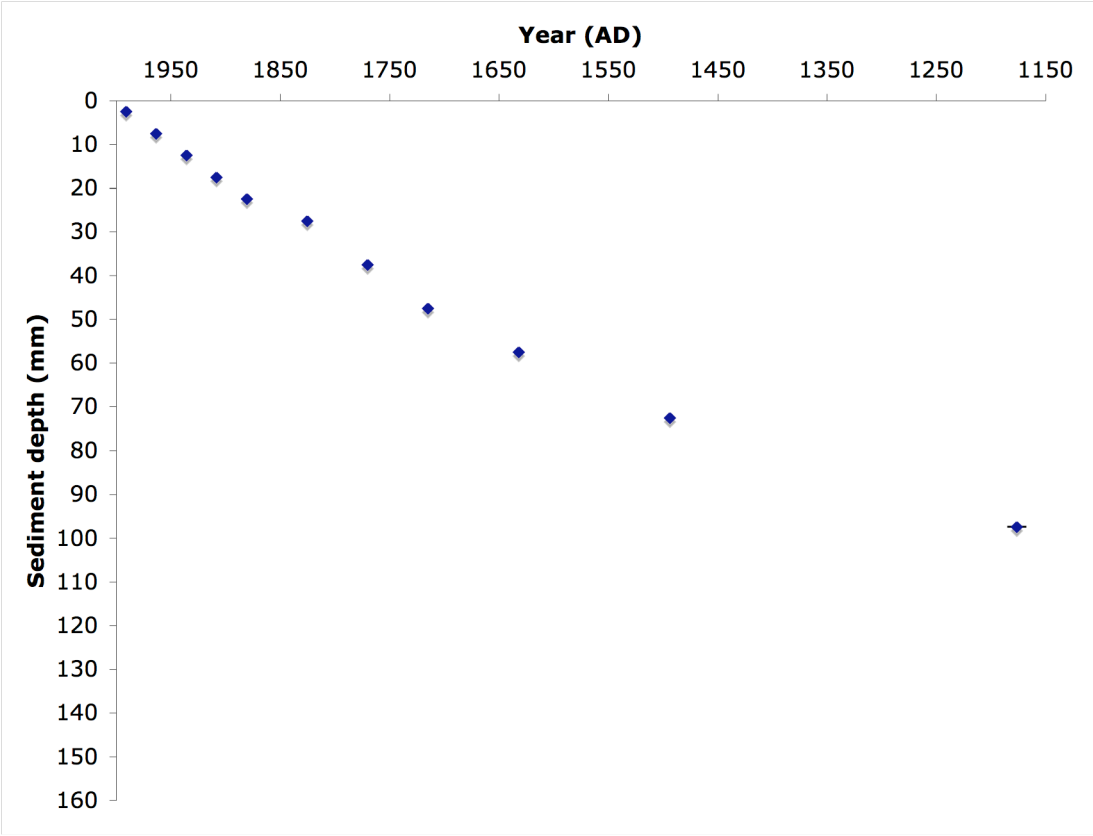


*Figure 6.5 The derived chronology (age against depth in mm) for the core Ar-2005 with extrapolated ages and the respective errors associated with the CRS model although these are small (refer to Table 6.1).*

### 6.6.2. Radiocarbon dating

Radiocarbon dating at the Poznan Radiocarbon Laboratory, Poland, by accelerator mass spectrometry (AMS) was conducted on a total of 5 bulk sediment samples from the lake Arachlei core. This is due to the dating period limitation of $^{210}$Pb. The radiocarbon dates were calibrated using the IntCal-04 atmospheric calibration set (Reimer 2004). The data presented from this thesis are from a sub-sampled part (35 cm) of a larger core where two radiocarbon dates have been analysed and discussed here. The age-depth model (Figures 6.6 and 6.7) was created using a Bayesian phase sequence model (Bronk Ramsey 2009). Bayesian analyses utilise prior knowledge and assumptions when generating a model from a particular data set (termed a prior) (Blockley et al. 2008). Blockley et al (2008) suggest that a *P_Sequence* model allows for a subtle and less rigid modelling of the data (compared to other depositional models) while still accounting for information that is not used in the simple sequence algorithm. This model recognises that many processes are a series of events and by taking into account the estimation of some factor (*k*), the relationship between the events and the overall stratigraphical processes, it is then possible to model such processes by using representative information on the individual event (ibid.).

A boundary for the model was applied for the date at which the core was collected in 2005. Furthermore, the three selected $^{210}$Pb dates (which had the greatest $^{210}$Pb activity values), used for the formulation of the sedimentation rate, were also selected and applied to the model as calendar dates (C_Date) to constrain the dates at the top of the core within the age model (Figure 6.6).

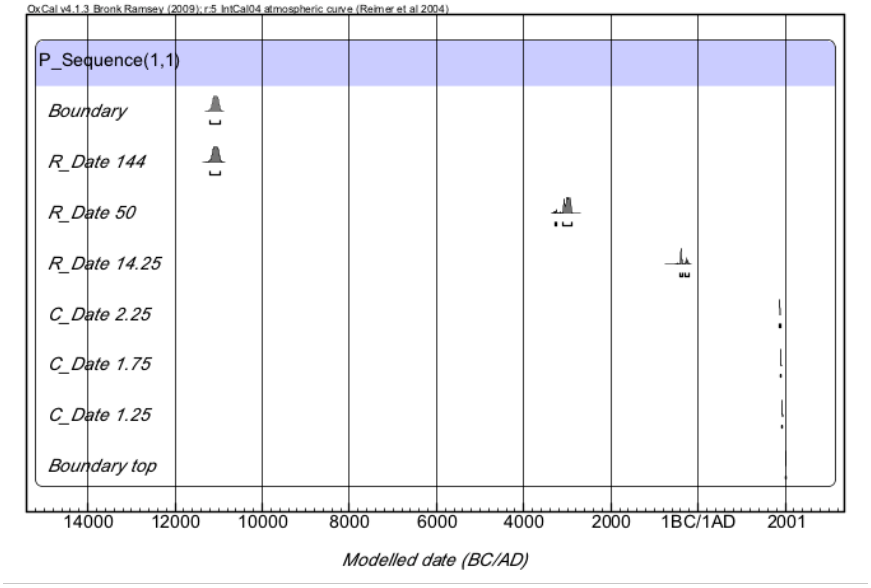


*Figure 6.6 The calibration of the radiocarbon dates (R_Date) for Ar-2005. The last date of the core is displayed also as a boundary for the core. Three calendar dates (C_Dates) associated with the $^{210}$Pb dates are also displayed along with the boundary top date, 2005, when the date was collected. The depth associated with each sample is in cm. The years were calibrated to BC/AD as $^{210}$Pb years (AD) were incorporated into the model.*

The resulting age model for the core can be seen in Figure 6.7 and the respective dates and errors in Table 6.2. This is calibrated to BC/AD although later converted to calendar years before present (BP) for the palaeoreconstructions. Years will be referred to as BP from now on. Please refer to the appendices for a table displaying the original radiocarbon dates and errors.

| Code name | Sediment depth (mm) | Date (cal years BC/AD) | Lower bound date (cal years BC/AD) | Higher bound date (cal years BC/AD) |
|---|---|---|---|---|
| R_Date 1440 | 1440 | 11,299 | 11,184 | 10,955 |
| R_Date 500 | 500 | 3445 | 3264 | 2902 |
| R_Date 142.5 | 142.5 | 625 | 487 | 212 |
| C_Date 47.5 | 47.5 | 1714 | 1712 | 1716 |
| C_Date 22.5 | 22.5 | 1880 | 1879 | 1881 |
| C_Date 17.5 | 17.5 | 1908 | 1907 | 1909 |
| C_Date 12.5 | 12.5 | 1935 | 1933 | 1937 |
| C_Date 0 | 0 | 2005 | 2005 | 2006 |

*Table 6.2. Calibration of $^{14}C$ dates for the core AR_2005. $^{210}Pb$ dates used for the formation of a boundary model are shown.*

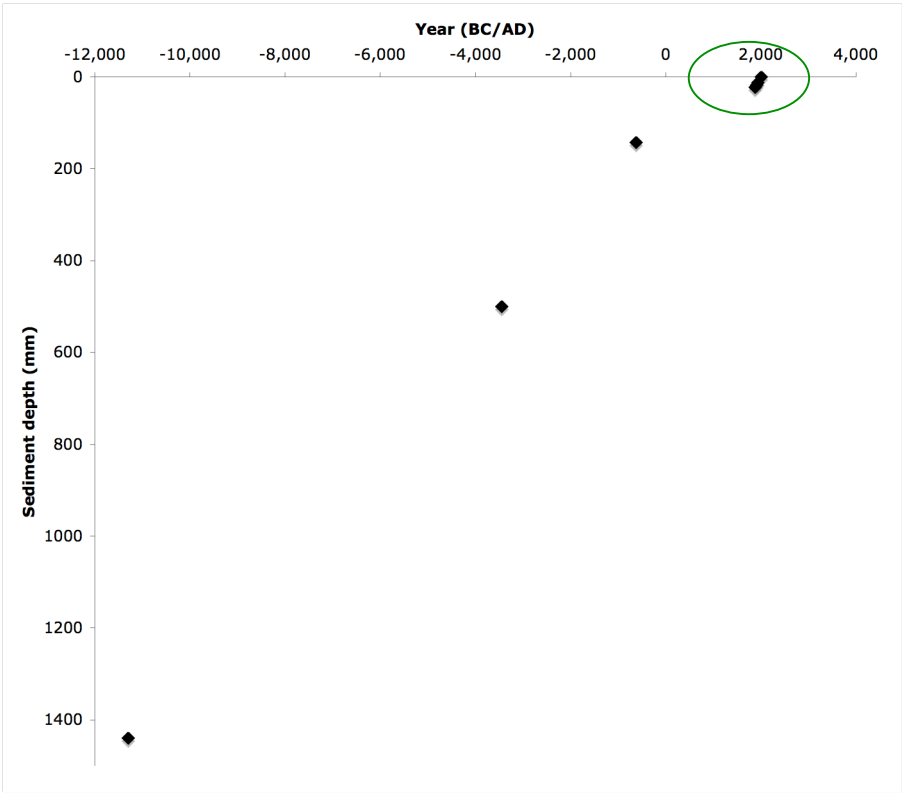


*Figure 6.7. The age-depth chronology derived for core Ar-2005 is displayed above. $^{210}Pb$ dates are shown in green circle. The R_Dates correspond to the sediment depth of the $^{14}C$ date and depths are in mm.*

### 6.6.3.SCP analyses

The SCP analyses for the core AR-205 are displayed in Figures 6.8 and 6.9. Both the concentrations per gram of dry weight (g/DM) on the age/depth scale and sediment depth (cm) are shown (Figure 6. 8 and 6.9 respectively).

Figure 6.8

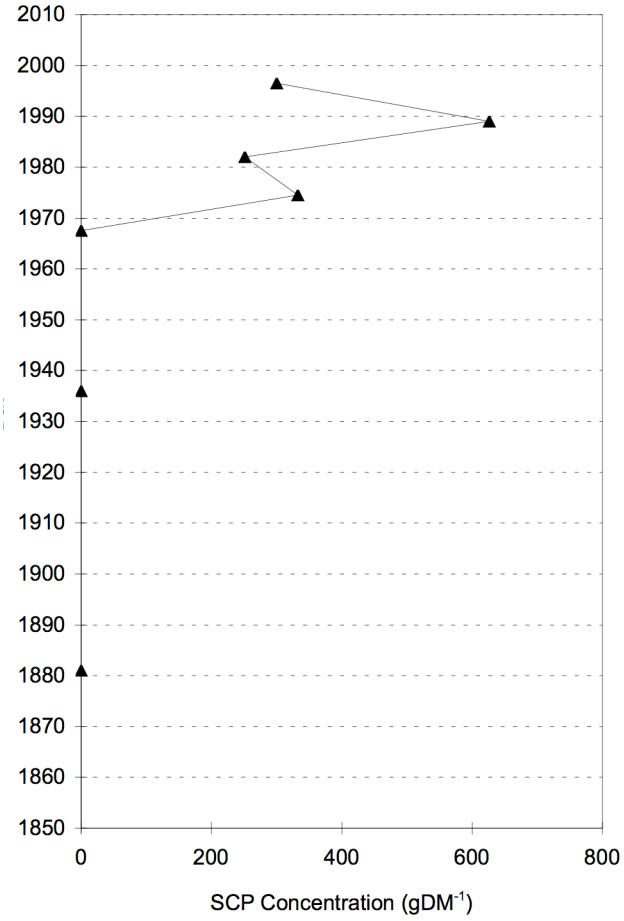


Figure 6.9

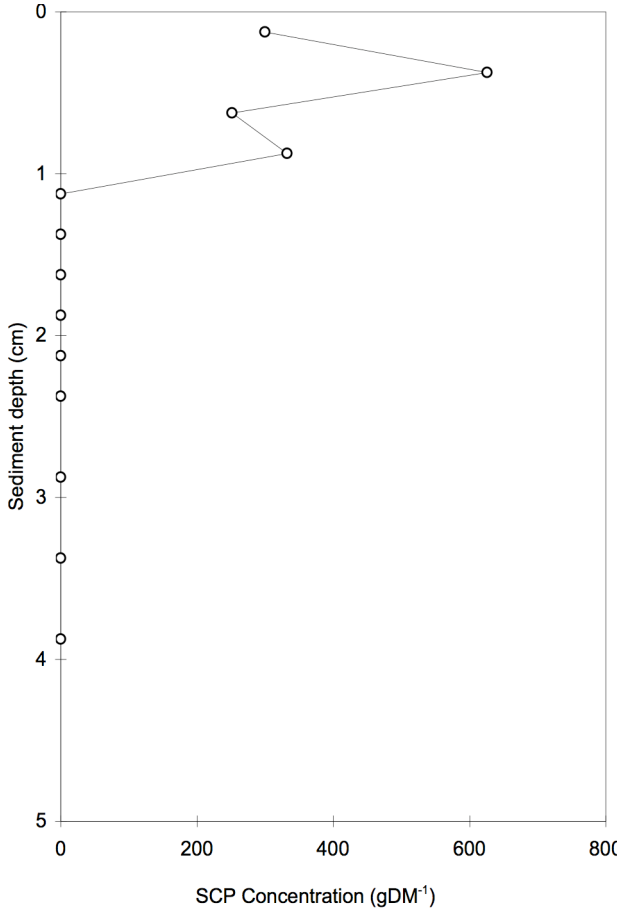


*Figure 6.8 SCP concentration (g/DM) plotted against calendar years AD (based on the CRS method applied to $^{210}$Pb dating) and Figure 6.9 SCP concentration against sediment depth (cm) for the core Ar-2005.*

Results from Ar-2005 show that the concentrations of SCPs are very low, particularly when compared to the results from XLW (Chapter 5), north east China. While SCPs do show a peak in concentrations at c. 1990 it is very important to outline that the absolute numerical values are in fact very low (peaking at 626 g.DM). SCP accumulation rates are not possible to calculate due to the very low concentrations in the core and so are not shown. Although the counts are low however, we can say that their presence corroborates the age model derived by the *P_Sequence* model created in OxCal as the age model they are plotted on is derived from $^{210}$Pb analyses only (Figure 6.7) SCP results however, cannot be used further as a means of independently dating due to the limitations associated with low counts.

### 6.6.4. Discussion on chronologies created for Lake Arachlei

OxCal v. 4.1 was used in order to calibrate $^{14}C$ ages and create a robust chronology where the $^{210}Pb$ ages could also be included. In order to do this three $^{14}C$ ages derived for the core Ar-2005 fall at the depths 144 cm, 50 cm and 14.25 cm. As the sampling depths for diatom analyses from core Ar-2005 are between 0 and 35 cm, $^{210}Pb$ analyses were also conducted on surface sediments. Unfortunately, there were insufficient funds to obtain multiple $^{14}C$ dates from samples where the analytical analyses were conducted for this project, which was why it was important to use $^{210}Pb$ methods to constrain the chronology. Errors will be taken into consideration when discussing the palaeoreconstruction for Lake Arachlei in this chapter. Sample resolution however for the record falls between 10 and 50 years.

## 6.7. Results

### 6.7.1. Bulk organic isotopes and core sedimentology

Figure 6.10 is a summary diagram of the lithological components (%DW, %LOI at 950$^{o}$C) and bulk organic isotopes ($\delta^{13}C$, %TOC, C/N). The analyses were conducted while samples were submitted for radiocarbon dating. As a result, the record is c. 800 years longer than the diatom record. This is due to the fact that subsampling for the diatom analyses was conducted after dates were received, so that the chosen samples cover the past c. 3000 years. For the purpose of discussing changes between the diatom and isotope record, the diatom zonation was applied.

The $\delta^{13}C$ and C/N record from Lake Arachlei show very little variation in productivity (see Table 6.3; standard deviation of 0.4‰ and 0.27 respectively). Firstly, what is most interesting is the representation of a dominant algal assemblage (< 12 C/N) at the site for the duration of the record. It is possible that this may raise concerns over taphonomy in the core as literature from the recent c. 50 years does argue a strong presence of macrophyte communities at the site. This will be further discussed in more detail in this chapter. A second observation about the record is that the overall variation in $\delta^{13}C$ over the reconstructed period is very low.

| | $\delta^{13}C$ (‰) | %TOC | C/N Ratio |
|---|---|---|---|
| **Mean** | -26.6 | 25.5 | 9 |
| **Standard Deviation (SD)** | 0.4 | 1.84 | 0.27 |

*Table 6.3. Summary of the mean and standard deviation for the isotopic analyses conducted on core Ar-2005.*

6.7.1.1. Pre-zone I (c. 3875 BP to c. 3200 BP)

In this zone, there is very little change in $\delta^{13}C$ with values fluctuating around – 26‰ (the mean of the entire record; Table 6.6). Although by only c. 3%, variability in %TOC shows an overall decreasing trend towards the transition with zone I. C/N also show a very small decreasing trend from c. 9.1 to c. 8.8. %DW and %LOI at 950$^{o}$C change very little during this zone, while %LOI at 550$^{o}$C show a small decreasing trend.

6.7.1.2. Zone I (c. 3200 BP to c. 2865 BP)

Decreasing trends in $\delta^{13}C$, %TOC and C/N can be seen during this zone. $\delta^{13}C$ declines from c. -26.8‰ to c. -27.6‰. Interestingly, %TOC shows a decline at this time, to c. 25%. C/N although variable, does also show this decreasing trend towards the transition with zone III. %DW again shows little change although %LOI at 550$^{o}$C and 950$^{o}$C increases by c. 2%, concurrent with the fall in C/N.

6.7.1.3. Zone II (c. 2865 BP to c. 2340 BP)

Zone II sees the beginning of an increasing trend in $\delta^{13}C$. %TOC shows a marked change after c. 2800 years BP, where values increase to c. 30%, after which values decline once more. A concurrent fall (increase) is seen for %DW (%LOI 550$^{o}$C and 950$^{o}$C) although by small values, c. 4% and 2% respectively. C/N shows a marked decline at c. 2695 years BP to the lowest values in the record (c. 8). The gradual declining trend seen in the record up until this point ends, after which values fluctuate between c. 9 and 9.2.

6.7.1.4. Zone III (c. 2340 BP to c. 1195 BP)

Zone III sees a very gradual increasing trend in $\delta^{13}C$. On entering zone III an increase is seen in %TOC to c. 25.5% at c. 2180 years BP. After c. 1935 years BP values settle and show little variation. C/N also remains stable during the zone. %DW demonstrates an increasing trend while %LOI 550$^{o}$C and 950$^{o}$C show an decreasing trend towards zone IV.

6.7.1.5. Zone IV (c. 1195 BP to c. 0 years BP)

$\delta^{13}C$ shows little variation over this zone, fluctuating around c. 26‰. %TOC also shows only minor fluctuations. C/N however shows variability during the zone. Values increase to c. 10 at c.1150 years BP, the highest point in the record. After c. 1060 years BP values decline and begin to fluctuate between c. 8.5 and c.9. Once again, %DW show little variation, while %LOI 950$^{o}$C increase by c. 4% in this zone, before declining towards the surface. %LOI 550$^{o}$C oscillates between c. 90 and 92% for the zone.

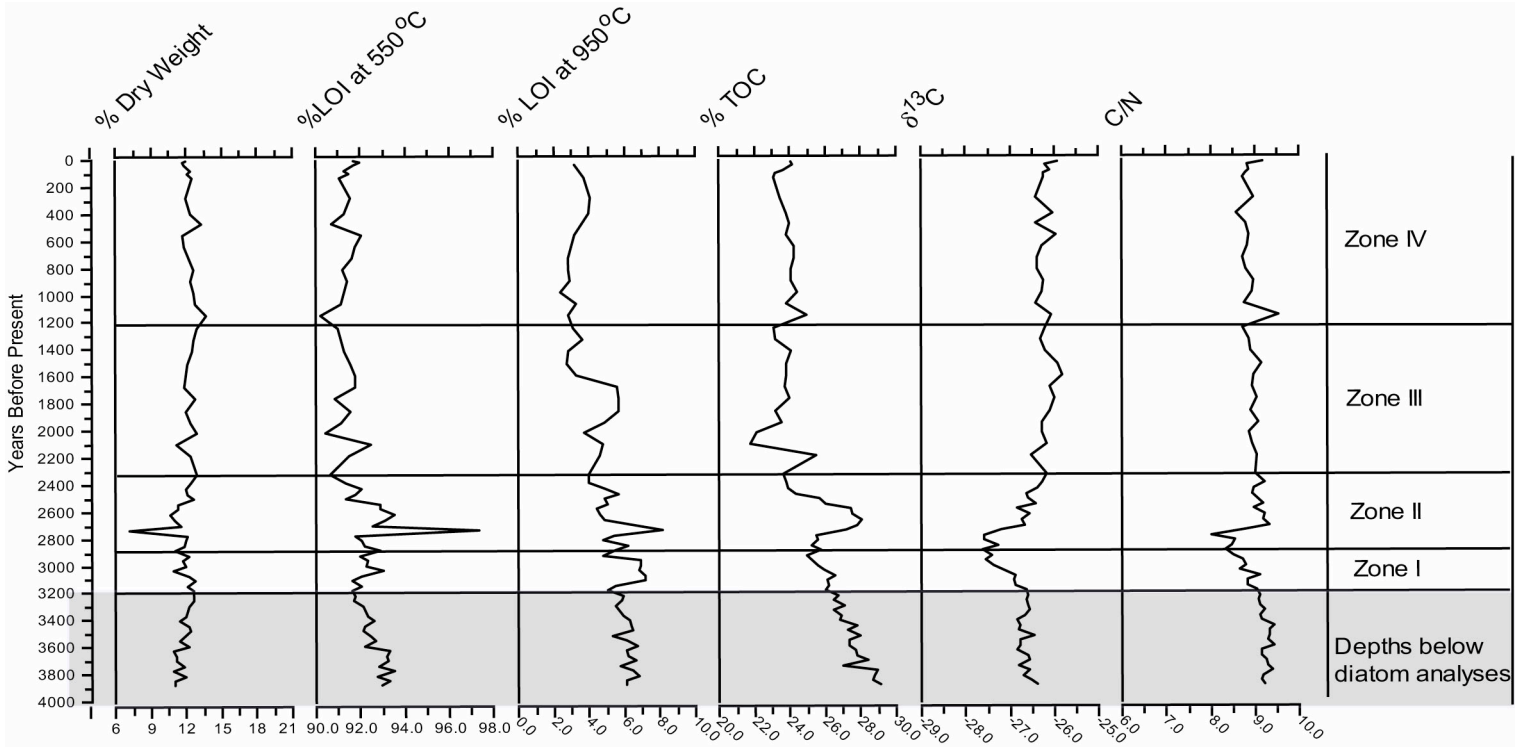


*Figure 6.10. A summary diagram for the analyses conducted on core Ar-2005. All the analyses have been conducted on the entire record. % DW, % LOI at 550°C, % TOC, % LOI at 950°C are shown along with $\delta^{13}C$ (‰) and C/N. Years are before present (2005). The zones shown are based on the cluster analyses conducted on diatom species data and applied here for comparison.*

### 6.7.2. Multivariate results on Ar_2005

6.7.2.1. DCA

Ordinations were carried out on species data > 2% in any one sample. DCA analyses resulted in a first axis eigenvalue of 0.232 (see Table 6.4). A gradient length for axis 1 of 1.898 suggests a linear response of the species data and as a result PCA analyses was conducted.

| DCA | 1 | 2 | 3 | 4 | Inertia |
|---|---|---|---|---|---|
| Eigenvalues | 0.232 | 0.124 | 0.059 | 0.039 | |
| Length of gradient | 1.898 | 2.875 | 1.476 | 1.095 | |
| Cumulative % variance of species data | 17.6 | 27.1 | 31.6 | 34.5 | |
| Sum of all eigenvalues | | | | | 1.318 |

*Table 6.4. DCA eigenvalues and gradient length results for axes 1 to 4.*

6.7.2.2. PCA

PCA resulted in eigenvalues for the first two axes of $\lambda_1$=0.421 and $\lambda_2$=0251 respectively (Table 6.5). The first two axes therefore capture 67.2% of the variation in the species data, with axis 1 capturing nearly two thirds of this (42.1%).

| PCA | 1 | 2 | 3 | 4 | Inertia |
|---|---|---|---|---|---|
| Eigenvalues | 0.421 | 0.251 | 0.124 | 0.060 | |
| Cumulative % variance of species data | 42.1 | 67.2 | 79.6 | 85.6 | |
| Sum of all eigenvalues | | | | | 1.000 |

*Table 6.5. PCA eigenvalues and cumulative percentage variance results for axes 1 to 4.*

The results of average link cluster analysis was applied to the PCA plot of sample core data from Ar-2005. A total of 4 groups was selected. The division of samples into groups is seen in Table 6.6. In order to reduce label crowding, species only of a N> 5 were displayed on the diatom species PCA plot.

| Class number | Samples |
|---|---|
| 1 | 1 to 27 |
| 2 | 28 to 46 |
| 3 | 47 to 57 |
| 4 | 58 to 100 |

*Table 6.6. Results from Average Link cluster analysis. Sample classification for the four chosen groups. This classification is adopted in Figure 6.11.*

Figures 6.11 and 6.12 display the PCA sample plot and diatom species vector plot, respectively. The sample plot shows the clear transition from the bottom core samples (class 4), dominated by *Puncticulata radiosa* and *Puncticulata bodanica* to further up core, where assemblages are dominated by species including *Epithemia adnata, Rossithidium petersenii* and *Stephanodiscus medius.* These assemblages are also seen on the stratigraphy. Class 1 shows a strong gradient of change along axis 2.

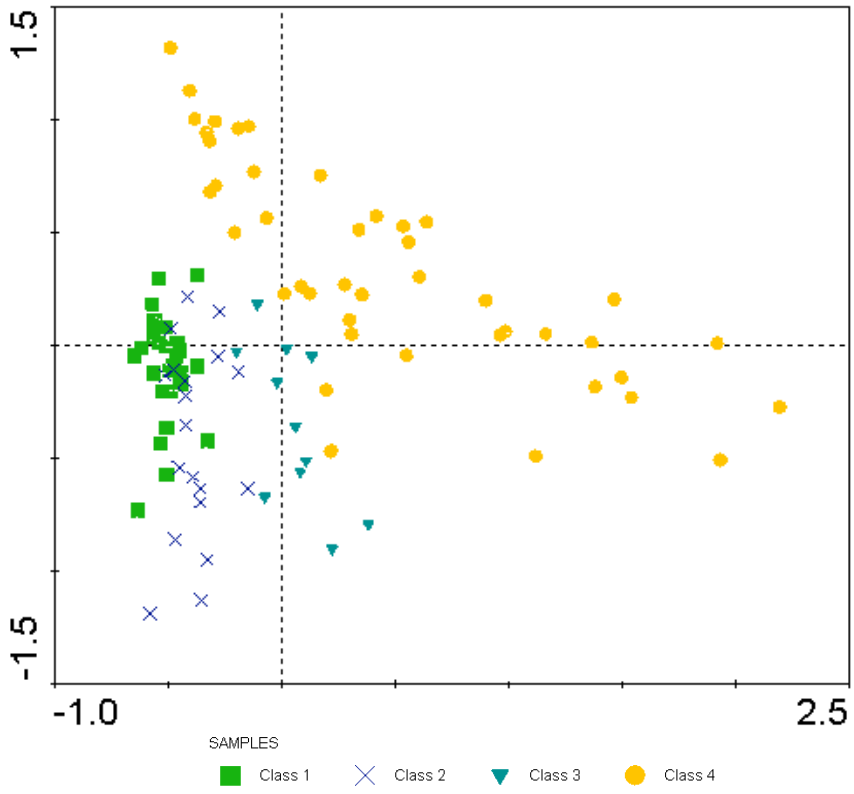


*Figure 6.11 PCA samples plot for the Ar-2005 diatom species data. Average link cluster analysis results are displayed on the stratigraphy to identify the four main zones of change in the core. Class one refers to the top of the core.*

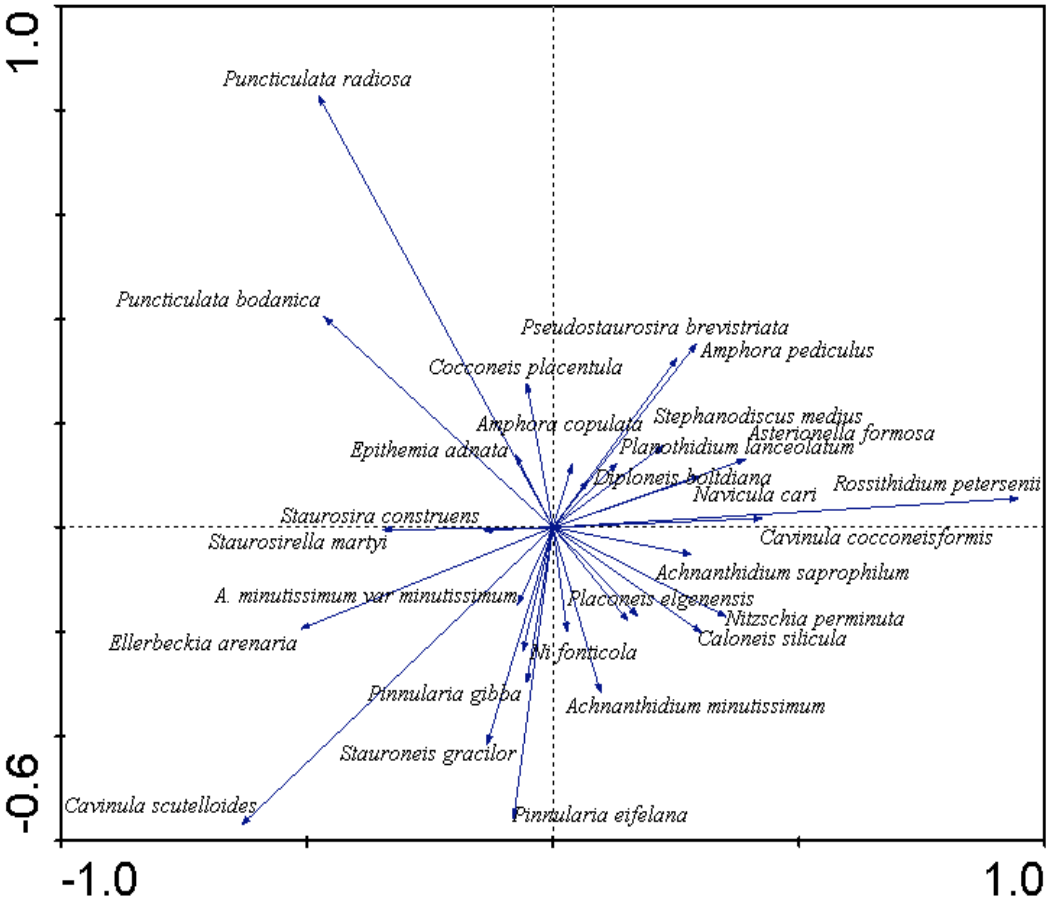


*Figure 6.12. PCA species plot for the core Ar-2005. Species N > 5% are only displayed for visual purposes.*

| Species name | PCA Axis 1 Score | PCA Axis 2 Score |
|---|---|---|
| *Puncticulata radiosa* | -0.4775 | 0.8276 |
| *P. bodanica* | -0.4656 | 0.4040 |
| *Stephanodiscus medius* | 0.2255 | 0.1575 |
| *Rossithidium petersenii* | 0.9460 | 0.0558 |
| *Cavinula scutelloides* | -0.6337 | -0.5692 |
| *Pinnularia eifelana* | -0.0799 | -0.5566 |
| *Staurosira elliptica* | 0.2539 | 0.2800 |

*Table 6.7. PCA axes 1 and 2 scores for the dominant species from core Ar-2005.*

The 10 samples in class 3 show a strong gradient along axis 2 and have an assemblage dominated by *E. adnata, Placoneis elginensis* and *Achnanthidium minutissimum* (Figures 6.11

and 6.12). This shift is seen in the stratigraphy at the beginning of zone III. Class 2 has a similar assemblage although there is a greater abundance of *Cavinula scutelloides, A. minutissimum* var *minutissimum* and *Ellerbeckia arenaria*. Class 1 also shows a gradient change along axis 2 which is seen in the stratigraphy in zone IV. These samples have a higher abundance of *Puncticulata* species, *E. arenaria, Staurosira martyi* and *C. scutelloides.* Once again this is clearly displayed in the stratigraphy (Figure 6.13).

### 6.7.3. Results from stratigraphy

Please refer to Figure 6.13 for the stratigraphy. Please note, that for the Lake Arachlei record years BP refers to calendar years before year 2005.

#### 6.7.3.1. Zone I (c. 3200 ± 825 years BP to c. 2865 ± 715 years BP)

Zone I sees the dominance of *Puncticulata radiosa,* at its highest abundances in the record. Other planktonic species, including *P. bodanica, Stephanodiscus medius* are also present. Abundances of *Staurosira elliptica* and *Amphora pediculus* show a slow increasing trend over the period. *Rossithidium petersenii* shows an increase at c. 3030 BP until c. 2990 BP, declining until entering zone II. Valve concentrations also show a peak at the same time, declining in the same trend as the species *R. pertersenii.* PCA axis 1 scores reach high values, although PCA axis 2 shows a decline in axis scores at c. 3010 BP corresponding to a decline in abundances of the planktonic species *P. radiosa* and *P. bodanica,* as well as an increase in the benthic/epiphytic species *Navicula cari, Amphora pediculus.* Preservation and abundances of total diatoms were high permitting a minimum of 300 valves to be counted per slide. Diatom to chrysophyte ratios (D:C) vary between 57-82 for zone I while planktonic:benthic (P:B) diatom ratios vary between 50 and 78.

#### 6.7.3.2. Zone II (c. 2865 ± 700 years BP to c. 2340 ± 200 years BP)

In zone II, planktonic species continue to dominate the record. While *P. radiosa* shows a decreasing trend, there is an increase in relative abundances for *P. bodanica* and *S. medius.* This is captured by the downward trend of PCA axis 2 scores. Values of epiphytic/benthic taxa remain low for the zone as do benthic abundances. However *R. petersenii* shows the highest percentage abundances for the record during zone II, reaching the highest abundances (c. 60%) at c. 2660 years BP. Once again, this is reflected by PCA axis 1 scores. Abundances of *P. eifelana* are introduced to the record at c. 2480 BP until c. 2375 BP, before decreasing once more at the transition with zone III. Total valves counted are once again > 300 valves per slide, however at c. 2615 years BP and c. 2635 BP and respectively, concentrations and total valves counted begin to decline. D:C shows an increasing trend after entering zone II, after which values decline after c. 2480 years BP. P:B remain high in the zone varying between 48 and 70.

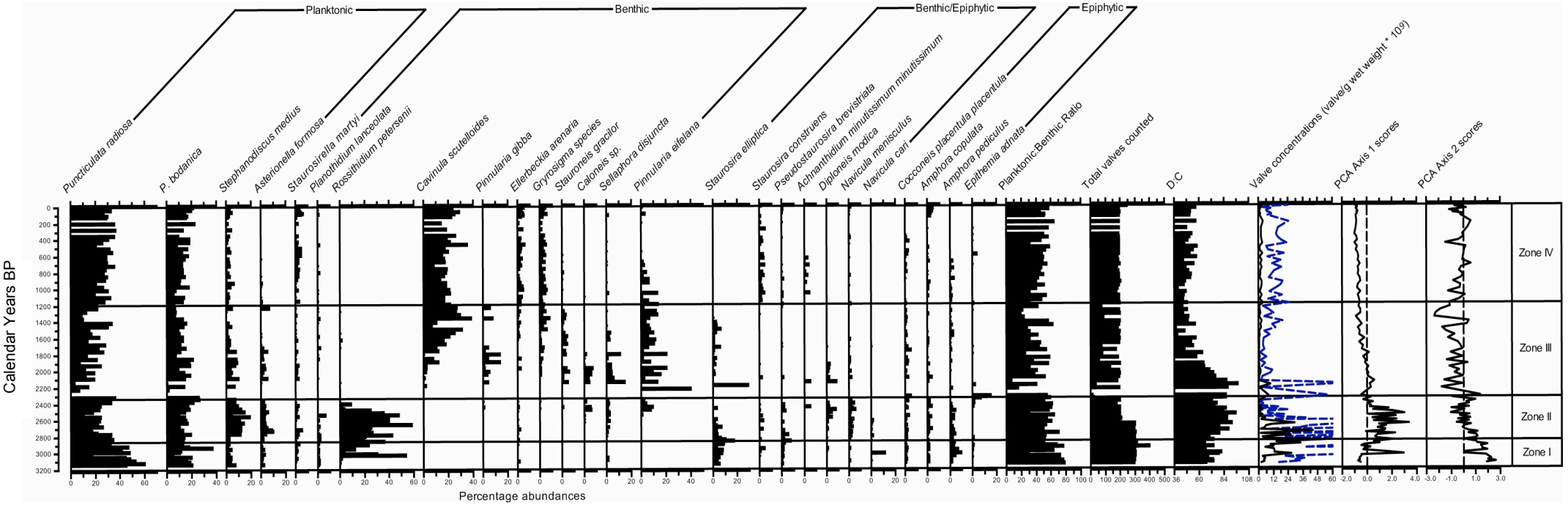


*Figure 6.13. Stratigraphy of Ar-2005 diatom percentage abundances. Species N > 5 are displayed only and species are grouped under relevant respective habitat preferences. Valve concentrations (with a 6x exaggeration), total valves counted, PCA axes 1 and 2and D:C are shown. Zones applied result from average link analysis applied to species data (of abundances > 2%). Please note that 0 years BP corresponds to the date on which the core was collected in 2005*

6.7.3.3. Zone III (c. 2340 ± 200 years BP to c. 1193 ± 1200 years BP)

At the transition with zone II and III, a small number of valves were counted per slide, in some cases < 50 valves. After c. 2225 years BP this increases once again. In zone III, there is an overall decrease in the abundance of planktonic taxa. A small increasing trend is seen in the valve abundances of *P. radiosa* however, over the zone. Benthic species have a greater percentage abundance during zone III. For example, *Cavinula scutelloides* shows an increasing trend after c. 2010 years BP throughout the zone. PCA axis 1 scores show very little change through zone III, although a small decreasing trend is seen, which is most likely reflecting the overall decreasing trend in planktonic species, while PCA axis 2 scores show a small overall decreasing trend, although axis scores are very variable throughout the zone. These scores are most likely reflecting the variation in the assemblages of benthic/epiphytic species, for example at c. 1410 years BP the peak in PCA axis 2 scores occurs at the same time as the decline in *C. scutelloides* and increase in *P. radiosa*, two species which are correlated with PCA axis 2. After c. 2140 years BP valve concentrations fall to low abundances and remain so for the rest of the record. Total valves counted remain at c. 200 per slide in zone II although there are some samples where values fall below this number. D:C for zone III decline after c. 2010 years BP after which they remain lower than 65. Planktonic:Bethic ratios for this zone are more variable ranging between 7 and 52.

6.7.3.4. Zone IV (c. 1193 ± 1200 years BP to 0 years BP)

Abundances of *P. radiosa* and *P. bodanica* increase once more in zone IV. *C. scutelloides* also increases and varies between c. 15 and 30%. While abundances of *P. eifelana* decline after entering zone IV, other benthic species (e.g. *Ellerbeckia arenaria* and *Gyrosigma species*) remain, although at low abundances. The presence of other benthic/epiphytic species is also seen, including *S. construens* and *Achnanthidium minutissimum.* Once again, total valves counted remains at c. 200 per slide. PCA axis 1 scores remain steady for the zone, although showing a decreasing trend, which may be reflecting the overall declining trend in benthic/epiphytic species. PCA axis 2 scores, are variable reflecting the percent abundance changes in the dominant planktonic species. D:C remain steady for zone IV with values less than 60, while P:B range between 32 and 50 for the zone and increase to 65 at c. 200 years BP.

### 6.7.4. Time series results

Timeseries analyses were conducted on PCA axis 1 and 2 scores as well as $\delta^{13}C$ and C/N data. Timeseries analyses were conducted in order to summarise general trends in the data over the period of reconstruction, and to detect any significant changes in the data.

#### 6.7.4.1. Timeseries results of bulk organic isotope analyses

GAMM2 was selected for timeseries analyses on a basis that it had a lower AIC value. However, as Figure 6.15 shows, as can sometimes happen with palaeodata in timeseries analyses, the autocorrelation structure in the model has caused problems. Essentially, the model finds it hard to distinguish autocorrelation between the data series compared with actual change. As a result, GAMM1 has also been shown here as this ignores autocorrelation structure (Figure 6.15).

Timeseries results from $\delta^{13}C$ analyses (Figure 6.14) show a change towards lower values during the period c. 3030 and 2700 years BP. Once again, this corroborates the changes seen in both PCA axes 1 and 2 seen above. However, based on this model there are no significant changes outside of this trend. When looking at the figure generated by GAMM2, Figure 6.15, a more general trend is outlined only. However, the changes seen between c. 2800-3000 years BP as significantly different from this increasing trend. Further significant changes are also seen between c. 1760 and 1585 years BP where there is an increase in $\delta^{13}C$. The overall trend of increasing productivity is clearly seen.

C/N ratios show a significant decrease in values between c. 2990 and 2770 years BP, followed by a later increase at c. 2695 years BP and again at c. 1150 years BP (Figure 6.16).

Figure 6.14

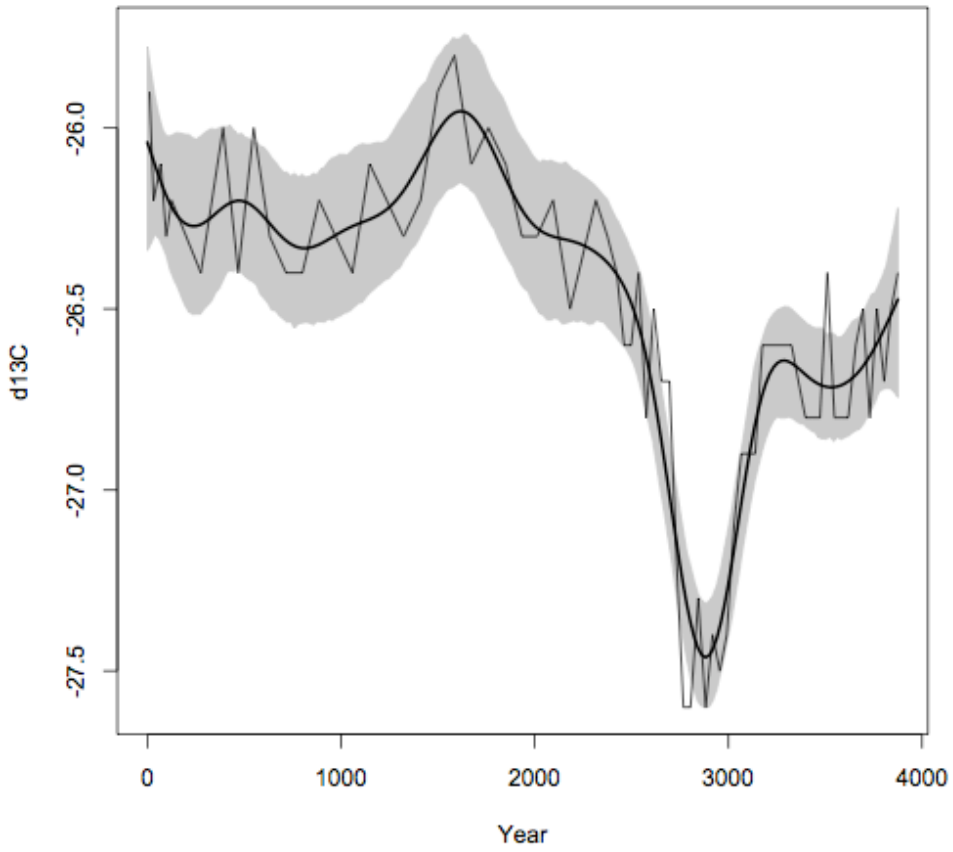


Figure 6.15

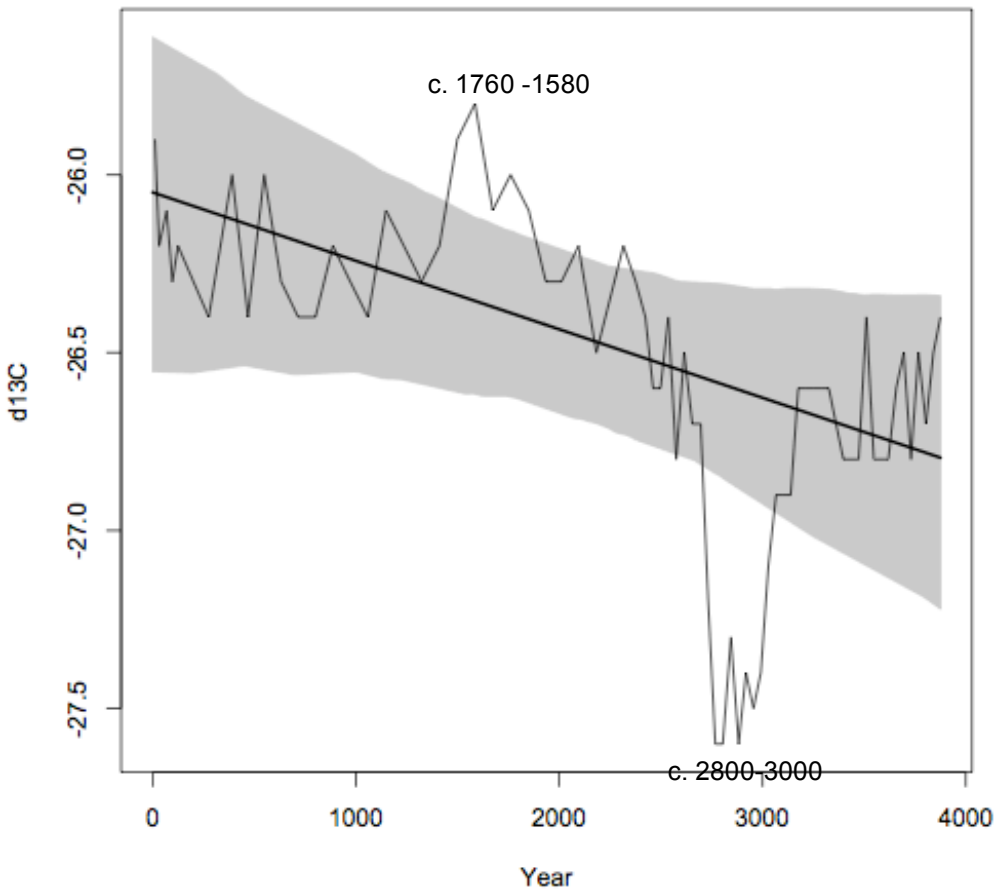


*Figure 6.14. Timeseries results showing fitted GAMM1 model selected for $\delta^{13}C$. 6.15 shows the GAMM2 model applied to $\delta^{13}C$ data, with autocorrelation structure. Units of $\delta^{13}C$ are in (‰). 95% confidence levels are also displayed. Outside of these modelled smoothers, there are significant changes in palaeoproductivity. Please note that the Year is BP (2005).*

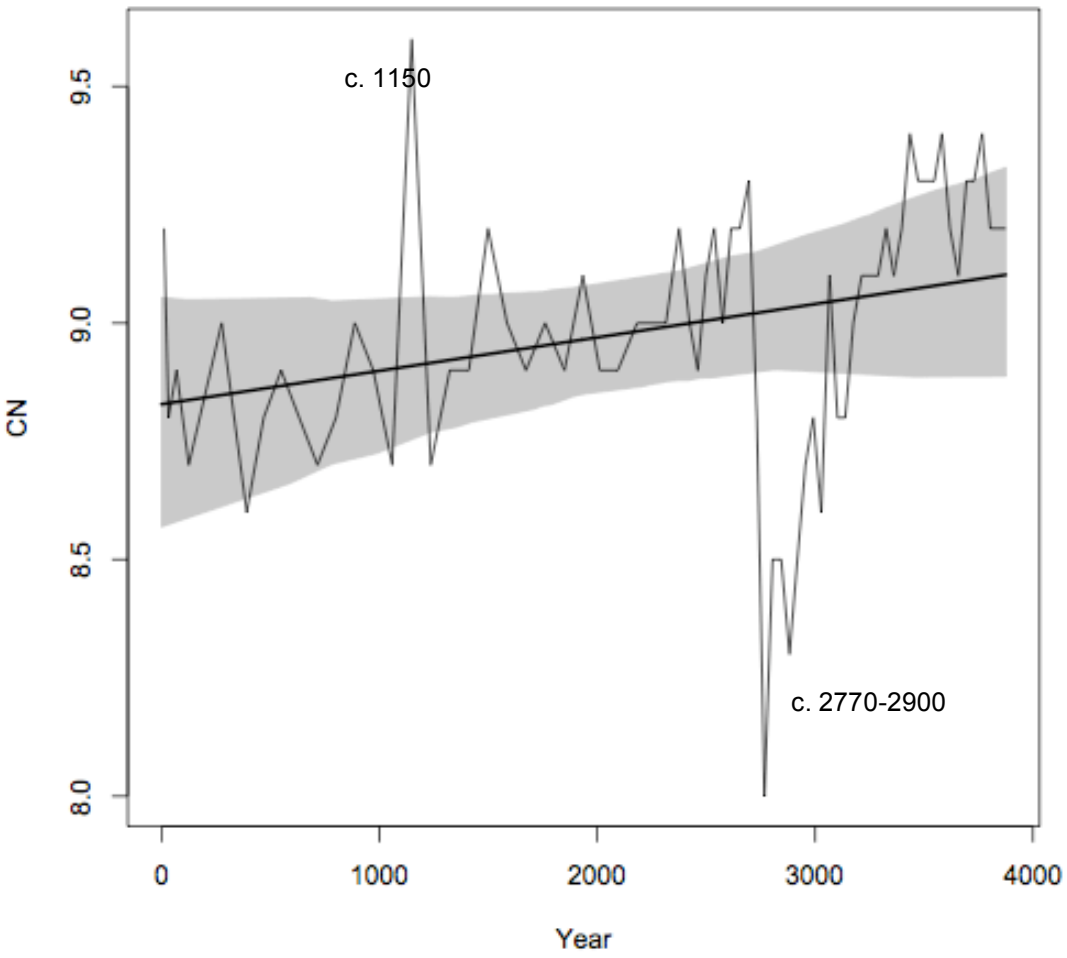


*Figure 6.16 The GAMM2 model applied to C/N data, with autocorrelation structure. 95% confidence levels are also displayed. Outside of these modelled smoothers, there are significant changes in palaeoproductivity. Please note that the Year is in before present (2005).*

6.7.4.2. Timeseries results from diatom PCA axes scores

Results for PCA axis 1 (Figure 6.17) shows that there are a number of significant shifts in axis scores at the bottom of the record. The GAMM1 model was selected for the analyses. The grey shaded band corresponds to the 95% confidence level, so that anything outside of the area is significant change. It should be noted here that the axes for PCA 1 have been reversed, this is sometimes an outcome of using the program R for plotting. This does not affect the data itself but only the plotting format of the axes.

Timeseries results for diatom PCA axis 1 species scores shows significant changes between the period c. 3030 years BP and 2315 years BP. On the basis of the diatom species data this suggests that there are significant changes in the abundances of *Rossithidium petersenii* and planktonic assemblages.

PCA axis 2 scores (Figure 6.18) demonstrate that there are a number of significant shifts in diatom axis scores over the duration of the record, which are associated with increase (positive) and decreases (negative) in *Puncticulata radiosa* (Table 6.7). Once again a number of significant shifts are seen in the bottom of the record, as mentioned demonstrating the shift between benthic and planktonic species.

Other examples of significant changes in diatom axis 2 scores are between c. 1410 to 1455 years BP, as well as at c. 1365 BP, 460 BP and 200 years BP.

Figure 6.17

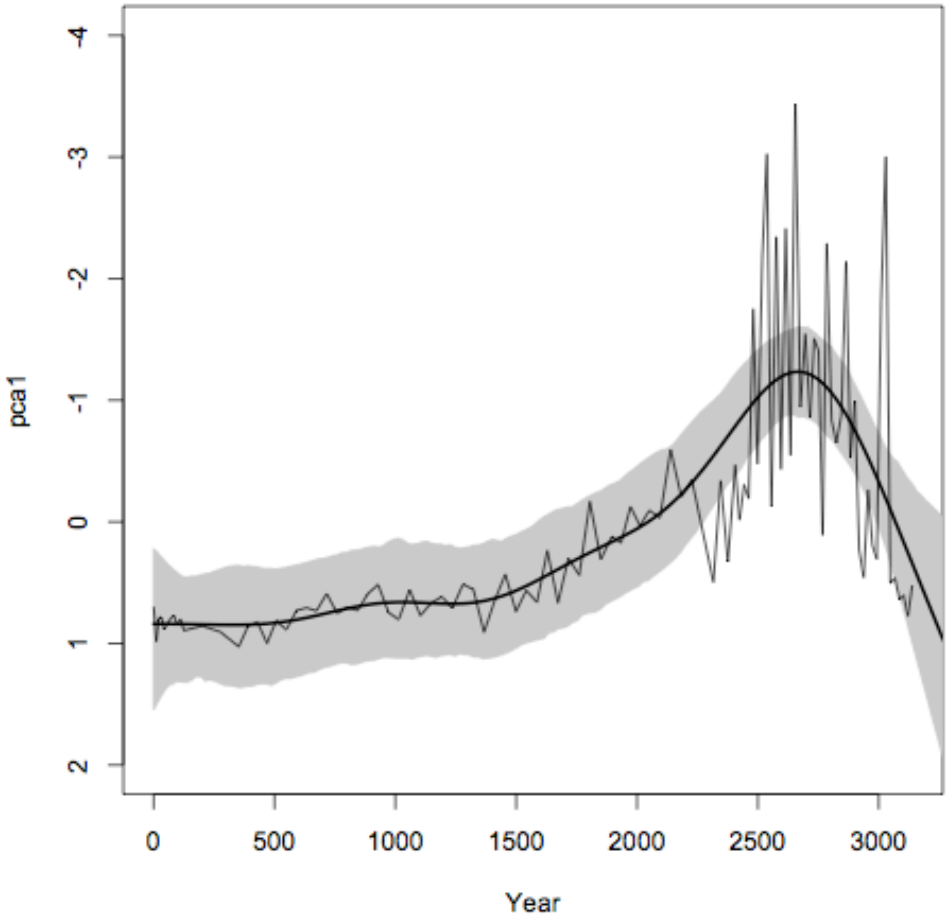


Figure 6.18

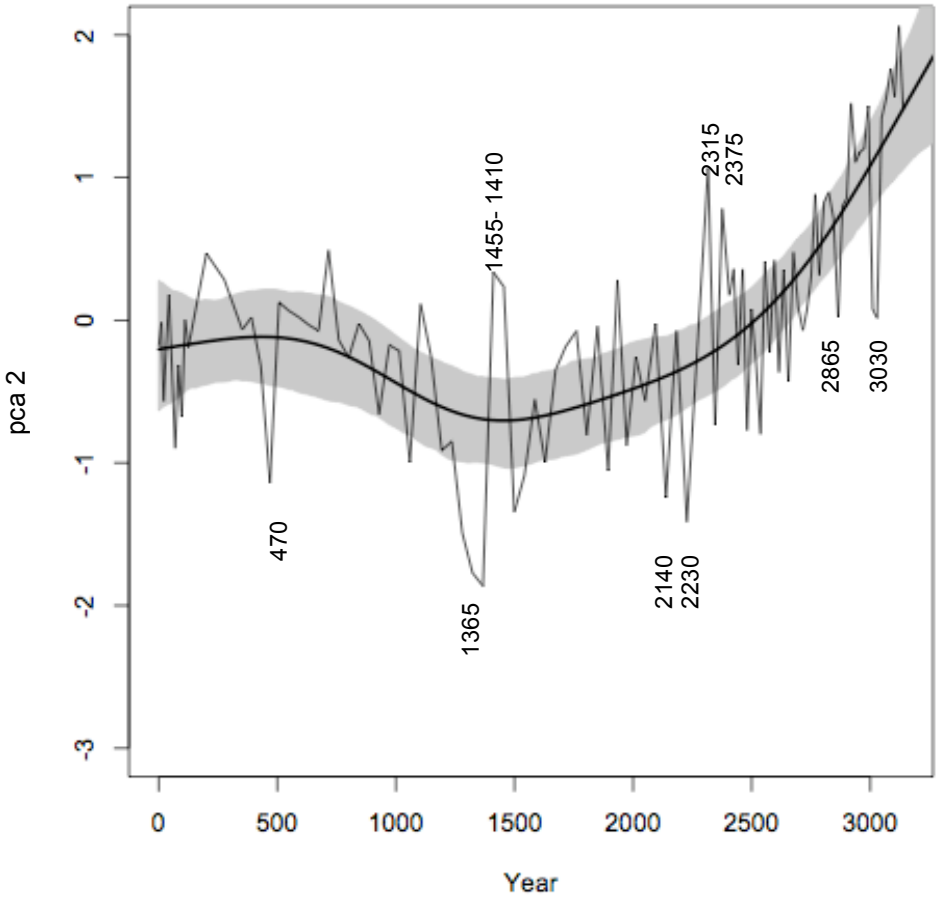


*Figure 6.17 Timeseries results conducted on PCA axis 1 and 6.18) PCA axis 2 scores. The results show the fitting of a GAMM1 model to the data without auto-correlation structure. Please note that years are in Years BP (before 2005). The ages displayed on the plots are average years based on my derived chronology. Please note that the axis 1 scores have been reversed for display purposes and in order to compare with PCA axis scores on Figure 6.13. This is as a result of adopting the software program R to create the analysis, which can sometimes reverse the axis plotting scores.*

### 6.7.5. SiZer results from Lake Arachlei

Results from SiZer analyses conducted on PCA axes scores from Ar-2005 show a number of trends. Firstly, when discussing the increase (red) and decrease (blue) trends, it must be noted here that the scale is reversed for axis 1. As highlighted in Section 6.7.4.2 this is a result of the reversal of the PCA axes, sometimes a feature of the program R. As SiZer analyses follow on from timeseries, the same interpretation applies here so that when discussing increasing and decreasing trends across the bandwidths the interpretation of the colours is reversed. This is only applicable for PCA axis 1 (Figure 6.19), after which the interpretation is as outlined in Section 5.3.7. Therefore:

- Ar_2005 PCA axis 1 scores – increasing trends are in blue and decreasing trends are in red
- Ar_2005 PCA axis 2 scores – increasing trends are in red and decreasing trends are in blue

The main trend identified in PCA axis 1 SiZer results (Figure 6.19) from ARAC are that of a decreasing trend (red for this plot) from the beginning of the record at c. 3200 years BP to c. 2500 years BP for the bandwidths greater than c. 3200 years. Between the bandwidths 3162 and 1000 years, this trend occurs between the years c. 2500 and 750 years BP. In the centennial size bandwidths (316 to 100 years) the following decreasing trend is seen between the years c. 2560 to 2330, 2100 to 1250, and 1250 to 500 years BP. On further smaller bandwidths (100 years) significant decreases are seen between 2000 to 2100 and 830 to 500 years BP. A small increasing trend (blue for this plot) is seen between the bandwidths 316 and 800 years, which occurs between c. 3200 and 2750 years BP in the ARAC record. After the 316 year bandwidth a decrease is seen at 2750 years BP lasting c. 100 years.

SiZer results from PCA axis 2 scores (Figure 6.20) show that longer than the 3162 year bandwidth there is a decreasing trend lasting from the beginning of the record until c. 1420 years BP which later shifts to a significant increasing trend from c. 1165 years BP to present day. Between the millennial and 316 year bandwidth a significant decrease in scores is seen after 3200 years, decreasing in duration with the shorter bandwidths. After 316 years this occurs between c. 2900 and 2600 years BP. The increasing trend in axes scores, after the 1000 year bandwidth lasts for a shorter duration in the record, between c. 1165 and 750 years BP.

6.19

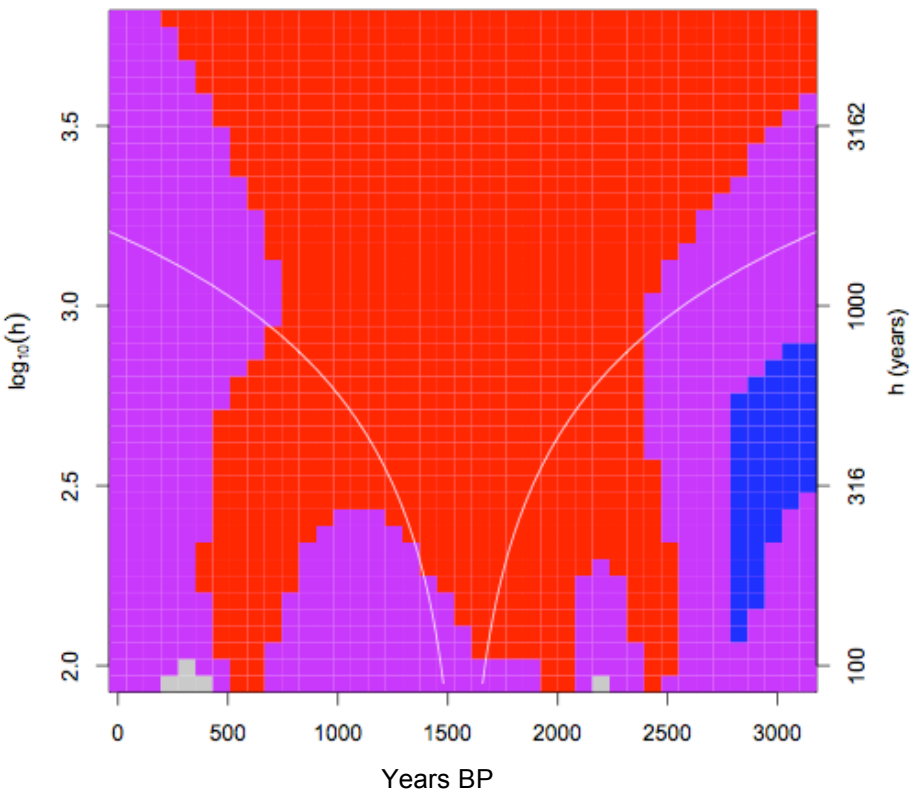


6.20

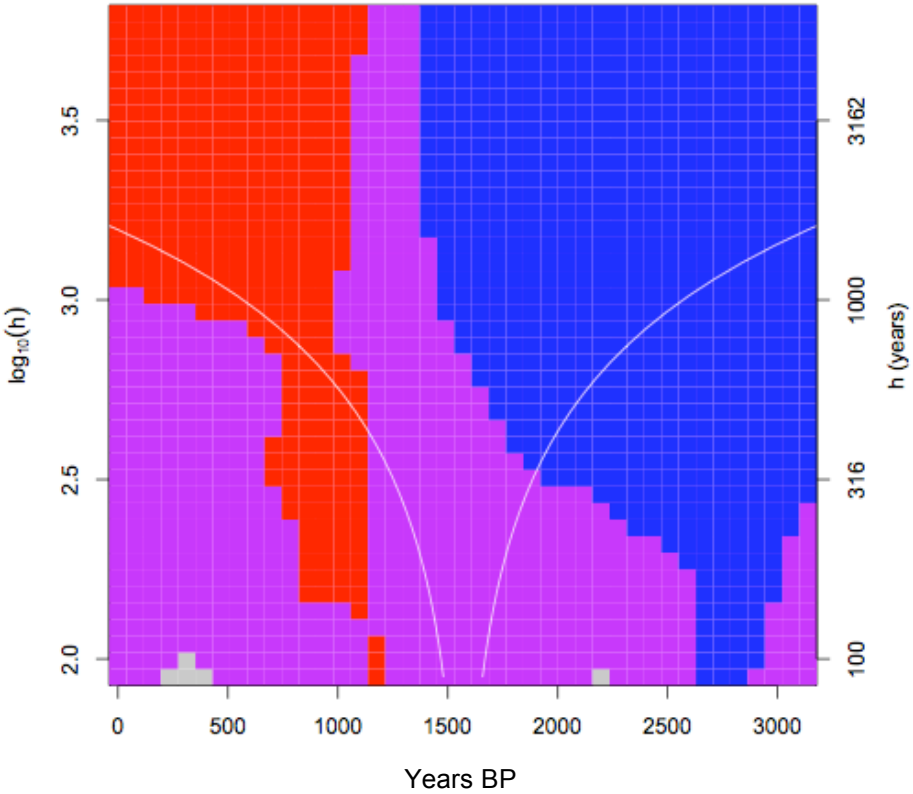


*Figures 6.19. SiZer results from PCA axis 1 and 6.20. PCA axis 2 scores of Lake Arachlei. Y-axis represents the bandwidth applied to the data (h) and right hand y-axis the equivalent bandwidth in years. Blue (red) corresponds to decreasing (increasing) trend in data, although this is reversed for 6.19 due to vagaries of the program R. The age scale is in calendar years BP (0 = 2005)*

Timeseries results (Figure 6.17) show significant increasing and decreasing trends between 3200 and 2300 years BP for PCA axis 1. SiZer identifies greater variability in the record at shorter bandwidths. Based on PCA axis 2 timeseries results, significant changes are seen at c. 3030, 2865, 2300, 2140-2230, 1455-1365, 470 and after 200 years BP. Results of bulk organic isotope analyses from the same ARAC record identify distinct changes in $\delta^{13}C$ between 3000 and 2800 and C/N between c. 2880 and 2750 years BP. The period 2100 to 1250 years BP is represented by large bandwidths in SiZer results for axis 2 and within this time timeseries results demonstrate a clear significant increase between c. 1410 and 1365 years BP for the axis (Figure 6.18). In summary, based on SiZer results the following main periodicities in the data (both axis 1 and 2) are seen between c. 3200 to 2600, 2100 to 1250 and 850 to 500 years BP. Comparing the data with the timeseries results it can be concluded that the dominant changes are seen between c. 3030-2800, 1410-1365 (particularly after 1400) and 800-500 years BP.

## 6.8. Discussion

As outlined in Section 5.4, results from cluster analyses (Table 6.6) will be adopted in order to divide palaeoenvironmental data into three time periods for the discussion. Class 2 and 3 were grouped together for the discussion, due to the more preferable time period they created and for ease with comparing the results with other published data. However, reference to the zones will sometimes be made to further emphasise stratigraphical changes.

### 6.8.1. Ecological interpretation of diatoms from Lake Arachlei

The planktonic species *Puncticulata radiosa* dominates the beginning of the Lake Arachlei record. This species can competitively dominate assemblages with high lake water temperatures due to their high growth rates (Table 6.8) (Hickman and Reasoner 1998). An assemblage change is later seen towards one dominated by the species *Rossithidium petersennii. R. petersenii,* is a benthic species which has an ecological preference for oligotrophic water with low pH and conductivity (Table 6.8). On the basis of diatom ecology, the Ar-2005 stratigraphy suggests that there is a change towards lower summer lake water temperatures (fall in *P. radiosa*) through zone I and into zone II (Figure 6.13). As the species is benthic, it may also reflect a fall in lake water level, increasing the benthic area habitat for *R. petersennii* and other benthic species. Prokopenko (pers. comm.) also suggest that changes in summer temperatures have a significant affect upon the duration of the following winter's ice cover at Lake Hovsgol (south west of Lake Arachlei; Figure 1.2), with a decline in temperatures causing longer ice cover. As a result, this may suggest that the decrease in *P. radiosa* may reflect earlier ice on and later ice off days as well as or instead of reductions in lake water level

at Lake Arachlei. In more recent years, evidence has shown the lakes within the Ivan-Araklei system are sensitive to changes in lake water level, demonstrating quasiperiodic (7-11 years) and longer cycles with a significant amplitude of water level but constant salinity (Bazarova et al. 2006; Shishkin 1973).

Later assemblages differ to the earlier ones (e.g. zones III and IV), with the introduction of *Cavinula scutelloides. C. scutelloides* is a benthic/epipelic species which mainly occurs in lake waters but can also survive on wet places (Table 6.8), which may be suggesting lake level fluctuations at Lake Arachlei (Van Dam et al. 1994). The presence and increase of *Ellerbeckia arenaria* after c. 1600 years BP also suggests a lake that experienced periodic changes in lake water level as this species is aerophilic and therefore tolerant of periodic exposure to the atmosphere (Schmid and Crawford 2001; Van Dam et al. 1994). It is around the same time that abundances of chrysophytes increase (e.g. D:C ratios). Chrysophytes are able to switch between autotrophy, heterotrophy and even phagotrophy in stressful conditions (Betts-Piper et al, 2003). Their increase at this time, compared to diatom abundances, may suggest highly variable lake conditions.

In conclusion, the general ecological trend that can be interpreted from Lake Arachlei on the basis of diatom ecology is one of variable (decreased) lake levels (e.g. PCA axis 1 timeseries results; Figure 6.17). This is supported firstly by the introduction of *R. petersenii* and later by the introduction of aerophilic species (e.g. *C. scutelloides* and *E. arenaria).* Variations in PCA axis 2 timeseries results also demonstrate variations in the abundance of the planktonic species *P. radiosa,* which suggests periods of increased/decreased lake water temperatures and/or changes in winter ice cover duration.

| Diatom species name | Ecology | Reference |
|---|---|---|
| *Rossithidium petersenii* | Low conductivity and low pH to circumneutral. Oligotrophic state and 100% oxygen saturation preference. Benthic habitat. | (Keatley et al. 2008; Van Dam et al. 1994) |
| *Puncticulata radiosa* | Planktonic, high summer water temperatures. Eutrophic, above 75% oxygen saturation of waters and rarely outside of water bodies. | (Hickman et al. 1998; Kirilova et al. 2010); |
| *Achnanthidium minutissimum* var *minutisimum* | Benthic/epiphytic, sometimes tychoplanktonic. Oxygen loving, pioneer species, phosphorous specialist. pH circumneutral and also at pH < 5.5. Abundant at the beginning of stratification and autumn turnover at XLW following macrophyte decay. Opportunistic species with wide tolerance of trophic state, high oxygen requirement. | (Brown et al. 2008; Cholnoky 1968; Kuhn et al. 1981; Reavie and Smol 1998; Van Dam et al. 1994; Watchorn et al. 2008) |
| *Staurosira ellipitica* | Opportunistic, widely found in fresh water bodies (e.g. cosmopolitan). Alkaliphilious (pH > 7). Mesotrophic to eutrophic. Above 100% oxygen saturation. | (Patrick and Reimer 1966; Van Dam et al. 1994; Weckstrom and Juggins 2006) |
| *Staurosira martyii* | Benthic, epipsammic, brackish - freshwater | (Nelson and Bradley 2009) |
| *Cavinula scutelloides* | Low light conditions, benthic, epipelic. Widely found in freshwater bodies (e.g. cosmopolitan). Alkalibiontic (exclusively above pH >7), eutrophic and sometimes found outside of water bodies. | (Patrick et al. 1966; Van Dam et al. 1994; Witkowski et al. 2004) |
| *Puncticulata bodanica* | Planktonic, high oxygen saturation (100%) and oligotrophic status. | (Algaebase 2010; Van Dam et al. 1994) |
| *Pinnularia eifelana* | Moss and stone (epiphytic/epilithic) | (Nikulina 2008) |
| *Stephanodiscus medius* | Spring and early summer, higher temperatures. Meso/eutrophic | (Kirilova et al. 2010) |
| *Ellerbeckia arenaria* | Benthic, alkalibiontic and alkaliphilic, oligotrophic and high oxygen saturation (100%). Permanent submersion and occasional drying or mainly occurring on wet and moist/temporary places. | (Prather and Hickman 2000; Schmid et al. 2001; Schmidt et al. 2004; Van Dam et al. 1994) |
| *Asterionella Formosa* | Alkaliphilios (mainly occurring at pH >7), mesotrophic to eutrophic and rarely occurring outside of water bodies. | (Van Dam et al. 1994) |

*Table 6.8. Ecological preferences of the dominant diatom species from core Ar-2005. Relevant references of literature consulted is shown.*

### 6.8.2. Environmental reconstruction between c. 3140 to 2230 years BP

Drying trends in palaeorecords, associated with Neoglacial cooling, have been identified in regions of Mongolia, Siberia and China, following the earlier climatic “optimum” in the Holocene between c. 8000 – 6000 BP and are attributed in part to the decreasing trend in solar insolation (refer to Chapter 1). It should be noted that the duration and nature of climate associated with the Holocene “optimum” varied spatially in regions of northern Eurasia (Prokopenko et al. 2007). The same therefore likely applies to the initiation of the arid trend following the “optimum” (as

discussed in Chapter 1, Section 1.7). Superimposed upon this mid-late Holocene drying trend are events of relative decreased or increased water levels thought to result from changes in effective moisture. The climatic mechanisms responsible for these lake level changes vary spatially across these regions with lower (higher) summer temperatures, decrease (increase) in potential evapotransporation and increased (decreased) precipitation thought to play important roles in increasing (decreasing) water levels (Mischke et al. 2008; Schwanghart et al. 2008).

At Lake Arachlei, these environmental changes are concomitant with significant reductions (increases) in planktonic (benthic) species (Figures 6.10 and 6.13). In particular, abundances of *R. petersenii* increase between the period c. 3000-2000 years BP, and *P.radiosa* species decline. During this period, valve concentrations increase and this is likely to be a reflection of the smaller valve size of the species compared to the planktonic assemblage at Lake Arachlei. Based on diatom ecology, a general trend to cooler summer lake temperatures is suggested and/or a reduction in lake water levels. Interestingly, significant changes between c. 3000 and 2800 years BP are also outlined by the fall in $\delta^{13}C$ and C/N ratios suggesting a movement towards decreased algal productivity. However, higher valve abundances during this period were observed, compared with the rest of the palaeorecord. Several studies have highlighted the possibility to distinguish between the benthic and planktonic algal composition of $\delta^{13}C$ values. In particular, it is suggested that benthic algae have higher $\delta^{13}C$ values while planktonic algae have lower values (Doi et al. 2009; France 1995). However, as outlined in Section 6.7, the range of $\delta^{13}C$ values for the core Ar-2005 are between c. −27.5 and −26‰, which is only a small range so further interpretation of these data will not be attempted here (Table 6.1). Evidence from Hulun Lake, Mongolia (refer to Figure 1.2), demonstrates a reduction in lake water levels between 3050-2800 cal years BP (Xiao et al. 2009). However, Fowell et al (2003) argue that for the period between c. 4500-1600 cal years BP, Lake Telmen, north central Mongolia, experienced “maximum humidity”, although superimposed upon this trend between c. 3150 – 2940 BP were events of extreme aridity. Other literature also suggests a trend to a more arid climate (decreased precipitation:evaporation; P:E) (as discussed in Section 6.1). For example, Prokopenko (2007) demonstrates that there is a significant warming seen in the Lake Baikal watershed between 4000 and 2500 years BP. This increased summer warming is supported by general circulation models (GCM) of the region over this time and evidence of negative moisture balance after c. 3540 years BP at Gun Nuur, Mongolia (Bush 2005; Dorofeyuk and Tarasov 1998). Dali and Daihai lakes (located along the modern day EASM boundary) also show a similar period of low lake level/arid phases between c. 3150 – 2650 years BP.

As outlined in Chapter 1 Dongge cave records also show intervals of decreased monsoonal intensity throughout the Holocene, for example at c. 2700 years BP (Wang et al. 2005), reflected by significant changes in timeseries records from Ar-2005. These events are considered to be reflections of teleconnections between the North Atlantic (Bond event 2) (Bond et al. 2001; Bond et al. 1997) also leading to reduced Westerly intensity in regions of arid

Eurasia and enhanced EAWM and SH intensity. Evidence from Lake Hosvgol, NW Mongolia, demonstrates that the decrease in abundances of planktonic species (e.g. *P. bodanica)* reflects a change to more oligotrophic, cold lake water and a reduction in lake water levels during arid phases (Prokopenko et al. 2007).

### 6.8.3. Environmental reconstruction between c. 2230 to c. 930 years BP

Total valves counted are at their lowest in zone III, particularly in the interval after c. 2300 years BP. This was a result of increased clastic material in the samples and a reduction in the total diatom valve abundances, rather than dissolution. After c. 2350 years BP (entering zone III; Figure 6.13), a shift is once again seen in the diatom assemblage from Lake Arachlei with an introduction and increase in benthic species including *Cavinula scutelloides, Pinnularia gibba, Pinnularia subcapitata* (Table 6.8). The species *R. petersenni* is no longer present in the record suggesting a lake environment different to that between c. 3000 and 2300 years BP. After c. 2300 years BP there is also a rapid increase in chrysophytes cysts, reflecting a possible decrease in lake productivity as shown by the fall in diatom productivity seen at the lake (Figure 6.13; Sandgren et al. 1995; Zeeb and Smol 2001). However, $\delta^{13}C$ continues to demonstrate an increasing trend suggesting increased within lake productivity. A significant change in $\delta^{13}C$ is also seen between c. 1760 to 1580 years BP (Figure 6.14), which is concomitant with the increase in *C. scutelloides* abundances.

It is clear that the Ar-2005 record does not reflect rapid, significant environmental change after c. 2000 years BP, compared to zones I and II. Rather, it suggests that the Ar-2005 reconstruction is demonstrating a continued trend of possible regional aridity and absence of significant climate oscillations as earlier in the record. As discussed in Section 6.1, at around this time there is evidence of an arid climate, with reduced effective precipitation and decreased lake water levels (e.g. Bush 2005; Fowell et al. 2003; Prokopenko et al. 2007; Xiao et al. 2009).

Timeseries results (PCA axis 2 scores) show a significant change between 1401-1365 years BP, although it is most notable after c. 1400 years BP. This more notable change reflects a decline in *P. radiosa* suggesting a significant lake water level reduction, associated with decreased precipitation and/or effective moisture in the region. Other arid climate oscillations have been identified, for example in regions of Mongolia between c. 1540 and 1310 years BP or after c. 1410 cal years BP (Fowell et al. 2003). Further records from the region have also identified such periods of decreased Westerlies and enhanced SH associated with north Atlantic variability e.g. a period of a drying (and cooling), coincident with Bond event 1 (Bond et al. 2001; Bond et al. 1997). For example, Fowell et al (2003) identify a period of aridity between c. 1540 and 1310 cal years BP in Mongolia.

### 6.8.4. Environmental reconstruction between c. 930 years BP to present

It appears that at Lake Arachlei there is little ecological change (diatom and bulk organic isotope record) that may reflect environmental changes associated with the MWP and LIA. After c. 930 years BP increased abundances of planktonic species (*P. radiosa* and *P. bodanica*) suggest increased summer lake water temperatures (Table 6.8). The increasing trend in $\delta^{13}C$ continues towards the present day representing increased within lake productivity. Although *C. scutelloides* is at lower abundances in class 1 compared to class 2, it remains a dominant part of the assemblage. *E. arenaria* is also present in this class., indicating that the lake level at Arachlei remains variable. Interestingly, other lake palaeoenvironmental reconstructions from these regions of northern Eurasia have demonstrated evidence for the MWP and LIA. For example, humid periods at 950 – 650 cal years BP (MWP) and 450-150 cal years BP (LIA) at Lake Telmen, north central Mongolia (Fowell et al. 2003).

PCA axis 2 scores also suggest that at c. 460 and 200 years BP there is a significant change in the reduction of planktonic assemblages, the latter event also associated with a dramatic fall in the number of valves counted, argued to be due to lower diatom productivity or increased sedimentation as valve dissolution was not significant. Indeed, the last main change seen in the SiZer results is between c. 850 and 500 years BP. Once again this reflects the decrease in PCA axis 2 scores (e.g. *P. radiosa*) in Figure 6.18, at c. 470 years BP, although this is superimposed upon a background increasing trend after c. 1200 years BP. Planktonic:benthic ratios decline and at the same time abundances of *C. scutelloides* increase. It is possible that PCA axis 2 scores may be reflecting a change in climatic conditions (decline in *P. radiosa;* axis 2 scores of 0.8276; Table 6.7), namely a movement to colder summer temperatures (Table 6.8). This explanation is consistent with tree ring data presented by Penderson et al (2001) which identifies t severe drought episodes during the LIA. Furthermore, Mackay et al (2005) show quantitative evidence for colder/drier climate between c. 1300 and 1750 years AD coincident with the LIA (ice raft debris (IRD) event 0, or Bond event 0) and increased intensity of the SH. In conclusion, the record from Lake Arachlei reflects variations in precipitation (effective moisture) and summer temperatures in the region, driven by the intensity of summer Westerlies (warm and wet).

In recent years, evidence of changing ecological thresholds associated with recent warming has been well documented in remote regions of the Arctic (e.g. Hobbs et al. 2010; Ruhland et al. 2008; Smol et al. 2005; Solovieva et al. 2008). However, there is an absence of significant changes in diatom assemblages (PCA axis 1 and 2 scores) seen in the past c. 150 years at Lake Arachlei. This suggests the absence of significant anthropogenic impacts on the diatom record from Lake Arachlei. Furthermore, the environmental changes seen in the earlier parts of the record are more significant than those in recent centuries. SCP analyses conducted on core Ar-2005 can further quantify the absence of anthropogenic impact upon the lake, although this does not dismiss human catchment changes, which may have an impact upon the record. SCP

concentrations in the core Ar-2005 are very low (< 630 g/DM). Analyses of multiple cores of Lake Baikal have shown a complex pollution history of recent sediments over the lake's three basins. Cores located in the south of the basin, near to Irkutsk, have the highest SCP concentrations with a maximum of 5,200 g/DM and a cluster of cores in the south basin all with values greater than 3000 g/DM (Rose et al. 1998). Higher values also occur in the north basin, ranging between c. 1,000 and 3,000 g/DM, while the central basin has concentrations < 1,000 g/DM (core Baik-25) representing hemispheric background levels (ibid.). Concentrations less than <1,000 g/DM are argued to represent the hemispheric background concentrations of SCPs, as they are similar to concentrations found in other remote areas of the northern Hemisphere (e.g. Spitsbergen, Canadian Arctic) (Rose 1995; Rose et al. 1998). Evidence from Ar-2005 of low concentrations, as with core Baik-25 from Lake Baikal, also suggests the presence of only background figures of SCP contamination at the lake. It is likely therefore that changes in the recent sediments (e.g. past 150 years) from Lake Arachlei are not a response to anthropogenic induced atmospheric contamination and as a result are likely to reflect within-lake processes or natural succession.

## 6.9. Conclusions

1. The Lake Arachlei diatom record appears to reflect changes in lake water level, most likely associated with changes in Westerly strength and precipitation amount and/or effective moisture. This is consistent with evidence of regional climate change from semi-arid Northern Eurasia.

2. The isotope data provide evidence for changes in productivity. $\delta^{13}C$ displays an overall increasing productivity trend although a significant fall in values is seen between c. 2800 and 3000 years BP. C/N ratios also show an overall declining trend in values over the duration of the record, all from a phytoplankton source, with a significant fall between c. 2750 and 2880 years BP.

3. Against the trend of water level and productivity change, three periods of variability are identified in the Arachlei record, between c. 3200-2600, 2100-1250 and 850-500 years BP. These are coincident with evidence of North Atlantic IRD events 2 to 0 and, therefore, suggest teleconnections between these regions at this time.

4. The study suggests that diatom assemblage variation and within lake productivity is sensitive to teleconnection mechanisms, which are manifested by changes in Siberian High intensity and Westerly strength.

5. There is little evidence of recent atmospheric pollution at Lake Arachlei as SCP concentrations are at background levels.

## References

Algaebase 2010. http://www.algaebase.org/.

An C.B., Feng Z.D. and Barton L. 2006. Dry or humid? Mid Holocene humidity changes in arid and semi-arid China. Quaternary Science Reviews 25: 351-361.

Bazarova B. and Itigilova M.T. 2006. Long-term production dynamics of aquatic vegetation in the Arakhlei Lake (Eastern Transbaikalia). Biol Bull+ 33: 68-72.

Bengtsson L. and Enell M. 1986. Chemical analysis. In: B. E. Berglund (ed.), Handbook of Holocene Palaeoecology and Palaeohydrology. Blackburn, New Jersey.

Best E.P.H. 2006. Photosynthetic characteristics of the submerged macrophyte *Ceratophyllum demersum* Physiologia Planatarum 68: 502-510.

Blockley S.P.E., Bronk Ramsey C., Lane C.S. and Lotter A.F. 2008. Improved age modelling approaches as exemplified by the revised chronology for the Central European varved lake Soppensee. Quaternary Science Reviews 27: 61-71.

Bond G., Kromer B., Beer J., Muscheler R., Evans M.N., Showers W., Hoffmann S., Lotti-Bond R., Hajdas I. and Bonani G. 2001. Persistent solar influence on north Atlantic climate during the Holocene. Science 294: 2130-2136.

Bond G., Showers W., Cheseby M., Lotti R., Almasi P., deMenocal P., Priore P., Cullen H., Hajdas I. and Bonani G. 1997. A pervasive millennial-scale cycle in North Atlantic Holocene and glacial climates. Science 278: 1257-1266.

Bronk Ramsey C. 2009. Bayesian analysis of radiocarbon dates. Radiocarbon. 51: 337-360.

Brown L., May J. and Hunsaker C. 2008. Species composition and habitat associations of benthic algal assemblages in headwater streams of the Sierra Nevada, California. Western North American Naturalist 68: 194-209.

Bush A. 2005. $CO_2$/$H_2O$ and orbitally driven climate variability over central Asia through the Holocene. Quaternary International 136: 15-23.

Canoco v. 4.5; ter Braak C.J.F. and Šmilauer P. 2002. Ithaca.

Chen F., Yu Z., Yang M., Ito E., Wang S., Madsen D., Huang X., Zhao Y., Sato T. and Birks H. 2008. Holocene moisture evolution in arid central Asia and its out-of-phase relationship with Asian monsoon history. Quaternary Science Reviews 27: 351-364.

Cheney C. and Hough R.A. 1983. Factors controlling photosynthetic productivity in a population of Cladophora Fracta (Chlorophyta). Ecology 64: 68-77.

Cholnoky B.J. 1968. Die Okologie der Diatomeen in Binnengewasser. J. Cramer, Lehre, 699 pp.

Doi H., Kiluchi E., Shikano S. and Takagi S. 2009. Differences in nitrogen and carbon stable isotopes between planktonic and benthic microalgae. Limnology

Dorofeyuk N. and Tarasov P. 1998. Vegetation and lake levels in northern Mongolia in the last 12500 years as indicated by data of pollen and diatom analyses. Stratigraphy and Geological Correlation 6: 70-83.

Fowell S., Hansen B., Peck J., Khosbayer P. and Ganbold E. 2003. Mid to late Holocene climate evolution of the Lake Telmen Basin, North Central Mongolia, based on palynological data. Quaternary Research 59: 353-363.

France R.L. 1995. Carbon-13 enrichment in benthic comapred to planktonic algae: foodweb implication. Marine Ecology Progress Series 124: 307-312.

Frost-Christensen H. and Sand-Jensen K. 1995. Comparative kinetics of photosynthesis in floating and submerged *Potamogeton* leaves. Aquatic Botany 51: 121-134.

Hamana K. and Matsuzaki S. 1985. Distinct difference in the polymine compositions of Bryophyta and Pteridophyta. Journal of Biochemistry 97: 1595-1601.

Hickman M. and Reasoner M. 1998. Late Quaternary diatom response to vegetation and climate change in a subalpine lake in Banff National Park, Alberta. Journal of Paleolimnology 20: 253-265.

Hobbs W.O., Telford R.J., Birks H.J.B., Saros J.E., Hazewinkel R.R.O., Perren B., Saulnier-Talbot E. and Wolfe A.P. 2010. Quantifying Recent Ecological Changes in Remote Lakes of North America and Greenland Using Sediment Diatom Assemblages. PLoS ONE 5: 1-12.

IAEA/WMO 2006. Global network of isotopes in precipitation. The GNIP Database. http://isohis.iaea.org.

Juggins S. 1992. Zone v 1.2. Environmental Change Research Centre.

Juggins S. 2007. C2 v.1.5.2. Environmental Change Research Centre.

Keatley B., Douglas M. and Smol J. 2008. Prolonged ice cover dampens diatom community responses to recent climatic change in high Arctic lakes. Arctic, Antarctic, and Alpine Research 40: 364-372.

Kent M. and Coker P. 1992. Vegetation description and analysis: a practical approach,. Wiley, Chichester.

Khursevich G. 1976. History of development of diatom flora from lakes of Narachansky Basin. Nauka i tekhnika, Minsk.

Kirilova E.P., Cremer H., Heiri O. and Lotter A.F. 2010. Eutrophication of moderately deep Dutch lakes during the past century: flaws in the expectations of water management? Hydrobiologia 637: 157-171.

Krammer K. and Lange-Bertalot H. 1986. Bacillariophycea. I. Teil. Naviculaceae. Gustav Fisher Verlag, Stuttgart.

Krammer K. and Lange-Bertalot H. 1988. Bacillariophyceae 2. Tiel. Bacillariaceae, Epithemiaceae, Surirellaceae. Gustav Fisher Verlag., Stuttgart.

Krammer K. and Lange-Bertalot H. 1991a. Bacillariophyceae. 3. Tiel. Zentrische Diatomeen, Diatoma, Meridion, Asterionellla, Tabellaria, Fragilaria, Eunotia und Verwandte, Peronia und Actinella. Gustav Fisher Verlag., Stuttgart.

Krammer K. and Lange-Bertalot H. 1991b. Bacillariophyceae. 4. Tiel. Achnanthes, Navicula, Gomphonema, Kritsche Nachtraege, Literatur. Gustav Fisher Verlag., Stuttgart.

Kuhn D.L., Plafkin J.L., Cairns J. and Lowe R.L. 1981. Quantitative characterisation of aquatic environments using diatom life-form strategies. Transactions of the American Microscopial Society 100: 165-182.

Leps J. and Šmilauer P. 2003. Multivariate analysis of ecological data using CANOCO. University Press, Cambridge, 269 pp.

Lydolph P.E. 1977. Geography of the USSR. Elsevier, The Hague.

Mackay A.W., Ryves D.B., Battarbee R., Flower R.J., Jewson D., Rioual P. and Sturm M. 2005. 1000 years of climate variability in cetral Asia: assessing the evidence using lake Baikal diatom assemblages and the application of a diatom inferred model of snow thickness. Global and Planetary Change 46: 281-297.

Mackay A.W., Swann G.E.A., Brewer T.S., Leng M., Morley D.W., Piotrowska N., Rioual P. and White D. In review. Millennial scale variability in the north Atlantic thermohailine circulation drives hydrological variability and diatom productivity in Lake Baikal (central Asia) during the past 14,500 years.

Matafonov D.V., Kuklin A. and Matafonov P. 2005. Consortia in Aquatic Ecosystems of the Transbaikalia. Biology Bulletin 32: 490-495.

Mischke S., Kramer M., Zhang C., Shang H., Herzschuh U. and Erzinger J. 2008. Reduced early Holocene moisture availability in the Bayan Har Mountains, northeastern Tibetan Plateau, inferred from a multi-proxy lake record. Palaeogeography, Palaeoclimatology, Palaeoecology 267: 59-76.

Nelson K. and Bradley L.-A. 2009. Fragmentary evidence of great earthquake subsidence during Holocene emergence, Valdivia Estuary, south Central Chile. Bulletin of the Seismological Society of America 99: 71-86.

Nikulina T.V. 2008. Diatom algae of Atlansova Island (Kuril Island). Vladmir Ya. Levanidov's Biennial Memorial Meetings. Vladivostok, Dal'nauka, pp. 122-129.

Patrick R. and Reimer C.W. 1966. The diatoms of the United States. The Academy of Natural Sciences, Philadelphia.

Peck J., Khosbayer P., Fowell S., Pearce R.B., Ariunbileg S., Hanses B.C.S. and Soninkhishig N. 2002. Mid to late Holocene climate change in northcentral Mongolia as recorded in the sediments of Lake Telmen. Palaeogeography, Palaeoclimatology, Palaeoecology 83: 135-153.

Prather C. and Hickman M. 2000. History of a presently slightly acidic lake in northeastern Alberta, Canada as determined through analysis of the diatom record. J Paleolimnol 24: 183-198.

Prokopenko A., Khursevich G., Bezrukova E., Kuzmin M., Boes X., Williams D., Fedenya S., Kulagina N., Letunova P. and Abzaeva A. 2007. Paleoenvironmental proxy records from Lake Hovsgol, Mongolia, and a synthesis of Holocene climate change in the Lake Baikal watershed. Quaternary Research 68: 2-17.

R v. 2.7.1 Team R.D. 2008. Vienna.

Reavie E.D. and Smol J.P. 1998. Epilithic diatoms of the St. Lawrence river and their relationships to water quality. Canadian Journal of Botany 76: 251-257.

Reimer P.J., Baillie, M.G.L., Bard, E., Bayliss, A., Beck, J.W., Bertrand, C.J.H., et al, 2004. IntCal terrestrial radiocarbon age calibration, 0-26 cal kyr BP. Radiocarbon. 46: 1029-1058.

Rosch M., Fischer E. and Markle T. 2005. Human diet and land use in the time of the Khans-Archaeobotanical research in the capital of the Mongolian Empire, Qara Qorum, Mongolia. Vegetation History and Archaeobotany 14: 485-492.

Rose N. 1995. Carbonaceous particle record in lake sediments from the Arctic and other remote areas of the Northern Hemisphere. Science of the Total Environment, The 160: 487-496.

Rose N.L., Appleby P.G., Boyle J.F., Mackay A.W. and Flower R.J. 1998. The spatial and temporal distribution of fossil-fuel derived pollutants in the sediment record of Lake Baikal, eastern Siberia. Journal of Paleolimnology 20: 151-162.

Ruhland K., Paterson A. and Smol J. 2008. Hemispheric-scale patterns of climate-related shifts in planktonic diatoms from North American and European lakes. Global Change Biology 14: 2740-2754.

Sandgren C.D., Smol J. and Kristiansen J. 1995. Chrysophyte algae: Ecology, phylenology and development Cambridge University Press, Cambridge, 399 pp.

Schmid A.M.M. and Crawford R.M. 2001. *Ellerbeckia arenaria* (Bacillariophyceae): formation of auxospores and initial cells. European Journal of Phycology 36: 307-320.

Schmidt R., Kamenik C., Lange-Bertalot H. and Klee R. 2004. Fragilaria and Staurosira (Bacillariophyceae) from sediment surfaces of 40 lakes in the Austrian Alps in relation to environmental variables, and their potential for palaeoclimatology. Journal of Limnology 63: 171-189.

Schwanghart W., Schutt B. and Walther M. 2008. Holocene Climate Evolution of the Ugii Nuur Basin, Mongolia. Advances in Atmospheric Sciences 25: 986-998.

Schwanghart W., Schutt B. and Walther M. 2009. Holocene Climate Evolution of the Ugii Nuur Basin, Mongolia. Palaeogeography, Palaeoclimatology, Palaeoecology 279: 160-171.

Shahgedanova M. 2002. Climate at the present and in the historical past. In: M. Shahgedanova (ed.), The physical geography of northern Eurasia. Oxford University Press, Oxford. , pp. 70-103.

Shindell D., Schmidt G., Mann M., Rind D. and Waple A. 2001. Solar forcing of regional climate change during the Maunder Minimum. Science 294: 2149-2152.

Shishkin B.A. 1973. Seasonal and annual variations in biological regime of lakes in an ultracontinental climate (Trans-Baikal Region of USSR). Hydrobiologia 43: 253-261.

Simpson G. 2008. "Numerical analysis of biological and environmental data";. Environmental Change Research Centre, University College London.

Smol J., Wolfe A., Birks H., Douglas M., Jones V., Korhola A., Pienitz R., Ruhland K., Sorvari S., Antoniades D., Brooks S., Fallu M., Hughes M., Keatley B., Laing T., Michelutti N., Nazarova L., Nyman M., Paterson A., Perren B., Quinlan R., Rautio M., Saulnier-Talbot E., Siitoneni S., Solovieva N. and Weckstrom J. 2005. Climate-driven regime shifts in the biological communities of arctic lakes. Proceedings of the National Academy of Sciences of the United States of America: 4397-4402.

Solovieva N., Jones V., Birks J., Appleby P.G. and Nazarova L. 2008. Diatom responses to 20th century climate warming in lakes from the northern Urals, Russia. Palaeogeography, Palaeoclimatology, Palaeoecology 259: 96-106.

Van Dam H., Mertens A. and Sinkeldam J. 1994. A coded checklist and ecological indicator values of freshwater diatoms from the Netherlands. Netherlands Journal of Aquatic Ecology 28: 117-133.

Wang Y., Cheng H., Edwards R.L., He Y., Kong X. and An Z. 2005. The Holocene Asian monsoon: links to solar changes and North Atlantic climate. Science 308: 854-857.

Watchorn M., Hamilton P., Anderson T., Roe H. and Patterson R. 2008. Diatoms and pollen as indicators of water quality and land-use change: a case study from the Oak Ridges Moraine, Southern Ontario, Canada. Journal of Paleolimnology 39: 491-509.

Weckstrom J. and Juggins S. 2006. Coastal diatom-environment relationships from the Gulf of Finland, Baltic Sea. Journal of Phycology 42: 21-35.

Witkowski A., Latałowa M., Borówka R., Gregorowicz P., Bąk M., Osadczuk A., Święta J., Lutyńska M., Wawrzyniak-Wydrowska B. and Woziński R. 2004. Palaeoenvironmental changes in the area of the Szczecin Lagoon (the south western Baltic Sea) as recorded from diatoms. Studia Quaternaria 21: 153-165.

Xiao J., Chang Z., Wen R., Zhai D., Itoh S. and Lomtatidze Z. 2009. Holocene weak monsoon intervals indicated by low lake levels at Hulun Lake in the monsoonal margin region of northeastern Inner Mongolia, China. Holocene 19: 899-908.

Zeeb B.A. and Smol J.P. 2001. Chrysophyte scales and cysts. In: W. M. Last and J. P. Smol (eds.), Tracking Environemntal Change Using Lake Sediments volume 3. Springer, Netherlands, pp. 203-223.

# CHAPTER 7. Synthesis of project

## 7.1. Introduction

Chapters 5 and 6 have discussed the main environmental interpretations from lakes Xiaolongwan and Arachlei and the variability in SiZer and timeseries results from each of the lakes. In summary, both records are argued to represent changes in lake water level, which in turn is associated with variations in regional climate. The reconstructed environmental interpretations, based on diatom ecology and bulk organic composition change, were then compared with regional evidence of environmental change across the regions. SiZer results from both lakes identified significant changes in diatom assemblages coincident with evidence of North Atlantic ice raft debris (IRD) events as well as regional evidence of climatic change over the late Holocene. This section aims to go further by providing a synthesis between the records presented in this project. In particular diatom records will be used to compare with regional climatic indices of solar variability, east Asian summer monsoon (EASM) variability and north Atlantic IRD events. Diatom PCA axes scores are selected as they reflect the most significant changes in the data and also due to the long time period they cover at both lakes, making it possible for comparisons between them (particularly compared to bulk organic isotope results from Lake Xiaolongwan).

## 7.2. Evidence of palaeoenvironmental change in northern Eurasia

Figure 7.1 provides a summary of the diatom PCA scores from both Lake Xiolongwan and Arachlei as well as the Dongge cave $\delta^{18}O$ speleothem record, a proxy for EASM intensity, 60 $^{o}N$ total solar irradiance (TSI) a proxy of solar variability and hematite stained grains (HSG) from the north Atlantic, a proxy of IRD events and the subsequent reduced circulation of the North Atlantic thermohaline circulation (THC) (Bond et al. 2001; Bond et al. 1997; Steinhilber et al. 2009; Wang et al. 2005). The rationale behind comparing the records is to look at the main characteristics in the data presented in this project, to discuss the climatic signal and the role of teleconnection mechanisms between the north Atlantic and northern Eurasia. Mayewski et al (2004) have outlined that changes in insolation related to both the Earth's orbital variations and to solar variability have played a central role in the global scale change in climate over the last 11,500 years BP and that superimposed upon this trend are Holocene climate change events at intervals of approximately 2800–2000 and 1500 years. As discussed in Chapter 1.5, the past c. 3000 years is a key timeframe for investigating climatic change in the Holocene due to only minor changes in boundary conditions (compared to earlier intervals) and in particular there is a need to increase the high resolution data repositories of regions of northern Eurasia (e.g. PAGES-IGBP 2010).

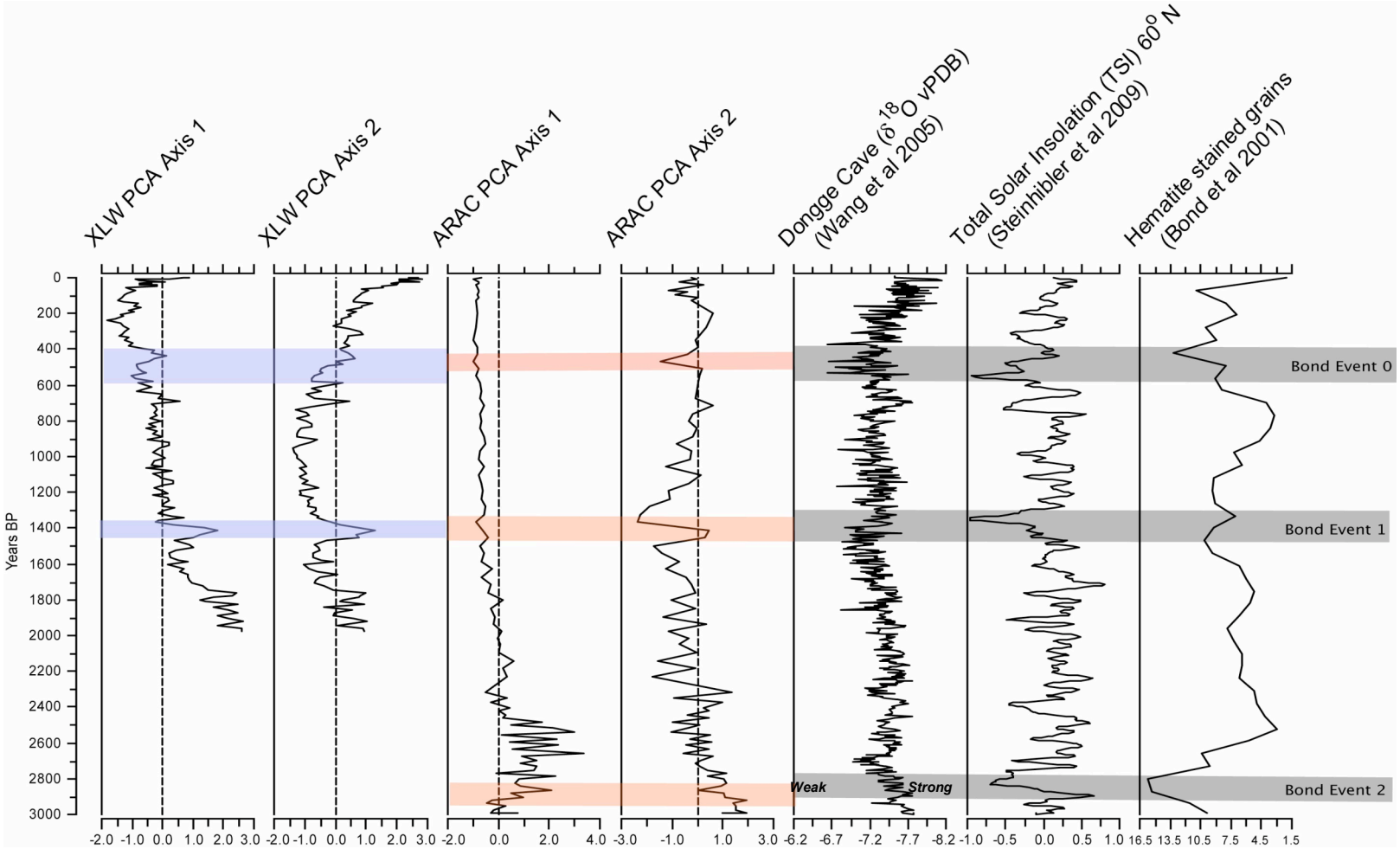


*Figure 7.1 PCA axis 1 and 2 scores from this project, for the Lakes Xiaolongwan-XLW (proxy of EAWM) and Arachlei-ARAC (proxy of summer climate e.g. Westerlies). $\delta^{18}O$ (‰) from the Dongge cave speleothem, Total Solar Irradiance from 60 °N where negative values correspond to minima and hematite stained grains from sediments in the north Atlantic, reversed so that troughs correspond with troughs in the other published data (sourced from NOAA-NCDC 2010 http://www.ncdc.noaa.gov/paleo/data.html). Relevant sources are displayed. The blue and pink bars correspond to the events, independent to each record, based on SiZer and timeseries results. Grey bars correspond to published dates when changes in each of the records is argued to correspond to Bond Events.*

As outlined in Chapter 5.4, the significant increases identified in PCA axis 1 scores from Lake Xiaolongwan reflect increased *Achnanthidium minutissimum* var *minutissimum* abundances which are interpreted as more dynamic lake environments during autumnal periods, while significant increases in PCA aixs 2 scores reflects an increase in the benthic species *Eunotia subarcuatoides,* which can tolerate high and abrupt variation in pH. The latter part of the PCA axis 2 record however represents the introduction of *Discotella woltereckii* after c. 55 years BP, although this is not highlighted in Figure 7.1 due to the possible role of anthropogenic contamination at the site at this time (Figure 5.14a and b). While bulk organic isotopic data for Lake Xiaolongwan covers only c. 300 years, significant shifts to increased algal productivity are highlighted at the same time as the introduction of *D. woltereckii.* Based on these data, it is believed that highlighted events in Figure 7.1 represent an intensified east Asian winter monsoon (EAWM) based on contemporary understanding of climate. Significant changes in PCA axis 2 scores from Lake Arachlei (Figure 7.1) demonstrate the decrease in *Puncticulata radiosa*, a planktonic species, which is believed to reflect lake water level reductions. Significant changes in PCA axis 1 scores are only identified between the period c. 3300 and 2300 years BP representing the variation in the species *Rossithidium petersenii* and the later trend reflects the increasing abundance of *Cavinula scutelloides.* For Lake Arachlei, these significant changes reflect reduced abundances of the warm lake water species indicator *P. radiosa* and an increase in benthic species, thereby reflecting reduced Westerly transport to the region and enhanced SH intensity (colder and drier periods). Bulk organic isotopic data for the core show an overall increasing trend in aquatic productivity, although a periodic decrease is highlighted between the periods c. 3000-2800 years BP, which may again be a reflection of more intensified winter conditions. These interpretations are supported, as demonstrated in Sections 5.4 and 6.8, by other relevant literature of palaeoenvironmental change.

Figure 7.1 summarises the significant changes highlighted in both the Lake Xiaolongwan and Arachlei records, based on timeseries and SiZer analyses conducted on PCA axes scores. The two most dominant periods fall between c. 1450-1350 and 600-350 years BP for Lake Xiaolongwan (Figures 5.9 to 5.12) and between c. 3030-2800, 1410-1365 (particularly after 1400) and 850-500 years BP for Lake Arachlei (Figures 6.17 to 6.20). The coloured bars in Figure 7.1 correspond directly to the data presented in the relative data chapters and have not been correlated. It is evident that for both records, there are significant intervals of environmental change that are occurring across similar time periods. They do demonstrate different durations and timings however, which may be a result of the different dating methods used for each of the reconstructions and also the errors associated with these techniques. However, it is possible to conclude that the changes seen in south east Siberia and north east China from these records are coincident with evidence of weakening of north Atlantic deep water (NADW) formation

(Bond et al. 2001), minima in solar variability (based on $^{10}$Be reconstructions by Steinhilber et al. 2009) and weakened EASM intensity (Wang et al. 2005). In particular events centred at c. 2800 (Bond Event 2), 1400 (Bond Event 1) and c. 500 years BP (Bond Event 0 or the LIA).

Cosford et al (2008) highlight that with weakened EASM intensity, high latitude cooling and low latitude aridity is seen when there is enhanced SH and EAWM intensity and increased north Atlantic ice rafting. Based on the Linhua $\delta^{18}$O record, this is particularly seen in the late Holocene between 3300-3100 and at 200 years BP (Figure 1.2; ibid.). Cosford et al (2008) go further to state that EASM intensity responds to internal climatic mechanisms that regulate oceanic and atmospheric circulation. Indeed, the mechanism that links solar activity to changes in climatic conditions (e.g. the monsoon) remains poorly understood because the magnitude of variance in solar radiation at these time-scales, estimated at 0.1% to 0.3% (1–2 mW/m$^2$) (Bard and Frank 2006; Lean et al. 1995) is seemingly insufficient to directly affect the sensible heating and pressure differentials that drive monsoonal circulation. Solar irradiance enhances stratospheric ozone formation through photochemical reactions and leading to further heating of the stratosphere through absorption of the excess UV radiation by ozone. Modelling studies indicate that this mechanism amplifies the global average warming due to the increase in irradiance by about 15–20% (Palmer et al. 2004; Shindell et al. 2001). However, to influence the climate system, this small radiative forcing requires an amplifying mechanism in the ocean-atmosphere system, such as a response to solar forcing by the North Atlantic Oscillation (NAO) (Mayewski et al. 2004). As such, a negative NAO associated with north Atlantic fresh water forcing (e.g. Bond events 2 to 0) will lead to an enhanced SH intensity, with colder and drier winter conditions and reduced westerly transport in summer months in Arid central Asia (ACA). In monsoon Asia dominanted areas, it will lead to an enhanced EAWM associated with enhanced SH intensity and weakend EASM intensity. It is argued here that these teleconnections are demonstrated through palaeoenvironmental interpretation of diatom ecological changes down core from both Lake Xiaolongwan and Arachlei. Furthermore, they appear to occur at similar times which is contrary to the argument of asynchroneity of environmental change (particularly in the mid-Holocene) between ACA and monsoonal Asia (Chen et al. 2008).

Outside of natural climate forcing, it cannot be ignored that in more recent years the role of anthropogenic forcing has been found to have a significant effect upon pristine lake environments (Ruhland et al. 2008; Smol et al. 2005; Solovieva et al. 2008). Hobbs et al (2010) outine that ecological responses of remote lakes to post-industrial environmental changes are complex and conclude that remote lakes will continue to shift towards new ecological states. In particular evidence has demonstrated the increase in the planktonic species *Cyclotella* in a response to increased warming over recent decades (Ruhland et

al. 2008; Smol et al. 2005; Wang et al. 2008). As outlined in Section 5.4.4 the introduction of *D. woltereckii* at Lake Xiaolongwan after c. 1970 AD may also be responding to the increase in mean annual temperatures (and decreased annual precipitation). However, this introduction is coincident with an increase in pollution indices at the lake and a peak in SCP concentrations (Figures 5.2 and 5.14a). As such, it may not be attributed to climatic change alone. At Lake Arachlei, on the other hand, little significant change is seen at the surface of the diatom and bulk organic geochemistry record. Furthermore, the absence of SCPs above background levels from the core argues that anthropogenic impact is minimal.

## 7.3. Further work

Throughout the completion of this project a number of elements can be proposed as future work. These would help to draw more distinct conclusions. Firstly, contemporary isotopic sampling of both lake waters and catchment soil and vegetation is not available for Lake Arachlei. This information would provide valuable information on lake-catchment processes and end-members for contemporary compositions of these variables, for down core interpretations. Contemporary sampling of dominant diatom habitats at the lake would also be useful in providing detailed information of present day diatom assemblages, in particular their habitats and ecologies, invaluable information for palaeoenvironmental reconstructions. As part of this further work, more detailed research on the numerous types of macrophytes (emergent and submerged) present at Lake Xiaolongwan would also be very valuable, especially with reference to disentangling the $\delta^{13}C$ record. Particular consideration should be made to the preferential method of carbon uptake (e.g. atmospheric $CO_2$ or DIC) and how these different pathways affect $\delta^{13}C$ composition of plants, in order to interpret the changes in productivity. Macrofossil analyses in particular would also be useful in looking at the representation of plant macrophytes in the lake and pollen analyses to look further at catchment/regional productivity changes in response to environmental change.

A second element which has had some attention drawn to it (Chapter 4) is the chronology derived for Lake Xiaolongwan. In order to make the age model for the cores X00/X06 and XLW2 more robust I propose that further independent radiometric dating should be carried out on the cores X00/X06. This would act as a method of corroborating the varve age model. In order to create a more robust chronology for Lake Arachlei, it is also proposed that further radiocarbon analyses should be conducted. In particular covering the sediment depths between 14.5 and 2.5 cm. This would bridge the gap between the $^{210}Pb$ age model and the first $^{14}C$ date from the Ar-2005 core. As such, this would aim to

create a more robust age model, using both techniques and reduce errors for those sections of the core.

Thirdly, in order to investigate further the conclusions drawn from the data presented in this thesis, for example the role of teleconnections during the late Holocene, I would suggest that a number of other sites should be analysed. This would include another site in both ACA and monsoon Asia, as well as a site that is positioned along the present monsoonal boundary. Bulk organic isotopic and diatom analyses would again be conducted so that the records are comparable with Lake Xiolongwan and Lake Arachlei. The timing, duration and intensity of environmental changes at these sites will be used to discuss further late Holocene environmental change in northern Eurasia, how they compare with other indices (e.g. of NADW formation and solar variability) of climate change and what role teleconnections play.

Finally as mentioned in Section 5.4.4 the role of recent anthropogenic impacts upon diatom assemblages, in particular the introduction of the species *D. woltereckii,* have been discussed. I believe that it would be interesting to investigate further the role of atmospheric deposition upon the sites and in particular nitrogen deposition (e.g. $^{15}N$ analyses on cores). For example, further information on the nitrogen sensitivity of certain species present in the lake today to increased loading.

## 7.4. Conclusions

1. The main periods of change in the diatom record of Lake Xiaolongwan occur between 1450-1350 and 600-400 years BP and at Lake Arachlei between 3000-2800, 1450-1350 and 500-400 years BP. These coincide with the dated periods of IRD events at 2800 (Bond Event 2), 1400 (Bond Event 1) and c. 500 years BP (Bond Event 0 or the LIA).

2. The proxies employed reflect increased EAWM intensity at Lake Xiaolongwan and reduced Westerly intensity at Lake Arachlei. Bulk organic isotopic data, however, do not document such dramatic changes in lake/catchment productivity compared to the shifts in the diatom assemblages.

3. The inferred changes in climate are closely linked to teleconnections between the North Atlantic ocean and modes of climatic variability, in particular the NAO. With phases of negative NAO, following freshwater forcing of the North Atlantic (after IRD events), reduced Westerlies occur leading to cooler summer temperatures over parts of northern Eurasia, in turn leading to weakened EASM intensity. Negative NAO index also leads to enhanced SH intensity in winter months and as such increased EAWM intensity.

4. The findings indicate that significant environmental variability in the late Holocene at both study sites (southern Siberia and north east China) is coincident with Bond Events 0,1 and 2. Nevertheless, evidence of environmental change outside of these three events is also seen.

5. Over the past c. 40 years, a dramatic change is seen in the diatom assemblages of Lake Xiaolongwan, possibly reflecting recent global warming and a degree of anthropogenic contamination as revealed by SCP and XRF analyses. No such recent change was observed in the Lake Arachlei diatom record and SCP concentrations were at background levels.

This study has contributed to the ongoing research in this region by disputing the argument of asynchroneity between monsoonal Asia and arid central Asia. The findings suggest that, during the late Holocene, periods of climatic perturbations in differing atmospheric systems (e.g. the EASM, EAWM, Westerlies and SH) occur at similar times. Indeed the thesis provides sufficient evidence to suggest the presence of teleconnections in these regions. Finally, this thesis has contributed to the current scientific focus of the PAGES (Focus 2) Programme, by providing high resolution palaeoecological records of environmental change in the late Holocene for a previously poorly studied region of the world.

## References

Bard E. and Frank M.J. 2006. Climate change and solar variability: What's new under the sun? Earth and Planetary Science Letters 248: 1-14.

Bond G., Kromer B., Beer J., Muscheler R., Evans M.N., Showers W., Hoffmann S., Lotti-Bond R., Hajdas I. and Bonani G. 2001. Persistent solar influence on north Atlantic climate during the Holocene. Science 294: 2130-2136.

Bond G., Showers W., Cheseby M., Lotti R., Almasi P., deMenocal P., Priore P., Cullen H., Hajdas I. and Bonani G. 1997. A pervasive millennial-scale cycle in North Atlantic Holocene and glacial climates. Science 278: 1257-1266.

Chen F., Yu Z., Yang M., Ito E., Wang S., Madsen D., Huang X., Zhao Y., Sato T. and Birks H. 2008. Holocene moisture evolution in arid central Asia and its out-of-phase relationship with Asian monsoon history. Quaternary Science Reviews 27: 351-364.

Cosford J., Qing H., Eglington B. and Mattey D. 2008. East Asian monsoon variability since the Mid-Holocene recorded in a high-resolution, absolute dated aragonite speleothem from eastern China. Earth and Planetary Science Letters 275: 296-307.

Hobbs W.O., Telford R.J., Birks H.J.B., Saros J.E., Hazewinkel R.R.O., Perren B., Saulnier-Talbot E. and Wolfe A.P. 2010. Quantifying Recent Ecological Changes in Remote Lakes of North America and Greenland Using Sediment Diatom Assemblages. PLoS ONE 5: 1-12.

Lean J., Beer J. and Bradley R. 1995. Reconstruction of Solar Irradiance since 1610 - Implications for Climate-Change. Geophysical Research Letters 22: 3195-3198.

Mayewski P., Rohling E., Curt Stager J., Karlén W., Maasch K., David Meeker L., Meyerson E., Gasse F., van Kreveld S. and Holmgren K. 2004. Holocene climate variability. Quaternary Research 62: 243-255.

NOAA-NCDC 2010. http://www.ncdc.noaa.gov/paleo/data.html.

PAGES-IGBP 2010. http://www.pages-igbp.org/index.html.

Palmer M.A., Gray L.J., Allen M.R. and Norton W.A. 2004. Solar forcing of climate: model results. Advances in Space Research 34: 343-348.

Ruhland K., Paterson A. and Smol J. 2008. Hemispheric-scale patterns of climate-related shifts in planktonic diatoms from North American and European lakes. Global Change Biology 14: 2740-2754.

Shindell D., Schmidt G., Mann M., Rind D. and Waple A. 2001. Solar forcing of regional climate change during the Maunder Minimum. Science 294: 2149-2152.

Smol J., Wolfe A., Birks H., Douglas M., Jones V., Korhola A., Pienitz R., Ruhland K., Sorvari S., Antoniades D., Brooks S., Fallu M., Hughes M., Keatley B., Laing T., Michelutti N., Nazarova L., Nyman M., Paterson A., Perren B., Quinlan R., Rautio M., Saulnier-Talbot E., Siitoneni S., Solovieva N. and Weckstrom J. 2005. Climate-driven regime shifts in the biological communities of arctic lakes. Proceedings of the National Academy of Sciences of the United States of America: 4397-4402.

Solovieva N., Jones V., Birks J., Appleby P.G. and Nazarova L. 2008. Diatom responses to 20th century climate warming in lakes from the northern Urals, Russia. Palaeogeography, Palaeoclimatology, Palaeoecology 259: 96-106.

Steinhilber F., Beer J. and Frohlich C. 2009. Total solar irradiance during the Holocene. Geophysical Research Letters 36: -.

Wang L., Lu H., Liu J., Gu Z., Mingram J., Chu G. and Li J. 2008. Diatom-based inference of variations in the strength of Asian winter monsoon winds between 17,500 and 6000 calendar years BP. Journal of Geophysical Research-Atmospheres 113: 1-9.

Wang Y., Cheng H., Edwards R., He Y., Kong X., An Z., Wu J., Kelly M., Dykoski C. and Li X. 2005. The Holocene Asian monsoon: links to solar changes and North Atlantic climate. Science 308: 854-857.

# Appendices

## i. Additional information on diatom identification

Lake Xiaolongwan taxonomy (refer to Section 5.2.4):

When identifying the small Fragilariaceae, it was concluded that the species *Staurosira construens* var*. venter* was present (Figures i, ii). Taxonomic characteristics include areolae that are occluded. The species can be defined from *Staurosira elliptica* on the basis of the areole, which are more stretched and less elliptical in *S. construens* var *venter*.

Another small sub round species that was identified by SEM was *Punctastriata discoidea* (Figure iii). Flower (2005) describe that the new species *P. discoidea* nov. sp. was chosen as under SEM it was clear that valve shape, spines and striae density separated the species from *P. ovalis* (Williams and Round). This species has a multi-seriate fascicle structure and reaches a size of up to 4µm diameter (Flower, 2005). Another distinguishing factor of this species is short distally expanded spines. As Figure iii shows, these were not seen in SEM analyses conducted upon cores X00/X06. New literature has highlighted the similarity of the species *P. glubokoensis* to *P. discoidea* (Williams et al. 2009). Williams et al (2009) conclude that the spines on both of these species differ, with the latter having more complex spines with additional horizontal projections. As spines were not identified in SEM from the Lake Xiaolongwan core, the species was defined as *P. discoidea*. Indeed, Williams et al (2009) conclude that the possibility remains that the two species are the same and that spine structure is the only means of distinguishing a difference.

***i*** ***ii*** ***iii***

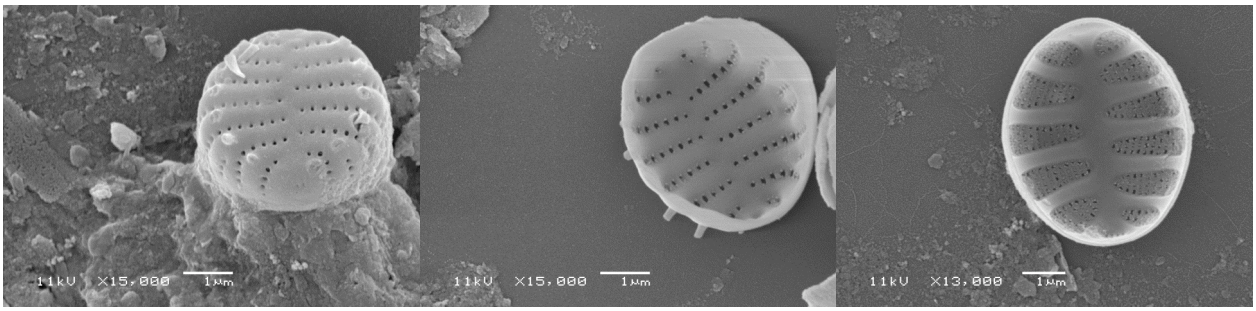


Figures i and ii, SEM photographs of *Staurosira construens* var*. venter,* showing the outer value and inner valve view respectively. iii, SEM photograph of *Punctastriata discoidea* from Lake Xiaolongwan sediments.

The species *Discotella woltereckii* was identified in the top sections of the Lake Xiaolongwan record. This is a member of the stelligeroid family and has a number of distinguishing factors that are distinct from the remaining forms. These have been outlined by Haworth and Hurley (1986) and Wunsam, Schmidt and Klee (1995). *D. woltereckii* is a species that has forked striations (unlike *D. stelligera*). This species also has marginal fultoportulae (mfp) spaced at every 4-5 striae typical of the species. *D. woltereckii* can be as small as 4.5µm in diameter. It was concluded that the species present in the core are small valves of *D. woltereckii* with short striae.

***iv*** ***v***

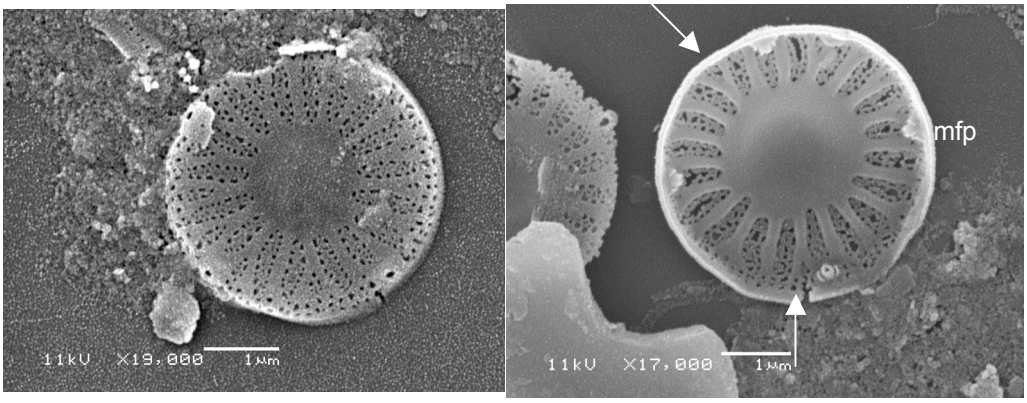


Figures iv and v, SEM photographs from Lake Xiaolongwan showing the species *Discotella woltereckii* (outer valve with some dissolution and inner valve respectively). Characteristic features including forked striae are highlighted by arrows and marginal fultoportulae (mfp) are also shown.

Lake Arachlei taxonomy (refer to Section 6.4.4):

Diatom taxonomy and identification for the Lake Arachlei core was more straightforward than the species identification from Lake Xiaolongwan. The main issue for Lake Arachlei was the presence of clay particles in the samples (evident in SEM pictures below), which could cover species and make identification more difficult. SEM and LM photographs will be shown here to indicate the dominant taxa identified from the core and key identification characteristics will be highlighted.

*Rossithidium peretsenii* (previously *Achnanthes petersenii)* was identified based on the characteristics identified by Krammer and Lange-Bertalot (1991b) which is of a length between 8.5 and 42.5µm and a valve width of 4 to 5µm.

***vi***

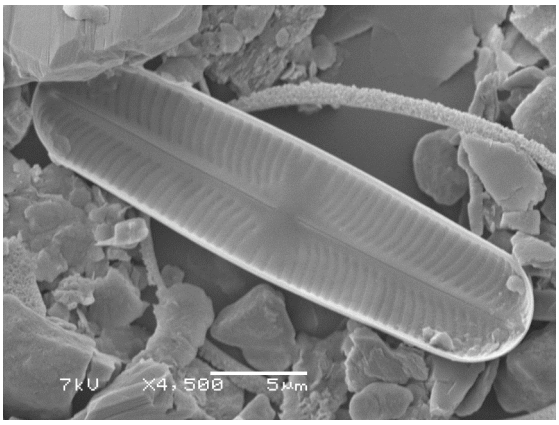


Figure vi, SEM photograph of *Rossithidium pertersenii* from the Lake Arachlei core.

*Punctastriata bodanica* (previously *Cyclotella bodanica*) was identified based on the characteristics defined in Krammer and Lange-Bertalot (1991a) with a width between 20-80µm and the number of radial striae between 13-15 per 10µm. The same literature was used to identify the smaller centric species of *Punctastriata radiosa* (*Cyclotella radiosa*). This species has a size of 8-50µm and radial striae of 13-16/10µm.

***vii*** ***viii***

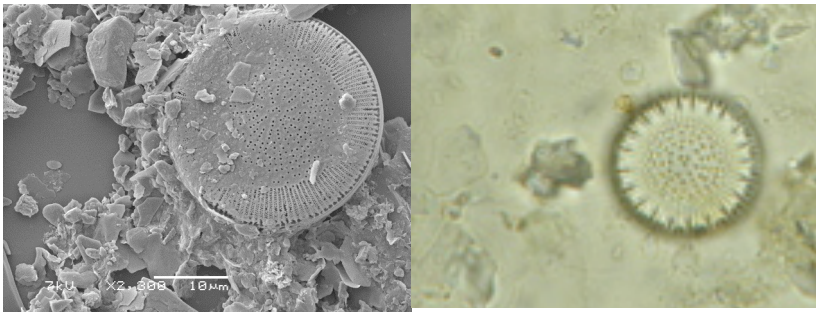

Figures vii, SEM photograph of *Punctastriata bodanica* from the Lake Arachlei core and viii, LM photograph of *Punctastriata radiosa* from Lake Arachlei.

**ii. Radiocarbon ages for core Ar-2005**

| Sample name | Sample depth (mm) | Lab no. | Age ($^{14}$C years) | Error ($^{14}$C years) | Calibrated age (BC/AD) |
|---|---|---|---|---|---|
| A2 1440-1450 | 1440 | Poz-23517 | 11,110 | 60 | 11,299 |
| A2 500-510 | 500 | Poz-23516 | 4,380 | 40 | 3,445 |
| A2 142.5-145 | 142.5 | Poz-30580 | 2,315 | 35 | 625 |

*Table 1. Analytical results of radiocarbon dating on core Ar-2005. Sample age in radiocarbon years as well as errors are shown. Calibrated age (BC/AD) for the samples is also provided based on calibration using the program OxCal v. 4.1 and the calibration curve IntCal 04. Refer to Table 6.2 for errors associated with the calibrated ages. Please note, $\delta^{13}$C values are not available for the dates.*

**References**

Flower R.J. 2005. A taxonomic and ecological study of diatoms from freshwater habitats in the Falkland Islands, South Atlantic. Diatom Research 20: 23-96.

Haworth E.Y. and Hurley M.A. 1986. Comparison of the stelligeroid taxa of centric diatom genus Cyclotella. In: M. Ricard (ed.), Proceedings of the 8th International Diatom Symposium. Koeltz Scientific Books, Koenigstein, pp. 43-53.

Krammer K. and Lange-Bertalot H. 1991a. Bacillariophyceae. 3. Tiel. Zentrische Diatomeen, Diatoma, Meridion, Asterionellla, Tabellaria, Fragilaria, Eunotia und Verwandte, Peronia und Actinella. Gustav Fisher Verlag., Stuttgart.

Krammer K. and Lange-Bertalot H. 1991b. Bacillariophyceae. 4. Tiel. Achnanthes, Navicula, Gomphonema, Kritsche Nachtraege, Literatur. Gustav Fisher Verlag., Stuttgart.

Williams D.M., Chudaev D.A. and Gololobova M.A. 2009. *Punctastriata glubokoensis* spec. nov., a new species of "fragilarioid" diatom from Lake Glubokoe, Russia. Diatom Research 24: 479-485.

Wunsam S., Schmidt R. and Klee R. 1995. Cyclotella-taxa (Bacillariophyceae) in lakes of the Alpine region and their relationship to environmental variables. Aquatic Sciences-Research Across Boundaries 57: 360-386.